Oxytocin Receptor Expression and Function in the Retinal Pigment Epithelium

By

Nathaniel W. York

A dissertation submitted in partial fulfillment of

the requirements for the degree of

Doctor of Philosophy

(Endocrinology and Reproductive Physiology)

at the

University of Wisconsin-Madison

2018

Date of final oral examination: 05/25/2018

Submitted for the Approval of the Final Oral Committee:

Bikash Pattnaik, Assistant Professor, Pediatrics

De-Ann Pillers, Professor, Pediatrics, University of Illinois at Chicago

Nader Sheibani, Professor, Ophthalmology and Visual Science

Aparna Lakkaraju, Associate Professor, Ophthalmology and Visual Science

Ian Bird, Professor, Obstetrics and Gynecology

Thesis Abstract

Oxytocin (OXT) is well-known for its role in labor and lactation but OXT and its receptor are involved in processes throughout the body, from maintaining muscle to driving blood vessel growth. In this study, I focus on the role oxytocin plays in the visual system, something that has remained unexplored since oxytocin was discovered in the eye in 1983. We have previously shown that oxytocin receptor (OXTR) is expressed and functional in the retinal pigment epithelium (RPE) and that OXT is present around the adjacent cone photoreceptor outer segments. In this work I further characterized the signaling pathway at work in the RPE and then explored potential downstream regulations. Using our knowledge of OXTR signaling I looked into the potential for OXT to influence the function of the inwardly rectifying K^+ channel, Kir7.1, which is a key component of RPE health and disease. I demonstrate that OXT can induce the inhibition of this channel and that this inhibition is prolonged, suggesting a long-lasting effect of OXT on the RPE. In addition to exploring the potential for OXT to influence cellular excitability I have explored the potential for OXT to influence retinal vascular growth. Focusing on the production and secretion of growth factors that control angiogenesis, I found that OXT does not appear to influence retinal vascular growth through its action in the RPE. In addition, I looked for the pattern of OXTR expression in the retina of the mouse not only to explore when OXT could begin to play a role in the retina but also to characterize the animal as a model for future study on OXTs impact on vision. Interestingly, I found that the mouse exhibits a different pattern of OXTR expression than the primate, with expression of OXTR throughout the retina and inconsistent expression in the RPE. This suggests a possible difference in the role played by the peptide between primates and humans and suggests that mice may not be an ideal model for OXTs role in the RPE. In total, this work represents a first step towards understanding of the role of OXT in the retina.

Table of Contents

Dedication

First and foremost, I would like to dedicate this work to my wife, Ali York. Since high school you have been there to support me, and I would not be the person I am today if it wasn't for you. I am sure it has been annoying at times, but competing with you has always driven me to push myself further. Every moment of every day, the good and the bad, is a little bit better when I get to share it with you. Also, we have a cat who is pretty cute, so that's nice.

I also want to thank my parents, who have provided endless love and support throughout my life. Whether I wanted to be a railroad conductor, a paleontologist, a comedian or a doctor you were always there to tell me I could do it. You taught me the value and necessity of hard work and the importance of leaving your comfort zone. You raised a beautiful family, with three great sisters and a very difficult son. You have both offered me a model of someone I should strive to be and everything I am, I am because of you.

Acknowledgments

Most importantly I would like to acknowledge and thank my mentor, Dr. Bikash Pattnaik. Over the last five years your door has always been open to me, whether to talk about new directions or to trouble shoot a particularly difficult problem. You always encourage discussion and debate and have allowed me to talk out my problems, even if it might take a while for me to come to the obvious solution. Your constant guidance and support have helped me develop as a scientist and a person and I want to thank you very much for this opportunity and experience.

I would also like to acknowledge Dr. Pawan Shahi, who joined the lab around the same time as me and has served as a constant during the last five years. Whether it be to offer advice, help or just good conversation, you have done a lot to shape my experience and working alongside you has been a pleasure.

Dr. De-Ann Pillers was another member of our lab group who has had a tremendous impact on my graduate career and my development as a scientist. Her advice and guidance has been invaluable during this process and her focus on what I needed to complete my degree is what made it possible for me to graduate in five years.

They say, “it takes a village” and in this case that is absolutely true. This work wouldn’t be possible if it wasn’t for the support of everyone in our lab. Katie, Yu, Andi, Luo, and Liu, thank you for all of your help, both by supporting me and my work but also by providing an environment that it is a joy to work in. This extends to all of the great undergrads who have come through the lab but especially Allie, Hannah and Dalton, who all worked with me and helped make this possible.

Finally, I would like to acknowledge my wife, Ali. From reading and editing pretty much every paper of mine since high school to listening to me practice talks over and over again, she has always been there to support me in my research. She is there to encourage me and to listen to my complaints. This would not be possible without your love and support.

Thank you all.

Abbreviations

$[Ca^{2+}]_e$	Extracellular Ca^{2+} concentration
$[Ca^{2+}]_i$	Intracellular Ca^{2+} concentration
$[K^+]_e$	Extracellular K^+ concentration
AM	Acetoxymethyl ester
CaV	Voltage gated Ca^{2+} channels
CCE	Capacitative Ca^{2+} entry
CM	Conditioned media
CNS	Central Nervous System
COX	Cycloxygenase
DAG	Diacylglycerol
ER	Endoplasmic Reticulum
ERG	Electroretinogram
GFP	Green-flourescent protein
GPCR	G-protein Coupled Receptor
HEK293	Human Embryonic Kidney cell line
hfRPE	Human fetal RPE
HGF	Hepatocyte growth factor
hPSC	Human Pluripotent Stem Cell
HR	Hepes Ringer Bath solution
ICROP	International Classification of ROP
IGF-1	Insulin-like Growth Factor-1
IP_3	Inositol trisphosphate
IPM	Interphotoreceptor Matrix
IRBP	Interphotoreceptor retinal binding protein
K-ATP	ATP-sensitive Kir channel
Kir	Inwardly rectifying K^+ channel
K_v	Voltage gated K^+ channel
LCA	Lebers congenital amaurosis
MC4R	Melanocortin-4 receptor
OTA	desGly-NH_2-d$(CH_2)_5$[D-Tyr^2,Thr^4]OVT
OXT	Oxytocin
OXTR	Oxytocin Receptor
PBS	Phosphate buffered saline
PEDF	Pigment Epithelium Derived Factor

PFA	Paraformaldehyde
PIP_2	Phosphatidyl inositol 4,5 bisphosphate
PKA	Protein Kinase A
PKC	Protein Kinase C
PLC	Phospholipase C
POS	Photoreceptor Outer Segments
Px	Postnatal day x
qPCR	Quantitative PCR
R_a	Access Resistance
RDDH5	11-*cis*-retinol dehydrogenase
REC	Retinal endothelial cell
RGR	RPE-retinal G protein-coupled receptor
RNA_i	RNA interference
ROI	Region of Interest
ROP	Retinopathy of Prematurity
RPE	Retinal Pigment Epithelium
SRIRS	Simultaneous RPE isolation and RNA stabilization
SVD	Snowflake Vitreoretinal Degeneration
TM	Transmembrane
VEGF	Vascular Endothelial Growth Factor
α-MSH	Alpha melanocyte stimulating hormone

List of Tables and Figures

Chapter 1: Introduction and Literature Review

1.1 Introduction

The eye is our window to the world, allowing us to perceive and interact with our surroundings. Although we so often take it for granted, human vision is made possible by a complex and highly organized process that relies on the thin, neuronal tissue that lies in the posterior of the eye called the retina. The function and development of the retina is closely tied to the epithelial layer of cells that lies adjacent to the photoreceptors, the retinal pigment epithelium (RPE). In the Pattnaik lab, we focus on understanding and characterizing the function of the RPE and describing its impact on the retina. My focus, in this thesis, is to better understand the specifics of this interaction, which is not yet fully understood.

One interesting, and previously unexplored factor that could play a role in this regulation is oxytocin (OXT). A hormone that was first shown to be in the eye in 1983, oxytocin has not been studied within the eye to any depth (Gauquelin et al., 1983). Oxytocin has a diverse list of functions throughout the body, a list that continually grows as more work is done, which extends labor and lactation to behavior and feelings of love. Another one of these functions is the ability to stimulate angiogenesis in endothelial cells (Cattaneo et al., 2008). This, plus the lack of fetal OXT production until late in gestation, brought our focus to the peptide, as we were searching for a factor that could play a role in retinal vascular growth (Schubert et al., 1981). To better understand its function, we set out to determine precisely where OXT and OXTR were found, within the eye. In pursuit of this goal, a previous graduate student in the lab, Patrick Halbach, M.S., demonstrated that oxytocin receptor (OXTR) is expressed in the RPE, and that oxytocin is present around the photoreceptors of the retina (Halbach, 2013). This discovery reveals the exciting possibility of oxytocinergic signaling within the retina-RPE interface. The

implications of this signaling are not yet clear but in this thesis I hope to have taken steps to resolve this by focusing both on the direct effect of OXT on RPE cell function and by looking at the potential for OXT to influence retinal angiogenesis, as well as through further characterization of OXTR expression as it is observed in the primate and the mouse.

For us to understand the effect of oxytocinergic signaling in the RPE, and the potential impact of this signaling on the retina, we must first understand the role of the RPE within the retina and the mechanisms underlying this role. Stated plainly, the RPE is a barrier, separating the subretinal space from the vascular blood supply of the choroid. As an epithelial cell, one major function of the RPE is the transepithelial transport of fluid and waste from the subretinal space that surrounds the photoreceptors to the choroidal blood. Additionally, the RPE is responsible for the maintenance of the subretinal K^+ concentrations that potentiate the light response of the photoreceptors. Both of these functions rely partially on the inwardly rectifying K^+ channel Kir7.1, the predominant K^+ channel in the RPE (Yang et al., 2003). The RPE is also responsible for the diurnal phagocytosis of the photoreceptor outer segments, a process that is necessary to maintain a healthy and functioning photoreceptor population. The importance of the RPE is clear when you look at the consequences of RPE dysfunction and degradation, including Lebers Congenital Amaurosis (LCA) and Snowflake Vitreoretinal Degeneration (SVD), to name only a few (Pattnaik et al., 2015; Pattnaik et al., 2013). In addition to these functions, the RPE is responsible for the production of a number of growth factors. These are Vascular Endothelial Growth Factor (VEGF), Pigment Epithelium Derived Factor (PEDF) and Insulin-like Growth Factor-1 (IGF-1), among many others. In the mature, healthy eye, this VEGF secretion helps to maintain the choriocapillaris while PEDF acts to inhibit angiogenesis (King & Suzuma,

2000; Strauss, 2005). In addition to this, the RPE is thought to be the primary source of VEGF for choroidal neovascularization (Strauss, 2005). The RPE, therefore, has the potential to influence angiogenesis in the retina through the secretion of these growth factors, a potential that is explored in **chapter 3**.

Oxytocin receptor is a G-protein coupled receptor and as such its actions can be wide reaching, ranging from direct effects on the receptor and its second messengers to more delayed effects like alterations in gene expression. In the uterine myometrium, where its action was first described, its signaling is primarily through the heterotrimeric G-protein G $\alpha_{q/11}$ which activates phospholipase C (PLC) which then hydrolyzes phosphatidylinositol 4,5 bisphosphate (PIP_2) to diacyl glycerol (DAG) and inositol trisphosphate (IP_3) (Arrowsmith & Wray, 2014). IP_3 in turn activates a Ca^{2+} release from the endoplasmic reticulum (ER) and DAG goes on to activate MAPK signaling through Protein Kinase C (PKC). Around this framework, there is some disagreement in the literature about the exact mechanisms underlying the response to OXTR activation. I therefore set out, in **chapter 2**, to first describe the mechanism of OXTR signaling as it exists in the RPE before exploring the broader impacts of its actions. Following this characterization, I turned my focus to the potential regulation of Kir7.1, which as previously mentioned is a key component of many RPE functions. In addition to this, I attempted to describe the potential for OXT to influence the development of the retina, looking at its effect on vascular development through the production of angiogenic growth factors by the RPE in **chapter 3** and by characterizing the ontogeny of the receptor within the RPE during development in **chapter 4**. These studies were performed using commercially available human

RPE cells, isolated murine RPE cells, a heterologous HEK293 -OXTR cell line that we developed, and tissue isolated from mice and rhesus monkeys.

To provide background information and to support the aims of this study, the introduction of this thesis proposes to describe: 1) The importance of the RPE to retinal function and the mechanisms underlying this role, 2) The function and regulation of Kir7.1 in the RPE, 3) The history of oxytocin and a review of its actions throughout the body, 4) Oxytocin receptor regulation and the mechanisms and effects of its signaling, 5) Systemic and peripheral production of oxytocin, and 6) The development of the retina, looking at the role played by the RPE as well as normal and pathological retinal vascular development. In light of this review of current literature, I will then provide the three specific aims I proposed for this thesis, as they were accepted by my thesis committee. We will begin first with a review of the RPE.

1.2 The Retinal Pigment Epithelium

1.2.1 RPE Overview

The retinal pigment epithelium lies within the posterior of the eye, adjacent to the photoreceptors of the retina and the blood vessels of the choriocapillaris (Figure 1.1). As its name suggests, the RPE is a pigmented monolayer of polarized epithelial cells. The apical membrane of these cells consists of microvilli that extend towards and between the light-sensitive photoreceptors, facilitating the interaction of the two cell types. The basolateral membrane of the RPE lies on top of Bruch's membrane, a barrier that sits between the RPE and the choriocapillaris. The function of the RPE is facilitated by this close physical proximity to the photoreceptors and the blood supply, allowing the RPE to provide necessary nutrients to the photoreceptors, including glucose, retinol and fatty acids (Strauss, 2005). Ion channels on the apical membrane of the RPE are also key mediators of photoreceptor function, ensuring that the ionic composition surrounding the photoreceptors is conducive to photoreceptor excitability (Steinberg et al., 1983; Strauss, 2005). To further support visual function the RPE is also responsible for the conversion of all-*trans*-retinol, taken from the photoreceptors, to 11-*cis*-retinal, which can be sent back to the photoreceptors to facilitate phototransduction (Baehr et al., 2003). The RPE is also very phagocytically active, daily phagocytosing the outer segments of both the rod and cone photoreceptors, digesting them and recycling usable elements like retinal back to the photoreceptors. This process is necessary to ensure photoreceptor excitability is maintained. The RPE is also responsible for the secretion of various growth factors to allow maintenance of the choriocapillaris as well as the photoreceptors while also being an epithelial barrier, maintaining the state of immune privilege that the retina enjoys. Finally, the

pigmentation of the RPE allows it to absorb light and protect against free radical formation within the retina (Boulton & Dayhaw-Barker, 2001).

Through these diverse roles, the RPE is clearly an integral part of the visual system and is absolutely necessary in maintaining visual function. This necessity is clearly demonstrated when these functions are disrupted, resulting in degeneration of the retina and a loss of visual function that leads to blindness (Strauss, 2005). Given the importance of the RPE to maintaining vision, a study of the RPE cannot be complete without a full understanding of the mechanisms underlying this maintenance. In the following sections, I will review what is known about each

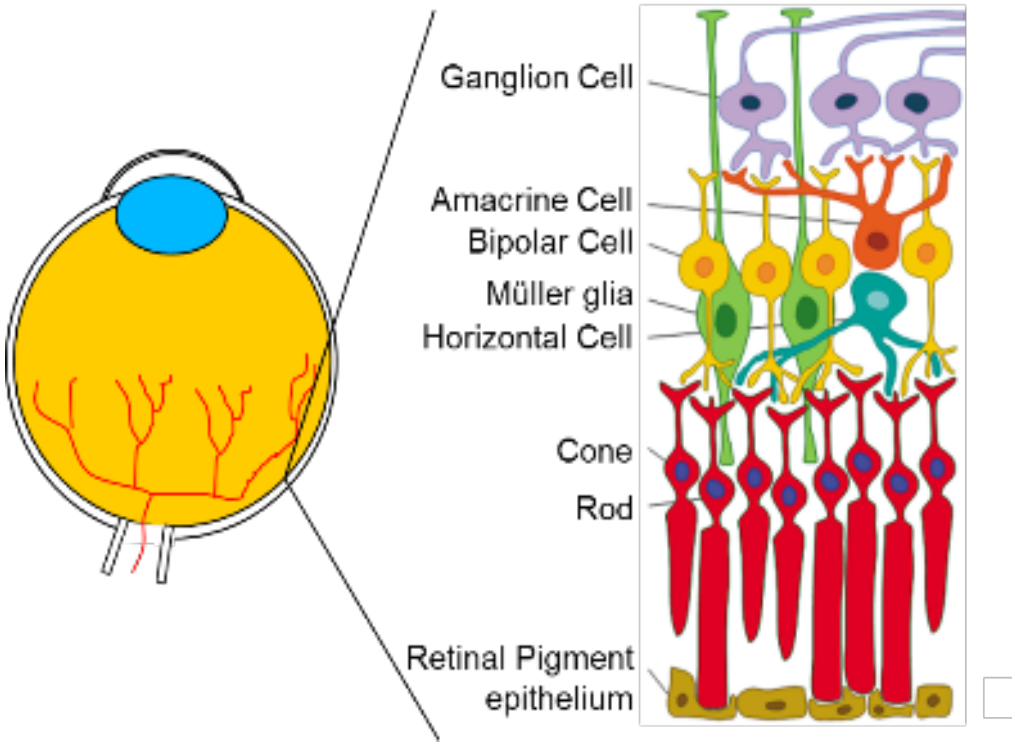

Figure 1.1: Structure and location of retina. *Located in the posterior of the eye, light travels through the retina, from the ganglion cells to the photoreceptors, where it stimulates a visual response that is transduced in the opposite direction, traveling from the photoreceptors to bipolar cells to ganglion cells.*

Figure adapted from Gramage E. et al., (2014). The expression and function of midkine in the vertebrate retina. British Journal of Pharmacology, 171(4), 11, with permission.

of these functions, in more detail. While it is necessary to outline this information for the purpose of this thesis, I would point anyone interested in further detail to the excellent review entitled *The Retinal Pigment Epithelium in Visual Function* by Dr. Olaf Strauss (2005).

1.2.2 Fluid and Waste Transport

The RPE is a tight monolayer of epithelial cells, meaning that between RPE cells are tight junctions that prevent the open movement of ions and water between the choroid and the retina. The transport of these materials occurs instead through the RPE cells themselves. Primarily as a result of the robust metabolism in the neurons and photoreceptors of the retina there is a large amount of water produced that is secreted into the extracellular space (Strauss, 2005). This water adds to water from the vitreous that is passively pushed through the retina due to intra-ocular pressure towards the subretinal space and the RPE (Marmor, 1990). The transport and removal of this fluid is necessary to ensure that the close physical interaction between the RPE and the retina remains intact. There is a passive component to this fluid transport, which is primarily observed when the RPE is damaged. In the functioning, healthy retina, active transport in the RPE is the primary mechanism of fluid transport (Marmor, 1990).

The transport of water is primarily driven by osmotic pressure, established via Cl^- and K^+ movement and supported by the presence of aquaporin-1 (Figure 1.2) (Stamer et al., 2003). The energy for this transport is provided by the Na^+-K^+- ATPase, present on the apical membrane, which establishes a gradient of Na^+ that flows from the extracellular space to the intracellular space (Frambach et al., 1989; Strauss, 2005). This gradient provides the Na^+ required for the Na-HCO_3^- and Na^+-K^+-$2Cl^-$ cotransporters, which facilitate the uptake of HCO_3^-, Cl^-, and Na^+. This, in turn, supports a basolateral Cl^-/HCO_3^- cotransporter which helps to regulate pH by transporting

HCO_3^- out of the cell in exchange for an increase in intracellular Cl^{--} (Strauss, 2005). High activity of the Cl^-/HCO_3^- cotransporter results in a decrease in the efficiency of the efflux of Cl^-, while an increased intracellular acidification, due to HCO_3^- buildup, has the opposite effect. This means that intracellular pH can regulate Cl^- transport, which may be an important mediator of water transport from the retina during increased metabolic activity (Edelman et al., 1994; Strauss, 2005; Tsuboi, 1987).

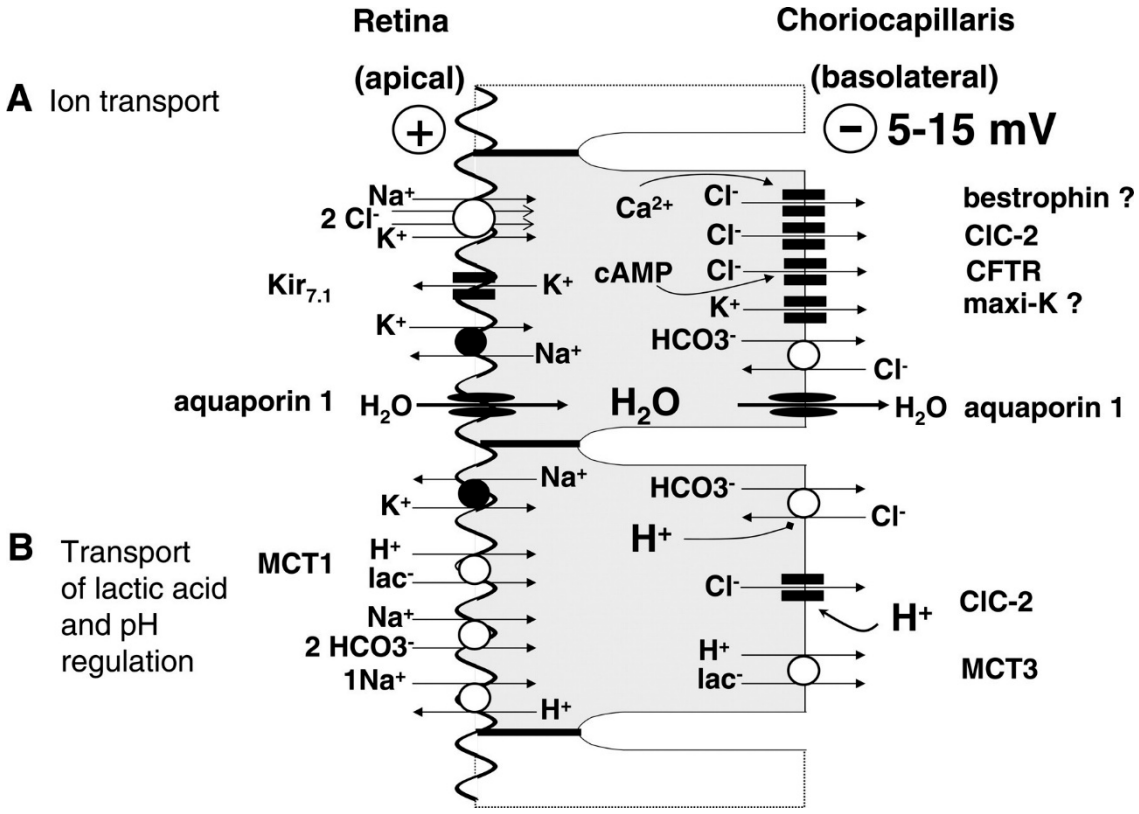

Figure 1.2. Epithelial transport and pH regulation*. A: transepithelial transport of ions across the RPE is shown. B: transport of lactic acid and pH regulation is also shown; CFTR, cystic fibrosis transmembrane conductance regulator; Kir7.1, inwardly rectifying K+ channel 7.1; maxi-K, large-conductance Ca2+-dependent K+ channel; MCT1, monocarboxylate transporter 1; MCT3, monocarboxylate transporter 3.*

Figure and some of caption reused from Strauss, O (2005). The Retinal Pigment Epithelium in Visual Function. Physiol Rev, 85(3), 845-881, as allowed by copyright.

In addition to Cl^-, K^+ is an important regulator of this fluid transport in the RPE, both through the transporters described above and through the presence of dedicated K^+ channels. With K^+ being brought into the cell by Na^+-K^+-$2Cl^-$ and Na^+-K^+-ATPase, K^+ channels primarily mediate the efflux of K^+ from the apical and basolateral membranes. Apical K^+ conductance is well described, with the efflux being predominately through the inwardly rectifying K^+ channel Kir7.1, which will be discussed in more detail in **section 1.3**. In contrast to the apical conductance, the channels responsible for the basolateral K^+ efflux have not yet been identified. A few channels that may fulfill this purpose include Ca^{2+} activated K^+ channels and M-Type K^+ channels (Pattnaik & Hughes, 2012; Ryan et al., 1999; Tao & Kelly, 1996; Zhang & Hughes, 2013).

In addition to water, the RPE is also responsible for the transport of metabolic waste from the photoreceptors to the choroid, a process that is also driven by ion movement. The predominant waste product of the photoreceptors is lactic acid, which is mostly produced in the outer segments. Lactic acid is brought into the RPE cell from the subretinal space via MCT1, a lactate-H^+ cotransporter, as well as the Na^+ dependent transporter for organic acids. It is then removed at the basolateral membrane by the similar lactate-H^+ cotransporter MCT3 and the Na^+/lactate exchanger (Kenyon et al., 1994; Strauss, 2005). These transporters, and therefore the transport of lactic acid, rely on regulation of intracellular pH. As was outlined above this regulation is achieved through the transport of HCO_3^-, tying lactic acid transport to the transporters and channels described above.

It is clear that fluid transport is important to maintaining a healthy retina. Therefore, understanding the regulation of this transport is necessary for us to be able to identify the

underlying causes of a subset of retinal diseases. In this thesis I show the regulation of the Kir7.1 ion channel by OXT in the RPE, giving it the potential to play a regulatory role in this fluid transport mechanism that we hope to explore further in the future.

1.2.3 The RPE and the Visual Cycle

The RPE plays a key role in maintaining the visual cycle. The light response of photoreceptors is mediated by the isomerization of 11-*cis*-retinal to all-*trans*-retinal within the opsin molecule. The visual cycle refers to the process through which this all-*trans*-retinal is recycled back to photoactivable 11-*cis*-retinal. This re-isomerization predominately occurs in the RPE, although some retinal from cones is regenerated in the Müller cells (Arshavsky, 2002). Herein I will focus on the visual cycle as it relates to the RPE.

Following the production of all-*trans*-retinal in the photoreceptor outer segments by rhodopsin, the all-*trans*-retinal is released to the cytosol of the photoreceptors where it is reduced to all-*trans*-retinol by retinol dehydrogenase (Strauss, 2005). The all-*trans*-retinol is then transferred to the RPE on a carrier protein, which may be interphotoreceptor retinal binding protein. Once inside of the RPE, the all-*trans*-retinol is esterified.

Loss of function studies have clearly demonstrated the role of RPE65 in the visual cycle. It was initially thought that the protein acts as a chaperone for the all-*trans*-retinylester, but it is now evident that it is responsible for the isomerization of all-*trans*-retinylester to 11-*cis*-retinol in a one-step conversion (Cai et al., 2009; Moiseyev et al., 2005; Redmond et al., 1998). Following this isomerization, 11-*cis*-retinol is oxidized to 11-*cis*-retinal by 11-*cis*-retinol dehydrogenase (RDH5).

There is an alternate pathway through the RPE-retinal G protein-coupled receptor (RGR). In this alternative pathway, the same all-*trans*-retinol that is esterified in the other pathway is converted into all-*trans*-retinal by a retinol dehydrogenase (not RDH5) then converted to 11-*cis*-retinal by RGR consuming light energy (Chen et al., 2001; Maeda et al., 2003).

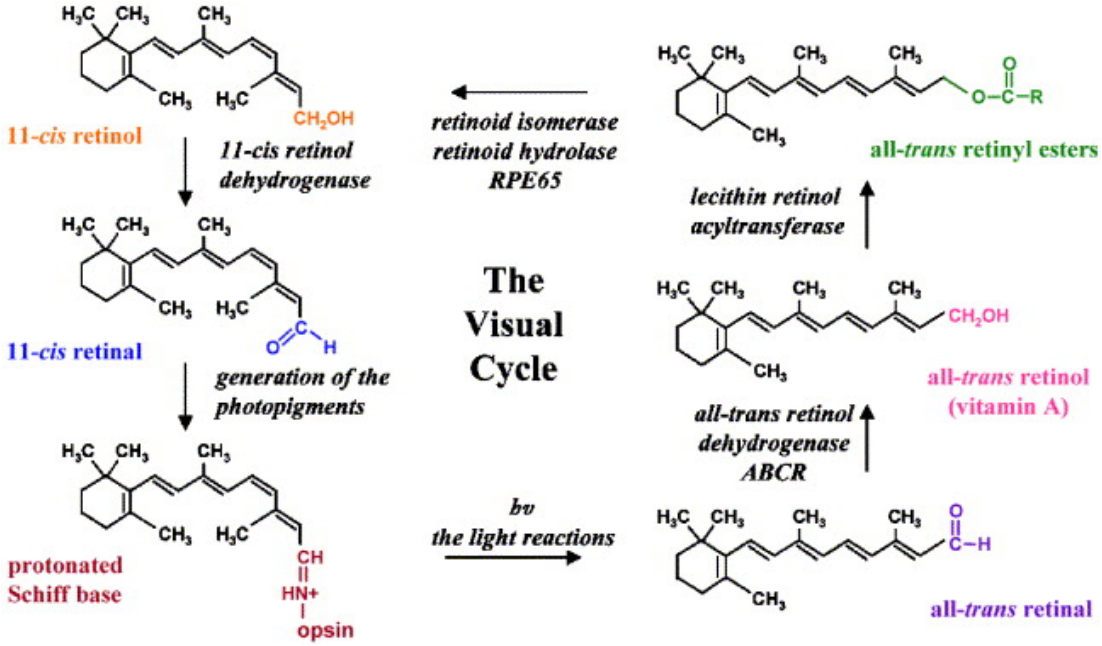

Figure 1.3: The visual cycle. *Schematic of the reactions of the visual cycle involved in the interconversion of vitamin A and 11-*cis *retinal.*

Figure and caption reused from Thompson D., Gal A., (2003). Vitamin A metabolism in the retinal pigment epithelium: genes, mutations, and diseases. Progress in Retinal and eye research, 22(5), 21, with permission

These two pathways work together to maintain retinal availability, with the RGR pathway producing 11-*cis*-retinal after light onset and the RDH5 pathway producing it for the recovery from that of light exposure (Strauss, 2005). Following its production, 11-*cis*-retinal is transported back to the photoreceptors, a process facilitated by interphotoreceptor retinal binding protein (IRBP), whose mechanism is not understood (Gonzalez-Fernandez, 2003).

1.2.4 Phagocytosis

As the photoreceptors are exposed to intense levels of light, photo-damage occurs to proteins and lipids, which begin to accumulate. Additionally, retinal itself generates photo-oxidative radicals (Strauss, 2005). Combined, these two factors lead to the accumulation of toxic substances within the photoreceptor outer segments (POS). In order to maintain photoreceptor function, these substances must be removed and digested. This is accomplished through a coordinated shedding of the POS tips and the regeneration of new POS from the base of the outer segments. The shed POS are phagocytosed by the RPE where they are digested. Some material is recycled to the photoreceptors, utilizing processes similar to the visual cycle (Bok, 1993). This process follows a circadian rhythm, with rod POS degeneration occurring in the morning and cone POS degeneration occurring at night (Young, 1978). The regulation of circadian phagocytosis appears to be complex and differs between rods and cones, with evidence for the involvement of both central and local regulatory factors (Strauss, 2005; Teirstein et al., 1980).

The substances responsible for allowing the photoreceptors and the RPE to coordinate this POS shedding and phagocytosis has not been identified, suggesting that the shed POS alone may be sufficient to initiate phagocytosis by the RPE. Studies done with isolated rod outer segments have delineated the process of photoreceptor phagocytosis (Figure 1.4). Phagocytosis begins with the shed POS binding to the apical portion of the RPE. This leads to POS ingestion, which continues for 4 hours, after which the cells are not responsive to further binding for 1-2 hours (Hall & Abrams, 1987). Ingestion is mediated by intracellular signaling that involves a rise in in IP_3 through activation of MerTK receptor, which associates with myosin IIA to reorganize

cell shape, as well as binding of the integrin and CD36 receptors on the RPE (Finnemann & Silverstein, 2001; Heth & Marescalchi, 1994; Strick et al., 2009). The rise in IP_3 and the subsequent increase in intracellular Ca^{2+} are thought to act together to regulate phagocytosis, with IP_3 stimulating ingestion and Ca^{2+} acting together with Protein Kinase C to shut it off (Hall et al., 1991; Heth & Marescalchi, 1994). The cAMP second messenger system also appears to play a role, regulating the rate of phagocytosis through β-adrenergic stimulation and stimulation of adenosine A_2 receptors (Gregory et al., 1994; Hall et al., 1993). It is possible that ion channels in the RPE also play a role in the initiation and maintenance of phagocytosis. L-type Ca^{2+} channels appear to play some role in the regulation of phagocytosis, as their

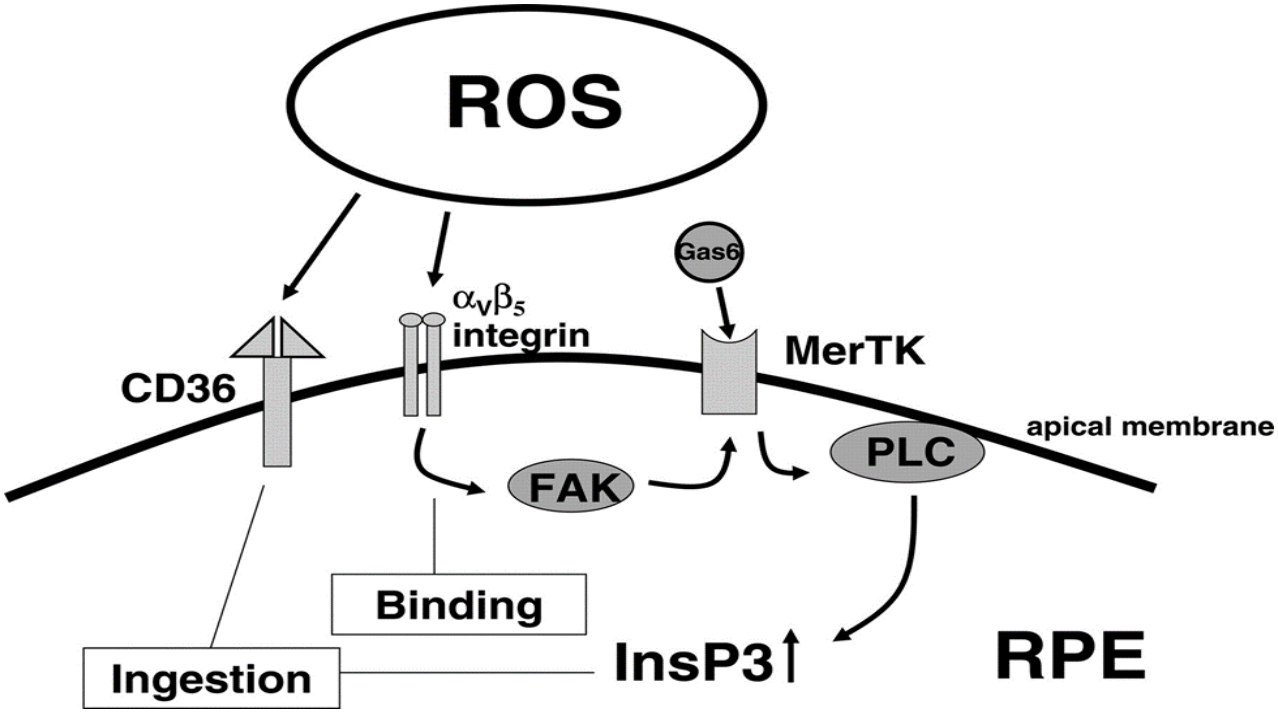

Figure 1.4: Initiation of rod outer segment (ROS) phagocytosis. *Initiation begins when ROS binds to apical membrane. Binding induces a rise in IP_3 which intern leads to ingestion, which involves the macrophage receptor CD36; CD36, macrophage phagocytosis receptor; FAK, focal adhesion kinase; Gas6, growth-arrest-specific protein 6; MerTK, receptor tyrosine kinase c-mer; PLC, phospholipase C; POS, photoreceptor outer segment.*

Figure and some of caption reused from Strauss, O (2005). The Retinal Pigment Epithelium in Visual Function. Physiol Rev, 85(3), 845-881, as allowed by copyright.

inhibition with pharmacological blockers decreases phagocytosis in human RPE cultures (Karl et al., 2008). These channels are sensitive to membrane potential and are activated with membrane depolarization, potentially implicating other ionic modulators of membrane potential, like Kir7.1 (Strauss et al., 1997).

Most work exploring RPE phagocytosis is done in rod photoreceptors. We have previously shown that oxytocin, present in the cones, can induce a rise in Ca^{2+} through a mechanism very similar to the one that regulates phagocytosis of rods (York et al., 2017). My work demonstrated that OXT can induce the inhibition of Kir7.1. An interesting possible implication of these findings is that OXT may play a role in the initiation or maintenance of cone POS phagocytosis through G-protein coupled signaling or modulation of ion channels.

1.2.5 Growth Factors and Angiogenesis

The RPE is known to secrete a number of growth factors, as well as other factors that are necessary to maintain the retina and the choriocapillaris. These include Vascular Endothelial Growth Factor (VEGF), Pigment Epithelium Derived Factor (PEDF) and Insulin-like Growth Factor 1 (IGF-1). The secretion of these factors has been shown to be primarily at opposite sides of the RPE. PEDF is secreted into the subretinal space whereas VEGF is secreted through the basal membrane toward the vascular choroid that lies beneath Bruch's membrane (Strauss, 2005).

In the mature, healthy eye, VEGF secretion helps to maintain the choriocapillaris while PEDF acts to inhibit angiogenesis (King & Suzuma, 2000; Strauss, 2005). In addition to this, the RPE is thought to be the primary source of VEGF for choroidal neovascularization (Strauss, 2005).

The regulation of these secretions by the RPE are similar to what is known about other secretory tissues. For example, in the RPE, secretion of VEGF has been shown to be dependent on voltage activated Ca^{2+} channels (L-type), where activation of these channels through membrane depolarization induces release of VEGF (Rosenthal et al., 2007). This is like what is seen in pancreatic β-cells, where depolarization in response to closure of Kir6.2 results in activation of L-type Ca^{2+} channels and the release of insulin. The L-type channels in the RPE differ from those seen in excitable cells because their activation is also regulated by tyrosine kinase instead of exclusively by membrane voltage. These tyrosine kinases shift the voltage-dependent activation of the channels to more negative membrane potentials, closer to the resting potential of the RPE, activating the channels with less significant depolarization (Strauss, 2005). One of these tyrosine kinases, a cytosolic subtype of tyrosine kinase, $pp60^{c\text{-}src}$ is activated by the IP_3/Ca^{2+} second messenger system and stimulates tyrosine kinase activity, linking the growth factor secretion with GPCRs like the oxytocin receptor (Mergler & Strauss, 2002).

The role in growth factor secretion was the original focus of my work on oxytocin. I started by looking for a factor that could influence the pathogenesis of retinopathy of prematurity (ROP), which is driven by VEGF. In this thesis, I explore the possibility for OXT to influence the expression and secretion of VEGF and other angiogenic factors as well as the impact of this OXT treatment on retinal endothelial cell growth.

1.3 Function and regulation of Kir7.1

1.3.1 Kir 7.1 Overview

Inwardly rectifying K^+ channels are so named because they exhibit an alteration in K^+ conductance as voltage is changed, with a larger inward conductance than outward conductance, at a given voltage (Figure 1.5) (Nichols & Lopatin, 1997). This inward rectification appears to violate the Nernst equation, which would predict an outward rectification, resulting in these channels being dubbed "anomalous" rectifier K^+ currents (Hagiwara & Takahashi, 1974; Hibino et al., 2010). This current does not, however, result from the channels' ability to break the laws of physics. Instead, the inward rectification results from blockage of the open pore by intracellular divalent cations like Mg^{2+} and linear polyamines like spermine (Kumar & Pattnaik, 2014). As a result of this pore block, Kir channels exhibit little K^+ current at potentials positive to E_k but a large K^+ conductance at potentials negative to E_k (Hagiwara & Takahashi, 1974; Hibino et al., 2010; Miyazaki et al., 1974; Sakmann & Trube, 1984). This results in cells with high expression of Kir having a membrane potential close to E_k and a suppression of spontaneous electrical activity (Hibino et al., 2010). In cells that are electrically excitable, like neurons and muscle, Kir conductance helps regulate action potential

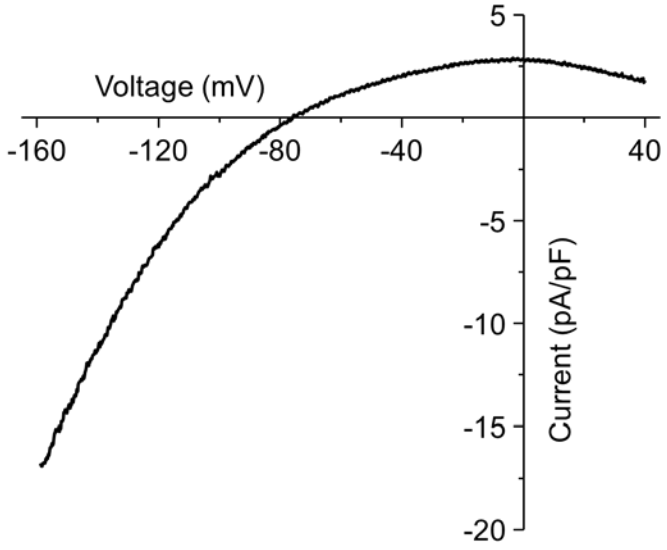

Figure 1.5: *I-V Plot of Kir7.1 current density*

duration as a result hyperpolarization of the cell, as well as the independence of Kir channels to voltage (Hagiwara & Takahashi, 1974; Hibino et al., 2010; Sakmann & Trube, 1984).

The first Kir currents were identified in 1949 and the first members of the Kir family where cloned in 1993 (Dascal et al., 1993; Ho et al., 1993; Katz, 1949; Kubo et al., 1993). This new family of potassium channels was shown to consist of two transmembrane domains per subunit, differentiating them from the family of voltage gated K^+ (Kv) channels that consist of six transmembrane domains. Despite this difference, Kir channels retained the H5-loop that determined the K^+ selectivity in Kv channels. Since the original discovery of Kir channels there have been seven subfamilies of Kir that, depending on their structure and location, have been shown to play a significant role in regulating cellular excitability in both active and passive ways.

My focus, Kir7.1, is the most recently identified member of the Kir family of ion channels and shares only 38% homology with its closest relative in the Kir family, Kir4.2 (Hibino et al., 2010). Its expression is found in a diverse number of tissues, including the intestinal tract, the kidney, the heart, the uterus and of most important consideration for this thesis, the eye, where it is localized to the retinal pigment epithelium (RPE) (Kumar & Pattnaik, 2014; Nichols & Lopatin, 1997).

Expressed on the apical membrane in the RPE, Kir7.1 is key to maintaining K^+ homeostasis in the subretinal space and in supporting the transepithelial transport that is dependent on ion transport, as described in the **section 1.2**. Kir7.1 is a weak inward rectifying channel, which is differentiated from a strong inward rectifying by the presence of a larger outward K^+ current at positive membrane potentials. This weak rectification is key to the K^+ recycling role of Kir7.1, allowing K^+ ions to move out of the RPE and into the subretinal space.

In this chapter we will look at Kir7.1 in detail, exploring its structure, function, regulation and impact in the RPE and throughout the body.

1.3.2 Kir7.1 structure

Channels that belong to the inwardly rectifying K^+ family contains the same structural hallmarks; two transmembrane domains (TM1 and TM2) that are connected by a pore forming loop (H5) and a cytoplasmic amino and carboxyl terminal domain (Figure 1.6) (Hibino et al., 2010). A single subunit is not capable of forming an ion channel, instead the functional channel is composed of a tetrameric complex made up of 4 subunits (Yang et al., 1995). In this tetramer the H5 loop forms a K^+ selectivity filter that is mediated by the T-X-G-Y(F)-G sequence,

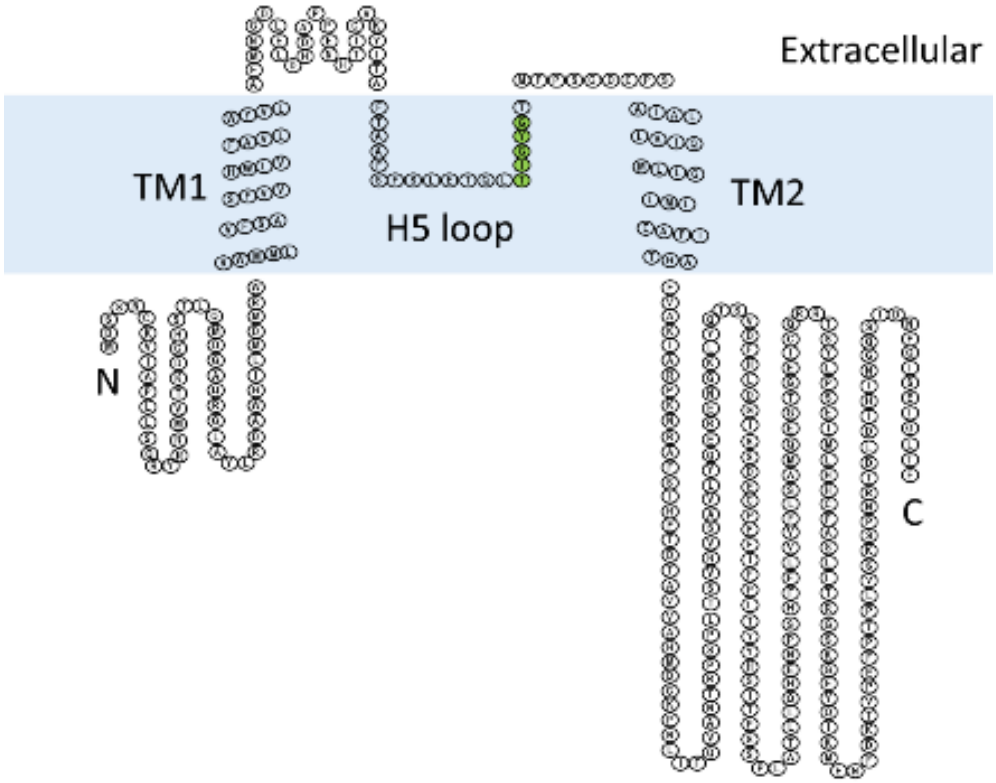

Figure 1.6: Topology of single Kir7.1 subunit. *Two transmembrane domains (TM1 and TM2) are joined by a pore forming H5 loop. The K^+ selectivity sequence, conserved among K^+ channels, is shown in green. Cytoplasmic amino and carboxyl terminal domains flank this region.*

conserved among K^+ channels. This filter underlies the characteristic inward current of these ion channels, which arises not from a structural selectivity towards inward K^+ movement but a blockage of outward K^+ current by intracellular cations. Kir channels are insensitive to membrane voltage due to a lack of the s4 voltage sensor present in voltage-gated cation channels. This means that, in the absence of a specific regulator, Kir channels are open at all membrane potentials. While Kir channels have been shown to form heterotetramers, Kir7.1 is thought to exclusively form a homotetramer (Kumar & Pattnaik, 2014).

Despite a common structure among Kir channels, Kir7.1 exhibits some unusual characteristics. As mentioned before, Kir7.1 has a weak inward rectification, allowing K^+ ions to move out of the cell more freely than other Kir channels. Like all Kir, channels Kir7.1 is sensitive to inhibition by Ba^{2+} and Cs^+ in the bath solution, however, it is much less sensitive to these ions, with IC_{50} values approximately 10 times higher than other Kir channels (Krapivinsky et al., 1998). The single channel conductance of Kir7.1 is also much smaller than observed in other family members, with an estimated conductance of 50 fS (Krapivinsky et al., 1998). Finally, while other Kir channels exhibit a sensitivity to extracellular K^+ ($[K^+]_e$), characterized by a saturation of conductance with $[K^+]_e$ higher than 150mM, Kir7.1 conductance appears to be non-saturating except at low concentrations of K^+ (1-2mM) (Döring et al., 1998; Lopatin & Nichols, 1996; Shimura et al., 2001).

While it was initially thought that Kir7.1 was almost independent of $[K^+]_e$, $[K^+]_e$ in fact has an inverse relationship with K^+ conductance through Kir7.1 at physiological membrane potentials (Shimura et al., 2001). As a result of this relationship, a decrease in $[K^+]_e$ leads to an increase in K^+ conductance at potentials that are physiologically relevant. The basis for these

differences is thought to be M125, present in the pore region, which differs from all other Kir channels, which contain a conserved R at the equivalent amino acid (Figure 1.7). This is supported by replacement of methionine 125 with arginine in Kir7.1 (M125R), which results in an increase in single-channel conductance, an increase in Ba^{2+} sensitivity and a return of the $[K^+]_e$ sensitivity observed in other channels (Döring et al., 1998; Krapivinsky et al., 1998). This not only suggests that this residue is key to Kir function, but it influences pore blockage by Mg^{2+} and polyamines. Furthermore it suggests that electrostatic interactions between the K^+ occupying this outer pore region and Mg^{2+}, polyamines and $[K^+]_e$ could underlie the inward rectification and current saturation, and the change from Arg to Met is sufficient in Kir7.1 for these interactions to be partially disrupted.

Figure 1.7: Comparison of Kir pore regions. *Arginine is conserved in all Kir channels except Kir7.1. This conserved Arg is likely responsible for some of the unique characteristics of Kir7.1.*

Reused from Krapivinsky G.,Medina I. ,Eng L., Krapivinsky L., Yang Y., Clapham D., (1998) A Novel Inward Rectifier K+ Channel with Unique Pore Properties, Neuron, 20 (5), 995-1005, 1998, with permission from Elsevier.

1.3.3 Kir7.1 function in the RPE

In the RPE, Kir7.1 is found on the apical membrane. That is not true for all cells that express Kir7.1, however. For example, in thyroid follicular cells and renal epithelia, Kir7.1 is localized to the basolateral membrane (Hibino et al., 2010; Nakamura et al., 1999; Ookata et al., 2000). This pattern of localization follows the Na^+-K^+-ATPase, supporting the role of Kir7.1 in K^+ recycling, as it facilitates the return of K^+ brought in by the pump.

In the RPE recycling K^+ is key to maintaining visual function. Following illumination of the retina, [K^+] in the subretinal space decreases from 5mM to 2mM (Dornonville de la Cour, 1993). This depleted K^+ results in a negative shift in the *I-V* relationship of Kir7.1, as well as an increase in K^+ conductance (Döring et al., 1998; la Cour et al., 1986). As a result, subretinal [K^+] can be replenished by Kir7.1 due to its weak rectification allowing the efflux of K^+ ions. This negative shift in the *I-V* relationship of Kir7.1 also leads to a hyperpolarization of the apical membrane of the RPE, due to the major role the channel has in determining membrane potential.

The effect of a light-induced K^+ decrease on Kir7.1 has broader impacts on other ion channels in the apical membrane and throughout the RPE. In response to decreased K^+, the Na^+-K^+-$2Cl^-$ cotransporter activity is reduced, resulting in a decrease in Cl^- transport into the cell across the apical membrane (Bialek et al., 1995; Bialek & Miller, 1994). This decrease in apical Cl^- conductance in turn leads to a reduced basolateral Cl^- conductance and hyperpolarization of the basolateral membrane. Additionally, as a response to the apical hyperpolarization, there is a reduction in the activity of the voltage dependent Na^+-HCO_3^- cotransporter leading to a decrease in intracellular pH of approximately 0.35 pH (Yuan et al., 2003). As was discussed in Chapter 1.2.2, a decrease in intracellular pH can reduce the activity of the Cl^-/HCO_3^-

cotransporter, increasing the transport of Cl^- across the basolateral membrane and therefore increasing the absorption of water from the subretinal space.

The light-induced response of the RPE can be observed via the electroretinogram (ERG) as the c-wave (Strauss, 2005). As a result of the photoreceptor light response and subsequent decrease in subretinal K^+ there is a hyperpolarization in the apical membrane of the RPE. The apical and basal membranes are electrically coupled by the cytoplasm as well as a paracellular shunt pathway, meaning that hyperpolarization of the apical membrane subsequently hyperpolarizes the basal membrane (Quinn & Miller, 1992). This basal hyperpolarization is smaller than what is observed on the apical membrane, resulting in an increase in the transepithelial potential of the RPE (V_b-V_a), which is observed as the c-wave in the ERG (Oakley, 1977).

The dependence of apical hyperpolarization on Kir7.1 is evident following suppression of the channel, which results in an abolished c-wave (Shahi et al., 2017). The impact of Kir7.1 on apical membrane potential could include the development of a “light peak” response by the RPE. Following the c-wave there is a slow forming depolarization of the RPE that reflects depolarization of the basal membrane as a result of Cl^- conductance (Gallemore et al., 1988). While altering apical [K^+] alone can induce a c-wave, this light peak response requires photoreceptor stimulation by light to occur (Samuels et al., 2010). As a result, researchers suggested the existence of a yet unidentified “light peak substance” that is released from the photoreceptors, inducing depolarization of the RPE. In **chapter 2** I will demonstrate that OXT can induce the depolarization of the RPE through the inhibition of Kir7.1, demonstrating that

Kir7.1 could be a target of this “light peak substance” and the cause of its resulting depolarization.

The importance of Kir7.1 to the RPE and to larger visual function is clear when you look at the consequences of a dysfunctional channel. Hereditary diseases known as channelopathies have been associated with Kir7.1 mutations. The most widely studied of these is Snowflake Vitreoretinal Degeneration (SVD), which is an autosomal dominant disease that results in degeneration of the vitreous humor, cataracts, retinal detachment, and the development of crystalline deposits in the retina (Hibino et al., 2010). Patients with this disease have been found to be heterozygous for an R162W mutation in the gene for Kir7.1 (KCNJ13), resulting in a premature depolarization of the RPE cells leading to Ca^{2+} overload and cell death (Hejtmancik et al., 2008; Kumar & Pattnaik, 2014; Pattnaik et al., 2013).

In addition to SVD, a Kir7.1 mutation has also been implication in Lebers Congenital Amaurosis (LCA), a diseased characterized by a dysfunctional retina and visual impairment that begins early in life (Pattnaik et al., 2015). In one case, reported by our lab, a nonsense mutation (W53X) which results in a nonfunctional channel has been implicated in the pathogenesis of the disease (Pattnaik et al., 2015). The possibility that other mutants can induce the disease is also being explored. Given the clear importance of this channel to RPE health its potential regulation by OXT is of great interest. To understand this potential, it is important to more closely examine the regulation of Kir7.1.

1.3.4. Regulation of Kir7.1

Like all Kir channels, Kir7.1 lacks the voltage dependence observed in Kv channels. It also lacks direct the modulation by ATP found in the K-ATP subfamily of Kir channels. That is not to say, however, that it lacks functional regulators completely. In the kidney Kir7.1 has been shown to be regulated by protein kinase A (PKA) and protein kinase C (PKC) (Zhang et al., 2008). This regulation is dependent on two sites, S287 and S201, both present on the C-terminal domain. Zhang et al. demonstrate that PKA-induces activation of the channel through S287 and that PKC inhibits the channel through S201.

Additionally, Kir7.1, as well as other Kir channels have been demonstrated to be influenced by both extracellular $(pH)_e$ and intracellular $(pH)_i$. A $(pH)_o$ of below 6.0 induces a strong inhibition of Kir7.1 current while the channel appears relatively insensitive to changes between 6.5 and 9.0 (Kumar & Pattnaik, 2014; Yuan et al., 2003). The effect of $(pH)_i$ is more complex, with K^+ conductance showing a biphasic response to alterations (Yuan et al., 2003). Changes in $(pH)_i$ from 7.2 to 6.8 results in an activation in Kir7.1 while further reduction to 6.0 leads to inhibition following transient activation (Kumar & Pattnaik, 2014). Increasing $(pH)_i$ results in a rapid inhibition (Kumar & Pattnaik, 2014; Yuan et al., 2003). This change in intracellular pH may play a significant role in the K^+ recycling observed in the RPE. As described above, the light response induces a decrease in intracellular pH of ~ 0.35. This level of acidification would likely increase Kir7.1 mediated K^+ conductance and increase the ability of the RPE to respond to a reduced subretinal $[K^+]$ concentration.

Like other Kir channels, Kir7.1 is also activated by phosphatidylinositol (4,5) bisphosphate (PIP_2). While it exhibits a weaker binding affinity for PIP_2 than Kir2.1 or 4.1, it is

stronger than that observed in some Kir family member, especially the ATP dependent Kir6.2 (Rohács et al., 2003). As a result of this activation, Kir7.1 current is dependent on the concentration of PIP_2 on the membrane and can be modulated by depletion of the phospholipid. This has been demonstrated for Kir7.1 through direct alteration of intracellular PIP_2, disruption of PIP_2 interactions with Kir7.1 using neomycin and indirectly through the inhibition of lipid kinases responsible for synthesizing PIP_2 as well as the of G-protein Coupled Receptor (GPCR) mediated activation of phospholipase C (PLC) (Hatcher-Solis et al., 2014; Pattnaik & Hughes, 2009). In a channel that doesn't exhibit sensitivity to voltage, PIP_2 provides a mechanism for modulating channel function. It is this regulation by PIP_2 that caused me to hypothesize a relationship between OXTR and Kir7.1. OXTR activation by OXT results in the hydrolysis of PIP_2, removing it from the membrane. I propose that this is the mechanism of the inhibition observed in **chapter 2**.

Finally, a recent study by Ghamari-Langroudi et al. demonstrated regulation of Kir7.1 by the G-protein coupled receptor MC4R in hypothalamic neurons (Ghamari-Langroudi et al., 2015). MC4R activation by agonist α-MSH results coupling of the receptor to $G\alpha_s$, which in turn stimulates the production of cAMP by adenylyl cyclase and the activation of PKA. The inhibition of Kir7.1 was independent of this pathway, however, acting instead in a novel, G-protein independent manner. While this kind of direct action between GPCRs and K^+ channels has been demonstrated previously, it had not been shown in Kir7.1 and, as the authors of the study suggest, it indicates the possibility of Kir7.1 regulation by other GPCRs (Ghamari-Langroudi et al., 2015).

1.3.5. Function of Kir7.1: Beyond the RPE

Like OXT, the role of Kir7.1 is not limited to its function in the RPE. Kir7.1 expression can be found in neurons, the intestines, the heart and the uterus. Recent work on neurons in the paraventricular nuclei that express MC4R have demonstrated that GPCR-mediated inhibition of Kir7.1 is essential for depolarization to occur (Ghamari-Langroudi et al., 2015). In this study they suggest that Kir7.1 may be playing a role in mediating eating behavior through these neurons because α-MSH is implicated in inhibiting food intake and blocks Kir7.1 while AgRP has been shown to stimulate food intake and is demonstrated to open Kir7.1 (Ghamari-Langroudi et al., 2015). The α-MSH mediated effect in neurons is also relevant to the scope of my thesis, as α-MSH, working with OXT itself, is known to stimulate dendritic release of OXT via MC4R, as is discussed in more detail in **section 1.4.2** (Sabatier et al., 2003).

In other recent work it was demonstrated that Kir7.1 is present in uterine myometrium, and that it plays a role in the initiation of contractions during parturition (McCloskey et al., 2014). Kir7.1 expression decreases as parturition approaches and this decrease in expression and subsequent depolarization of the myometrium is necessary for the initiation of organized contractions. Kir7.1 has also been found in thyroid follicular cells and intestinal epithelial cells where it plays a similar K^+ recycling role, as described previously in the RPE. In these cells Kir7.1 is found in the basolateral membrane, where it colocalizes with Na^+-K^+-ATPase (Nakamura et al., 1999). Given the number of systems affected by Kir7.1, the findings I present in this thesis have implications far beyond the RPE.

1.4 Oxytocin

1.4.1 Oxytocin Overview

Like all neurohypophysial hormones (hormones secreted from the posterior pituitary), Oxytocin (OXT) is a nonapeptide hormone, the structure of which was first proposed in 1953, making it the first peptide structure to ever be identified (Figure 1.8) (Du Vigneaud et al., 1953).

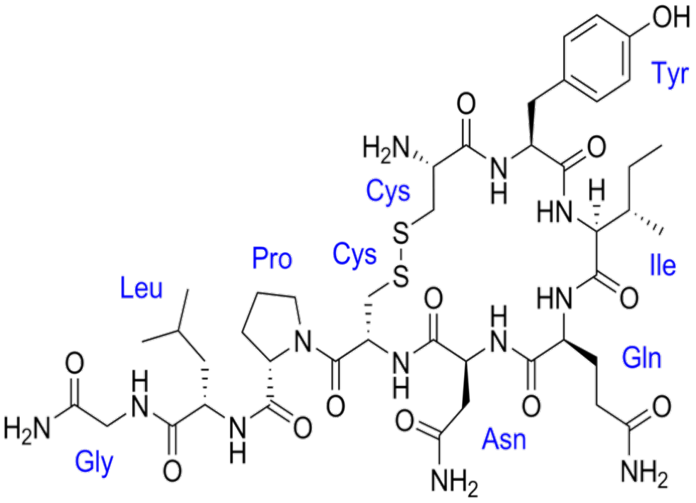

Figure 1.8: Structure of Oxytocin.

As with all peptides secreted from the posterior pituitary, OXT is a nonapeptide that contains a disulfide bridge between Cys residues 1 and 6. These peptides are differentiated into either the OXT or vasopressin families based on the identity of the amino acid at position 8 (Gimpl & Fahrenholz, 2001). Peptides in the OXT family are characterized by a neutral amino acid at this position while peptides in the vasopressin family have a basic amino acid (Gimpl & Fahrenholz, 2001).

Both OXT and vasopressin are very closely related and appear to have diverged early in evolution, following duplication of an existing sequence and subsequent mutations (Leng et al., 2005). Their family members have performed a wide variety of functions throughout evolutionary history but in humans, OXT was initially identified for its role in the initiation of parturition and lactation. Since its discovery, the role of OXT has continued to expand. It has been implicated in the regulation of sexual and social behavior, skeletal muscle regeneration and influence over metabolic activity in adipose tissue (Elabd et al., 2014; Gimpl & Fahrenholz,

2001). Recent work in our lab has demonstrated the presence of OXT in the extracellular matrix of the cone photoreceptors, along with the expression of its receptor in the RPE (Halbach et al., 2015). The presence of its receptor in the RPE, as well as the close proximity of the peptide to that receptor, suggests that OXT has the ability to affect the function of the RPE and therefore the retina itself.

Primarily produced in the hypothalamus and secreted from the posterior pituitary, oxytocin is a hormone that travels through the blood, transporting it to its peripheral targets. This release into the blood does not appear to account for the neurological role played by OXT, based on studies of peripherally administered OXT that found less than 1% of OXT administered into the blood supply makes it to the cerebrospinal fluid (Mens et al., 1983). In addition to the discovery of oxytocinergic neurons that project into the brainstem, spinal cord and other parts of the hypothalamus, some have attempted to address this issue by suggesting that dendritic release of neuropeptides into the brain allows peptides to be released and then diffuse to targets throughout the brain (Leng et al., 2005; Ludwig & Leng, 2006). This mechanism is supported by an increased half-life of peptides in the brain when compared to the blood, with OXT's half-life increasing from 2 minutes to 20 minutes (Mens et al., 1983). Peripheral production of OXT, independent of the hypothalamus, including testicular interstitial cells, the corpus luteum and the placenta has also been described (Ivell, 1986). Regardless of how OXT reaches the cell in question, its action is mediated through the oxytocin receptor (OXTR), a G-protein coupled receptor that will be discussed in more depth in **section 1.5**.

1.4.2 Oxytocin Production and Secretion

The promoters for human OXT are stimulated by the estrogen receptors ERα and ERβ, as well as the thyroid hormone receptor THRα and the retinoic acid receptors RARα and RARβ, suggesting many methods of potential regulation in different cell types (Richard & Zingg, 1990, 1991).

While OXT production has been described in peripheral tissues, the predominate production is from the hypothalamus, where both oxytocin and vasopressin are synthesized in the supraoptic and paraventricular nuclei of the hypothalamus by magnocellular neurons (Brownstein et al., 1980; Gainer, 1998; Leng et al., 2005). While almost all of the supraoptic neurons project into the posterior pituitary and contain either oxytocin or vasopressin, the paraventricular nucleus contains neurons that are involved in neuroendocrine functions and thus target other sites. These neurons include parvocellular oxytocin cells that project into the brainstem, spinal cord and other parts of the hypothalamus, potentially distributing OXT to these areas (Leng et al., 2005).

While OXT and vasopressin genes are both present on the same chromosomal locus, their transcription occurs in opposite directions (Gimpl & Fahrenholz, 2001). They are both also expressed with a “carrier protein”, neurophysin, contained within the same gene. In humans, the OXT-neurophysin 1 gene is mapped to chromosome 20p13 (Rao et al., 1992). This gene contains three exons, the first of which contains the transcript for the OXT prepropeptide as well as a 5’ non-coding promoter region and a tripeptide processing signal (Gainer, 1998; Gimpl & Fahrenholz, 2001). The first nine amino acids of neurophysin are also in the first exon, with the central part being encoded by exon two and the COOH-terminal encoded on exon 3. The

OXT prepropeptide encoded by this gene is packaged in neurosecretory vesicles and is cleaved as it moves down the neuronal axons, which extend into the posterior pituitary (Brownstein et al., 1980).

Oxytocin moves with neurophysin in a 1:1 complex and it appears to be necessary for proper packaging and targeting of oxytocin to the axon terminal, prior to its secretion (Gimpl & Fahrenholz, 2001). This interaction between neurophysin and OXT is heavily dependent on pH, with strong binding occurring at the acidic pH (~5.5) of the neurosecretory granules (Gimpl & Fahrenholz, 2001). As a result of this pH dependence, upon stimulation of the neuron and secretion of the OXT:neurophysin complex, the two components dissociate in the plasma as a result of its neutral pH (7.4).

Following the production of OXT it is stored in its OXT:neurophysin complex within neurosecretory vesicles until a stimulus is received that induces its secretion. There have been a wide range of stimuli that have been described to induce this secretion. Perhaps the most important of these stimuli can be found in the release of milk during lactation, as animals who are deficient in OXT are not able to feed their offspring (Young et al., 1996).

Stimulation of mechanoreceptors in the nipple by babies initiates the release of oxytocin and in mice it has been shown that during nursing OXT release occurs in a pulsatile manner, with most OXT release being synchronized across OXT containing neurons (Lincoln & Wakerley, 1974). This pulsatile nature of OXT release during lactation appears to be necessary for milk release as the mammary gland rapidly desensitizes to continuous exposure to the peptide (Leng et al., 2005). It is likely that this pulsatile nature of secretion occurs in all mammals, as a similar intermittent milk let-down has been observed in humans (Leng et al., 2005; Ramsay et al.,

2004). The release of OXT is driven by action potentials, and action potentials that occur in frequent bursts, as observed during milk letdown, release more oxytocin than solitary action potentials occurring infrequently (Leng & Brown, 1997). The increase in OXT release is a result of high frequency bursts of action potentials effectively priming neurons for OXT release. As each burst travels down the neuron they progressively depolarize the cell due to a progressive increase in voltage-dependent Ca^{2+} entry as well as a mobilization of intracellular Ca^{2+} stores (Leng & Brown, 1997; Leng et al., 2005). The increase in intracellular Ca^{2+} facilitates OXT release and the higher the level of Ca^{2+} the more hormone is released (Fisher & Bourque, 2001). The bursting effect also helps ensure the action potentials spread throughout the entirety of the neuron, as a single magnocellular neuron branches extensively and may have as many as 2000 neurosecretory endings (Leng et al., 2005; Nordmann, 1977). Successive action potential bursts progressively increase the extracellular $[K^+]$ surrounding the axons, depolarizing the cells and increasing the chance that the action potentials successful propagate past branch points, where they may otherwise fail (Leng et al., 1988).

In addition to lactation, OXT also plays an important role in the initiation of labor. This role is driven by a positive feedback loop that is established between the contracting uterus and the oxytocin containing neurons in the hypothalamus. The oxytocin needed to feed the demand created by this positive feedback is built up in preparation for labor, with stores of oxytocin expanding by around 50% (Leng et al., 2005; Russell et al., 2003). This expansion is not driven by an increase in production but instead by reduced secretion. This reduction in the secretion of OXT is mediated by an opioid, Dynorphin, which actively inhibits the release of OXT through k-opioid receptors (Brown et al., 2000). Dynorphin is co-secreted with OXT and its

effects are strongest in midpregnancy, with its effects declining as parturition approaches, enabling OXT to be released.

Outside of its role in parturition and lactation, OXT has been implication in modulation of behavior. As OXT has limited ability to reenter the brain as a result of the blood-brain barrier, its actions are likely a result of release within the brain. As was mentioned previously, there are parvocellular neurons that project into the CNS, however large amounts of oxytocin is released from dendrites of magnocellular OXT neurons in both the supraoptic and paraventricular nuclei (Sabatier et al., 2003). In addition to autocrine action, dendritically secreted OXT is thought to diffuse and have "neurohormone-like" actions in other parts of the CNS (Ludwig & Leng, 2006). This mechanism of action is supported by the presence of OXT receptors throughout the CNS, despite the absence of oxytocin neuron projections nearby. Furthermore, it has been shown that OXT release from the dendrites can be stimulated in a manner that decouples it from systemic release (Sabatier et al., 2003). Instead OXT release is thought to be the result of localized increases in intracellular [Ca^{2+}] ([Ca^{2+}]$_{i)}$ that allows the release of substantial amounts of OXT from the dendrites without the presence of action potentials that can stimulate systemic release. An example of the role of Ca^{2+} in the dendritic OXT release can be seen with the peptide α-MSH, which is associated with many of the same behavioral effects as OXT, including grooming, yawning and stimulation of sexual behavior (Sabatier et al., 2003). α-MSH acts through melanocortin-4 receptors (MC4Rs) to trigger the transient increase in [Ca^{2+}]$_i$ as a result of mobilization of intracellular stores, resulting in the secretion of OXT (Sabatier et al., 2003). The dendritic release of oxytocin also appears to be primed by some peptides, including OXT itself. Priming involves increasing the availability of OXT containing vesicles and, as it can

be driven by OXT itself, it can be self-sustaining, resulting in a prolonged release of OXT in response to an initial stimulation, allowing it to have long lasting behavioral effects (Leng et al., 2005).

To summarize, much of OXTs behavioral effects are likely the result of stimulation of magnocellular neurons by afferent signals that induce a transient increase in $[Ca^{2+}]_i$, stimulating the dendritic release of OXT, independent of systemic release. The OXT release is sustained by autocrine action of OXT on the magnocellular neurons while it also diffuses throughout the CNS, allowing it to influence behavior.

1.4.3 Oxytocin in the eye

Oxytocin was first detected in human and rat eye through the use of a specific radioimmunoassay on HPLC fractions (Gauquelin et al., 1983). In this study Guaquelin et al. also showed, in the rat retina, that OXT levels were modified by light and that detected levels were smaller in the night than during the afternoon (Gauquelin et al., 1988). They initially hypothesized that the origin of this retinal OXT was systemic, likely from the hypothalamus. However, they later found that this day/night rhythm was observable in the retina and the Harderian glands, which are present in the eye, while the pineal gland, which is present in the brain, did not exhibit any rhythm, suggesting that the OXT might be produced within the eye (Gauquelin et al., 1988).

More recently work in our lab has used immunohistochemistry to show the presence of OXT in the extracellular matrix surrounding the outer segments of the cone photoreceptors, localizing OXT to a specific region of the retina, directly adjacent to the RPE, where we have

shown OXTR to be expressed (Halbach et al., 2015). Our results may be indicative of cone PR expression of OXT, which could explain the increase in OXT during the day, when cones are most active. However, we do not have any data to support the expression of OXT mRNA in the cone photoreceptors or anywhere else in the retina, meaning that the source of OXT in the retina remains unknown.

1.5 Oxytocin Receptor

1.5.1 Oxytocin Receptor Overview

Oxytocin receptor is a G-protein coupled receptor that binds to OXT and stimulates the activation of a heterotrimeric G-protein to initiate a cellular response. While initially thought to be limited to expression in the uterus and mammary glands where it mediates smooth muscle contraction to facilitate labor and lactation, respectively, the role for OXT and therefore its receptor has expanded to include additional physiological and complex behavioral functions. With this expansion in our understanding of the role played by OXT has come, by necessity, an expansion in our study of OXTR and its signaling in new tissues from the heart to the eye. In this section we will discuss the structure and mechanism of OXTR function as well as explore the role it and OXT have been shown to play in reproduction and beyond.

1.5.2. Oxytocin receptor structure

The oxytocin receptor is a member of the rhodopsin-type GPCR family. It contains the seven transmembrane α-helices that are highly conserved across the GPCR family along with an extracellular NH_2-terminal domain and an intracellular COOH-terminal domain (Figure 1.9). In humans its NH_2-terminal domain contains three possible *N*-glycosylation sites while in mouse and rat there are only two (Gimpl & Fahrenholz, 2001). There appears to be different glycosylation patterns in different tissues, resulting in different observed molecular masses, however glycosylation does not appear to have any effect on the binding characteristics of the receptor or its functional properties (Gimpl & Fahrenholz, 2001; Kimura et al., 1997).

Independent of this glycosylation the expected molecular mass of OXTR is around 45 kDa, based on its amino acid sequence.

The activation of OXTR, like other GPCRs, is thought to be through a conformational change following ligand binding that results in a change in the orientation of transmembrane domains 3 and 6, resulting in G protein binding sites being exposed (Gimpl & Fahrenholz, 2001). The receptor activation appears to be dependent on an Asp residue in the second transmembrane domain and a tripeptide (E/DRY) at the interface of this transmembrane

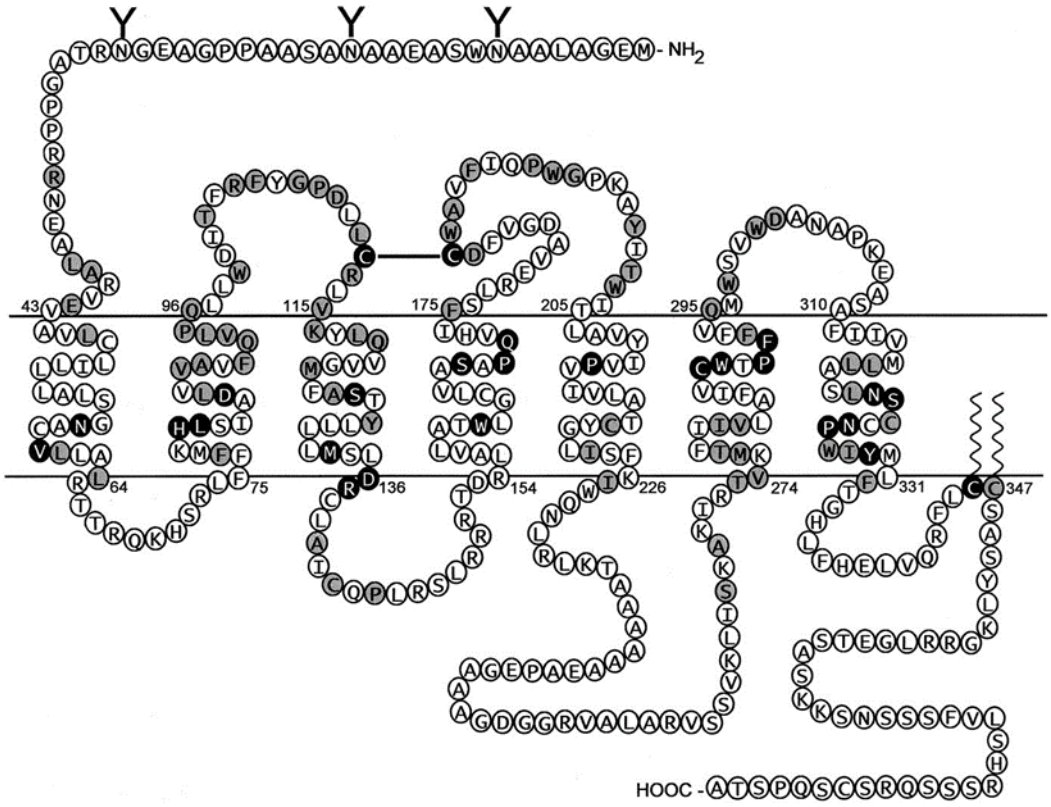

Figure 1.9: Schematic structure of the human OT receptor with amino acid residues shown in one-letter code. *The residues are marked in the same manner as in Fig. 3, i.e., residues conservative within the OT/vasopressin receptor subfamily are outlined in gray, and residues conservative for the whole G protein-coupled receptor superfamily are outlined in black. The putative N-glycosylation ("Y") and palmitoylation (at C346/C347) sites are marked.*

Figure and caption reused from Gimpl.G., & Fahrenholz, F. (2001). The oxytocin receptor system: structure, function, and regulation. Physiol Rev, 81(2), 629-683, as allowed by copywrite

sequence and the first intracellular loop (Bockaert & Pin, 1999; Gimpl & Fahrenholz, 2001). In the human OXTR, the Asp residue is Asp-85 and alterations of this residue disrupt receptor function, leading to an inactive receptor, while mutation of the R residue in the DRY motif to A results in a constitutively active receptor (Fanelli et al., 1999). The discovery led to the hypothesis that the Arg from the DRY motif is constrained in a hydrophilic pocket formed by polar residues in the transmembrane domains 1, 2, and 7 and that protonation of the Asp in this motif pushed the Arg out of the pocket, leading to rotation of the transmembrane helices relative to each other and resulting in cytoplasmic exposure of buried domains that mediate G-protein coupling (Fanelli et al., 1999; Gimpl & Fahrenholz, 2001; Neumann & Landgraf, 2008).

More recently, crystallographic studies done to better understand the structure of rhodopsin, a light sensitive G-protein coupled receptor, suggest more minor changes in structure upon activation, with a relaxation of the GPCR and increase in flexibility of its cytoplasmic loops that allows an induced fit of the heterotrimeric G-protein (Salom et al., 2006). This was supported by high-angle X-ray scattering performed on vertebrate visual rhodopsin which showed consistent conformational changes within the crystal structure but also suggested that rhodopsin was dimerized on the membrane and that interaction between the rhodopsin molecules mediate structural changes in response to light (Imamoto et al., 2015). OXTR has also been shown to be present in dimeric or oligomeric complexes on the cell surface so a similar activation mechanism is possible in its case (Devost & Zingg, 2003; Neumann & Landgraf, 2008; Terrillon et al., 2003). Despite this, while the dimeric structure appears to be more responsive it has been clearly demonstrated that a monomeric GPCR is capable of activating a G-protein (Whorton et al., 2007).

OXT binding to the receptor is mediated by residues within the transmembrane domains, as well as ones in the extracellular domains, and it is thought to bind in a narrow cleft created by the ringlike "binding pocket" arrangement of the transmembrane domains (Gimpl & Fahrenholz, 2001). The binding site is conserved amongst the vasopressin, OXT and vasotocin subtypes of this GPCR family following substitution of conserved Gln and Lys residues in these structures with Ala that reduced receptor affinity for agonists (Barberis et al., 1998). It is likely that all ligands closely related to OXT can bind to this central receptor pocket in OXTR. In the case of vasopressin, cross reactivity is clearly observed, with OXT binding to OXTR with only a 10x greater affinity than observed with vasopressin (Kimura et al., 1994). In addition to interacting with the extracellular loops that forms this binding pocket the agonist also forms contacts with the extracellular NH_2-terminus of the receptor. In contrast antagonists appear to prefer contact sites located more deeply within the binding pocket (Neumann & Landgraf, 2008).

Two important modulators of OXTR function are cholesterol and divalent cations. The presence of a high-cholesterol environment and divalent cations like Mg^{2+} are necessary for the receptor to exist in a high-affinity state (K_d= ~1nM) and it can reversible switch between that state and a low affinity (K_d= ~100nM) one (Fahrenholz et al., 1995; Klein & Fahrenholz, 1994). It is possible that there are multiple affinity states that lie in between but these states have proven difficult to characterize (Neumann & Landgraf, 2008). The effect of cholesterol on OXTR is not simply due to a change in the membrane fluidity, instead it is suggested to be mediated by critical residues on extracellular domain 3 and 4 (Neumann & Landgraf, 2008). Cholesterol is also shown to stabilize OXTR against thermal or proteolytic degradation, with OXTRs present in

cholesterol-rich microdomains like caveolae being significantly more stable than their partners in cholesterol-poor domains (Gimpl & Fahrenholz, 2000, 2002). It is possible that OXTR in this high cholesterol environment has different signaling characteristics, as demonstrated by a switch from proliferation induced by OXT to growth-inhibition following C-terminal fusion of OXTR to caveolin, which forces the receptor into lipid-rafts (Guzzi et al., 2002; Neumann & Landgraf, 2008).

1.5.3. Mechanism of OXTR signaling

OXTR signaling, like all GPCR signaling, is mediated through coupling of the receptor to heterotrimeric G-protein, composed of an α-, β- and γ-subunit. Upon ligand binding this G-protein undergoes a conformational change that allows for GDP, bound to the α-subunit, to be replaced with GTP. This G-protein activation can be blocked with compounds like GDPβS, used in **chapter 2**, which bind to the Gα-subunit but cannot be exchanged for GTP, leaving the G-protein inactive, even after receptor activation occurs. In the case of OXTR it is the $G\alpha_{q/11}$ class GTP binding proteins that, working together with Gβγ, stimulates the activity of the β-isoform of phospholipase C (PLC). After activation, PLC hydrolyzes PIP_2 in the membrane into inositol trisphosphate (IP_3) and 1,2-diacylglycerol (DAG). IP_3 travels to IP_3 receptors on the endoplasmic reticulum and stimulates the release of Ca^{2+} from intracellular stores.

The rise in intracellular Ca^{2+} stimulates several different cellular responses. In addition to altering neuronal firing patterns and influencing neurotransmitter secretion, Ca^{2+} can also form a Ca^{2+}-calmodulin complex and stimulate smooth muscle contraction and the synthesis of nitric oxide. The role of extracellular Ca^{2+} in the rise in intracellular Ca^{2+} is somewhat controversial, with some early studies suggesting that voltage-operated Ca^{2+} channels (L-Type)

played a role in the OXT mediated Ca^{2+} while others demonstrated that inhibition of these channels with nifedipine did not affect the $[Ca^{2+}]_i$ response to OXT (Inoue et al., 1992; Mironneau, 1976). A criticism of the study showing the effect of L-type Ca^{2+} channel inhibition was that the immortalized cells used no longer expressed the channels being studied. As a result, the question of the role of extracellular Ca^{2+} in the OXT response still needs to be definitively determined and is explored further in **chapter 2**.

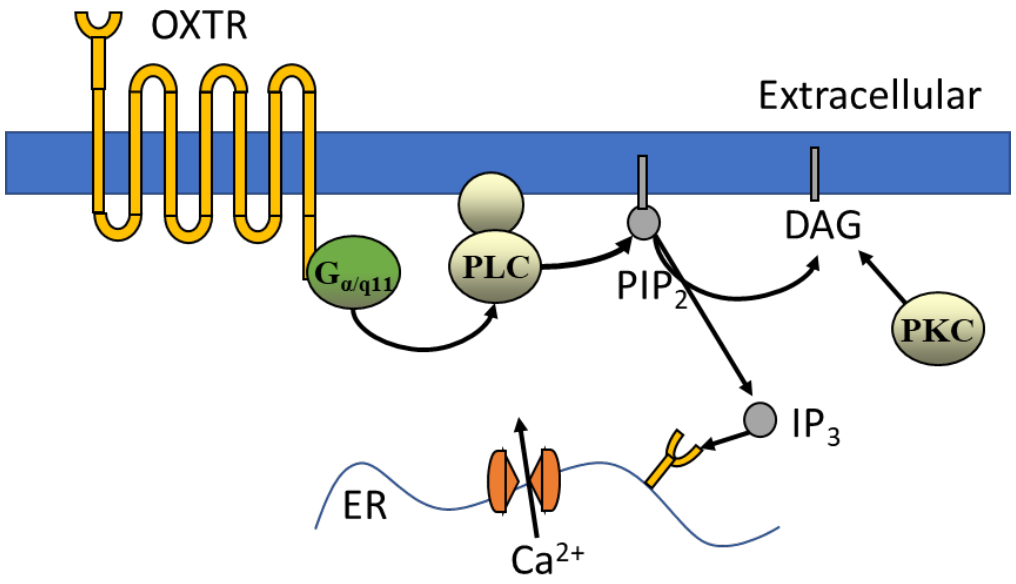

Figure 1.10: Schematic of canonical OXTR signaling. *OXTR activation leads to $G_{\alpha q/11}$ mediated activation of PLC, which hydrolyzes PIP_2 into IP_3 and DAG. IP_3 then induces the release of Ca^{2+} from the ER and DAG associates with PKC, leading to further downstream signaling.*

1.5.4. Oxytocin Receptor in the Uterus

OXTR in the uterus has been heavily studied and its role there is considered the "classical" function of OXT. Its role in the initiation of labor and parturition also serves as a good illustration of the diverse effects OXTR can mediate within a cell and throughout a tissue. Although OXT is not required for normal labor, it serves as a potent uterotonic agent and is

used clinically to induce labor (Nishimori et al., 1996). As labor approaches, the uterine sensitivity to OXT increases dramatically because of a significant increase in the density of OXTR. The increase in density reaches its peak early in labor, with elevated mRNA levels and an increase in the number of myometrial oxytocin receptors (Gimpl & Fahrenholz, 2001). The change occurs together with an increase in the ratio of estrogen to progesterone. Estrogen has been demonstrated to increase OXTR expression while progesterone suppresses this effect. Thus, the change in relative levels of estrogen and progesterone results in increased OXTR expression (Adachi & Oku, 1995). The expression of OXTR is not limited to the myometrium, however. It is also observed in the decidua, where the levels of OXTR increase by five times during parturition (Gimpl & Fahrenholz, 2001).

The role of hypothalamic OXT during parturition is not clear. Circulating OXT does not increase in labor until after full cervical dilation, from the time when the fetal head is visible to the time when it is delivered (Leake et al., 1981). Instead of systemic OXT, it is thought that locally produced peptide may be acting in a paracrine or autocrine manner within the uterus. OXT is locally expressed in the amnion, chorion and decidua of the placenta during pregnancy, supporting the possibility of this type of signaling (Chibbar et al., 1993). Furthermore, in the rat this expression has been shown to increase by more than 150-fold during parturition, quickly returning to normal following the cessation of labor (Lefebvre et al., 1992). This is 70-fold greater than the level observed in the hypothalamus, which only sees an approximately 3 fold increase during labor (Lefebvre et al., 1992). This increase is not reflected in the local levels of OXT peptide however, possibly as a result of OXT metabolism by local oxytocinases (Mitchell & Chibbar, 1995). This local production of OXT would explain the lack of a detectable change in

circulating hormone and supports the hypothesis that OXT is acting in a local paracrine, instead of endocrine, manner.

The role of OXT in parturition is dependent on the tissue in which the receptor is expressed. In the myometrium OXT directly induces contractions through PLC mediated release of intracellular calcium. Increases in the gap junction protein, connexin-43, in preparation for labor, allow this Ca^{2+} response to travel throughout the myometrium in synchronized, powerful contractions. In the decidua however, OXTR plays a different and less clearly defined role. OXT has been shown to stimulate the release of the prostaglandins $PGF_2\alpha$ and PGE from the decidua (Blanks & Thornton, 2003; Wilson et al., 1988). $PGF_{2\alpha}$ is a key regulator of luteolysis and is necessary for the decrease in progesterone that allows the induction of labor. This production of $PGF_{2\alpha}$ has been shown, in bovine endothelial cells, to be a result of OXT mediated production of cyclooxiginase-2 (COX-2) (Asselin et al., 1997). However, in mice oxytocin has a luteotrophic effect that must be overcome by $PGF_{2\alpha}$. In mice that do not express cyclooxygenase-1 (COX-1) there is a reduction in the level of $PGF_{2\alpha}$. As would be expected, these mice demonstrate a lack of luteolysis and delayed labor that is recovered following surgical luteolysis. However, double KO mice that lack COX-1 and OXT expression exhibit luteolysis and labor initiation on the normal day, suggesting that OXT has luteotrophic effects that oppose the actions of prostaglandins like $PGF_{2\alpha}$ (Gross et al., 1998).

1.6 Retinal Development and Retinopathy of Prematurity

1.6.1. Introduction

The Retina is an accessible, relatively simple, neural tissue that can be manipulated without many of the lethal consequences that could be expected from study of other tissues in the central nervous system. As a result, the development of the retina has been widely studied and characterized. In the mature retina there are ten distinct layers and no less than nine different cell types, each playing a specific role (Willermain et al., 2014).

Light stimulates the photopigments in the outer segments of the rod and cone photoreceptors, which are located adjacent to the RPE. These photoreceptors form synapses with horizontal cells and bipolar neurons. The bipolar neurons in turn synapse with ganglion cells directly or indirectly, thorough amacrine neurons. These ganglion cells then project their axons down the optic nerve and to the visual cortex of the brain (Wallace, 2011). Müller cells, a type of glial cell within the retina work to support this process of phototransduction.

All these cells can trace their lineage to multi-potent progenitor cells. These progenitor cells exhibit a directionality in the order of cell production and differentiation, with the multi-potentiality of the dividing progenitors declining as the retina matures and development continues (Reese, 2011). This means that early progenitor cells are capable of producing all types of retinal cells but that once the production of a particular cell type has begun within a progenitor cell line, all subsequent clones of that cell will never include members of that cell type (Wong & Rapaport, 2009). This effect appears to be driven by alterations in the retinal microenvironment, as new cell types are produced in the retina the retinal microenvironment

progressively changes, altering transcription factors expressed by the progenitors (Agathocleous & Harris, 2009).

Another key component of retinal development is the growth of the vascular network necessary to supply the inner retina with the oxygen and nutrients required to support vision. As the retina matures, the vascular network within the eye undergoes a dramatic reorganization. Initially supported by an arterial network in the vitreous called the hyaloid network, the retina is later supported by retinal vasculature that spreads across the inner surface of the retina (Fruttiger, 2007). As the retinal vasculature develops the hyaloid network regresses. The growth of the retinal vasculature is key to development and dysregulation or abnormal vessel growth can lead to severe visual complications. The formation of new blood vessels in the adult retina, called neovascularization, is a causative factor in several diseases, including retinopathy of prematurity (ROP), diabetic retinopathy and age related macular degeneration. It is therefore important to understand how the vasculature of the retina is developed so that we may understand how to prevent and treat diseases like these.

1.6.2 The coordinated development of the RPE and Retina

The development of the RPE is closely tied to the development of the photoreceptors and the neural retina. The close relationship between the two is evident in the fact that the RPE is capable of transdifferentiating into neural retina in many vertebrate species (Del Rio-Tsonis & Tsonis, 2003). The origins of both tissues arise from the optic cup, a neural structure which invaginates, with the cells on one side of the invagination eventually becoming the RPE and the cells on the other side eventually becoming the neural retina (Strauss, 2005). The remaining lumen that separates the two is then filled with the interphotoreceptor matrix (IPM), a material

that begins to encourage the maturation of the RPE. This is accomplished in part due to the presence of retinoic acid and the exchange of this retinoic acid between the RPE and the neural retina, an exchange mediated by interphotoreceptor retinal binding protein (IRBP) (Gonzalez-Fernandez, 2003). Synthesized in both the RPE and primordial photoreceptors, IRBP is produced from the beginning of IPM formation, at the same time as RPE specific protein, RPE65 is formed (Strauss, 2005). The onset of RPE maturation is marked by the onset of melanogenesis, when the neuroectodermal cells differentiate into RPE and Bruch's membrane begins to form (Jeffery, 1998; Strauss, 2005). During this period the RPE polarizes and forms short microvilli and basolateral membrane infoldings and approximately 75% of the apical structures seen in the mature RPE are present (Strauss, 2005). At this point the RPE is able to begin to interact with the primordial photoreceptors, allowing them to differentiate.

The differentiation of these primordial photoreceptors is tightly coordinated with the final maturation of the RPE. The primordial photoreceptors extend their outer segments towards the RPE and the RPE, in turn, extends its apical microvilli towards the growing outer segments and forms deep basolateral membrane infoldings (Strauss, 2005). These apical microvilli develop into two distinct types. The first are long microvilli, which ensure maximal apical surface area, and the second are short microvilli, which mediate outer segment phagocytosis. In addition to these structural changes, the photoreceptors and RPE also exhibit coordination in gene expression, with genes like RGR opsin and bestrophin being expressed in the RPE at the same time that photoreceptor electrical activity begins (Bakall et al., 2003; Tao et al., 1998).

The impact of the RPE on photoreceptor and retinal development is partially mediated through the secretion of growth factors. One of these factors is VEGF, through which the RPE could influence vascular growth, both in the choriocapilaris that lie below Bruch's membrane and the retinal vasculature (Adamis et al., 1993). Additionally the RPE is responsible for the secretion of pigment-epithelium-derived factor (PEDF), which has been shown to play a neuroprotective role in the mature retina and helps support the normal development of photoreceptors, in addition to helping to control ocular vascular growth through the inhibition of angiogenesis (Dawson et al., 1999; Jablonski et al., 2000; King & Suzuma, 2000).

Further evidence of the coordination between the RPE and retina in development are the local adaptions observed in the RPE to different functions of the retina. In the macula, where photoreceptor density is higher than the periphery, the RPE cells are adapted to allow for a higher turnover rate of shed photoreceptor outer segments, with higher expression of the enzymes required for turnover (Hayasaka et al., 1981). The cells of the macula are also much smaller and have a higher melanin content than those of the periphery (Strauss, 2005). The RPE also forms different types of sheaths around photoreceptor outer segments depending on whether the photoreceptors are rods or cones (Strauss, 2005). As a result, the apical structure of RPE in the cone heavy macula are different than RPE cells found in the periphery of the retina. This close relationship between the photoreceptors and the apical processes of the RPE has implications for our understanding of the role of OXTR in the RPE. The presence of OXTR in these apical processes is shown in **chapter 4**, suggesting that it could play a role in signaling between the two layers.

1.6.3 Retinal vascular development

The process of vascular growth in the retina is thought to occur primarily through the process of angiogenesis, through which proliferating endothelial cells from existing vessels sprout new vessels, extending the vasculature (Risau, 1997). Some studies have also suggested that the process of vasculogenesis, or the *de novo* formation of blood vessels, plays a role in the establishment of early retinal vasculature. In the early 1970's "spindle-shaped" cells were found anterior to growing vessels that were suggested to be vascular precursor cells that migrate over the retinal surface and establish the early retinal vasculature (Ashton, 1970). However more recent work has suggested that these cells are instead astrocytes that grow ahead of vasculature and that the vessel growth was a result of angiogenic sprouting (Gariano, 2010; Gariano et al., 1996). The door is not completely shut on a role for vasculogenesis however, as cells expressing both a marker for vascular precursors (CXCR4) and retinal endothelium (CD39) were found in advance of forming retinal vasculature (McLeod et al., 2006).

The process of retinal blood vessel growth is guided by specialized endothelial tip cells that have been identified at the edge of growing vasculature in the retina. These tip cells form bundles of filopodia in the direction of vascular growth (Fruttiger, 2007). In addition to these tip cells there are endothelial stalk cells, which are highly proliferative and have fewer filopodia. These cells work to ensure the stability of new sprouts and form the new vascular lumen (Blanco & Gerhardt, 2013). Filopodia bundle formation in the endothelial tip cells is controlled by VEGF receptor-2 (VEGF2R) mediated signaling and pushes vascular growth towards areas with high concentrations of VEGF (Gerhardt et al., 2003). VEGF expression is mediated by hypoxia, with retinal astrocytes at the leading edge of the vasculature expressing and secreting

higher levels of the growth factor in areas of low O_2 (Stone et al., 1995). As a result, a VEGF gradient exists, guiding retinal vascular growth from normoxic areas to hypoxic areas. There are likely other factors that play a role in guiding endothelial tip cell migration, although they have not been clearly described. Receptors for axon guidance molecules have been demonstrated to be involved in vascular growth in other tissues, however none of them have been associated with retinal vascular growth (Fruttiger, 2007). Additionally, there are factors that act in support of VEGF's actions, including insulin-like growth factor 1 (IGF-1), which acts to enhance the maximum level of VEGFR activation (Smith, 2004).

As the tip cells direct vascular growth in the retina, the region behind them grows into a dense capillary plexus that sits in the inner surface of the retina. This capillary plexus begins adjacent to the optic nerve and extends towards the periphery of the retina and as it does so it is remodeled and starts to form a less uniform vascular tree, with distinguishable arteries and veins (Fruttiger, 2007). Capillary free zones begin to form in the vicinity of arteries, as a result of endothelial cell migration and selective apoptosis of endothelial cells driven by leukocytes (Hughes & Chang-Ling, 2000; Ishida et al., 2003). This process is possibly driven by VEGF as well, as capillary pruning has been shown to be defective in mice that express only the $VEGF_{120}$ isoform of VEGF (Stalmans et al., 2002). A deeper plexus of the retinal vasculature develops out of this original, primary plexus, penetrating the retina perpendicularly to the primary plexus (Fruttiger, 2007). Vessels sprout and grow along Müller cells into the retina and then spread across the inner and outer boundary of the inner nuclear layer, parallel to the primary plexus (Fruttiger, 2007). This process begins to occur as the primary plexus reaches its most peripheral extent (Gariano, 2010; Provis, 2001).

1.6.3.1 Comparison of Human and Murine vasculature

As with many areas of research, the mouse provides a powerful tool to study the blood vessel growth in the retina. In the human, retinal vascular growth begins before mid-gestation in humans and other primates and is almost complete by birth, making it difficult to study (Gariano, 2010; Provis, 2001). Mice, however, don't begin to develop their retinal vasculature until birth and the entire process is completed within three weeks, making the mouse a much more accessible and convenient model for studying this development (Figure 1.11)(Connolly et al., 1988).

While vascular development can vary significantly between strains of mice, in the widely used C57Bl/6 strain we see growth of the primary plexus out from the optic nerve towards the periphery during the first week after birth, with it reaching the edge of the retina by approximately postnatal day 7-8 (p7-8) (Stahl et al., 2010). In humans this process occurs

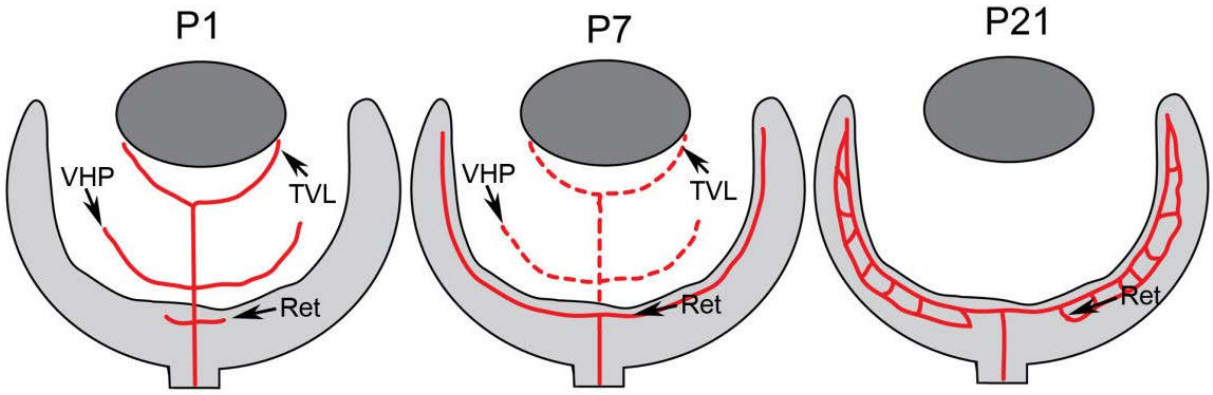

Figure 1.11: Vascular development in the mouse retina. *Mouse retinal vasculature develops after birth extending out from the optic nerve, reaching the periphery by day 7-8. By postnatal day 21 the vasculature is fully mature, with multiple vessels connecting the different layers.*

Figure adapted from Edwards M. et al., (2011). Lama1 mutations lead to vitreoretinal blood vessel formation, persistence of fetal vasculature, and epiretinal membrane formation in mice.BMC Dev Bio, 11(60), 1, as allowed by copywrite

beginning during the fourth month of gestation and the vessels reach the periphery by the 7th or 8th month (Anand-Apte & Hollyfield, 2010). The formation of the deep plexus in the mouse begins at P7, with the deeper plexus on the outside of the inner nuclear layer reaching the retinal periphery by P12 and the plexus on the inner portion of the inner nuclear layer forming between P12 and P15 (Stahl et al., 2010). While this process occurs simultaneously throughout the retina in mice, in humans it appears to occur in a directed manner, progressing from the posterior to the anterior (Gariano, 2010).

1.6.4 Pathogenesis of ROP

Retinopathy of Prematurity (ROP) is the most common disorder of retinal vascular growth and it is the leading cause of blindness in children. The pathogenesis of ROP is closely tied to retinal oxygen levels and is driven primarily by alterations in the production of VEGF and IGF-1, which mediates responsiveness to VEGF. As mentioned in the previous sections, the vascularization of the human retina continues from 4 months of gestation to birth. Infants born prematurely therefore have incompletely vascularized retinas, with peripheral avascular zones. The more premature an infant the larger the area of this avascular zone.

Following birth, the normal blood vessel growth that would occur *in utero* is incomplete and as the retina continues to mature and become more active the vasculature cannot supply sufficient O_2, resulting in an increasingly hypoxic retinal environment. This process is described as the first phase of ROP and is characterized by a decrease in VEGF and IGF-1 in response to the abundance of O_2 (Smith, 2004). In the second phase, retinal neovascularization occurs, driven by the hypoxia of the retina, and can lead to retinal detachment, scarring and eventually

blindness (Cavallaro et al., 2014). The neovascularization of this phase results from significantly increased VEGF as a result of retinal hypoxia.

Given the importance of VEGF in the vascularization of the retina it makes sense that it plays a prominent role in pathogenesis of this vascular disease. Hypoxia drives the production of VEGF by astrocytes and directs vascular growth to areas with limited O_2. When ROP was first described a connection was quickly made between the use of high levels of supplemental O_2 and increased instances of the disease (Cambell, 1951). The use of supplemental O_2 leads to a state of hyperoxia in the retina and results in reduced VEGF and IGF-1 production and a cessation of normal vessel growth characterized in Phase I of ROP (Smith, 2004). Despite this role for O_2 in the pathogenesis of ROP it is clear that the causes are more complex, as limitations on the amount of supplemental O_2 have been successful in reducing instances of ROP by 52% but they have not eliminated the disease (Chen et al., 2010). In fact, as modern medicine has made it possible for infants of extremely low gestational age to survive we are seeing that these infants have an increased susceptibility to the development of ROP (Sahin et al., 2014). This persistence of ROP suggests that other factors, related to prematurity itself are also responsible for the pathogenesis of the disease.

In the clinic, ROP is described according to the international classification of ROP (ICROP), which divides the retina into three concentric zones, moving outward from the posterior to the anterior retina (Figure 1.12a)(Prematurity, 2005). Zone 1 is a circle with the center as the optic disc, a raised disc on the retina where the optic nerve enters, and a radius of twice the distance from the disc to the fovea (Shah et al., 2016). The second zone extends from zone 1 to the ora serrata, the nasal junction between the retina and the ciliary body. The third

zone contains the remaining portion of the retina. Within these zones the extent of ROP is documented as the number of "clock hours" involved, with the nasal side of the right eye as 3 o'clock and the temporal side of the same eye as 9 o'clock (Shah et al., 2016). The inverse is true for the left eye. The degree of vascular changes observed during ROP are classified into 5 different stages (Figure 1.12b) (Hellström et al., 2013; Shah et al., 2016). In stage 1, a demarcation line can be observed between the vascular and avascular retina. In stage 2, this demarcation line forms a three-dimensional ridge that rises above the plane of the retina. In stage 3 ROP this ridge is observed to have fibrovascular growth out of the retina and into the vitreous, posterior to the ridge. Stage 4 is characterized by partial detachment of the retina, either not involving the fovea (Stage 4A) or involving the fovea (stage 4B). The final stage, stage 5, is characterized by total retinal detachment. Additionally, ROP can be classified as plus disease, defined by venous dilation and arterial tortuosity seen in the posterior pole of the

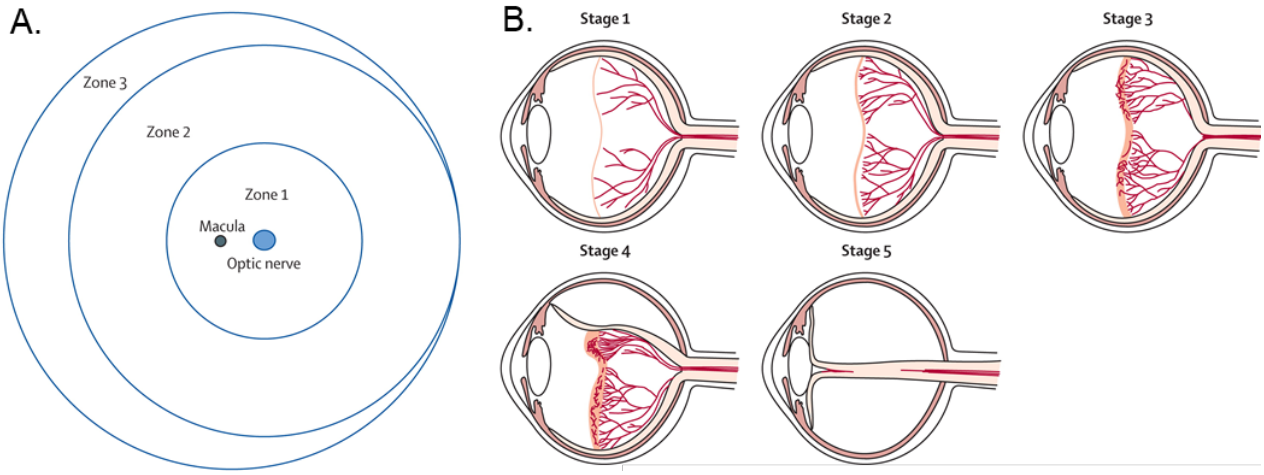

Figure 1.12: Zones and stages of retinopathy of prematurity. *A) The three zones that divide the retina are shown. The severity of ROP in a given shown are classified as stages, shown in panel (B).*

Figure adapted from Hellström A. et al., 2013. Retinopathy of prematurity, The Lancet, 382(9902), 13 with permission from Elsevier

retina. An intermediate classification of pre-plus disease is given in cases where vascular dilation and tortuosity is increased but less severe than plus. Finally, an uncommon and rapidly progressing form of ROP, characterized by severe plus disease and flat intraretinal neovascularization, is classified as aggressive posterior ROP.

1.6.5 Current Treatment for ROP

As the leading cause of childhood blindness in the world, the treatment of ROP is of worldwide interest. This is exemplified in the World Health Organization's "Vision 2020 Programme", which gives treatment of the disease high priority (Gilbert & Foster, 2001). Treatments for ROP are limited and imperfect. The most common and widely used therapies today continue to be ablative therapies. This treatment, first established as the preferred method of treatment in 1988, includes two techniques, cryotherapy and laser ablation (O'Keefe & Kirwan, 2006). Cryotherapy, in which a tool is used to freeze peripheral avascular regions of the retina, has fallen out of favor with the increased use of laser therapies, which generally have better patient outcomes (Mutlu & Sarici, 2013; O'Keefe & Kirwan, 2006). Laser therapy uses a laser to ablate the peripheral retina that lacks adequate vasculature, preventing the hypoxia that drives the neovascularization of ROP. While these treatments have been successful in reducing the instances and progression of ROP, patients still suffer from poor vision, especially when the avascular region of the retina was large (Mutlu & Sarici, 2013). Patients also exhibit retinal detachment in 12% of eyes that receive laser therapy, possibly as a result of macrophages in the vitreous of the eye acting as a second source of VEGF that cannot be removed with laser therapy (Naug et al., 2000). Other complications from this treatment can include corneal edema, intraocular hemorrhage and cataract formation (Mutlu & Sarici, 2013).

Regardless of these risks ablative therapy remains the “gold standard” for ROP treatment and the only evidence-based treatment available. However, there are a number of promising future treatments being explored.

One of these promising treatment is the use of anti-VEGF drugs. Taking a pharmacological approach to reducing VEGF without the tissue destruction seen in ablative therapies, these drugs hope to reduce the instances and progression of ROP without many of the complications seen with laser and cryotherapy. One major concern with the use of these drugs is the potential off target effects. For example, the humanized recombinant antibody Bevacizumab, which binds to all isoforms of VEGF-A, has had promising results but could potentially disrupt the other important vascular development occurring in the premature infants that are given it (Kong et al., 2008; Mintz-Hittner, 2010; Mutlu & Sarici, 2013). Originally an anticancer drug, intravenous Bevacizumab has been shown to cause systemic complications at high doses but no such complications have been reported from intravitreal injections (Taugourdeau-Raymond et al., 2012). It has not been approved for use in the eyes or in infants yet, although off label use has been growing, and is even suggested as a treatment by the American Academy of Pediatrics, American Academy of Ophthalmology, the American Association for Pediatric Ophthalmology and Strabismus and the American Association of Certified Orthoptists (Fierson et al., 2013). More selective inhibition of VEGF is also possible. Pegaptanib sodium is an anti-VEGF drug that specifically inhibits the $VEGF_{165}$ isoform of VEGF, potentially making it a safer alternative (Mutlu & Sarici, 2013). Some success has been shown with this drug, however it is not as widely used as Bevacizumab despite being approved for use in ocular neovascular disease in adults (Autrata et al., 2012; Mutlu & Sarici, 2013). These are

not the only two drugs being explored for ROP but they represent the most widely studied ones.

Treatment options being explored extend beyond targeting VEGF, specifically. Propranolol, a β-adrenergic receptor antagonists, is being explored as a potential treatment option. Systemic application of the drug has been shown to reduce the levels of retinal VEGF and IGF-1 as well as retinal neovascularization in mice with oxygen-induced retinopathy (Ristori et al., 2011). Others, however, have found it difficult to repeat these results using up to 30 times the standard human dose in mice, and a recent study on the safety of propranolol treatment in premature infants with ROP was stopped due to increased mortality in the group receiving treatment (Chen et al., 2012; Ristori et al., 2011). Gene therapies have also been proposed as possible treatments, using viruses to deliver genes regulating angiogenesis or small interfering RNA to block various pro angiogenic factors to the retina to prevent neovascularization. The potential for this gene delivery has been shown in a rat model of ROP but further study is needed (Chowers et al., 2001).

1.7 Conclusion

In this introduction I have highlighted the importance of the RPE in maintaining a healthy retina and functioning vision, emphasizing the role played by Kir7.1. Additionally, I have outlined the process and timeline of vascular growth in the developing retina and examined a consequence of dysregulation of this growth in ROP. In this thesis I attempt to determine how oxytocin and its receptor, which we have previously localized the photoreceptor outer segments and the RPE respectively, might be involved in these processes. As I have stated, our

understanding of how oxytocin acts throughout our body is continuously expanding. I expect my work will add some clarity to the role of oxytocin in the eye as well as reveal new potential roles for it elsewhere.

1.8 Statement of Specific Aims

The discovery of OXT present around the cone photoreceptor outer segments and the expression of OXTR by the RPE suggests the presence of oxytocinergic signaling in the retina. Given the importance of the RPE to retinal function and maintenance, understanding the effect of this signaling could have a significant effect on our understanding of retinal health and disease. In this thesis I explore the impacts of this signaling, focusing on direct effects on the RPE through the modulation of Kir7.1, as well as indirect regulation of retinal development through the production and secretion of growth factors by the RPE. To study these effects I have developed the following global hypothesis as well as three specific aims in an effort to address this hypothesis.

Global Hypothesis: Oxytocin receptor signaling in the RPE directly impacts RPE physiology and indirectly influences retinal vascular growth during the development of the retina.

AIM #1: Explore the effects of OXTR signaling on Kir7.1 in the RPE

Hypothesis: Kir7.1 function is inhibited by PIP_2 hydrolysis in response to OXT activation of the OXTR in the RPE.

Approach: OXTR is G-protein Coupled Receptor (GPCR) whose main mechanism of action involves the hydrolysis of phosphatidylinositol 4-5 bisphosphate (PIP_2), a membrane

associated phospholipid. PIP_2 is known to regulate inwardly rectifying K^+ channels. The inhibition of Kir7.1 is therefore a likely consequence of OXTR activation. To test this, I used the whole cell patch clamp technique on HEK-OXTR cells transfected with an eGFP fused Kir7.1 plasmid. I used the same technique to record from freshly isolated mouse RPE cells and observed an inhibition of Kir7.1 current in both cell types, with depolarization in the RPE cells. I will follow up on these findings by using pharmacological blockers and visual markers of PIP_2 to confirm the mechanism of Kir7.1 inhibition and determine that it is a direct action of the OXTR signaling pathway.

Impact: This aim will support a role for OXT in regulation of RPE function and will expand our understanding of the processes that underlie the maintenance of vision. In addition, the regulation of Kir7.1 by OXT could have implications in other tissues, including the uterine myometrium.

AIM #2: Oxytocin and the development of the retinal vasculature in ROP

Hypothesis: The lack of exposure to a late gestational surge in OXT is responsible for abnormal vascular growth in ROP.

Approach**:** Retinopathy of prematurity (ROP) is a disorder that is caused by abnormal growth of blood vessels into the vitreous of the eye. The RPE forms the blood-retina barrier, and it plays an important role in maintaining normal vascular growth (Dawson et al., 1999; Nishijima et al., 2007; Sakamoto et al., 1995). OXT levels are tightly controlled during pregnancy, with levels increasing significantly from 32-40 weeks while almost all infants born with ROP have a gestational age of less than 31 weeks, which suggests that OXT may be

involved in the pathogenesis of ROP. To determine the role of OXT in ROP I will establish the effect of OXT on the transcription and secretion of specific angiogenic growth factors by the RPE, utilizing molecular and biochemical techniques. Furthermore, to determine the angiogenic effect of this production I will utilize migration and tube forming assays, developed to analyze angiogenesis.

Impact: Identifying OXT as a culprit in the development of ROP would open the door for a study into whether OXT treatment in premature infants could reduce the cases of ROP.

Aim #3: Describe the Ontogeny of the Oxytocin receptor in the RPE

Hypothesis: Oxytocin receptor is expressed by the RPE during the period of retinal vascular growth.

Approach: I will identify and quantify OXTR transcript molecular expression during retinal gestation in the mouse. Expression levels will be determined at five day intervals, starting from birth. If OXTR is expressed at birth, prenatal mice eyes will be examined to discover the exact time point of OXTR expression during pregnancy. The ultimate goal is to correlate the expression of OXTR with RPE and retinal markers.

Impact: Describing the expression of OXTR in the mouse will provide insight to the possible time point where OXT can have an impact on retinal development. In addition to the developmental impact, this study will provide the groundwork for future use of the mouse model in studies of OXT's role in developmental eye diseases.

Chapter 2: Oxytocin Receptor Signaling in the RPE

Oxytocin (OXT)-stimulated inhibition of Kir7.1 activity is modulated by PIP_2-dependent Ca^{2+} response of the Oxytocin receptor in the Retinal Pigment Epithelium in vitro

Nathaniel York[1,2,3,7§], Patrick Halbach[1,2,3,7§], Michelle A. Chiu[2,3,7], Ian M. Bird[1,4], De-Ann M. Pillers[2,3,5,7], Bikash R. Pattnaik[1,2,3,6,7#]

From the [1]Endocrinology-Reproductive Physiology Program, the [2]Division of Neonatology& Newborn Nursery, the [3]Departments of Pediatrics, [4]Obstetrics & Gynecology, [5]Medical Genetics, [6]Ophthalmology &Visual Sciences, and [7]the McPherson Eye Research Institute, the University of Wisconsin,-Madison, WI 53715

Originally Published in Cellular Signaling, Volume 37, September 2017, Pages 93-102 (York et al., 2017) with added data to complete this thesis. Original manuscript, as published, is included at the end of this document, in **Appendix 2**.

ABSTRACT

Oxytocin (OXT) is a neuropeptide that activates the oxytocin receptor (OXTR), a rhodopsin family G-protein coupled receptor. Our localization of OXTR to the retinal pigment epithelium (RPE), in close proximity to OXT in the adjacent photoreceptor neurons, leads us to propose that OXT plays an important role in RPE-retinal communication. An increase of RPE $[Ca^{2+}]_i$ in response to OXT stimulation implies that the RPE may utilize oxytocinergic signaling as a mechanism by which it accomplishes some of its many roles. . In this study, I used an established human RPE cell line, a HEK293 heterologous OXTR expression system, and pharmacological inhibitors of Ca^{2+} signaling to demonstrate that OXTR utilizes capacitative Ca^{2+} entry (CCE) mechanisms to sustain an increase in cytoplasmic Ca^{2+}. These findings demonstrate how multiple functional outcomes of OXT-OXTR signaling could be integrated via a single pathway. In addition, the activated OXTR was able to inhibit the Kir7.1 channel, an important mediator of subretinal waste transport and K^+ homeostasis.

Keywords: calcium imaging, cell signaling, hormone receptor, inositol 1,4,5-trisphosphate (IP3), ion-channel, retina, oxytocin, RPE, oxytocin receptor

2.1 Introduction

Oxytocin (OXT) is a cyclic nonapeptide produced in the paraventricular and supraoptic nuclei of the hypothalamus (Gimpl & Fahrenholz, 2001). Although best known for its association with parturition and lactation, OXT also has numerous central and peripheral effects, including, but not limited to, the modulation of sexual and social behavior, influence over metabolic activity in adipose tissues, and skeletal muscle maintenance (Elabd et al., 2014; Gimpl & Fahrenholz, 2001).

The RPE is a monolayer of polarized cells that serve as a physical and protective blood-retina barrier and act as a facilitator of phototransduction in the photoreceptors (Strauss, 2005). The RPE also mediates the bidirectional transport of nutrients between the choroid and photoreceptors, maintains the ionic composition of the subretinal fluid, and facilitates phagocytosis of photoreceptor outer segments that are shed on a daily basis. It is not fully understood how the RPE and photoreceptors coordinate their function. What is known, however, is that autocrine and paracrine signaling in the RPE involves G protein-coupled receptors (GPCR), including the dopaminergic, adrenergic, P_{2Y}-purinergic, and serotoninergic receptors (Barnard et al., 1994; Gallemore & Steinberg, 1990; Nash et al., 1999; Nash & Osborne, 1997; Quinn et al., 2001; Versaux-Botteri et al., 1997).

We have shown that OXT is a potential mediator of retinal physiology given its presence in the cone photoreceptor extracellular matrix (Halbach et al., 2015). Moreover, the oxytocin receptor (OXTR) is expressed in the retinal pigment epithelium (RPE), where we have shown that OXT can induce an increase in intracellular [Ca^{2+}] ($[Ca^{2+}]_i$), leading to my hypothesis that oxytocinergic signaling may serve as a means for communication between cone photoreceptors

and the RPE (Halbach et al., 2015). OXTR is a GPCR and like the aforementioned receptors, it activates a phospholipase C (PLC)-mediated signaling pathway, thereby stimulating PIP_2 hydrolysis and resulting in a rise in $[Ca^{2+}]_I$ (Fahrenholz et al.).

Facing the photoreceptor outer segments on the apical membrane of the RPE cell is the inwardly rectifying potassium (Kir7.1) channel (Strauss, 2005; Yang et al., 2003). As its name suggests, Kir7.1 exhibits a large inward K^+ current at hyperpolarized membrane potentials. However, at physiological membrane potentials, the channel facilitates the efflux of intracellular K^+ (Hughes & Takahira, 1996; Shimura et al., 2001). This, combined with its co-localization with Na^+-K^+-ATPase, makes Kir7.1 integral to the maintenance of the K^+ transport needed for transepithelial fluid transport (Bialek & Miller, 1994; Griff et al., 1985; La Cour, 1992). Kir7.1 function is also directly mediated by PIP_2, supporting the possible regulation of Kir7.1 by OXTR through PLC-activated PIP_2 hydrolysis (Pattnaik & Hughes, 2009). Understanding how Kir7.1 is regulated is clinically important, as disrupted Kir7.1 function is a known cause of the retinal diseases of Snowflake Vitreoretinal Degeneration and Lebers Congenital Amaurosis – Type 16 (LCA16) (Hejtmancik et al., 2008; Pattnaik et al., 2015; Sergouniotis et al., 2011). A direct impact of Kir7.1 on retinal function and vision can be clearly seen following RNA interference (RNA_i) knockdown of Kir7.1 in mice, resulting in a characteristic and abnormal electroretinogram (ERG) (Pattnaik et al., 2015).

In this study I sought to delineate the mechanism by which OXT elicits an increase in $[Ca^{2+}]_i$ and how this may affect Kir 7.1 function in the RPE by using cultured hfRPE cells. I also studied a human embryonic kidney (HEK293) cell line with heterologous expression of human OXTR to study the effects of OXTR on the Kir7.1 channel without the complex interactions

inherent in the intact RPE cell. In this cell line I was able to demonstrate the necessity of G-protein mediated signaling and PIP_2 hydrolysis for Kir7.1 inhibition by OXTR. Additionally, I used adult mouse RPE cells to demonstrate the link between Kir7.1 channel function and OXT-OXTR signaling.

2.2 Materials and Methods

Reagents

All chemical reagents were purchased from Sigma-Aldrich (Sigma-Aldrich, St. Louis, MO), Thermo Fisher Scientific (Thermo Fisher Scientific, Waltham, MA), or Gibco (Grand Island, NY), unless otherwise specified.

Solutions

HEPES Ringers (HR) extracellular bath solution was prepared using (mM) 135 NaCl, 5 KCl, 1.8 $CaCl_2$, 1 $MgCl_2$, 10 HEPES, 10 glucose, and adjusted to pH 7.4 with NaOH. K^+ inhibition solutions require the same composition with 115mM NaCl and the addition of 20 mM $BaCl_2$ or $CsCl_2$. Ca^{2+}-free extracellular bath solution was prepared using (mM) 135 NaCl, 5 KCl, 1 $MgCl_2$, 10 glucose, 10 HEPES, 2 EGTA-KOH, and adjusted to pH 7.4 with NaOH. Final concentrations of 0.01, 0.1, 1, 6, 10, or 100 µM OXT were prepared in either HR or Ca^{2+}-free extracellular solutions. Extracellular solution containing the Ca^{2+} channel blocker nifedipine was prepared by diluting to 10 µM final concentration in HR. A final concentration of 60 µM 2-APB (Tocris Bioscience, Bristol, UK), an IP_3R inhibitor, was prepared in HR.

Cell Culture

Passage 1-3 cryopreserved Primary Clonetics™ Human RPE cells (hfRPE) (LONZA, Walkersville, WA) were cultured using a previously published protocol (Halbach et al., 2015).

HEK293 cells were obtained from ATCC (Manassas, VA). To generate HEK-OXTR line, cells were transfected with a pcDNA6/HisC plasmid-containing human OXTR via nucleofection (4-D Nucleofector, LONZA) as per the manufacturer's instructions. Cells were cultured in a 60 mm culture dish in complete growth medium (DMEM + 10% Fetal Bovine Serum + 1% Pen-Strep). Twenty-four h after transfection, culture media was supplemented with 10 µg/mL blasticidin (Thermo Fisher Scientific) to select for cells expressing the OXTR-containing plasmid. Individual surviving cell colonies were selected and grown in culture media containing blasticidin in 24-well plates. OXTR expression was verified by indirect immunofluorescence and Ca^{2+} imaging. OXTR positive cells were cryo-preserved and subcultured for experimental usage.

hfRPE culture media was prepared using MEM alpha base medium, 1% N-2 supplement, 1% glutamine, 1% pen-strep, 1% MEM non-essential amino acids, taurine, hydrocortisone, and 3, 3', 5-triiodo-thryonine. HEK cell culture complete growth media was prepared using 10% FBS and 1% PenStrep diluted in DMEM.

Ca^{2+} imaging

hfRPE cells were grown on coverslips and incubated in 5 µM FURA-2 penta-acetoxymethyl ester (AM) in hfRPE culture media + 0% FBS for 30 minutes in a dark environment. Selective Oxytocin antagonist, desGly-NH_2-d$(CH_2)_5$[D-Tyr^2, Thr^4]OVT, (OTA) was generously provided Dr, Maurice Manning (University of Toledo, OH). 100uM OTA was included in FURA incubation solution as well as perfused solutions. HEK-OXTR cells grown on coverslips

were incubated with 5 µM Fura-2 AM in serum-free DMEM under the same conditions. Following incubation with FURA-2 AM, coverslips were rinsed x 3 in HR solution and transferred to the recording chamber (Warner Instruments, Hamden, CT) on the microscope stage (Nikon FN1, Nikon Instruments Inc., New York, NY). hfRPE cells were continuously perfused with HR or Ca^{2+}-free solution containing tested compounds (OXT, nifedipine, 2-APB, OTA) and were exchanged using a gravity-feed 8-valve solution exchange system with a ValveLink Pinch Valve (Automate Scientific, Berkeley, CA) controlled through ValveLink8.2 (Automate Scientific, Berkeley, CA). HEK-OXTR cells were continuously perfused with HR, and HR solution containing OXT or ATP was exchanged using the same system.

Images were acquired every 10 s using a 20X water immersion objective (NA = 0.5) and Lambda LS lamp (Shutter Instruments, Novato, CA). The 300 ms shutter speed and 340 and 380 nm excitation wavelengths were controlled by the Lambda 10-2 controller (Sutter Instruments), and emission was set to 518 nm. Image frames from the CoolSnap HQ Photonics camera (Nikon) were digitized and stored for off-line analysis. Background and calibration images were similarly acquired and used to obtain absolute changes in fluorescence values. All distinct, visible cells in a visual field had regions of interest defined using NIS software thresholding intensity feature to identify cells by intensity at 380nM excitation and the amplitude of the R (340/380) was measured.

The calcium concentration was calculated using the equation: $[Ca] = Kd*(R-R_{min})/(R_{max}-R)(F_{max}^{380}/F_{min}^{380})$, assuming the K_d to be 225 nM in the cytosolic environment (Grynkiewicz et al., 1985). Calibration values were determined using 10 µM ionomycin to permeabilize cells to

Ca^{2+} and expose them to [0] Ca^{2+} solution or HR to obtain min and max values, respectively. Values were determined separately for hRPE and HEK-OXTR cells.

Live-Cell Fluorescence Imaging

Plasmids encoding the PH domain of phospholipase Cd1 fused to GFP (PH-GFP kindly provided by T. Balla, NIH) or GFP fused to C1 domains from protein kinase C (PKC-GFP kindly provided by T. Meyer, Stanford) were used for live-cell fluorescence imaging (Oancea et al., 1998; Varnai & Balla, 1998). After 24 hours of plasmid transfection into HEK-OXTR cells using TransIT-LT1 (Mirus Bio, Madison, WI), cells were dissociated and plated onto laminin-coated coverslips (12 mm #1; Thermo Fischer Scientific).

Imaging was performed between 48 to 72 h post-transfection while cells were perfused with HR alone and OXT dissolved in HR. Using 470 nm excitation and 525 nm emission, images were acquired every 10 s. 10 µM OXT was used to stimulate cells. The images were analyzed off-line using scans of either membrane or cytoplasmic 'regions of interest' (ROI).

Animal Handling and RPE isolation

Mouse RPE was isolated from 6-8 wk old C57BL6 mice (The Jackson Laboratory, Bar Harbor, ME) used for research in accordance with the recommendations of the guide for the care and use of laboratory animals by Association for Research in Vision and Ophthalmology (ARVO) with housing and care reviewed and approved by the UW-Madison Animal Care Committee. Mice were anesthetized and sacrificed by cervical dislocation. The eyes were enucleated, immediately placed in chilled 0 Na, Ca-Mg free (0Na-CMF) solution (135mM NMDG-Cl, 5mM KCl 10mM HEPES, 10mM Glucose, 2mM EDTA-KOH and pH adjusted to 7.4) and

washed two times. An incision was made in the scleral buckle with the sharp needle. Vannas scissors were used to cut along the scleral buckle to open the eye, and the anterior cornea, iris and lens were discarded. With the use of surgical forceps, the thin layer of retina was removed. The posterior eye cup with the intact retinal cells was then transferred to an enzymatic solution (0.375 mg/ml Adenosine, 0.3mg/ml L-Cysteine, 0.25 mg/ml Glutathione, 0.05mg/ ml Taurine, 2.5 µl/ml papain and 5 µl/ml DNAse (0.8mg/ml-stock) dissolved in 0Na-CMF solution for digestion and incubated in 2ml tube at 37°C for 30 mins. The reaction was stopped using 0.01% BSA solution and the eye cups were washed gently with warm HEPES ringer solution (135mM NaCl, 5mM KCl, 10mM HEPES, 10mM Glucose, 1.8mM $CaCl_2$, 2mM $MgCl_2$ and pH adjusted to 7.4).

Electrophysiology

For electrophysiology using HEK-OXTR cells, $1.8x10^5$ cells were plated in a 35 mm dish overnight. The following day, cells were transfected with an N-terminal GFP-labeled Kir7.1 plasmid using a standard TransIT LT-1 protocol at 37 ^oC for 24 h, after which the cells were transferred to coverslips and placed in reduced-serum media at 37 ^oC overnight. Cells were selected for recording by the presence of GFP fluorescence in the membrane.

For electrophysiology using murine RPE cells, cells were isolated from 8wk old C57BL/6 mice by enzymatic digestion of the eye cup. Following digestion, RPE cells were identified by their morphology. Recordings were performed in either perforated or whole cell patch configuration. During the recording, HR was used in the bath. Once current was stable, RPE cells were perfused with 10µM OXT whereas HEK-OXTR cells were perfused with 0.1-10 µM OXT. Potassium ion current in cells was blocked using 20 mM $CsCl_2$ to identify the proportion of total

current for which Kir channel was responsible. The pipette solution contained 30 mM KCl, 83 mM K-gluconate, 5.5 mM EGTA-KOH, 0.5 mM $CaCl_2$, 0.5 mM $MgCl_2$ and 10 mM HEPES. For recordings with GDPβS (Sigma-Aldrich, St. Louis, MO), internal solution was supplemented with 5mM GDPβS immediately prior to recording, with new solution made every 1-2 hours to prevent loss G-protein inhibition. All recordings were performed using an electrophysiology rig built around a Nikon FN1 microscope and consisting of a fixed stage (Nikon, USA), PATCHSTAR micropositioner (Scientifica, East Sussex, UK), low noise amplifier, D/A convertor, and pClamp-10 software (all from Molecular Devices, Sunnyvale, CA). Iused a micropipette with a 5-7 MΩ tip and recordings were made using a 2 sec ramp protocol from -150 mV to 50 mV to monitor Kir7.1 current while holding cells at -60 mV in the inter-pulse interval.

For cells recorded in perforated patch configuration, 120 µg/mL amphotericin B and 100 µg/mL of pluronic F-127 (Sigma-Aldrich, St. Louis, MO) were added to the internal solution. To create this solution 1.2 mg of amphotericin B was dissolved in 40 µL of DMSO and 1 mg of F-127 was dissolved in 20 uL of DMSO (Husch et al., 2011). Both solutions were mixed together and the resulting 60 µL was added to 1mL of pipette solution. After a giga-ohm seal was achieved cells were monitored continuously for an increase in capacitance and reduction in access resistance (R_a), signifying a perforated patch. Perforated patch recordings were performed using the same hardware and recording protocols as whole cell patch recordings.

Statistical analyses

Data from the Ca^{2+} imaging and electrophysiology experiments were analyzed using the Student's *t*-test. All curve fitting, statistical tests, and plotting of data was performed with Origin (OriginLab Corporation, MA). The dose-response was calculated with the equation y =

R_{min} + (R_{max} - R_{min}) / (1 + 10^ ((LogEC_{50} - x) * HillSlope)). Ca^{2+} response decay and current inhibition during perforated patch were fit with the exponential equation $y = y_0 + Ae^{R0x}$ using Origin. Confidence interval for the ratio of means was calculated using method described by Cochran (1977, sect. 6.4, eq. 6.13) (Cochran, 1977). Data are expressed as mean ± SEM. Significance was determined to be present at $P<0.05$.

2.3 Results

Dose-response effects of OXT in activating hfRPE cell $[Ca^{2+}]_i$

We have previously shown that OXT induces an increase in hfRPE $[Ca^{2+}]_i$, so we used $[Ca^{2+}]_i$ as a variable to determine the dose-dependent response to OXT (Halbach et al., 2015). hfRPE cells were stimulated by OXT concentrations ranging from 0.01 to 100 µM, and $[Ca^{2+}]_i$ represented by R (340/380), was measured. OXT concentrations of 0.01, 1, and 100 µM showed a progressive increase in $[Ca^{2+}]_i$ (Figure 1A). 100 µM OXT induced an average increase in R (340/380) of 0.2 (Figure 1A). Using R values normalized to R_{peak} (0.63; R/R_{peak}), a dose-response curve was generated (Figure 1B). The dose-response curve exhibited a sigmoidal shape with EC_{50} 0.341 µM OXT and Hill coefficient 0.77 ± 0.07.

Selective inhibition of hfRPE Ca^{2+} response by selective OXTR antagonist

To demonstrate that the observed Ca^{2+} response was specifically mediated by OXTR I utilized the potent selective OXTR antagonist, desGly-NH_2-d$(CH_2)_5$[D-Tyr^2, Thr^4]OVT (OTA). Following pre incubation with 100 µM OTA I observed a reduction of response relative to HR controls performed on the same day (Figure 2A-B). On average, while 10 µM OXT was able to elicit a 4 ± 0.5 (n=39/2 coverslips) fold increase in intracellular calcium, pretreatment of cells

with 100 µM OTA significantly reduced the Ca^{2+} response to a 1.3 fold ± 0.1 (n=55/3 coverslips) fold increase (P<.001, Figure 2B). The OXT-induced initial increase of hfRPE $[Ca^{2+}]_i$ is not dependent on extracellular Ca^{2+}

In addition to mobilizing stored intracellular Ca^{2+} via IP_3R, activation of OXTR is thought to stimulate CaV channels, thereby causing an influx of extracellular Ca^{2+} (Murtazina et al., 2011; Sanborn et al., 2005; Wray, 2007). Thus, to determine whether extracellular Ca^{2+} contributed to the OXT-induced transient increase in hfRPE $[Ca^{2+}]_i$, hfRPE cells were exposed to OXT in HR, the CaV specific inhibitor nifedipine in HR and to Ca^{2+}-free extracellular solution. (Figure 3). I found that 10 µM OXT induced an increase of 1.3 ± 0.2 µM $[Ca^{2+}]_i$ in cells tested using HR solution and 0.61 ± 0.13 µM in cells perfused with HR solution including nifedipine. Ca^{2+}-free solution was used to determine the gross effect of extracellular Ca^{2+}, including CaV channels. Stimulation of hfRPE cells in Ca^{2+}-free extracellular solution with 10 µM OXT induced a 0.69 ± 0.11 nM increase in $[Ca^{2+}]_i$ (Figure 3C). I compared the average $[Ca^{2+}]_i$ response to OXT in HR, Ca^{2+} free medium and HR-nifedipine (Figure 3D), and fit a 1st order equation for the average Ca^{2+} time to decay from peak response. Elevated Ca^{2+} returned to baseline, with time constants (τ) of 0.35 ± 0.02 (r^2 =.99), 0.34 ± 0.03 (r^2 =.99), and 0.20 ± 0.005 (r^2=.99) min for Ca^{2+}-free, nifedipine, and Ringer's solution, respectively (Figure 3E).

2-APB reduces the OXT-induced increase of hfRPE $[Ca^{2+}]_i$

In non-retinal tissues, OXTR activation by OXT is known to cause the PLC-mediated generation of IP_3, IP_3-IP_3R binding and an increase in $[Ca^{2+}]_i$ due to IP_3R-mediated mobilization of $Ca^{2+}$from intracellular stores (Arrowsmith & Wray, 2014). To determine whether the OXT-induced increase of hfRPE $[Ca^{2+}]_i$ is similarly initiated through the IP_3R-mediated mobilization,

we used the IP_3R antagonist, 2-APB. In the presence of 60 μM 2-APB we found that the Ca^{2+} response to 10 μM OXT was virtually abolished in hfRPE cells (Figure 4). Figure 4B demonstrates the significance of this inhibition by comparing the average $[Ca^{2+}]_i$ response from an entire visual field of hfRPE cells to 10 μM OXT , in the presence and absence of 60 μM 2-APB. The fold increase in $[Ca^{2+}]_i$ relative to pre-OXT baseline supports that there is a significant inhibition of OXT effect by 2-APB ($P<.0001$) (Figure 4C). While 2-APB has also been shown to inhibit TRP channels, the maintenance of a $[Ca^{2+}]_i$ response in the presence of Ca^{2+}-free solution suggests that TRP channels are not required for the OXT-mediated response, supporting that our observation that inhibition is through IP_3R.

Development of HEK-OXTR cell line

To facilitate further study of OXTR signaling, we generated a stably-transfected HEK293-OXTR cell-line. In three independent experiments, we measured intracellular $[Ca^{2+}]_i$ during stimulation with 10 μM OXT or 100 μM ATP, in a total of 947 cells. OXT increased $[Ca^{2+}]_i$ 6.0 ± 0.2 fold relative to baseline ($P<0.001$, Figure 5C). This was similar to the effect of ATP, which increased $[Ca^{2+}]_i$ by 5.6 ± 0.1 fold relative to baseline ($P<0.001$, Figure 5C). HEK293 cells not expressing OXTR were used as a negative control and displayed an increase in intracellular Ca^{2+} when stimulated with ATP, but not with OXT (Figure 5C). These observations are consistent with our work identifying OXT-OXTR signaling in hfRPE cells (Halbach et al., 2015).

Visualization of OXT-induced GPCR signaling

To support our findings in hfRPE and provide visual evidence that OXTR activation by OXT induced the PLC-mediated hydrolysis of PIP_2 to generate IP_3, we used live-cell fluorescence

imaging to visualize the production of IP_3 and DAG. GFP probes to the Plekstrin Homology domain (PH-GFP) were used to detect membrane PIP_2, and PKC-GFP was used to detect DAG, as both signaling molecules are used by the GPCR-PLC activation pathway. When HEK-OXTR cells were treated with OXT, PH-GFP fluorescence translocated from the membrane micro-environment to the cytoplasm, an indication of PIP_2 hydrolysis by PLC to form IP_3. Figure 6A is a plot of cytoplasmic fluorescence intensity measured over time in a single PH-GFP expressing cell exposed to 10 μM OXT. Immediately following OXT treatment, there was an increase in cytoplasmic fluorescence (Figure 6A, upward deflection) followed by slow return to the baseline level. On average, OXT treatment of cells resulted in a 1.2 ± 0.2 fold reversible increase of cytoplasmic fluorescence (Figure 6B, $p < 0.001$, n=35).

I performed a similar experiment using PKC-GFP transfected cells. As shown in Figure 6C, one representative cell shows cytoplasmic GFP before (Figure 6C, left panel), and after (Figure 6C, right panel) OXT treatment. During the treatment with 10 μM OXT, GFP fluorescence was noticed primarily in the membrane microenvironment and cell nucleus (Figure 6C center panel; Video). Plotting of fluorescence intensity in the cytoplasm (Figure 6D) versus time indicated a reversible decrease (Figure 6D, downward deflection) in fluorescence intensity upon treatment of HEK-OXTR cells with OXT. Measurement of the average fluorescence intensity showed that OXT treatment resulted in a decrease in the cytoplasmic fluorescence level to 0.80 ± 0.02-fold of that in non-treated cells ($p < 0.0001$, n=8) which recovered to 0.9 ± 0.03-fold upon washing of OXT (Figure 6E).

OXTR activation inhibits RPE Kir7.1 channel function

Kir7.1 channels are present in the RPE apical membrane and are regulated by membrane PIP_2 (Logothetis et al., 2007). Given the importance of Kir7.1 to RPE-Retina interaction and our demonstration of its contribution to an OXTR signaling mechanism, I was keen to test whether these two signaling pathways are connected (Pattnaik & Hughes, 2009). As the RPE cell contains a complex microenvironment that could mask the interaction between Kir7.1 and OXTR, I first used the HEK-OXTR stably transfected cell line model. An N-terminal GFP-fused Kir7.1 protein was transiently expressed. Whole cell current was recorded in bath solution, and during treatment with 100nM OXT and 20mM $BaCl_2$ or 20 mM $CsCl_2$. Figure 7A shows the time course of a whole-cell recording from a single transfected HEK-OXTR cell. A large inward current at -160mV, characteristic of Kir7.1, was subsequently reduced following OXT treatment (green bar), and almost completely blocked by Cs^{2+} (blue bar). Depolarization of the membrane was also observed (red trace) following OXT treatment in this single cell. Figure 7B is an IV plot in which I observed an average whole-cell (n=9) current of -22.0 ± 2.6 pA/pF (black trace) which was reduced to -6.6 ±0.6 pA upon treatment with OXT (Figure 7B, red trace) measured at -160 mV. This 68 ± 3% decrease in total current corresponds to a 72 ± 3 % decrease in K^+ current and was statistically significant (Figure 7F, $P<0.001$). Despite what was observed in Figure 7A, on average there was no significant alteration of membrane potential. Chinese hamster ovary cells stably expressing the muscarinic (M1) receptor GPCR were used as a positive control. These cells displayed a similar reduction in inward Kir7.1 current amplitude when exposed to the M1-receptor agonist carbachol (66% decrease; $P<0.001$ results not shown), suggesting that the inhibition is GPCR-dependent.

To validate the physiologic relevance of our results showing inhibition of Kir 7.1 by OXT in a heterologous expression system, whole-cell patch clamp recordings were performed on RPE cells freshly dissociated from mouse eye cups. An example of the morphology of selected cells can be seen in Figure 7C. In 7 cells I observed an average membrane potential of -58.7 ± 1.9 mV. As illustrated in Figure 7D, a plot of whole-cell current amplitude at -160mV shows the reduction of inward current in response to 10 µM OXT (Figure 7D, black bar). In the same figure depolarization of the cell can also be observed in response to OXT and Cs^{2+} treatment. A plot of the current-voltage curve shows the average whole cell current in HR before and after 10 µM OXT treatment (Figure 7E, n=7). The three treatment conditions show equal current at a voltage consistent with E_k (~-88 mV), further demonstrating that the observed effect is through modulation of K^+ channels. This plot demonstrated a 22 ± 2% decrease in whole cell current following OXT treatment, corresponding to a 62 ± 5% decrease in K^+ current ($p<.005$) and an average depolarization by 11.4 ± 3.3 mV ($p<.005$).

In Figure 7F, I compare the proportion of the K^+ current following OXT treatment to the K^+ current before treatment in mouse RPE (n=3), and HEK-OXTR (n=9) cells. The overexpression of OXTR and Kir7.1 compared to that in the mouse RPE cells is likely the reason for the greater decrease in current observed in HEK-OXTR cells.

Inhibition of Kir7.1 by OXT is reliant on PIP_2 hydrolysis and independent of $[Ca^{2+}]_i$

To determine whether the observed inhibition of Kir7.1 was a result of PIP_2 hydrolysis I took multiple approaches. First, HEK-OXTR cells with transient Kir7.1 eGFP expression were recorded from in the perforated patch configuration while the temperature of the bath solution was maintained at 37°C. Recording in perforated patch configuration ensures that the

intracellular environment was not disrupted by the internal solution of the pipette during whole cell recordings and maintaining a temperature of 37°C mimics physiological conditions in an attempt to create the optimal conditions for PIP_2 regeneration. These conditions allow us to accurately define the kinetics of the inhibition to determine whether it is consistent with what would be expected by PIP_2 hydrolysis. Following OXT treatment of these cells I observed a rapid inhibition of Kir7.1 current that did not exhibit any recovery over the entire period of recording (Figure 9). On average (n=6) I observed a reduction of inward current, recorded at -160mV, from -757.4 ± 148.9 pA to -255.2 ± 76.7 pA. I also observed an average depolarization from -62mV to -34mV. I fit a 1^{st} order equation for the average time to decay of inward current and observed a time constant (τ) for the inhibition of 18.4 ± 2.3 (r^2=.99) (Figure 9 B).

While the rapid inhibition is consistent with PIP_2 hydrolysis, the lack of recovery is not what would be expected from PIP_2, which should yield a gradual increase in current as the membrane population of the phospholipid are replenished. To identify whether the mechanism of inhibition is independent of PIP_2 hydrolysis entirely I performed whole cell configuration recordings on our transfected HEK-OXTR cells and utilized a non-hydrolyzable GTP analogue, GDPβS, in the internal solution to block G-protein activation and therefore the PLC mediated signaling cascade (Figure 10). In the presence of this GTP analogue I observed that the OXT mediated Kir7.1 inhibition was completely abolished with no significant alteration in I-V current profile (n=6). The absence of OXT mediated inhibition in the presence of GDPβS suggests that the effect of OXT on Kir7.1 relies on G-protein activation and the subsequent hydrolysis of PIP_2.

2.4 Discussion

Oxytocin is present in the cone photoreceptor extracellular matrix and OXTR is expressed in the adjacent RPE cells, leading me to suggest that oxytocinergic signaling may be of physiologic significance in the retina (Halbach et al., 2015). In the present study, we show that OXT increases hfRPE $[Ca^{2+}]_i$ through a GPCR-mediated mechanism whereby the OXT binding to OXTR causes downstream activation of PLC and PIP_2 hydrolysis. In addition, I have shown that heterologously expressed Kir7.1 channels in HEK-OXTR cells, as well as endogenous mouse RPE cell Kir7.1 channels are subject to OXTR inhibition. I propose a model by which OXT-OXTR signaling between photoreceptor and RPE cells may also occur *in vivo*, as summarized in Figure 8.

The dose-response curve of $[Ca^{2+}]_i$ induced by OXT in hfRPE exhibited a sigmoidal profile similar to previously reported dose-response curves for OXT, indicating that OXT-OXTR signaling may be of physiologic relevance (Evans et al., 1997; Sinclair et al., 2010). In the present study, hfRPE had a reported EC_{50} of approximately 341 nM OXT. Previously reported K_d values for OXTR range from 0.96 to 215 nM OXT (Crankshaw et al., 1978; Fahrenholz et al., 1995; Gimpl et al., 1997; Pliska et al., 1986; Quehenberger et al., 1992). Within this range, however, there exist distinct high- and low-affinity subgroups of OXTR. As demonstrated by Gimpl and colleagues (1995), the affinity state of OXTR is cholesterol-dependent, such that addition of exogenous cholesterol can promote a shift of about 20% of the low affinity OXTR to an approximately 200-fold higher affinity state (K_d = 0.96 nM) (Gimpl et al., 1995). Our finding of an EC_{50} of 341 nM OXT in hfRPE suggests that OXTR was in a low affinity state under our experimental conditions. Variable OXTR K_d values have been shown with alterations in culture media cholesterol, serum,

and Mg^{2+} concentrations (Copland et al., 1999; Gimpl et al., 2000; Pliska & Kohlhauf Albertin, 1991; Soloff & Fields, 1989). The hfRPE cells were cultured in non-FBS containing media and thus did not contain adequate exogenous cholesterol to promote the high affinity variant of the OXTR. It is also true that RPE cells are highly polarized cells with a distinct plasma-membrane composition when compared to other epithelial cells, and thus they may demonstrate sensitivity to OXT that could be unique (Strauss, 2005).

Although OXT likely increases hfRPE $[Ca^{2+}]_i$ by binding and activating the OXTR, OXT also has some affinity, albeit low, for the vasopressin V_{1a} receptor, which when activated can also stimulate an increase in $[Ca^{2+}]_i$ (Friedman et al., 1991; Sermasi & Coote, 1994). In addition to being highly homologous and closely related to OXTR, vasopressin V_{1a} is known to be present and functional in the RPE. We have shown previously that the OXT-induced increase in hfRPE $[Ca^{2+}]_i$ was reduced by 87% in the presence of 500 nM of the OXTR-specific antagonist, L-371,257, providing strong evidence that the OXT-induced increase in hfRPE $[Ca^{2+}]_i$ was mediated through the OXTR, even when a supraphysiologic dose (6µM) was used (Halbach et al., 2015). The other specific OXTR antagonist, OTA, in this paper also significantly reduced the Ca^{2+} response to OXT (10 µM), further supporting the activation of OXTR in the RPE. Based on these finding, I used 10µM OXT to ensure maximal activation of cells during perfusion experiments.

Studies in the myometrium and OXTR-COSM6 cells have demonstrated activation of a Gßγ-mediated pathway as a consequence of GPCR activation, resulting in increased ERK1/2 phosphorylation (Gimpl & Fahrenholz, 2001; Mitchell, 2001; Zhong et al., 2003). This suggests that OXT may be stimulating the increase in $[Ca^{2+}]_i$ through mechanisms other than the $G\alpha_q$-

mediated activation of PLC. Our data, however, support the $G\alpha_q$-mediated mechanism of oxytocinergic signaling in the RPE (Figure 8). We propose that binding of OXT from the retina leads to OXTR-mediated hydrolysis of the RPE membrane PIP_2 by PLC and generates two cellular responses: 1) the inhibition of Kir7.1 channels in the RPE apical membrane, and 2) IP_3 binding to the IP_3R that causes release of Ca^{2+} from intracellular stores. The effect is abolished in the presence of 2-APB, in agreement with published work on OXTR signaling in myenteric neurons (Che et al., 2012). 2-APB has also been described as a TRPC inhibitor, however, the sustained Ca^{2+} response in Ca^{2+}-free solution I have demonstrated shows that the 2-APB mediated inhibition demonstrated found in our system is through the IP_3R (Lievremont et al., 2005).

The association of OXTR activation with extracellular Ca^{2+} influx through CaV is somewhat controversial in uterine function, the best characterized model of OXT signaling to-date. In my RPE work, the rapid initial OXT-induced increase in $[Ca^{2+}]_i$ occurs consistently in the presence of nifedipine, as well as Ca^{2+}-free solution, demonstrating nifedipine insensitivity in agreement with work published by Inoue and colleagues (Arrowsmith & Wray, 2014; Inoue et al., 1992). However, I observed a reduction in the amplitude of the Ca^{2+} response from HR to nifedipine and Ca^{2+}-free solution, which corresponds to an increase in time constant (Figure 3D-E). This suggests that extracellular calcium is involved in part in the OXT-mediated response after the initial IP_3-mediated Ca^{2+} release. I suggest that this response is likely mediated by voltage-activated Ca^{2+} channels, given the lack of distinction between the responses observed in Ca^{2+}-free solution and nifedipine.

Utilizing HEK-OXTR cells exposed to OXT, we were able to demonstrate by live cell fluorescence imaging that PLC hydrolysis of PIP_2 is a source of IP_3 and DAG using PH-GFP and PKC-GFP, supporting our observations and hypothesis about its role in the RPE. Using this heterologous system I also investigated whether a loss of PIP_2 affects direct gating of RPE Kir7.1 channels (Pattnaik & Hughes, 2009). In development of our Kir7.1 eGFP, we generated both N-terminal and C-terminal fused constructs. The N-terminal fused construct exhibited measurable current whereas the C-terminal fused construct did not, suggesting that the C-terminal GFP, but not the N-terminal GFP, interfered with Kir7.1 channel function (Pattnaik et al., 2015). The activation of OXTR with OXT therefore inhibits Kir7.1 channel in both HEK-OXTR cells and the mouse RPE and the N-terminal GFP does not interfere with the cellular signaling events explored in this study.

All Kir channels demonstrate PIP binding to the same general cytoplasmic location; however, the affinity of Kir channels for PIP_2 and other PIP groups is determined by differences in the amino acid sequence mediating interaction with the lipid tail group (D'Avanzo et al., 2013; Rohacs et al., 1999). Relative to other Kir channels, Kir 7.1 has a weak affinity for PIP_2 which results in a more pronounced inhibition by PIP_2 hydrolysis compared to other Kir channels (Du et al., 2004; Pattnaik & Hughes, 2009). I observed an OXT-mediated decrease in the Kir7.1 channel current by 15.5 pA/pF or 68±3% in HEK-OXTR cells (Figure 7B) and a smaller but still significant decrease in whole cell current in mouse RPE cells. After removing non-K^+ current by subtracting the Cs^{2+}-insensitive component, the percent inhibition between the two cell types was identical, with the remaining difference likely due to overexpression of Kir7.1 in the HEK-OXTR cells (Figure 7E). Furthermore, mouse RPE was significantly depolarized in

response to OXT treatment. The RPE membrane potential regulates the ion and waste transport functions of the RPE, making oxytocin a potential regulator of outer retina function. In view of the discovery by Ghamari-Langroudi and colleagues (2015) that Kir7.1 can be inhibited by a GPCR independently of G-protein coupling, our future studies will determine if this also occurs in OXT-mediated OXTR activation in the RPE (Ghamari-Langroudi et al., 2015). Given the recent discovery of a role for Kir7.1 in the initiation of uterine contractions by McCloskey and colleagues (2014), I propose that the signaling mechanism discovered in our study is also involved in parturition (McCloskey et al., 2014).

It has recently been demonstrated that Kir7.1 can be inhibited by GPCRs through a G-protein independent mechanism in MC4R neurons (Ghamari-Langroudi et al., 2015). Given this revelation, and a lack of recovery from inhibition observed after OXT treatment, I set out to determine whether a similar mechanism could be at play in our recordings. Perforated patch recordings were done at 37˚C to both ensure that intracellular mechanisms were not disrupted by the whole cell recording and that temperatures were optimal to support recovery of PIP_2. In spite of these efforts, the lack of current recovery persisted, suggesting that an alternate mechanism of inhibition may be at play. I also utilized a non-hydrolyzable analogue for GTP, GDPβS, to block G-protein activation and prevent the PLC mediated hydrolysis of PIP_2 in response to OXTR activation by OXT. In the presence of GDPβS I observed a complete loss of OXT mediated current inhibition. This demonstrates that, unlike the direct inhibition of Kir7.1 by MC4R, the OXT mediated inhibition is reliant on G-protein coupled signaling and the hydrolysis of PIP_2. The response is not dependent on $[Ca^{2+}]_i$ because, while Ca^{2+} can impact Kir7.1 current, $[Ca^{2+}]_i$ is clamped by EGTA during whole cell recordings so the inhibition I

observe is not a result of IP_3 mediated Ca^{2+} release. Our data therefore demonstrates the necessity of PLC mediated PIP_2 hydrolysis on Kir7.1 inhibition, however it does not explain the lack of recovery in current that I observe. One possible explanation lies with the internalization of OXTR. OXTR exhibits internalization following exposure to OXT in a clathrin-dependent manner and sequence analysis of Kir7.1 protein reveals the presence of the C-terminal sequence (YSHI [244-247 aa]) that resembles sequence motifs that favor clathrin coated vesicles (Kumar & Pattnaik, 2014; Smith et al., 2006). The possibility therefore exists that the clathrin mediated internalization of OXTR also results in the internalization of Kir7.1 and the long-term loss of current. While this hypothesis needs to be tested, it would not be the first example of a Kir internalization through clathrin-dependent mechanisms, as Kir1.1 (ROMK) is retrieved from the cell surface in the same manner as a result of an NPXY motif on its C-terminal domain (Zeng et al., 2002). Furthermore, Kir internalization has also been demonstrated to occur in a caveolin-dependent manner, mediated by the activation of PKC, suggesting that there are multiple potential pathways for OXTR to induce channel internalization (Jiao et al., 2008). Regardless of the mechanism of prolonged inhibition of Kir7.1 by OXT, the implications for the RPE-retina interface are interesting. Prolonged depolarization of the RPE could imply a role of OXT in regulating long term processes, like phagocytosis. The effect of OXT on the RPE through Kir7.1 clearly requires further study.

In summary, I have provided evidence of the following: 1) the OXT-induced $[Ca^{2+}]_i$ response is not dependent on extracellular Ca^{2+}, 2) the OXT-induced $[Ca^{2+}]_i$ response is not blocked by the CaV blocker nifedipine, and 3) the IP_3R inhibitor 2-APB inhibits the OXT-mediated $[Ca^{2+}]_i$ increase. Using a model in which OXTR is stably expressed in HEK-OXTR cells, I

have demonstrated an OXT-induced $[Ca^{2+}]_i$ increase, associated with PIP_2 hydrolysis through PH-GFP and PKC-GFP can be visualized in response to OXT. I have also shown that Kir7.1 is inhibited by OXT in both heterologous HEK-OXTR cells and in physiological RPE cells isolated from the mouse eye, resulting in depolarization of the RPE membrane potential and that this inhibition is G-protein dependent and prolonged. Control of membrane potential through Kir7.1 regulates the ion and waste transport functions of the RPE, and supports our hypothesis that oxytocin can influence outer retina function.

Statement of conflicts of interest

The authors declare that they have no conflicts of interest.

Author Contributions: Study concept and design: all authors. Acquisition, analysis and interpretation of data: NY, PJH, MC, BRP. Drafting of manuscript: NY, PJH, MC, DMP, BRP. Critical revision of manuscript: NY, IB, DMP, BRP. Final approval: DMP, BRP. Study supervision: BRP.

Acknowledgments

We thank Dr. Barbara Sanborn (Colorado State University) for the gift of the OXTR plasmid and for helpful discussion, Dr. Thomas Balla (NICHD, NIH) for the gift of PH-GFP, Dr. Maurice Manning (University of Toledo) for providing the selective oxytocin receptor antagonist and Dr. Tobias Meyer (Stanford) for the gift of PKC-GFP expression plasmids. We would also like to thank Dr. Jens Eickhoff (University of Wisconsin-Madison) for the help he provided with our calcium imaging statistics. We acknowledge members of the Pillers-Pattnaik research team for

helpful discussion and exchange of ideas. These studies were supported by the Meriter Foundation (BRP), McPherson Eye Research Institute M.D. Mathews Research Professorship (BRP), and the University of Wisconsin Department of Pediatrics (DMP, BRP). BRP is supported by NIH grant EY24995, and a core grant P30EY16665.

2.5 Tables and Figures

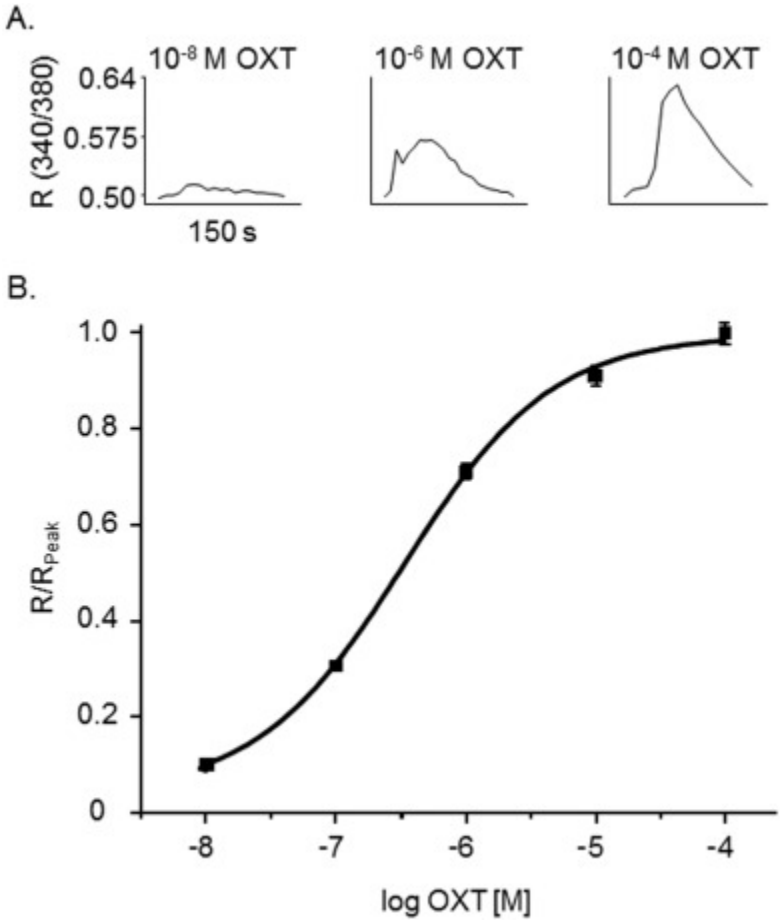

Figure 1: OXT activation of OXTR in hfRPE cells. (A) Representative traces of individual hfRPE cells during 0.01, 1, or 100 µM OXT bath solution showing a change in R (340/380). (B) OXT-activated increase in intracellular Ca2+-response curve normalized (R/Rpeak) to the average peak R (340/380), 0.18 ± 0.01, acquired at 100 µM OXT as a function of OXT concentration. Scatter plots represent the average of five experiments (n=150 cells for each dose, 0.01, 0.1, 1,

10, and 100 µMOXT) and are reported as mean ± SEM. The curve shown is the best fit of the data using the Hill equation. Values obtained for EC50 and Hill coefficient were 341 nM and 0.77± 0.07, respectively.

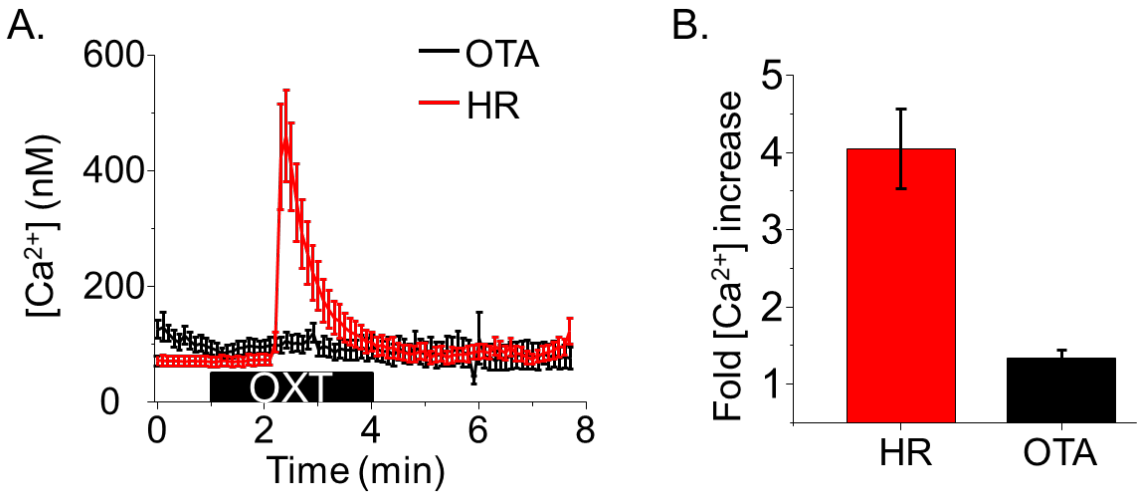

Figure 2: OXT mediated calcium response is specifically through OXTR. (A) Average response from all cells in a visual field on a coverslip incubated with OTA or HR only. (B) Average fold increase in calcium in HR (n=39 ROI / 2 coverslips) or after OTA incubation (n=55 ROI / 3 coverslips) ($P<0.005$).

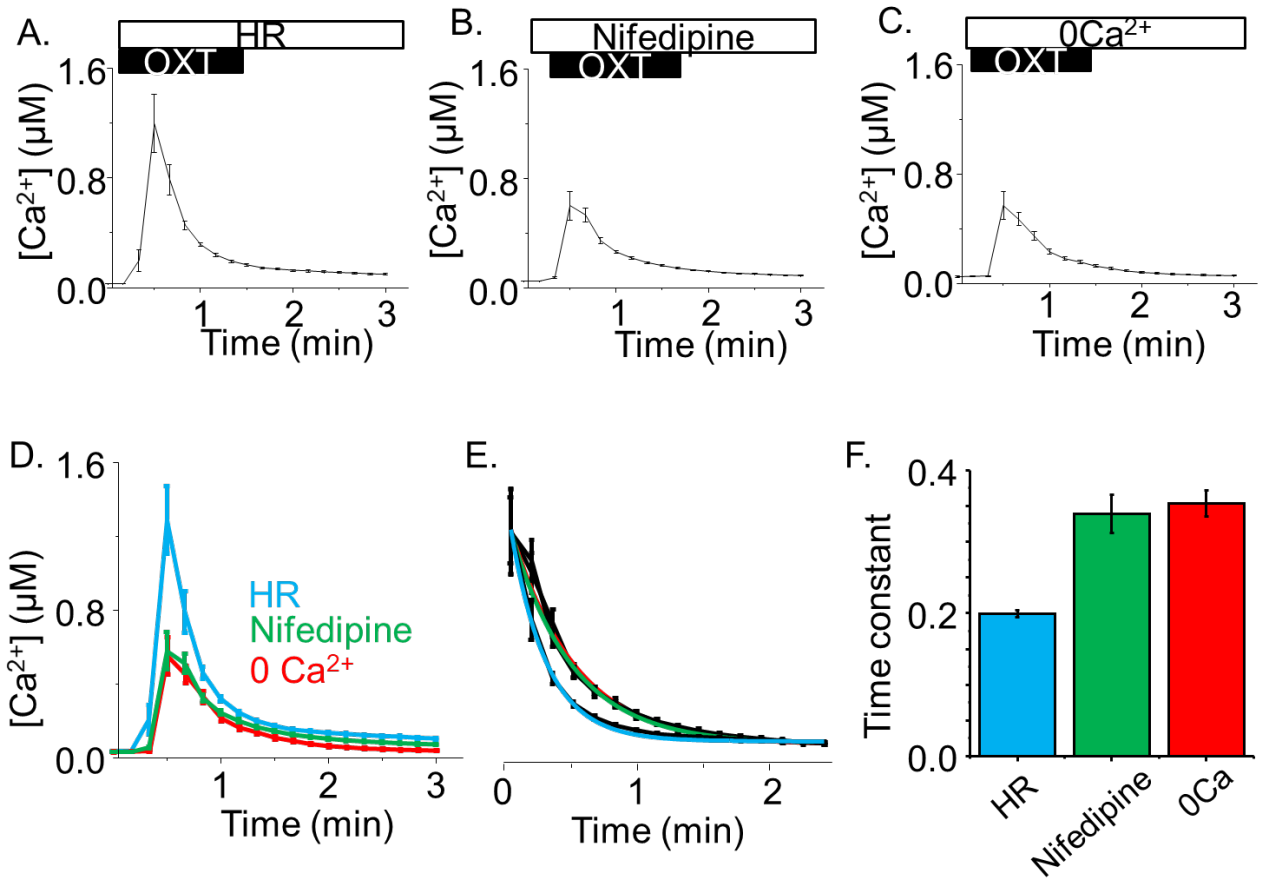

Figure 3: Effect of $[Ca^{2+}]_{ec}$ on hfRPE Ca^{2+} response to OXT (A) Average time course of hfRPE $[Ca^{2+}]_i$ in response to OXT treatment during incubation with HR solution (n=79 ROI / 2 coverslips). (B) Average time course of $[Ca^{2+}]_i$ in response to OXT treatment during incubation with nifedipine (n=158 ROI / 3 coverslips). (C) Average time course of $[Ca^{2+}]_i$ in response to OXT treatment during incubation with 0 Ca^{2+} solution (n=174 ROI / 4 coverslips). (D) Recordings in all three conditions aligned by their pre-treatment baseline to allow comparison of rise time and amplitude. (E) Rate of decay of each treatment, normalized to HR peak with exponential fit included in color. (F) Time constant for decay rate in the presence of these three treatments.

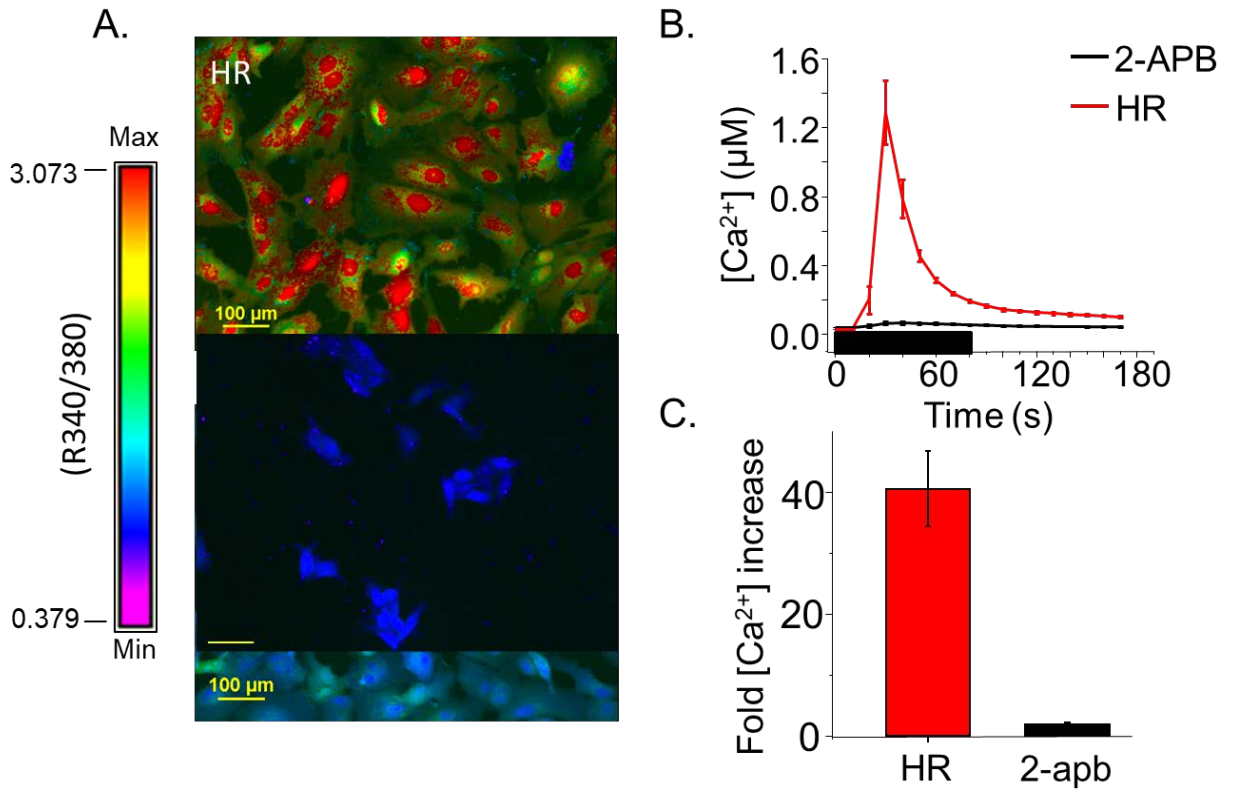

Figure 4: hfRPE OXT response is inhibited by the IP_3R antagonist, 2-APB. (A) Example of Ca^{2+} response to OXT in HR solution compared to OXT response in 2-APB treated cells. Color spectrum with max and min R (340/390) used to calculate $[Ca^{2+}]_i$ provided. (B) An average trace taken from an entire (20X) visual field of hfRPE cells showing the change in $[Ca^{2+}]_i$ when stimulated with 10 µM OXT in HR (pink) and 10 µM OXT in 60µM 2-APB (black). (C) Fold increase in $[Ca^{2+}]_i$ after 10 µM OXT treatment in HR (black) or 60µM 2-APB (red), relative to baseline taken by averaging five points prior to treatment. This plot demonstrates a significant inhibition ($P<.0001$) in the Ca^{2+} response in hfRPE cells following treatment with 2-APB.

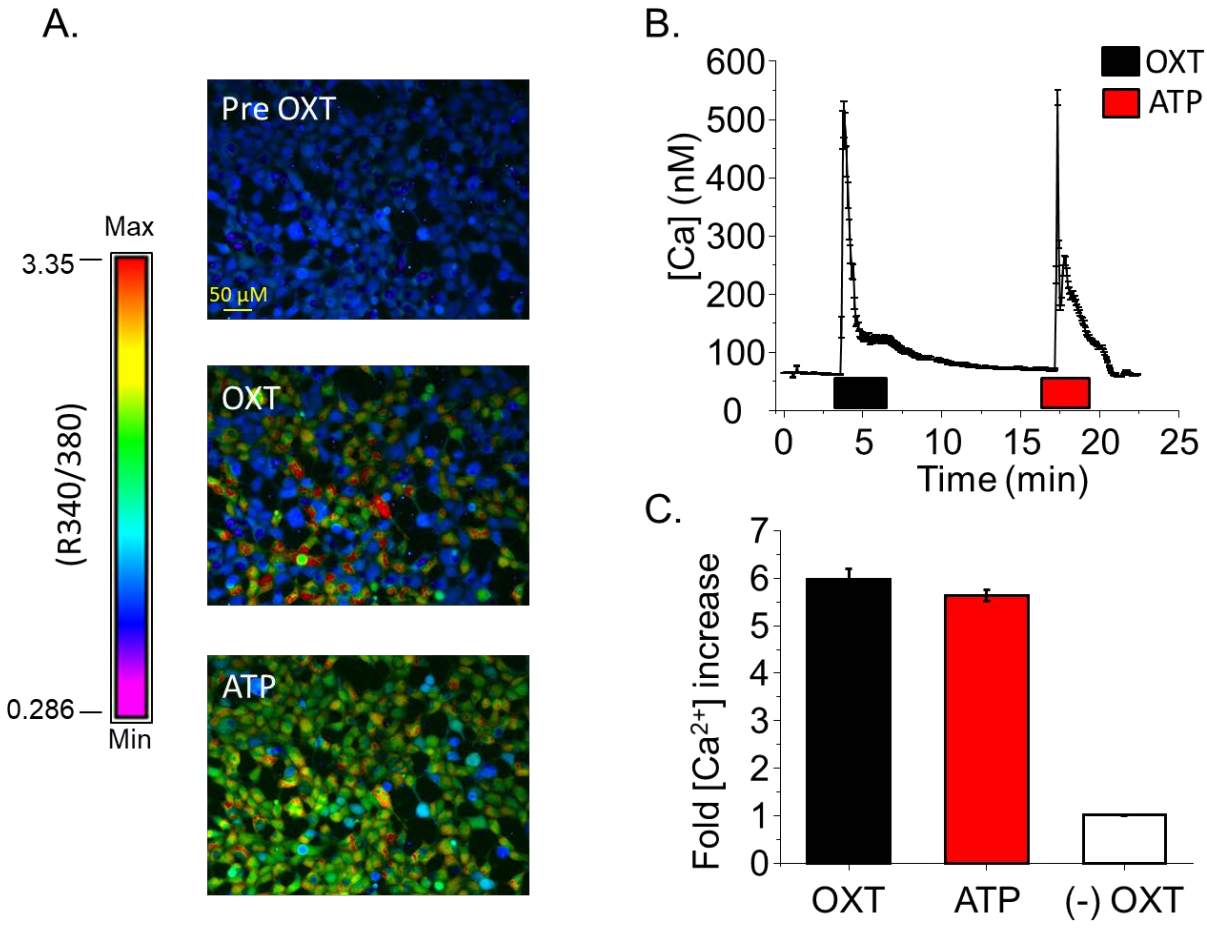

Figure 5: The $[Ca^{2+}]_i$ response upon OXT stimulation of HEK293-OXTR cells. (A) Representative images demonstrating $[Ca^{2+}]_i$ response to OXT and ATP. Color spectrum with max and min R (340/390) used to calculate $[Ca^{2+}]_i$ provided. (B) An average time course, from one coverslip, of change in $[Ca^{2+}]_i$ when stimulated with 10 µM OXT or 100 µM ATP. Horizontal bars indicate duration of agonist application. (C) Average fold increase in $[Ca^{2+}]_i$ in response to OXT or ATP taken from three independent experiments (n=947) HEK293 cells without OXTR expression are used as a negative control for OXT mediated $[Ca^{2+}]_i$ response (n=139).

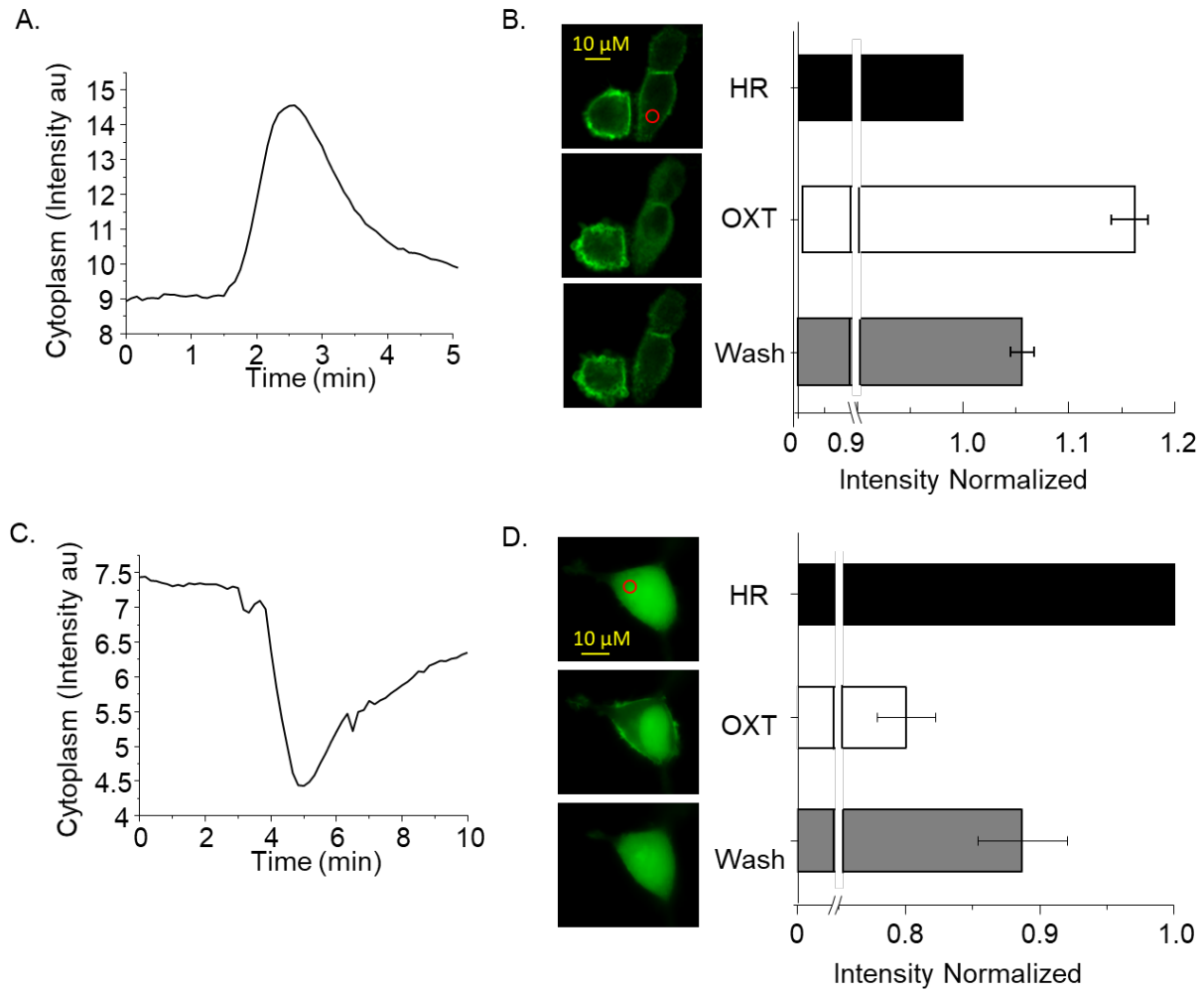

Figure 6: OXT activation of OXTR results in PIP2 hydrolysis in HEK-OXTR cells. (A) Representative GFP fluorescence time course within the cytoplasmic region of interest (ROI) shows that OXTR receptor activation in the presence of 6 µM OXT (horizontal bar) induced a translocation of the PIP2 indicator PH-GFP from the plasma membrane to the cytosol that was completely reversed upon removal of OXT. (B) The average of normalized fluorescence intensity change within the cytoplasmic domain as shown in the cell in 5A by OXT treatment. (C) The images of PKC-GFP (indicator of DAG) expressing cell shown were recorded at time 0 (left panel before), 5 (middle panel during) and 10 (right panel after) min during the treatment of OXT. (D) Time course of fluorescence intensity within the cytoplasmic ROI of cell in C showing a decrease in GFP fluorescence during treatment with OXT (horizontal bar). (E) Average plot of normalized fluorescence intensity values within the cytoplasmic domain from three experiments and reported as mean ± SEM.

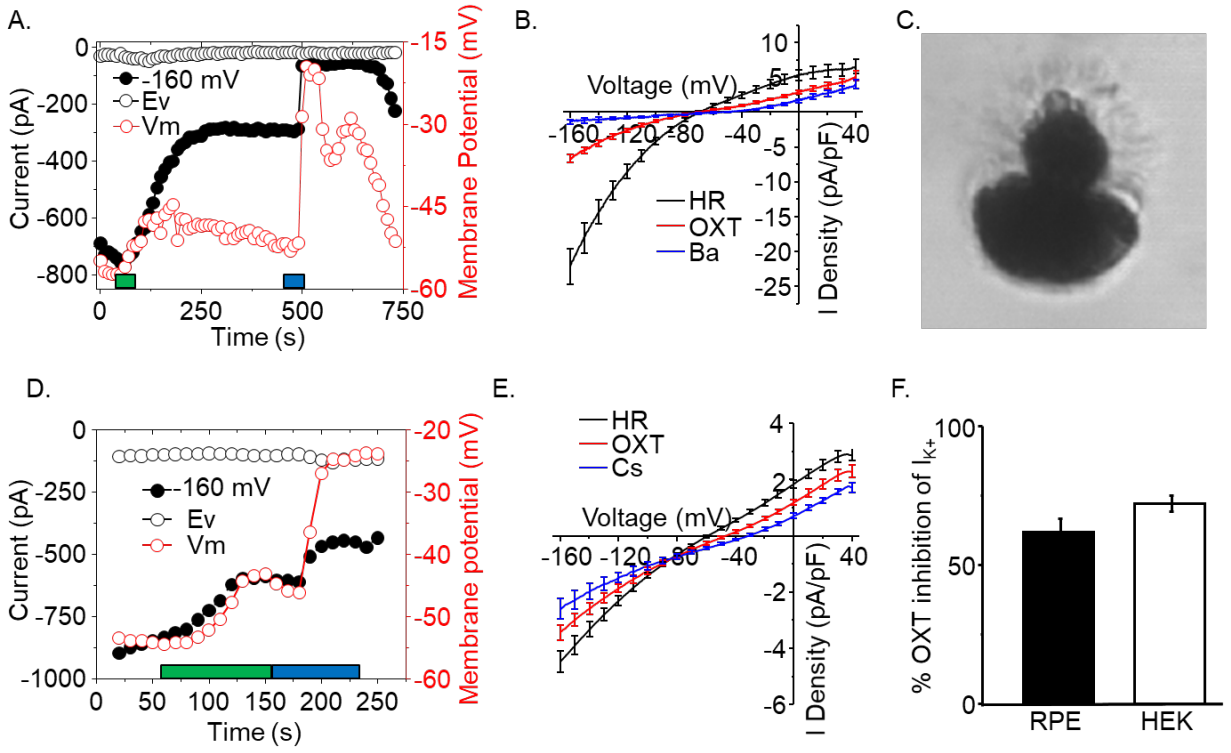

Figure 7: OXT activation of OXTR inhibits Kir7.1 channel. (A) Representative GFP fluorescence time course within the cytoplasmic region of interest (ROI) shows that OXTR receptor activation in the presence of 6 µM OXT (horizontal bar) induced a translocation of the PIP2 indicator PH-GFP from the plasma membrane to the cytosol that was completely reversed upon removal of OXT. (B) The average of normalized fluorescence intensity change within the cytoplasmic domain as shown in the cell in 5A by OXT treatment. (C) The images of PKC-GFP (indicator of DAG) expressing cell shown were recorded at time 0 (left panel before), 5 (middle panel during) and 10 (right panel after) min during the treatment of OXT. (D) Time course of fluorescence intensity within the cytoplasmic ROI of cell in C showing a decrease in GFP fluorescence during treatment with OXT (horizontal bar). (E) Average plot of normalized fluorescence intensity values within the cytoplasmic domain from three experiments and reported as mean ± SEM.

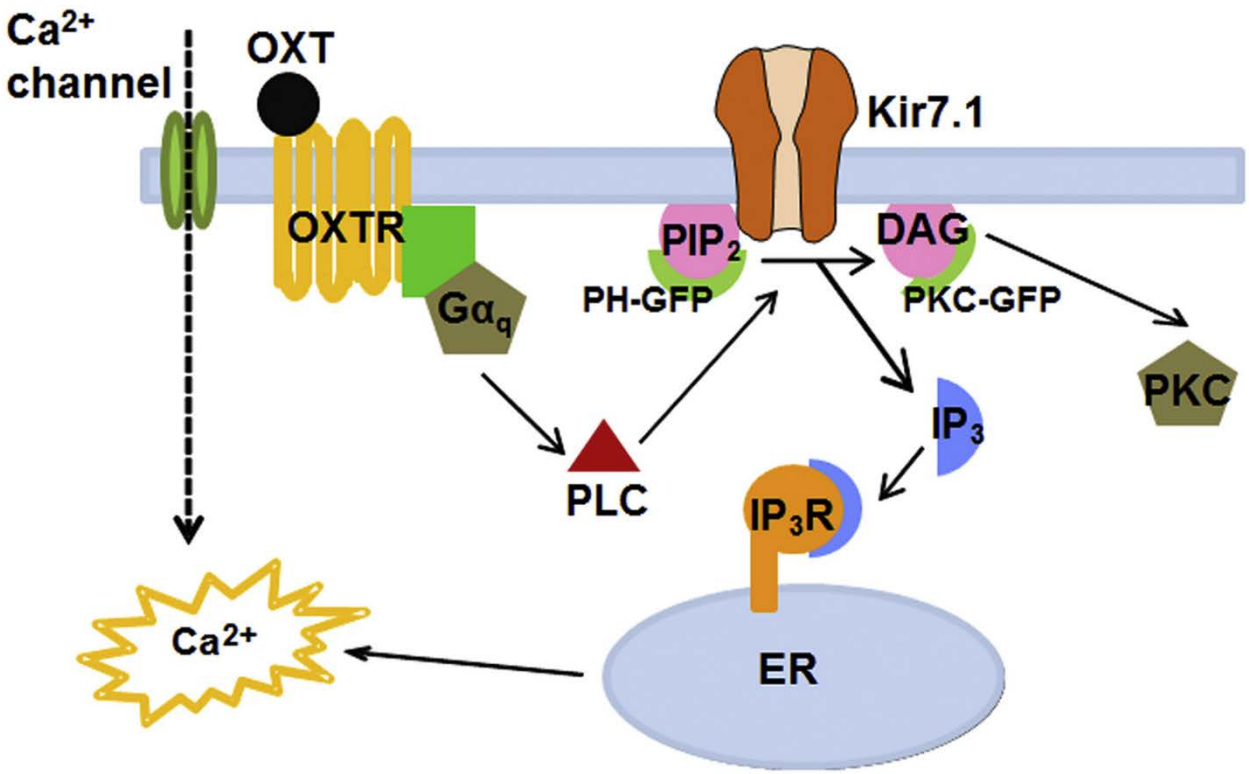

Figure 8: Summary of our findings regarding OXT-OXTR initiated cellular signaling events in the RPE. Binding of OXT ligand, either from cone photoreceptors or choroidal vasculature, to OXTR receptor in the RPE causes cytoplasmic membrane leaflet PIP2 to hydrolyze to IP3 and DAG. PIP2 hydrolysis inhibits RPE Kir7.1 channel to depolarize the membrane potential while IP3 binding to its receptor leads to the increase in cytoplasmic Ca2 +. These transient intracellular signaling responses neither involve Ca2 + channels nor does extracellular Ca2 + influence them in any substantive way

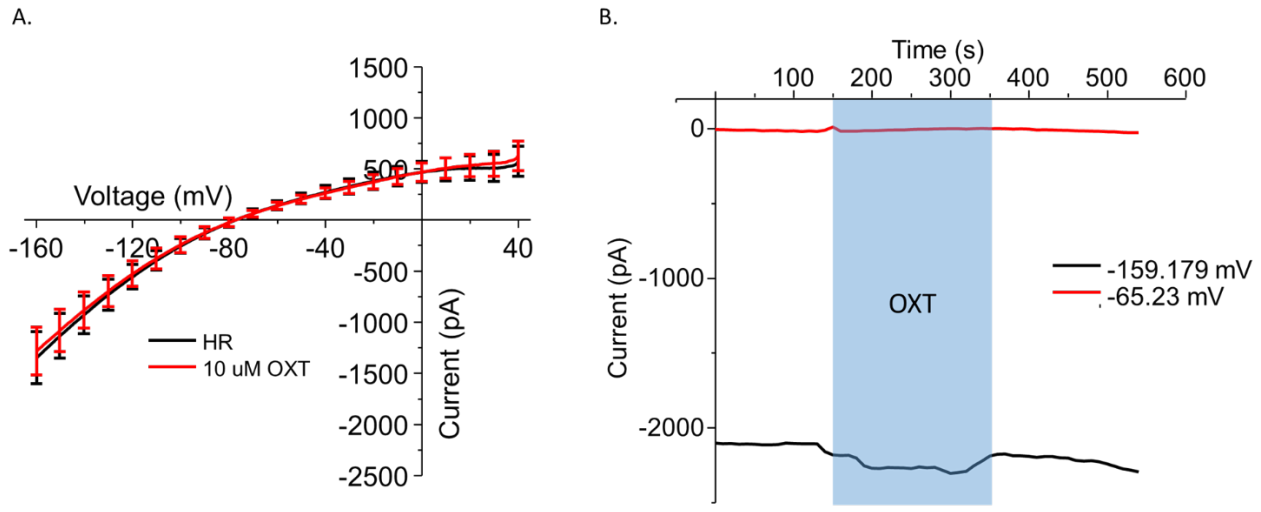

Figure 9: Kir7.1 inhibition is blocked by internal addition of GDPβS. (A) Average plot of current observed during RAMP protocol prior to 10 µM OXT treatment (black) and after treatment (red). There was no significant alteration in current in the presence of GDPβS ($P>0.05$; n=6). (B) Representative time-course of current during OXT treatment in the presence of GDPβS. Current observed during RAMP protocol at -160mV (black) and -65 mV (red) is represented. OXT treatment duration is shown in blue.

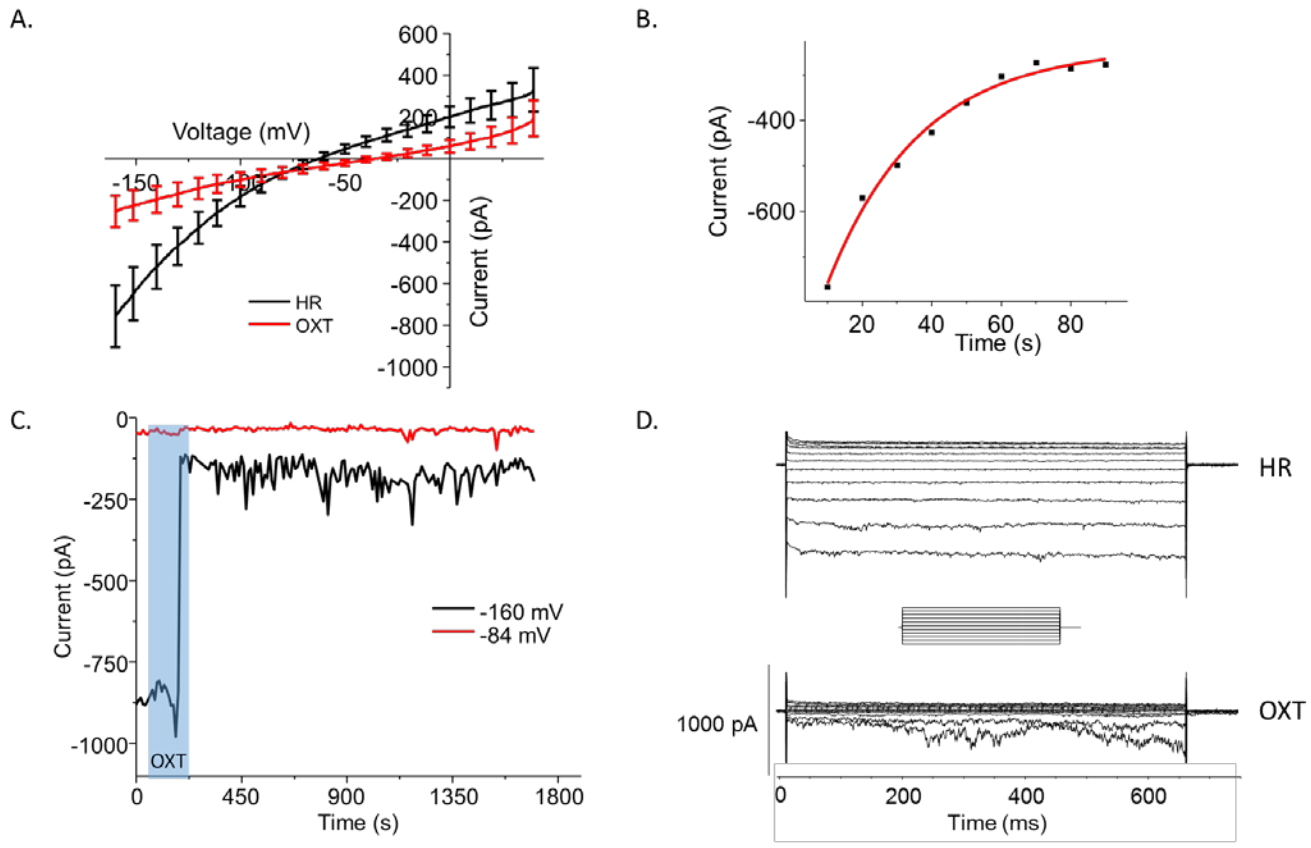

Figure 10: Perforated patch recordings of OXTR inhibition of Kir7.1 in HEK-OXTR cells. (A) I-V plot of average current during voltage RAMP from 40 mV to -160 mV. Current observed prior to OXT treatment (black) exhibits inward rectification characteristic of Kir channels and has a resting membrane potential of -62mV. Following treatment with 10 µM OXT current was significantly inhibited (red) ($P<0.05$; n=6) and there was an average depolarization to a resting membrane potential of -35 mV. (B) The time course of current inhibition in response to OXT, determined by plotting the average current values during inhibition and fitting an exponential curve. The time constant of this inhibition (tau) was 18.4. (C) Representative time-course of OXT inhibition of Kir7.1. Current observed during RAMP protocol at -160mV (black) and -84 mV (red) is represented. Duration of OXT treatment is represented with blue bar. Inhibition persisted throughout recording, exhibiting no signs of recovery, although there was fluctuation in current at -160mV. (D) STEP recordings from the same cell represented in C. 10mV steps, taken from 40 to -160mV, are shown prior to 10 µM OXT treatment (HR) and after OXT treatment (OXT).

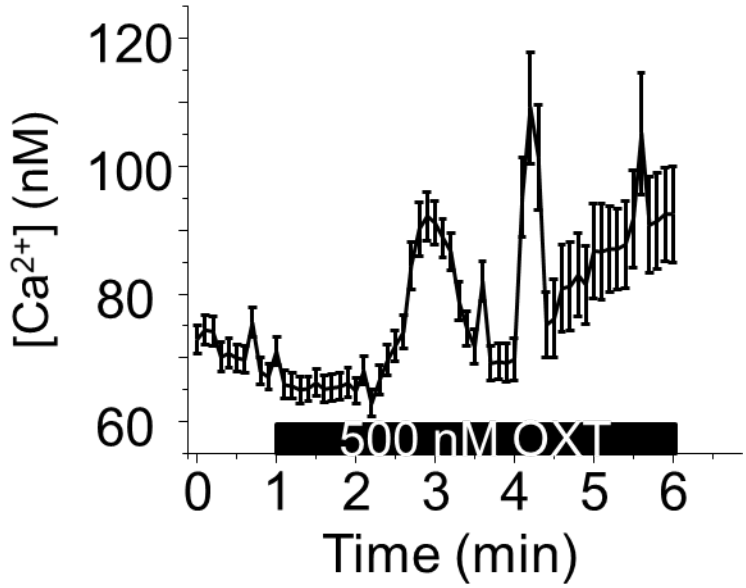

Figure 11. 500 nM OXT elicits a Ca^{2+} response in hRPE cells (n=42 ROI).

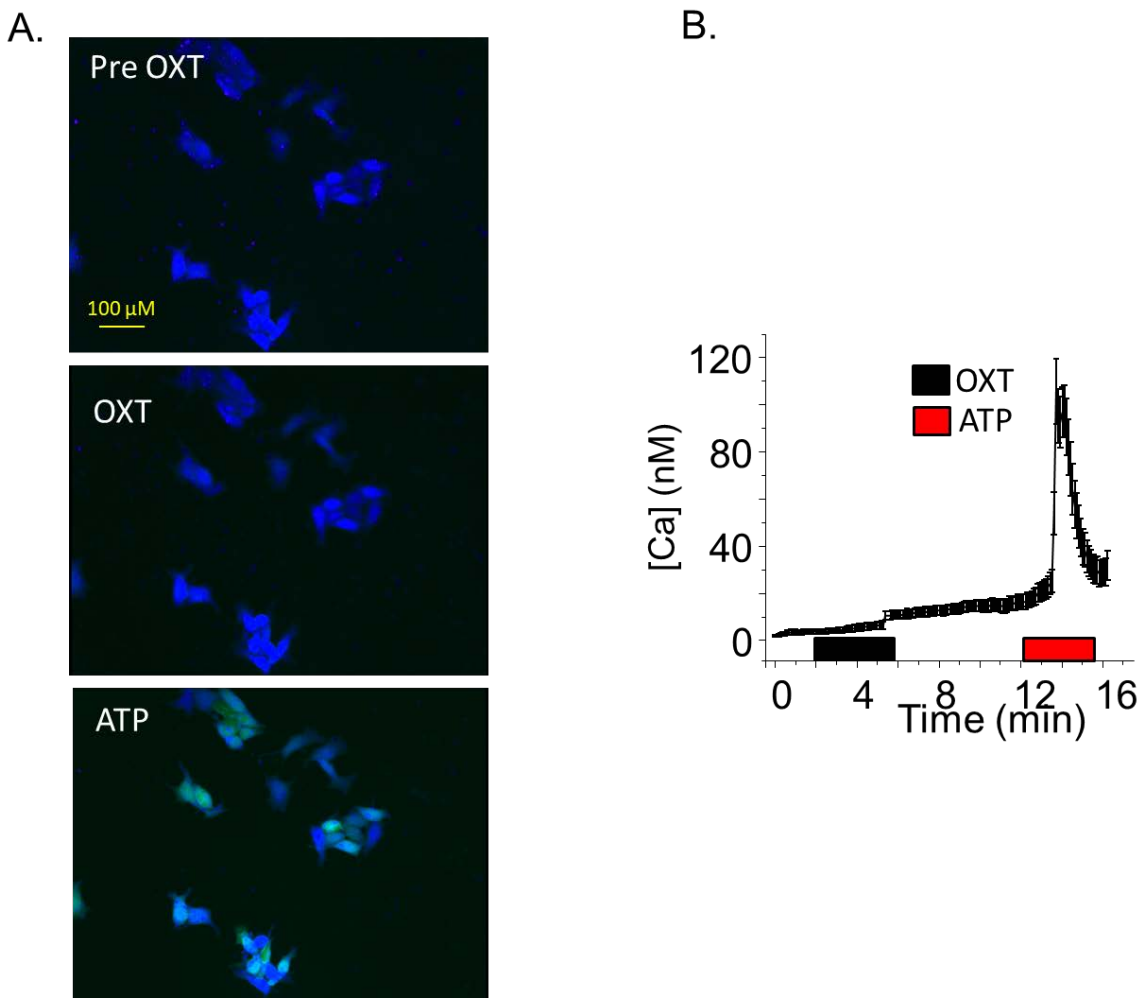

Figure 12. Control HEK cells do not respond to OXT treatment. (A) HEK cells without expressing OXTR, when treated with OXT (middle panel), showed no increase in intracellular Ca2 +. These cells responded normally to application of ATP (lower panel). (B) Average response of HEK cells to OXT and ATP during 15 min of experiment. Data is presented as mean ± SEM.

Chapter 3: Oxytocin Receptor and Retinal Angiogenesis

Nathaniel York[1,3,6], De-Ann M. Pillers[2-4], Nader Sheibani[5,6], Bikash R. Pattnaik[3,5,6]

From the [1]Endocrinology-Reproductive Physiology Program, the [2]Division of Neonatology& Newborn Nursery, the [3]Departments of Pediatrics, [4]Medical Genetics, [5]Ophthalmology &Visual Sciences, and [6]the McPherson Eye Research Institute, the University of Wisconsin-Madison, WI 53715

Abstract: Retinopathy of prematurity (ROP) is a disorder that is caused by abnormal growth of blood vessels in the retina. Understanding the pathogenesis of this disease is key to understanding how to treat it. OXT has previously been shown to influence blood vessel proliferation and its receptor has been found to be in the RPE, which forms the blood-retina barrier and plays an important role in maintaining normal vascular growth (Dawson et al., 1999; Nishijima et al., 2007; Sakamoto et al., 1995). OXT levels are tightly controlled during pregnancy, with levels increasing significantly from 32-40 weeks while almost all infants born with ROP have a gestational age of less than 31 weeks, which suggests that OXT has the potential to be involved in the pathogenesis of ROP. In this study I have explored this possibility, utilizing human fetal RPE, as well as murine RPE, to determine the effect of OXT stimulation on the expression of genes associated with angiogenesis. Additionally, I explored the impact of OXT on the secretion of VEGF by the RPE and utilized functional assays of angiogenesis to determine the angiogenic potential of conditioned media from RPE treated with OXT. I have determined that OXT does not alter expression of the primary genes associated with the pathogenesis of ROP but that it does have a small influence on the secretion of VEGF. Functional assays of angiogenic capacity suggest, however, that OXT does not have the ability to drive angiogenesis through its action on the RPE alone.

Key Words: Retinopathy of Prematurity, VEGF, Angiogenesis, Oxytocin, RPE, Oxytocin Receptor, Retina

3.1 Introduction

Retinopathy of prematurity is the leading cause of pediatric blindness in the world, with its severity increasing with decreasing gestational age. In what can be described as the 1st epidemic of ROP, a rise in instances was associated with the administration of high O_2 on premature infants. Following the institution of regulations limiting the percent O_2 that could be administered, the frequency of ROP declined. However, in the last 30 years we have seen an increase in cases, which correlates with an increased survival rate of low birth-weight infants (Shah et al., 2016). Given the multifaceted origin of the disease, this "2nd" epidemic of ROP suggests the possibility of an important mediator of angiogenesis that these infants of lower gestational age are not yet exposed to. While the pathogenesis of and history of ROP are discussed in more detail in **chapter 1**, here I explore whether OXT could play the role of this mediator.

The timeline of OXTs production correlates with this "2nd" epidemic of ROP, as fetal hypothalamic production of the peptide is significantly increased following 30 weeks of gestation; therefore depriving infants born prior to that time point of exposure to the peptide (Schubert et al., 1981). OXT mediation of angiogenesis is not completely novel, it has been shown to mediate human uterine vascular endothelial cell proliferation and migration (Cattaneo et al., 2008). In support of this hypothesis, early preliminary data from our lab suggested that OXT treatment of human fetal RPE induced an increase in expression of VEGF (Halbach, 2013). Additionally, I have demonstrated that OXT not only induces a rise in intracellular Ca^{2+} through the hydrolysis of PIP_2 in the RPE but it can also inhibit Kir7.1. Both effects have the potential to modulate the secretion of critical growth factors, including VEGF,

as a result of the L-type Ca^{2+} channels that can regulate growth factor release (Rosenthal et al., 2007). These channels are sensitive to membrane depolarization as well as IP_3/Ca^{2+} signaling due to their regulation by $pp60^{c\text{-}src,}$, a tyrosine kinase activated by this signaling that can stimulate these Ca^{2+} channels, increasing current and inducing growth factor release (Strauss et al., 1997). As a result, I hypothesize that OXT can influence the release of low levels of VEGF and other angiogenic factors from the RPE, providing a protective effect against ROP by protecting against the O_2 mediated inhibition of angiogenesis.

In this study, I utilized human fetal RPE (hfRPE) and isolated mouse RPE to determine whether OXT can influence angiogenesis *in vitro*. To demonstrate this influence, I have looked at the effect of OXT expression of 88 genes associated with angiogenesis as well as the secretion of VEGF, the major growth factor responsible for ROP. Additionally, I utilized two assays of angiogenesis, the migration and tube formation assays, to determine whether conditioned media from OXT treated RPE have a significant impact on vascular homeostasis, *in vitro*. In total, I found that OXT does not likely influence angiogenesis through the RPE. While I did not observe an alteration in the expression of major genes associated with ROP, I did observe some alterations in angiogenic genes. Additionally, I observed an increase in the secretion of VEGF to the apical compartment of our transwells. However, I did not observe any significant change in capillary morphogenesis or endothelial cell migration. These data therefore suggest that OXT has the potential to influence angiogenesis, through VEGF secretion or alteration of other angiogenic genes, but that it does not appear to be able to alter retinal endothelial cell growth through its action in the RPE.

3.2 Methods

Reagents

All chemical reagents were purchased from Sigma-Aldrich (Sigma-Aldrich, St. Louis, MO), Thermo Fisher Scientific (Thermo Fisher Scientific, Waltham, MA), or Gibco (Grand Island, NY), unless otherwise specified.

Cell Culture

Passage 1-3 cryopreserved Primary Clonetics™ Human RPE cells (hfRPE) (LONZA, Walkersville, WA) were cultured using a previously published protocol. (Halbach et al., 2015) hRPE culture was prepared in 3:1 mix of DMEM to F12, supplemented with 2% B27 without retinoic acid (Gibco, Grand Island, NY) and 1 % Pen/Strep. Cells were removed from liquid nitrogen and plated directly on transwells at a concentration of 100,000 cells/well. They were maintained in cell culture media containing 10% FBS for two days, after which the concentration was decreased to 2% FBS. After the cells reached confluence FBS was removed from the media and the cells were maintained in media alone.

mRNA isolation for qPCR

Due to the small number of cells on a transwell, all mRNA isolation was performed using the RNeasy micro kit (Qiagen, Germantown, MD). The protocol for that kit was as follows. The cells were lysed in their transwells using 75 µL of buffer RLT with 1% β-mercaptoethanol and the lysed cells were collected and vortexed for 1 minute and homogenized with a syringe and needle. 1 volume of 70% ethanol was then added and mixed by pipetting. The sample was then transferred to a MiniElute spin column, which had been stored at 4˚ C. All centrifugation steps

were done at 8000g for 15s unless otherwise noted. The column was centrifuged, the flow through was discarded and the column was washed with 350 µL of Buffer RWI, after which it was centrifuged again. DNase digestion was then performed to remove genomic DNA by adding 70 µL of a DNase 1 stock to 70 µL of Buffer RDD, mixing and incubating the mixture on the spin column for 15 minutes at room temperature. The column was then washed with 350 µL of Buffer RW1, followed by centrifugation and exchange of the collection tube for a fresh one. 500 µL of Buffer RPE was then added. The column was centrifuged again and the flow through discarded. 80% ethanol was then added to the column and spun for 2 minutes at 8000 g. The column was then placed in a new collection tube and dried by centrifuging at full speed for 5 minutes. Finally, the column was placed in a 1.5 mL collection tube and 14 µL of RNase-free water was added directly to the center. The sample was spun down for 1 minute at full speed to elute the RNA. RNA quality and concentration was determined using a NanoDrop One/One^{c} (Thermo Fisher Scientific, Waltham, MA).

Human Angiogesis RT^2 Profiler PCR Array

The protocol used for cDNA synthesis and for the Human Angiogenesis RT^2 Profiler PCR Array was found in the RT^2 Profiler PCR Array Handbook. First cDNA synthesis was performed on RNA that met the quality demands of the kit, namely an A_{260}:A_{280} ratio that was between 1.8 and 2.0 and a concentration measured from A_{260} of >40 µg/mL. Once quality had been assured 0.5 µg of RNA was used for synthesis of cDNA. This synthesis was performed using the RT^2 First Strand Kit (Qiagen, Germantown, MD). This is a two-step kit, with the first step involving creation of a genomic DNA elimination mix containing 500 ng of RNA, 2 µL of Buffer GE and RNase-free water to a total volume of 10 µL and incubating that mix for 5 minutes at 42˚ C. A

reverse transcription mix was then prepared containing, for 1 reaction, 4 µL 5X Buffer BC3, 1µL Control P2, 2µL RE3 Reverse Transcriptase Mix and 3µL of RNase-free water. The genomic DNA elimination mix was then added to this reverse transcription mix, mixed and incubated at 42˚ C for exactly 15 minutes. The reaction was then stopped by incubating at 95˚ C for 5 minutes. Finally, this mix was diluted with 91 µL of RNase-free water and either used immediately or frozen at -20˚ C.

Real-Time PCR was performed using the 96 well PCR array (PAHS-024Z) from Qiagen. Prior to opening the plate, the PCR mix was made containing 1350 µL 2x RT^2 SYBR Green Mastermix, 102 µL of the cDNA made in the previous step and 1248 µL of RNase-free water. The plate was then removed from -20˚ C and gently opened, after which 25 µL of the PCR mix was added to every well, with care taken to ensure equal volume distribution across the plate. The plate was then sealed with an optical adhesive film and centrifuged at 1000g for 1 minute. After centrifugation, it was ensured that no bubbles were present. After which, the plate was placed in the real-time cycler and the quantitation was performed. For this experiment, the Step One Plus thermocycler (Thermo Fisher Scientific, Waltham, MA) was used and the cycling conditions were as follows: 1 cycle of 95˚ C for 10 minutes and 40 cycles of 95˚ C for 15 seconds followed by 60˚ C for one minute. Fluorescence data collection was performed during the 1 minute at 60˚ C. Following these conditions, a melting curve analysis was performed to determine PCR specificity. Data was collected using StepOne software (Thermo Fisher Scientific, Waltham, MA) and exported to Excel. It was analyzed using the SABioscinces PCR Array Data Analysis Web-based software (Qiagen, Germantown, MD).

Mouse RPE isolation

Mouse RPE was isolated using the following protocol, shared with us from the Lakkaraju Lab. The mouse was euthanized and the eyes enucleated and placed in a 15mL centrifuge tube containing 1 mL/eye basic media (DMEM + 1X NEAA + 1X Pen/strep). The eyes were washed by inverting the tube 4X and then the basic media was completely removed. The eyes were then incubated in 1 mL/2 eyes in dispase solution. This solution consists of 2% (w/v) Dispase (Gibco, Grand Island, NY) solution made in basic media and sterilized with 0.22 µm filter. The eyes were incubated for 60 minutes at 37˚ C, with inversion every 15 minutes. The dispase solution was then removed and the eyes were washed two times with 1 mL/2 eyes basic media containing 20 mM HEPES (GMH). 1 mL/2 eyes GMH was then added and the eyes were transferred to a 100mm^2 Petri dish where they were dissected under a dissection scope. The anterior portion, including the cornea, lens and iris were removed and the eyecups were transferred to a second petri dish containing 1 mL/2 eyes GMH. Here the retina was gently removed, with care taken to try to keep the RPE attached to Bruch's membrane. Despite this care in most animals, much of the RPE peeled off with the retina. As much RPE as possible was then removed from the eye cup and retina, using forceps, and was collected win a 15 mL centrifuge tube containing 12 mL of basic media with 10 % FBS (GM). After collection from all eyes these RPE were centrifuged at 1000 rpm for 3 minutes at room temperature. The media was aspirated gently, and the cells were carefully washed two times with 1 mL of GM. This step had to be performed very gently to avoid disrupting the cell pellet. The cells were then resuspended in 1 mL of GM and centrifuged at 1500 rpm for 5 minutes at room temperature. Finally, the cells were re-suspended in GM at a density of 2 eyes/6.5 mm transwell and added to each transwell. Transwells were coated with collagen prior to plating at a concentration of 10 µg/cm^2 using Pure Col Type 1 Bovine collagen

(Advanced BioMatrix, San Diego, CA). This was done by mixing collagen with 70% ethanol at a concentration of 0.07 µg/mL and adding 50 µL of the mix to each transwell. This mix was allowed to dry overnight, after which it was washed with PBS and kept until used at 4˚ C. Following addition of the cells to the coated transwell they were kept at 37˚ C and 5% CO_2 for 48 hours before media was changed. Cells were treated with OXT 72 hours after plating and mRNA was isolated the following day.

ELISA

Protocol adopted from Human VEGF DuoSet ELISA Development System (R&D). Capture antibody was diluted to a working concentration indicated on the certificate of analysis provided with the antibody. All steps were performed at room temperature. PBS was made which consisted of 137mM NaCl, 2.7 mM KCl, 8.1 mM Na_2HPO_4 and 1.5 mM KH_2PO_4. PBS was brought to pH 7.2-7.4 and filtered. 100 µL of diluted capture antibody was added to each experimental well of a 96-well plate, which was then sealed and incubated overnight. Each well was then aspirated and washed three times with 0.05% Tween 20 in PBS. Plates were then be blocked with 1% BSA in PBS for at least 1 hr. 100 µL of collected media was added to wells, covered with adhesive strip and incubated for 2 hours. Previous wash step was then repeated. 100 µL of working concentration detection antibody was then added and incubated for 2 hours. Wash step was again repeated. 100 µL of a working dilution of streptavidin-HRP was added to each well followed by 20-minute incubation in dark. The wash step was performed again followed by addition of 100 µL of a 1:1 mix of H_2O_2 and Tetramethylbenzidine to each well and incubated for 20 minutes in dark. Finally, 50 µL of 2N H_2O_2 stop solution was added. Optical

density was measured using a Synergy HT microplate reader (Biot-TEK) set to 450nm and was corrected for optical imperfections by subtracting optical density readings at 540nm.

Tube formation Assays

Capillary morphogenesis was determined using a tube formation assay. Two methods were used to perform this assay, necessitated by the difference in available volume between the apical and basal media. For basal media, 24 well tissue culture plates were coated with 100 µL of cold Matrigel (10mg/mL, BD Biosciences), with care taken to ensure even coating of the well bottom. The plate was then placed at 37˚ C for at least 30 minutes to allow it to harden. Retinal endothelial cells (REC) were cultured and prepared by the Sheibani lab as described by them previously (Lavine et al., 2013). REC were taken from the incubator and removed from the plate with trypsin-EDTA and resuspended in DMEM containing 10% FBS. Cells were counted and then separated into different treatment conditions. Cells were then centrifuged at 12,000 RPM for 5 minutes and resuspended in the conditioned media (CM). CM was media that had been exposed to RPE cultures overnight, either with or without OXT. Media that had not been exposed to RPE cells was also used as a positive control. Cells were plated in the Matrigel coated plates at a density of 6.25×10^4 cells/well. Cells were incubated overnight and photographed the following morning with a Nikon microscope in a digital format. 5 separate regions of each well were imaged and the average number of branch points (nodes) and branches (tubes) were counted.

To measure the effect of apical media on tube formation, µ-angiogenesis 15 well slides (Ibidi, Madison, WI) were used. 10 µL of cold Matrigel (10mg/mL, BD Biosciences) was pipetted into each well of the slide and placed at 37˚ C for 30 minutes to an hour to solidify. While the

Matrigel was incubating, RECs were trypsinized and counted as described above. The cells were then centrifuged at 90g for 10 minutes and the supernatant was removed. Cells were then resuspended in serum free REC media at a concentration of $10x10^5$ cells/mL. For each well of the µ-angiogenesis slide, 10 µL of these cells was then taken and mixed with 40 µL of conditioned media from the apical compartment of the transwell, to get a final concentration of $2x10^5$ cells/mL. This 50 µL volume of cells was added to the µ-angiogenesis slide after the Matrigel had solidified. The cells were left at 31˚C overnight to allow for tube formation to occur and images were taken the following morning. Images were taken and saved at 2x magnification using an EVOS-XL microscope (Life Technologies, Grand Island, NY, USA), with two images taken of each well, one showing the top half of the well and the other showing the bottom half. Tube numbers were counted for each half and averaged to get the tube number for that well.

Transwell Migration Assay

The effect of conditioned media on REC migration was determined using the transwell migration assay. Costar transwell inserts (8-µm pore size, 6.5-mm membrane, Lowell, MA) were coated with fibronectin (2 µg/mL) on the bottom side at 4˚ C overnight. The inserts were then washed with PBS and then blocked using PBS with 1% BSA for 1 hour at room temperature. Retinal endothelial cells were trypsinized and counted, then centrifuged at 90g for 10 minutes. The cells were resuspended in conditioned media and 1×10^5 cells in 0.1 mL of conditioned media were added to each insert. The inserts were then placed in a 24 well plate containing 0.5 mL of conditioned media and incubated for 4 hours at 37˚ C. After incubation, cells were fixed with 2% paraformaldtehyde for 10 minutes at room temperature and stained with hematoxylin

and eosin. Membranes were mounted on a slide with the cells facing the slide and 10 separate fields were imaged for each sample. The average number of cells that migrated through the membrane was then determined.

3.3 Results

Varying concentrations of OXT do not influence major angiogenic genes in hRPE

To identify whether OXT might be influencing angiogenesis through alteration of gene transcription, I utilized the human angiogenesis RT^2 Profiler PCR array from Qiagen. The full panel results are listed in table 1. Genes identified to have a 2-fold change in regulation were qualified as either up or down regulated and can be seen in Figure 1. The genes that we primarily associate with the pathogenesis of ROP, VEGF and IGF-1, did not meet this threshold for up or down regulation. Both VEGF A and VEGF B saw no significant alteration in expression, with a 1.04 fold (P=0.7) and 1.08 (P=0.5) fold change observed, respectively. However, VEGF C was significantly altered by 1.97 fold (P=0.03). Like VEGF A and B, IGF-1 was not significantly altered, with a 0.85 (P=0.5) fold change in expression. One protein of interest which is significantly altered is Hepatocyte growth factor (HGF), which is a paracrine signaling molecule that has been shown to be involved in organ development, adult organ regeneration and wound healing (Nakamura, 1991). However, the Ct values for HGF were large (>30) so the effect of OXT may be exaggerated. Relevant to our hypothesis about the role of OXT in mediating ROP, these data suggest that there is an alteration in the expression of the VEGF-C isoform, but that this is effect is not large. However, the isoform primarily associated with angiogenesis, VEGF A, is not significantly altered.

VEGF and IGF-1 are not effected by OXT in mouse RPE

To determine whether the response I observed from the fetal cells would be different in adult RPE I isolated mouse RPE from adult mice and cultured them on transwells for 4 days, after which they were treated with 10 µM OXT. Following OXT treatment qPCR was performed to assay for expression of VEGF and IGF-1, two of the main regulators of retinal angiogenesis and key factors in the pathogenesis of ROP. The observed Ct for our gene of interest was compared to the Ct for 18s rRNA from the same sample, giving us a ΔCt, or relative expression for each sample (Figure 2A). The average difference between the ΔCt of our treated samples (n=4) to that of our untreated (n=3) samples revealed a ΔΔCt of 0.049 ± 0.37 for VEGF and a ΔΔCt of -0.67 ± 1.32 for IGF-1. These values correspond to a fold change of 0.97 (+1.3/-0.75) for VEGF in response to OXT and a fold change of 1.6 (+3.96/-0.64) for the IGF-1 in response to OXT (Figure 2B). These data demonstrate that in RPE from adult mice I see a trend towards increased expression of VEGF and IGF-1, however, as I observed in the human fetal RPE, this was not significant.

Apical VEGF secretion is significantly altered by OXT

In addition to influencing the expression of angiogenic genes, I also sought to address the potential for OXT to mediate the release of VEGF. To determine the effect of OXT on this release, I utilized a human VEGF assay (DuoSet Elisa, R&D systems). I determined the concentration of VEGF found in media collected from fetal RPE transwells following overnight (16 hr) incubation with either no (0 µM) OXT, 0.1 µM OXT or 10 µM OXT. The measured concentration of VEGF was determined both for the apical and basal compartment of the transwells and compared to the level of VEGF detected from the same transwell following 16-

hour incubation in media without any OXT, done one day before OXT treatment (baseline). The results are expressed as a ratio of the VEGF levels measured during the treatment day relative to the VEGF levels measured during the baseline treatment. Despite a lack of significant changes in the expression of VEGF identified in our RT^2 Human angiogenesis assay, this ELISA identified a significant increase in the levels of VEGF secreted into apical media in response to the 10 μM OXT treatment. It induced an average secretion of 1.35 ± 0.07 (P=0.03) fold change relative to VEGF in the baseline measurement for each well (Figure 3A). A slightly smaller increase was observed in response to 0.1 μM OXT (1.16 ± 0.1 fold) and the untreated wells exhibited a ratio of 0.87 ± 0.04 fold, relative to the previous day's baseline. The observed ratios for OXT treatment were significantly greater than the untreated control (P=0.03 for 10 μM OXT; P=0.04 for 0.1 μM OXT). There was no significant change in the level of basal VEGF, with a 1.00 ± 0.05 fold change for untreated wells, 1.048 ± 0.1 fold change for 0.1 μM OXT treated wells and a 1.13 ± 0.03 fold change for 10 μM OXT treated wells (Figure 3B).

Conditioned media does not influence angiogenesis in retinal endothelial cells

To determine whether conditioned media could impact angiogenesis I assayed for capillary morphogenesis in retinal endothelial cells (REC) following incubation with conditioned media. Basal and apical media were assayed separately to allow me to identify any differential effect as a result of polarized secretion. Changes in cell migration were also studied using basal media but the limited volume in the apical compartment prevented me from performing that assay for apical media. Following treatment of retinal endothelial cells with basal media collected from RPE cells incubated with OXT, I observed no significant effect on either migration or capillary morphogenesis (Figure 4 A-C). Two measures of capillary morphogenesis, tube

formation and node formation, were assayed following incubation of retinal endothelial cells with conditioned media from RPE cells incubated with 10 μM OXT (labeled treated) and no OXT (labeled untreated) as well as media that had not been exposed to RPE cells at all (labeled Media ONLY). Following overnight incubation, I observed an average tube number of 57.3 ± 7.8 in response to unconditioned media, 61.0 ± 3.7 in response to untreated conditioned media and 58.3 ± 4.6 in response to OXT treated conditioned media. The difference between these three conditions was not significant ($P>.05$). The results for node number were similar, with an average node number of 33.5 ± 5.1 for unconditioned media, 40.5 ± 3.0 for untreated conditioned media and 38.0 ± 2.4 for OXT treated conditioned media. In our migration assay I observed the chemotaxic potential of our conditioned media by counting the number of retinal endothelial cells that migrate across a transwell, towards the conditioned media. In this study I used both 0.1 μM OXT and 10 μM OXT to determine if migration was dose dependent. I observed that an average of 28.6 ± 1.8 cells migrated in the presence of unconditioned media, 42 ± 3.0 cells migrated in the presence of untreated conditioned media, 42.9 ± 2.9 cells migrated with 0.1 μM OXT treated conditioned media and 41 ± 1.3 cells migrated with 10 μM OXT conditioned media. Interestingly these results show a significant increase in migration with of RPE conditioned media relative to unconditioned media ($P<.05$). However, the addition of OXT did not have any significant impact on migration ($P>.05$).

Similar results were observed from the capillary morphogenesis assay when apical media was used (Figure 5). Due to the smaller media volume in the apical compartment the assay was designed differently than with basal media, using μ-angiogenesis slides instead of a 24 well plate. As a result, tube number was much lower. Additionally, cell concentration was

low, but increasing the number of cells resulted in the formation of large masses of cells and no observable tube formation. At the concentration used, tube numbers were counted, and I observed an average tube number of 2.85 ± 0.33 in response to untreated media, 3.17 ± 1.76 in response to 0.1 µM treated media and 3.17 ± 0.60 in response to 10 µM OXT. The difference between the three conditioned was not significant ($P > 0.05$), confirming what I saw in the basal media and demonstrating again that OXT does not significantly impact angiogenesis of RECs *in vitro*.

3.4 Discussion

We have previously demonstrated that OXT is present in the cone extracellular matrix and that OXTR is expressed in the adjacent RPE cells. Additionally, we have shown that in the RPE OXTR signals through a PLC mediated signaling cascade stimulating the hydrolysis of PIP_2 as well as the inhibition of the inwardly rectifying K^+ channel Kir7.1. The role that OXT plays in the RPE-retina interface has not been discovered. In this study, I have hypothesized that OXT was playing a role in regulating growth factor expression, secretion, or both in a manner that could influence retinal angiogenesis during development of the eye. This hypothesis was based on the increase in fetal OXT production after approximately 30 weeks of gestation, corresponding with the late development of the intraretinal vasculature as well as preliminary data from our lab demonstrating that OXT might induce an increase in VEGF expression (Halbach, 2013). To determine whether this was the case, I cultured hfRPE cells on transwells to allow for them to form a polarized monolayer, which has been shown to be important for growth factor secretion (Sonoda et al., 2009). I found that OXT treatment of these hfRPE cells does not result in a significant alteration in the expression of VEGF but that it does induce significant changes in

some other angiogenic factors. Despite the lack of altered VEGF expression, I was able to observe an increase in the secretion of VEGF, specifically to the apical compartment of our studied transwells, which suggests the possible polarized secretion of VEGF towards the retina in response to OXT stimulation. The increase in secretion, however, did not have any significant effect in two functional assays of angiogenesis, the tube formation and migration assays. As a result, I have determined that OXT has the potential to influence vasculature growth, however this influence is likely not a major factor in the pathogenesis of ROP.

In my study of OXTs role mediating gene expression I compare the transcript levels off 88 different genes, identified as important regulators of human angiogenesis, in hfRPE cells treated with OXT concentrations (10 μM) to RPE cells that were not treated. Following 16 hours of incubation I observed a greater than two-fold change in 14 genes (Figure 1). Of principle concern though for our hypothesis that OXT might be implicated in the pathogenesis of ROP through alteration in the transcription of the genes VEGF and IGF-1 and I did not see a greater than 2-fold change in any VEGF isoform or in IGF-1. These data suggest then that OXT is not likely to impact ROP pathogenesis through transcriptional regulation of angiogenic genes. However, one possible weakness of this study lies in the inherent immaturity of the hfRPE. Despite being cultured to a monolayer (TER > 800 Ω) and developing pigmentation, the RPE cells used are of fetal origin and the possibility that their immaturity or a lack of exposure to the retinal environment results in an altered response to OXTR exists. To address this concern, I also looked at the level of VEGF and IGF-1 production expression in mouse RPE. These cells, isolated from the mouse eye and cultured on transwells for no more than 4 days before OXT treatment, were treated under the same conditions as the hfRPE and transcript levels were

assayed. Like our observations in the hfRPE I observed no significant alteration in either IGF-1 or VEGF, relative to 18s rRNA. Using both of these cell types, from two different species, these data clearly demonstrate that, while OXT does induce a change in the expression of a number of angiogenic factors, it does not have an impact on genes associated with ROP.

It remained possible though that, while OXTR does not alter the expression of these angiogenic genes it does induce their secretion. Like in many secretory cells the secretion of growth factors from the RPE is in part controlled by L-Type Ca^{2+} channels on the cells membrane. IP_3/Ca^{2+} signaling has been shown to modulate growth factor secretion through $pp60^{c\text{-}src}$, a receptor tyrosine kinase that alters the voltage sensitivity of L-Type Ca^{2+} channels (Strauss et al., 1997). Additionally, Kir7.1 inhibition results in membrane depolarization, which can increase channel activation. Together these represent two possible mechanisms through which OXTR could be inducing the secretion of growth factors. In this study, I focused on the secretion of VEGF, as it is the major regulator of angiogenesis in the retina and the key angiogenic factor involved in the pathogenesis of ROP. Following ELISA assay on media collected from hfRPE cells, cultured on transwells and treated with OXT, I found a trend towards increased concentrations of VEGF in the apical compartment with increasing concentrations of OXT, relative to what was observed in the same well prior to treatment. This increase in apical VEGF was significant when 10 µM OXT was used. This demonstrates that OXT can induce the secretion of VEGF, even if it is not altering its expression in a significant way. Furthermore, the fact that a rise in apical VEGF is observed while no such change was seen in the basal medium suggests that there may be polarized secretion from the RPE that favors release of VEGF towards the retina. However, differences in volume in the apical compartment

(200 µL) and basal compartment (600 µL) may result in the basal secretion being obfuscated. To determine if polarized secretion is definitively occurring, a detailed study is needed.

The alteration in VEGF secretion from hfRPE provides some support to the hypothesis that OXT could be playing a role in mediating angiogenesis in the retina. Furthermore, I did identify significant changes in some important angiogeneic genes (Figure 1) and it is therefore possible that these alterations support this role as well. As such I turned my sights towards identifying whether OXT could functionally impact angiogenesis using retinal endothelial cells. To look at the angiogenic potential of OXT treated RPE in its entirety, I collected media from hfRPE cells, conditioned with OXT, and studied its effect on both tube formation and migration of retinal endothelial cells. I looked at the impact of apical and basal media on tube formation separately, to try and identify whether polarized secretion might influence the retina and choroid differently. Demonstrated in Figure 4 A and B, I observed no significant alteration in tube number or node number during the tube formation assay in response to basal media from cells exposed to OXT relative to those left untreated. In fact, I observed no influence of RPE exposure on tube formation at all, with media alone resulting in a statistical equivalent number of both measures. I had similar results in response to apical media, with no difference in the number of tubes found in media treated with OXT than media that was untreated (Figure 5). Additionally, no effect was found on cell migration, with no change in the number of cells migrating as a result of OXT exposure in basal media. Interestingly, in this case I did observe a significant increase in migration in media that had been exposed to RPE, suggesting that the RPE itself, independent of OXT, can impact retinal endothelial cell migration but not their

proliferation. These data provide functional proof that OXT does not influence retinal angiogenesis through its action in the RPE.

In conclusion, the data presented in this study suggest that the role of OXT in the RPE is not to regulate retinal vasculature through the production of VEGF or IGF-1. I have demonstrated the following: 1) OXT does not influence the expression of major genes involved in ROP in both human fetal and adult mouse RPE but OXT can alter expression of other important angiogenic genes 2) OXT does induce an increase in secretion of VEGF from hfRPE cells and this secretion may favor the apical compartment, 3) conditioned media from OXT treated RPE cells does not influence angiogenesis in retinal endothelial cells. Taken as a whole, these data suggest that OXT does not play a role in regulating retinal angiogenesis through production of VEGF. However, OXT does have an impact on the expression of some angiogenic genes and it may influence the secretion of VEGF, suggesting that OXT has the potential to influence angiogenesis, even if it does not do so in the retina, findings that are important to future studies on OXT throughout the body.

Acknowledgements

The work in this chapter would not have been possible without the help of Divya Sinha, whose expertise with RPE culture made our transwell cultures possible. Additionally, the angiogenesis assays were made possible by Mitra Farnoodian, who trained me and provided oversight, and Yong-Seok Song, who provided me with RECs and advice.

3.5 Tables and Figures

Layout	1	2	3	4	5	6	7	8	9	10	11	12
A	AKT1 1.73	ANG 7.33	ANGPT1 -1.84	ANGPT2 -1.35	ANGPTL4 1.07	ANPEP -10.04	ADGRB1 1.42	CCL11 1.35	CCL2 1.05	CDH5 -1.51	COL18A1 -1.01	COL4A3 1.12
B	CTGF 1.73	CXCL1 1.02	CXCL10 1.03	CXCL5 1.01	CXCL6 1.33	CXCL9 -1.14	EDN1 1.58	EFNA1 -1.23	EFNB2 1.07	EGF -1.22	ENG -2.44	EPGB4 -1.11
C	ERBB2 1.22	F3 1.4	FGF 1 1.5	FGF2 1.16	FGFR3 -1.42	FIGF -1.59	FLT1 1.03	FN1 1.13	HGF -14.43	H1F1A 1.29	HPSE -1.77	ID1 -1.05
D	IFNA1 2.55	IFNG -4.19	IGF1 -1.17	IL1B -1.94	IL6 1.27	CXCLB -1.2	ITGAV 1.07	ITGB3 1.88	JAG1 1.11	KDR -1.45	LECT1 -1.01	LEP -1.37
E	MDK 1.26	MMP14 1.35	MMP2 -1.02	MMP9 1.61	NOS3 -2.11	NOTCH4 1.06	NRP1 -1.31	NRP2 1.22	PDGFA 1.21	PECAM1 -1.13	PF4 1.56	PGF -1.09
F	PLAU 2.53	PLG 1.07	PROK2 1.64	PTGS1 2.96	S1PR1 -1.07	SERPINE1 2.61	SERPINF1 1.37	SPHK1 1.11	TEK -3.53	TGFA 1.32	TGFB1 1.31	TGFB2 1.41
G	TGFBR1 -1.03	THBS1 1.35	THBS2 -1.64	TIE1 -2.16	TIMP1 1.06	TIMP2 1.01	TIMP3 1.33	TNF -2.38	TYMP 1.27	VEGFA 1.04	VEGF B 1.08	VEGF C 1.97

Table 1: Plate layout of each gene assayed with fold change expression listed below.

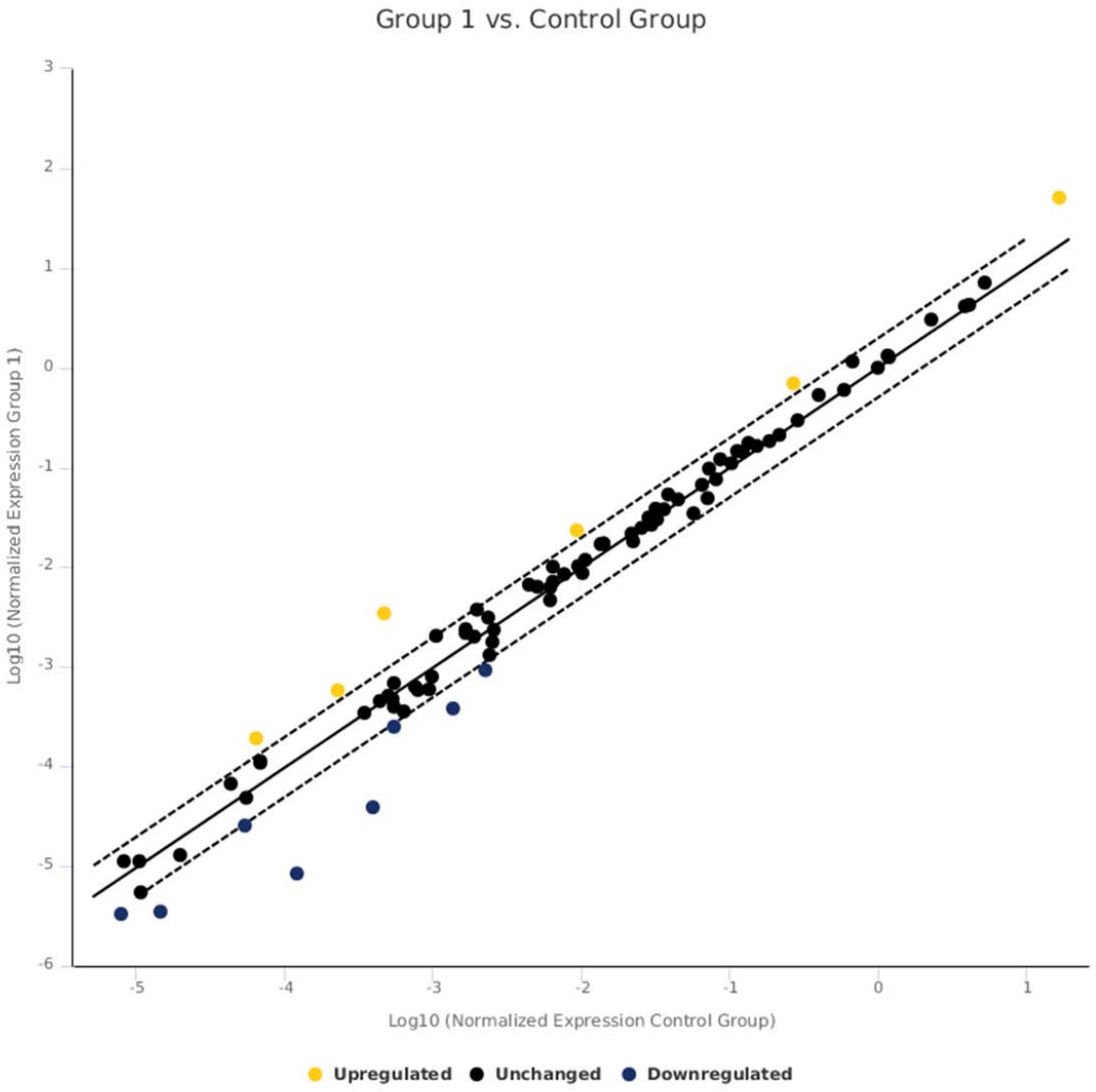

Figure 1: Fold Change in Gene Expression in response to OXT treatment. The Y-Axis shows the log10 of normalized expression of OXT treatment (group 1) while X-Axis shows the Log10 of normalized expression of untreated controls. The genes identified as being upregulated or downregulated greater than two-fold are listed in table 2.

Gene	Fold Regulation
ANG (Angiogenin)	7.21
GAPDH	3.02
PTGS1 (prostaglandin –endoperide synthase)	2.92
SERPINE1 (Serpine -1 –phosphate receptor)	2.56
IFNA1 (Interferon, alpha 1)	2.51
PLAU (Plasminogen activator urokinase)	2.49

Gene	Fold regulation
HGF (Hepatocyte growth factor)	-14.66
ANPEP (Alanyl (membrane) aminopeptidase)	-10.21
IFNG (Interferon gamma)	-4.26
TEK (TEK tyrosine kinase, endothelial)	-3.59
ENG (Endoglin)	-2.48
TNF (Tumor Necrosis Factor)	-2.42
TIE1 (Tyrosine Kinase with Ig-like and EGF-like domains 1	-2.20
NOS3 (Nitric oxide synthase 3 (endothelial cell)	-2.14

Table 2: Fold Change in Gene Expression in response to OXT treatment. Genes with altered expression (greater than 2-fold change) are listed here. The upper table lists genes with increased expression while the lower table shows genes with decreased expression.

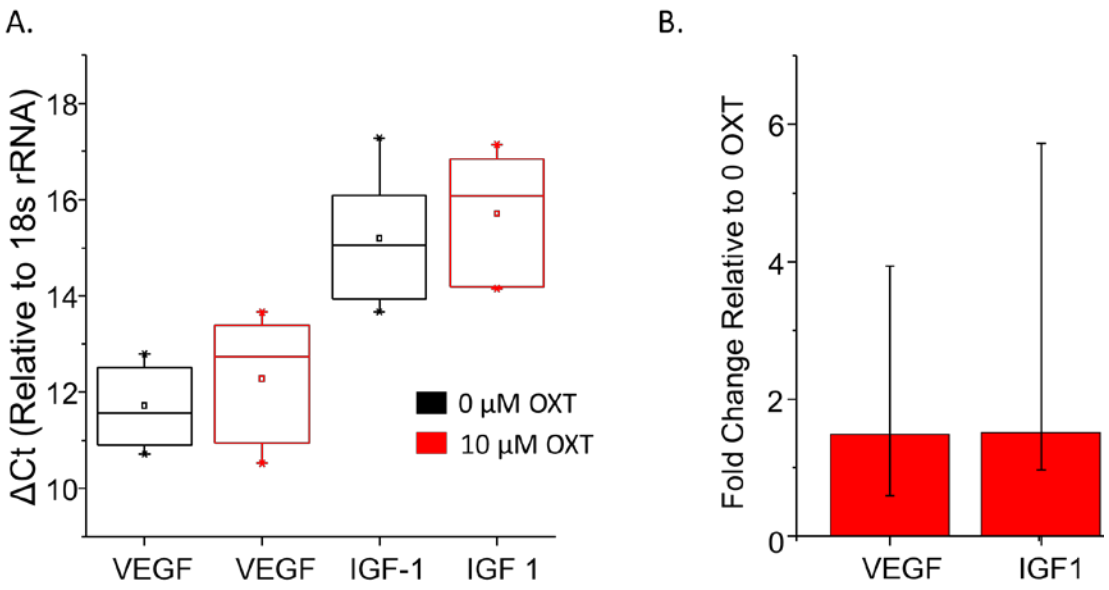

Figure 2: Effect of OXT on VEGF and IGF-1 expression in adult mouse RPE. (A) Box plot for ΔCt (VEGF/IGF1 Ct – 18s rRNA Ct) of VEGF and IGF-1 expression observed with 0 µM OXT and 10 µM OXT treatment. There was no significant change in the expression of either gene in response to the OXT in the samples assayed. (B) A representation of the fold change in VEGF and IGF-1 in response to OXT, relative to their untreated counterparts. There was no significant change in the expression of either gene.

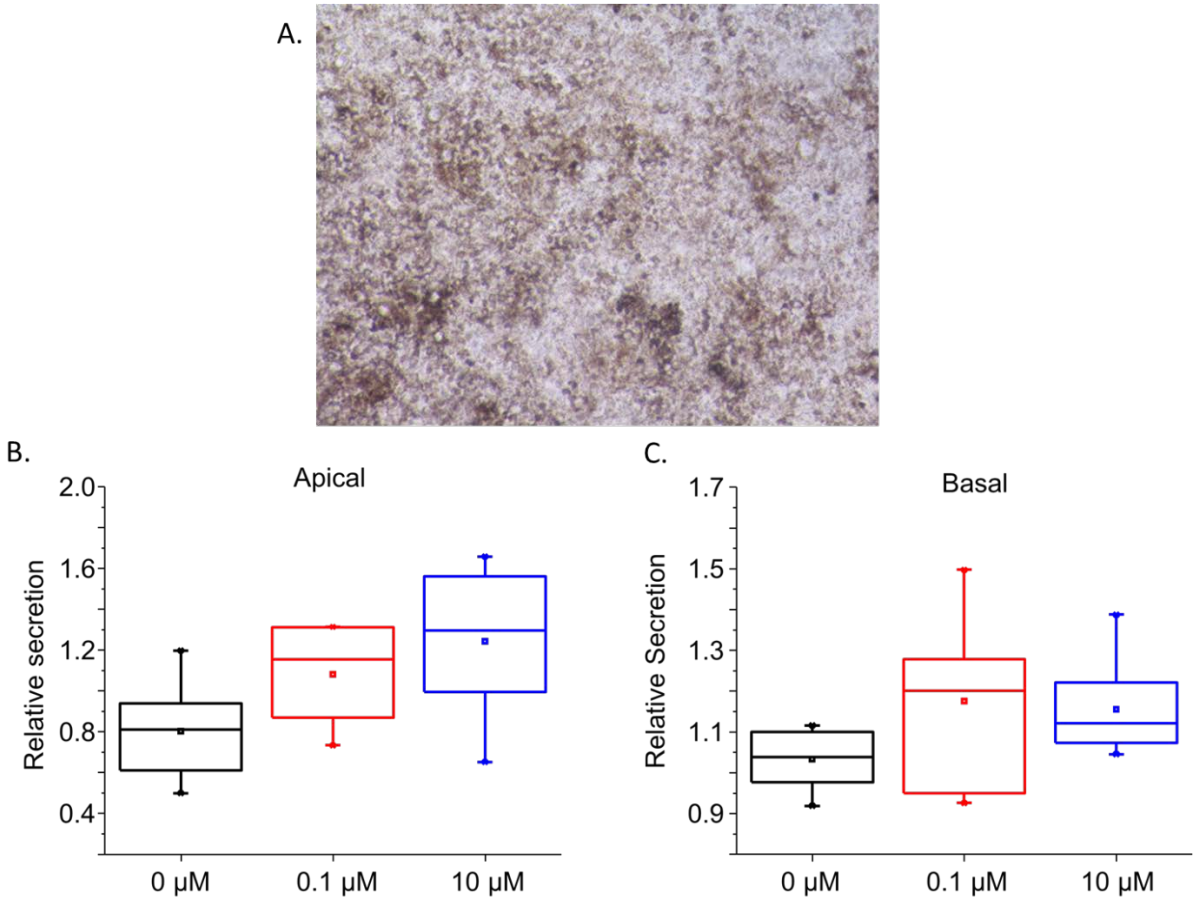

Figure 3: Polarized effect of OXT on secretion of VEGF by hfRPE. (A) Representative image of transwell used for ELISA and gene expression. (B) Box plot of apical levels of VEGF in response to OXT treatment (0-10 µM) expressed as a ratio of observed VEGF after 16hr treatment to observed VEGF in the same well during incubation with untreated media for 16 hours the day prior. 10 µM OXT induced a significant increase in VEGF relative to the untreated sample ($P<0.05$;n=8 for each condition). (C) Box plot of basal levels of VEGF during OXT treatment (0-10 µM) expressed in the same manner. No significant effect of OXT treatment was observed relative to the untreated sample (n=8 for each condition).

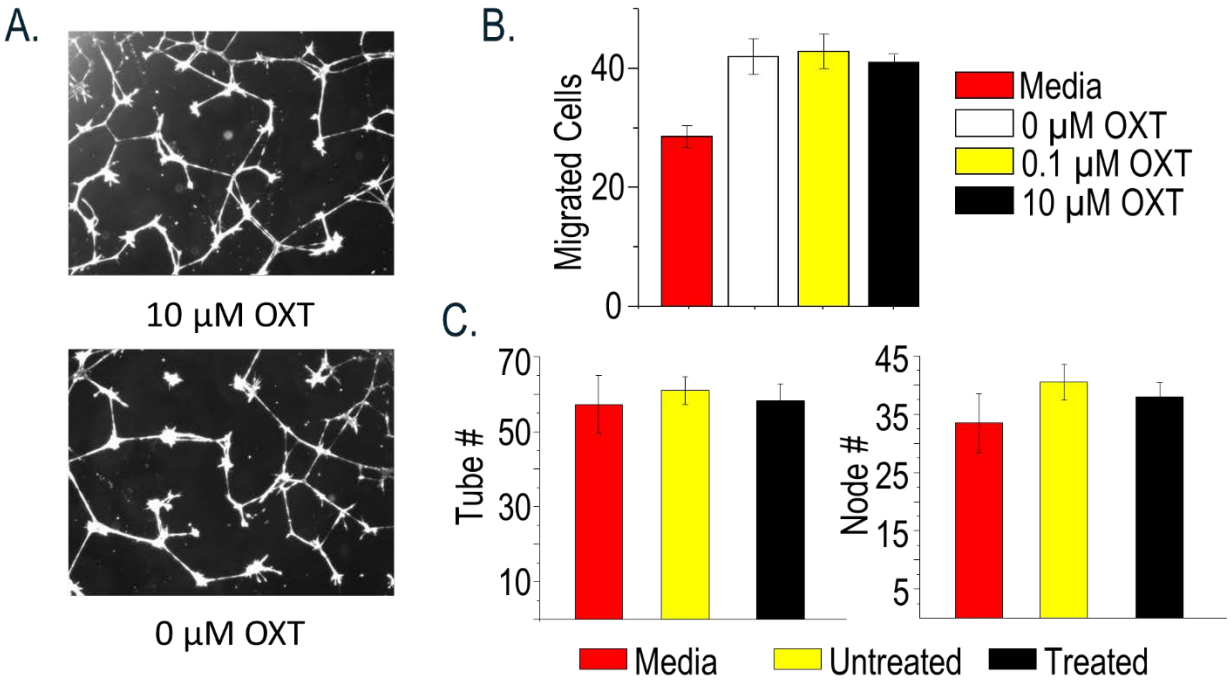

Figure 4: Impact of OXT on vascular homeostasis. (A) A representative image of retinal endothelial cells grown in conditioned media of RPE cells treated with 10 µM OXT or with No OXT. (B) Results of Tube formation assay represented. Tube number represents the number of projections formed between retinal endothelial cells while node # refers to the number of nodules from which these projections extend. There was no significant difference in the number of either when comparing untreated and treated RPE. (C) Results from migration assay, expressed as the number of cells that migrated across a transwell. While the exposure of media to the RPE induced an increase in migration this effect was not influenced by OXT at all.

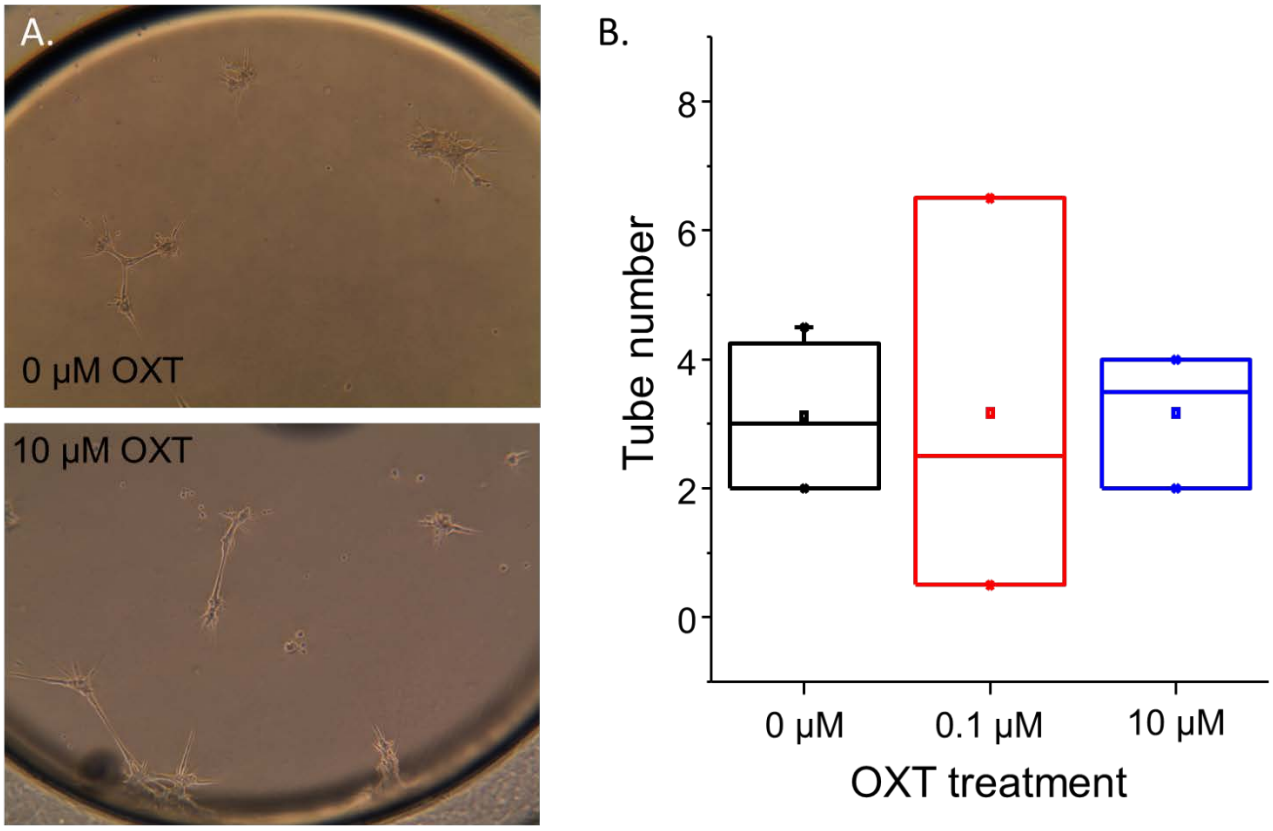

Figure 5: Tube formation is not altered by media from OXT treated cells. (A) Representative images of cells not treated with OXT (top) and untreated (bottom). (B) Box plot of tube average tube number following treatment of REC's with conditioned media containing 0 µM OXT (n=4), 0.1 µM OXT (n=3) and 10 µM OXT (n=4). No significant difference was seen across treatments.

Chapter 4: Ontogeny of OXTR in the RPE and broader expression in the mouse retina

Nathaniel York[1,3,6], Allison Lutz[3], De-Ann Pillers[2,3,4], Bikash Pattnaik[3,5,6]

From the [1]Endocrinology-Reproductive Physiology Program, the [2]Division of Neonatology& Newborn Nursery, the [3]Departments of Pediatrics, [4]Medical Genetics, [5]Ophthalmology &Visual Sciences, and [6]the McPherson Eye Research Institute, the University of Wisconsin-Madison, WI 53715

Abstract:

The role of oxytocin in the retina is not well understood. We have previously demonstrated the presence of both OXT and OXTR in the primate retina and have demonstrated that it is functionally active. Understanding the timeline of OXTR expression could provide a guide to understanding how OXT may be impacting the retinas development. In this study I have attempted to determine the ontogeny of OXTR within retina of the mouse, focusing on the timeline covering retinal maturation and vascular development. On average I found no significant change in the expression of OXTR during this time-period. This was likely the result of a large variation in the level of expression in the RPE that was independent of age or gender. I also found that, unlike what has been previously observed in primate retinas, the mouse expresses OXTR throughout the retina. These data have implications not only for our understanding of the mouse as a model of human retinal function and development, but for the broader understanding of the role the endocrine system might play in supporting and regulating vision.

4.1 Introduction

We have previously demonstrated that OXTR is present and functional in the RPE (Halbach et al., 2015). We have shown that in the RPE OXT specifically activates OXTR, leading to a G-protein mediated signaling activation in which PLC hydrolyses PIP_2 into IP_3 and DAG, resulting in a Ca^{2+} response that is dependent on the release of intracellular Ca^{2+}. Additionally, I have demonstrated that activation of OXTR by OXT can induce the inhibition of Kir7.1, and that this inhibition is reliant on G-protein coupling, unlike the direct inhibition observed by Ghamari-Langroudi, M., et al. (Ghamari-Langroudi et al., 2015). I have also explored whether OXT can influence angiogenesis in the retina and found that there was no evidence of such a relationship. These data do not eliminate the potential for OXT to influence retinal development however. The effect of OXT on other growth factors, like PEDF, have not been thoroughly studied and could be important in regulating retinal development. As a result, while we know that OXT can functionally impact the RPE, we still do not know what the implications of this effect are *in vivo* or when this signaling might occur. Given the complex role the RPE plays in retinal development and function, determining the ontogeny of OXTR expression is key to understanding when OXT could begin to have an impact on the retina and provide a guide in determining the role of oxytocinergic signaling *in vivo*. To perform this study I have utilized the mouse, which is commonly used to study development of the retina especially in the context of retinal vasculature development and disease such as retinopathy of prematurity.

The photoreceptors and the RPE develop in a coordinated fashion. Both are derived from the optic neuroepithelium which itself originates from a patch of cells, named the “eye field” that is present on the anterior neuroectoderm (Fuhrmann et al., 2014). The optic

neuroepithelium then forms the optic vesicle with the anterior portion normally forming the organized neural retina and the posterior forming the RPE. By 18 weeks of gestation in humans the RPE can be seen as a well-defined layer. At the same time the photoreceptors are developing, appearing as a well-defined layer by 21 weeks and forming outer segments at 28 weeks (Gupta et al., 2016). Human retinal vasculature development begins later than the RPE, starting at approximately 16 weeks of gestation. The retina is supplied at first by hyaloid vasculature, originating from the optic nerve, which must regress as the eye continues to develop (Stahl et al., 2010). The hyaloid regression occurs during the development of the intraretinal vascular, with the nasal retina being fully developed by 36 weeks and the temporal vessels being fully developed by 40 weeks, a process discussed in more detail in **chapter 1.6**. The human eye is therefore fully developed and vascularized by term.

In the mouse, the eye is not fully developed at birth, giving it the potential to provide valuable information on eye development in a more accessible way, since the development occurs outside of the uterus. The development of the RPE continues in the mouse beyond birth, with cell numbers rising until 15 days after birth (Bodenstein & Sidman, 1987). At the same time, the retinal vasculature is developing as well and serves as a good measure of the maturity of the eye. C57Bl/6 mice at birth have immature retinal vasculature and persistent hyaloid vessels, which regress as the intraretinal vasculature develops outward from the optic nerve towards the retinal edges, reaching them at approximately p8 and forming the superficial vascular plexus (Stahl et al., 2010). At approximately p7 the other two vascular layers, the deep and intermediate plexuses begin to form and all three are fully mature by 21 days after birth.

Using vasculature as a marker of development for the purpose of this study I consider a 21-day old mouse eyes as of equivalent maturity to those of a human at birth.

I have used C57Bl/6 mouse eyes, collected at days ranging from postnatal day 0 (P0) to adulthood to determine the ontogeny of the OXTR in the RPE. While initial results suggested there was a lack of OXTR expression prior to P15, more precise measurements using qPCR have shown that OXTR expression is highly variable in the mouse RPE but that the average expression remains unchanged in the postnatal eye. Additionally, I found that OXTR expression is not limited to the RPE in the mouse retina, instead I observed expression throughout the retina. This expression was more consistent than the expression observed in the RPE and much different than what I have observed in the primate. These new data suggest not only that the mouse is not likely to be a good model for oxytocinergic signaling in the RPE but that OXT's role may extend beyond the RPE in the animal. Considering this new information, I shifted my focus back to the rhesus monkey. In rhesus retina, I have confirmed our previously reported results showing OXTR expression in the RPE. Here I have expanded on that work, clearly demonstrating the expression of OXTR in the apical processes of the RPE, co-localizing with Kir7.1 and surrounding the photoreceptor outer segments.

In conclusion, while I have, on average, demonstrated a persistent expression of OXTR in the postnatal mouse RPE this expression varies dramatically between individual animals. Furthermore, I have shown that the expression of OXTR is found throughout the mouse retina, not just the RPE. This differs from the primate retina, where I show robust expression of OXTR along with Kir7.1 channels in the apical processes of the RPE.

4.2 Methods

RPE cell isolation using simultaneous RPE isolation and RNA stabilization (SRIRS)

To attempt to isolate mRNA from RPE cells specifically we utilized the SRIRS method, described by Wang et al (Xin-Zhao Wang et al., 2012). Mice were euthanized using either decapitation or CO_2, depending on the age of the mouse. The mouse eyes were then enucleated and kept in HR solution on ice during transfer to the lab. The eye was then placed in PBS in a 100 mm dish and the anterior segment and retina were removed. For samples where retina was collected retinae were placed in 200 µL RNAprotect (Qiagen, Germantown, MD). The eye cup of both eyes was then placed in 200 µL of RNAprotect and incubated for approximately 10 minutes at room temperature. The eye cups were then briefly vortexed to detach the RPE and the eye cup was removed from the solution. The RPE suspension was then centrifuged at 690 x g for 5 minutes to pellet the RPE cells. The RNA protect was removed and total RNA was extracted using the RNeasy Micro Kit (Qiagen, Germantown, MD) according the manufactures instructions for isolation of mRNA from <500 cells.

Single retinal and RPE cell collection

Retinal and RPE cells were isolated according to a protocol described previously by our lab (Shahi et al., 2017). Dispersed single RPE cells and retinal cells were placed on 12 mm #1 round coverslips and left to settle on the Nikon FN1 stage. About 2–5 cells (1 cell at a time) were picked using the recording pipette by applying negative pressure, and then expelled into a PCR tube containing RNA*later*® (AMBION, Austin, TX) by applying positive pressure. A single freeze-thaw cycle was used to disrupt the cell membrane to isolate the total RNA.

mRNA isolation

See **Chapter 3** for full mRNA isolation procedure. One alteration to general procedure was made. RPE cells were homogenized using a disposable pestle grinder and centrifuged for 2 minutes at 16,000x g following homogenization. The resulting supernatant was then transferred to a new tube and one volume of 70% ethanol was added, followed by resumption of the general procedure.

cDNA synthesis and quantitative PCR

cDNA synthesis was performed using the SuperScript III First-Strand Synthesis System (Thermo Fisher Scientific, Waltham, MA). For each sample 100 ng of total RNA was used. This volume of RNA was added to 1 µL of random hexamers (50 ng/µL), 1 µL of dNTP mix and the total volume was brought to 10 µL with DEPC-treated water. This mix was then incubated for 5 minutes at 65˚C and placed on ice for at least 1 minute. During this incubation a cDNA synthesis master mix was prepared containing, per reaction, 2 µL of 10X RT buffer, 4 µL 25mM $MgCl_2$, 2 µL 0.1 M DTT, 1 µL RNaseOUT (40U/ µL) and 1 µL SuperScript III RT (200 U/µL) enzyme. This mixture was added to the RNA/primer mixture, mixed and collected through brief centrifugation. RT PCR was then performed through incubation for 10-minutes at 25˚C followed by a 50-minute incubation at 50˚C and then terminated with an incubation at 85˚C for 5 minutes. The samples were then placed on ice and 1 µL of RNase H was added, followed by a 20-minute incubation at 37˚C. The samples were then immediately used or stored at -20˚C.

qPCR was performed using 3 technical replicates. For each replicate a volume of 1 µL of cDNA was used, along with 450 nM of the respective forward and reverse primers, 5 µL Power SYBR Green PCR Master Mix (Thermo Fisher Scientific, Waltham, MA) and water was used to bring the mix to a final volume of 10 µL per well. Primers used are listed in table 1. The Step

One Plus thermocycler (Thermo Fisher Scientific, Waltham, MA) was used and the cycling conditions were as follows: 1 cycle of 95˚ C for 10 minutes and 40 cycles of 95˚ C for 15 seconds followed by 60˚ C for one minute. Fluorescence data collection was performed during the 1 minute at 60˚ C. Following these conditions, a melting curve analysis was performed to determine PCR specificity. Data was collected using StepOne software (Thermo Fisher Scientific, Waltham, MA) and exported to Excel.

Tissue Fixation

Prior to performing IHC, mouse and rhesus tissue was fixed and frozen for sectioning. Fixation was performed with 4% paraformaldehyde (PFA) and tissue was prepared for freezing with incubation in progressively higher concentration sucrose solutions. For mouse eyes the entire eye was fixed. Following enucleation extraocular tissue was removed from the eye and the eye was washed in PBS. A small incision was made near the edge of the cornea using a 31-gauge needle. The eye was then placed in 4% paraformaldehyde solution for 15 minutes to fix. Following fixation, the eye was washed once in PBS and then placed in 5 % sucrose solution at 4˚C for 30 minutes. The eye was then transferred to a 10 % sucrose solution, where it was incubated for approximately 2 hours at 4˚C, until the eye sunk. The eye was then placed in 30% sucrose solution where it was incubated overnight at 4˚C. The next morning the tissue had again sunk to the bottom of the container and was prepared for freezing. This was done in a metal block, with holes drilled into, approximately the size of a large pen. Aluminum foil was wrapped around a pen and placed within a hole to ensure easy removal of the tissue. T he eye was placed within this foil mold. A 1:1 mixture of Tissue-Tek OCT (VWR, Radnor, PA) and PBS was then added to the eye and the tissue was placed at -80˚C to freeze. The tissue was then

sent to the Translational Research Initiatives in Pathology (TRIP) Lab on the UW Madison campus, where sectioning was performed. Sections were cut into 15 µM sections. For rhesus eyes the anterior segment of the eye was removed prior to fixation. The posterior segment was fixed using the same method described above and the tissue was exposed to progressively increasing concentrations of sucrose, imbedded in OCT and frozen, just as with the mouse eye. Sectioning was also performed in the same manner.

Immunohistochemistry

Frozen tissue sections were thawed to 25°C, rehydrated using PBS (Life Technologies, Grand Island, NY, USA), and blocked in PBS containing 10% goat serum, 5% BSA, and 0.3% Triton X-100 for 30 minutes at 25°C. The tissue was incubated with anti-OXTR primary antibody (1:100) diluted in incubation solution (1:3 blocking solution to PBS) overnight at 4°C in a humidified chamber. The sections were washed three times in PBS and incubated for 1 hour at 25°C with secondary antibody Alexa-Fluor 594 (1:100, goat anti-rabbit; Invitrogen), and 4',6-diamidino-2-phenylindole (DAPI) (1:1000; Molecular Probes, Inc., Eugene, OR, USA) diluted in incubation solution. Secondary antibody controls were tested for all experiments. The sections were washed three times in PBS and then incubated for 4 hours at room temperature with anti-Kir7.1 antibody (Alomone Labs, Jerusalem, Israel) diluted in incubation solution. The sections were then washed three times in PBS and mounted using Fluoromount (Sigma-Aldrich Corp.). Images were acquired using a Nikon C2 confocal system (Nikon, Melville, NY, USA) with a Nikon TiE microscope. A 20X objective was used with a numerical aperture of 0.75. Images were analyzed with NIS-Elements Advanced Research software (Nikon).

Statistical Analysis

qPCR data was analyzed using the comparative ΔCt method to determine relative expression. Ct for each technical replicate were averaged and the average Ct for the internal control was subtracted from this value, giving a ΔCt, which denotes expression relative to this internal control. ΔCt was then exponentially transformed into a relative expression (Relative expression = $2^{-\Delta Ct}$). For comparisons against adult mice ΔΔCt was calculated as $\Delta Ct_{p(x)} - \Delta Ct_{adult}$. ΔΔCt was then exponentially transformed in to fold change, relative to adult (Fold change = $2^{-\Delta\Delta Ct}$).

4.3 Results

4.3.1 OXTR can be found at all gestational time points in the whole eye

To determine whether mouse eye expression of OXTR differed throughout retinal development, the levels of expression were assayed in mice from postnatal day 0 (p0), p5, p10, p15 and adult. Following euthanasia, mouse eyes were enucleated, snap frozen in liquid nitrogen and then mRNA was isolated from the entire globe. cDNA was made and PCR was then performed to determine whether OXTR was present. We observed a consistent level of OXTR expression relative to β-Actin at all tested time points suggesting that whole eye OXTR expression remains relatively stable during the time associated with retinal maturation and vascular growth in the mouse eye (Figure 1a). However, when we isolated the RPE using the SCRIRS method we observed a reduction in expression in early gestational age, with no OXT detectible prior to day 10 (Figure 1b). To better measure expression of the receptor with more sensitivity and determine if these results could be confirmed, we set out to measure OXTR expression in the RPE using qPCR.

4.3.2 qPCR demonstrates that OXTR expression is not significantly altered during the period of vascular development

To determine whether the level of expression observed in the whole eye in the days following birth is consistent with that observed in the RPE, we isolated mRNA from the RPE specifically and quantified the expression of OXTR using qPCR. Utilizing the SCRIRS method described by Wang et al. we isolated RPE cells and extracted total RNA (Xin-Zhao Wang et al., 2012). cDNA was synthesized from isolated mRNA and qPCR was performed using the primers in table 1. Within each sample relative expression (ΔCt) was determined through comparison to Ct for 18s rRNA (Figure 2A). Average ΔCt of each group was subtracted from that of adult mice (ΔΔCt) and then average fold change was calculated ($2^{-\Delta\Delta Ct}$) (Figure 2B). The mRNA isolated from RPE showed a less than significant ($p>0.05$) reduction in OXTR expression in younger mice, with fold change of 0.20 (+1.41/-.028) in P0, 0.046 (+0.089/-0.024) in P5, 0.24 (+2.52/-0.023) in P10, 0.043 (+0.42/-0.0056) in P15 and a 0.17 (+1.69/-0.017) in P20 mice, relative to adult mice. The sample sizes at each time point were as follows, P0 (n=4), P5 (n=5), P 10 (n=6), P15 (n=11), P20 (n=22), Adult (n=6). Within each time point we observed a large variation in the level of OXTR expression, which is illustrated in Figure 2A. To determine whether the observed variation was a result of sex differences we compared OXTR expression between male and female mice across all groups (Figure 3). We found that there was on average slightly higher expression in female mice but this was not statistically significant and the variability in expression persisted in both sexes ($p>0.05$). The relative expression, calculated as $2^{-\Delta Ct}$, was 7.45×10^{-6} ($+8.47\times10^{-6}/-6.9\times10^{-6}$) in male mice (n=13), while the female mice (n=13) had an average relative expression of 4.36×10^{-5} ($+3.79\times10^{-6}/-4.35\times10^{-5}$).

To identify the cause of variation in OXTR expression observed in these data I compared the Ct counts for OXTR to those observed for the RPE specific gene RPE65. While our isolation should yield mRNA predominately from the RPE I suspected that some variation may have been the result of retinal mRNA in our samples. This comparison would allow me to determine whether OXTR variation was a result of variation in the level of mRNA from the RPE. I observed a decrease in relative expression of OXTR to RPE65 with increasing gestational age, a decrease that was significant when comparing P0 and P5 to adult mice ($p<0.05$) (Figure 4). This decrease was a result of increased expression of RPE65 as mice aged (Figure 5), suggesting either that OXTR expression is massively increased, relative to RPE65, in younger mice or that majority of OXTR expression was not coming from the RPE at all in mice.

4.3.4 OXTR expression is observed in the mouse retina at low levels.

To determine whether there was some expression of OXTR in the retina, I then quantified the expression of OXTR from P20 mouse retinas collected during RPE isolation. In these samples I found consistent OXTR transcript presence (Figure 6). I compared the expression of OXTR to RpL13A and found a relative expression of $1.5x10^{-3}$ ($+2.8x10^{-3}/-7.5x10^{-4}$) (n=8). The OXTR expression was not significantly different than the level of expression observed in the RPE, which was $2.0x10^{-3}$ ($+0.031/-1.3x10^{-4}$) (n=11), relative to RpL13A. These relative expression levels suggest that there is expression of OXTR in the mouse retina and that it is equal to that observed in the RPE. The variation in expression in the RPE persists in these samples but did not appear in the retina (Figure 6A). Given the potential cross contamination of retina and RPE during my isolation process I looked specifically at RPE and retinal cell expression by enzymatic dissociation of the respective tissue followed by identification and

selection of individual cells under a microscope. In these grouped cells I was able to identify OXTR expression in both RPE and retina, clearly showing that OXTR is expressed in both tissues. I found expression, relative to RpL13A, of 1.57 in the retinal group and a relative expression of 0.031 in the RPE group indicating far lower expression in the RPE than the retina.

4.3.3 Immunohistochemical analysis of OXTR expression in mouse and rhesus retina

In immunohistochemical analysis of human and rhesus retina I have previously shown that OXTR expression is limited to the RPE, with no discernable expression within the neural retina. These data from the mouse however suggest that OXTR expression extends beyond the RPE. To determine the extent of this expression in the mouse and compare it to that in the primate I performed IHC on mouse and rhesus retina. My results demonstrate a difference in OXTR expression across these species. In the rhesus I observed OXTR expression primarily in the apical projections of the RPE demonstrated by its co-localization with Kir7.1 (green), which is also apically located (Figure 7). Closer analysis of the RPE confirms this co-localization, using NIS elements AR software to track regions of correlated fluorescent intensity (Figure 8). Additionally, I looked at the localization of OXTR relative to that of the cone photoreceptor outer segments, stained with PNA (green), where OXT has previously been found (Figure 9) (Halbach et al., 2015). I found that OXTR surrounds these outer segments, clearly showing the potential for oxytocinergic signaling. These results were confirmed with negative controls demonstrating that the staining observed was specific to OXTR (Figure 11).

When IHC was performed on mouse retina the localization of OXTR was much different, with OXTR antibody staining the entire retina (Figure 10). I observed strong OXTR staining in the retina and an apparent lack of OXTR staining in the apical process, again indicated by Kir7.1

(green). These results were also confirmed using negative controls (Figure 12). My qPCR data suggests that there is limited expression in the RPE of some mice while OXTR expression in the retina is largely consistent and these data support that. This result confirms my qPCR data, showing that the mouse exhibits expression of OXTR across the retina with much less consistence in the expression within the RPE.

4.4 Discussion

Prior to my work, the role of oxytocin in the retina has been largely unstudied. I have previously demonstrated that it is present in the human and rhesus RPE and that it is functional and can act through the modulation of the inwardly rectifying K^+ channel, Kir7.1. Here I expand beyond the primate and look at OXTR expression in the mouse retina. The mouse is a powerful tool for vision research and understanding and characterizing the expression of OXTR in the mouse retina is necessary to support future studies of the role oxytocin might play in the development and maintenance of the retina. I have demonstrated that the expression of oxytocin receptor is consistent, on average, in the mouse retina during its postnatal development. Within the RPE I observed a large variation in receptor expression that was not dependent on sex. Furthermore, I found, unlike what we have previously reported in primates, that the expression of OXTR is not limited to the RPE in mice but instead is expressed throughout the retina. These results are interesting as they suggest a possible difference in the role of OXTR in mice than in primates.

To determine the ontogeny of OXTR I initially looked at its expression in the whole eye. I observed a consistent level of expression from birth to postnatal day 15 using gel electrophoresis, comparing the OXTR band intensity to that of the B-Actin control (Figure 1).

However, I wanted to look more specifically at expression in the RPE in a quantifiable way. Therefore, I isolated the RPE and assayed the mRNA for OXTR expression, again using gel electrophoresis. I found a lack of expression in mice younger than 10 days old.

To get a more accurate idea of the levels of transcript present I utilized quantitative PCR and analyzed the observed expression relative to 18s rRNA, a structural component of cytoplasmic ribosomes. This analysis revealed a confusing and complicated picture of OXTR expression in the RPE and the retina. Looking at average expression, relative to 18s rRNA, our results were like those observed in the whole eye. I saw no significant change in the level of expression with age, although there was a general trend towards increased expression in older mice. However, these data are complicated by a large variation in the level of OXTR expression between mice of the same age. While my initial instinct was that this variation was a result of sex I did not observe any difference between male and female mice when they were directly compared (Figure 3).

The RPE isolation method used allows me to separate the RPE but it does not ensure a total lack of mRNA from other sources. To determine whether the variation observed was the result of different variation in the level of RPE mRNA relative to other mRNA, I compared the expression of OXTR to that of the RPE specific gene, RPE65. With this comparison I found a dramatic decrease in the level of OXTR expression as the mouse matured. This decrease in relative expression was the result of significantly reduced RPE65 expression in younger mice. This lower expression is consistent with previous literature which describes a proliferation of the RPE that continues at approximately 1,500 cells/day from birth to p15 (Bodenstein & Sidman, 1987). One possibility that might explain the consistent expression of OXTR,

independent of the level of RPE 65, is that a baseline level of OXTR is required in the retina for normal function. If this baseline level was required OXTR must be over expressed in individual RPE cells at an early age when the RPE is less abundant and that expression would be reduced to maintain basal levels in the mature eye when more RPE is present. Alternatively, the stable expression of OXTR despite changing RPE65 expression could suggest the presence of another source of OXTR from elsewhere in the retina.

To determine if there was an alternate source of OXTR in the mouse I compared expression in the RPE to that of isolated mouse retina. Using a different internal control, RpL13A, I found on average that the level of OXTR expression in the retina was the same as what we observed in the RPE. Interestingly, the variation I observed within the RPE was not present in the retina. This result was inconsistent with what I expected based on immunohistochemistry done on human and rhesus retina previously and suggest that the mouse may have a different pattern of OXTR expression than the primate (Halbach et al., 2015). To confirm these results and compare the OXTR expression in the mouse to the rhesus I analyzed OXTR protein localization within cryosections of mouse and rhesus retinas. In addition to OXTR, I stained these sections with antibodies against Kir7.1 to mark the RPE and help establish localization of the receptor within the polarized cells. The results confirmed my qPCR and our previous IHC data, showing robust staining throughout the mouse retina while the rhesus showed OXTR primarily in the RPE. In the mouse I observed a distinct lack of co-localization with Kir7.1 while in the rhesus I observed a strong co-localization with Kir7.1, demonstrated clearly in Figure 8. The lack of co-localization in the mice appears to be the result of a lack of expression in the RPE overall, at least compared to what I see in the retina. These

data are not inconsistent with what I have observed in our qPCR where I saw mice with wide ranging levels of OXTR expression. The IHC does, however, suggest that the source of that variation is not from regional differences in expression but instead results from a lack of expression throughout the RPE of certain mice but not others. There are some differences between mice and primate retinas including a predominance of rods in mice compared to primates who have a retina with a cone heavy fovea. Perhaps this difference could hint at a cause in differential expression of OXTR, however the reason for this lack of expression needs to be further explored.

We have previously demonstrated that OXT is present in the subretinal space, specifically, in the extracellular matrix of the cone photoreceptor outer segments. In this study I have now localized OXTR to the apical projections of the RPE, which project towards these outer segments. This fact is further demonstrated in Figure 9, where I show the projection of cone POS, labeled with PNA, into the OXTR expression apical processes. The presence of OXTR in close on the apical membrane in close proximity to the POS suggests that OXT from the retina can influence the RPE, indicating a potential role for the hormone in regulating the interactions between the RPE and retina. Furthermore, given the data discussed in **chapter 2**, the co-localization of OXTR to Kir7.1 in the primate suggests that this role could be through the G-protein mediated inhibition of Kir7.1. One possible role for OXTR could be in the regulation of POS phagocytosis by the RPE. In macrophages depolarization has been shown to play an important step in the initiation of phagocytosis (Link et al., 2010). Perhaps the prolonged depolarization we have observed in OXTR mediated inhibition of Kir7.1 is playing a similar role in the RPE, which exhibits continued phagocytosis over a period of 4 hours. Additionally, both

OXTR and Kir7.1 have both been shown to exhibit clathrin mediated endocytosis and their co-localization in the apical processes supports the potential for them to exist in the same submembrane lipid rafts where they could be endocytosed together or PKC could mediate the internalization of Kir7.1, as has been observed in other Kir channels (Jiao et al., 2008; Kumar & Pattnaik, 2014; Smith et al., 2006). This is the extent of the supporting evidence, however and much more work is certainly needed to definitively determine the role for OXTR in the retina, including higher resolution, sub membrane localization of the proteins.

In conclusion, this study has characterized the expression of OXTR in the mouse as well as the rhesus, demonstrating the following points; 1) OXTR expression in the whole eye is unchanged throughout development, 2) The same is true in the retina, with no significant alteration in the expression of OXTR from birth to adulthood, despite reduced RPE population at younger ages, 3) There is a large amount of variation in the expression of OXTR within the RPE that is not sex or age dependent, 4) In the mouse OXTR expression is not limited to the RPE and can be found throughout the retina, 5) In the rhesus retina OXTR protein is present in the apical processes of the RPE, surrounding the POS and co-localizing with the inwardly rectifying potassium channel Kir7.1. These data suggest a multifaceted role for OXTR in the eye across species with the potential to act both in the RPE and the retina. While mouse RPE has been previously shown to respond to OXT stimulation the functionality of the receptor in retinal cells needs to be further studied. My IHC also reveals species differences in the pattern of expression between mice and rhesus. In the primate my findings support a role for the interaction between Kir7.1 and OXTR on the apical membrane of the RPE in regulating RPE-retinal interaction.

Acknowledgments

I would like to thank everyone who helped me with the work done in this chapter, especially Allison Lutz and Hannah Labarge, who both provided invaluable help in performing all of the PCR needed for this chapter. The UW nonhuman primate services core graciously provided the rhesus eyes for use in our IHC experiments.

4.5 Tables and Figures

Table 1: Primer sequences used in Chapter 4		
Primer	Forward	Reverse
OXTR (qPCR)	TTGTACCGGTCATCGTGCTG	CTTCAGGTACCGAGCAGAGC
RPE65 (qPCR)	ATGTCACAGGCAGGATTCCC	ATGTGACATGGCCCTCCTTG
18s rRNA	GTAACCCGTTGAACCCCATT	CCATCCAATCGGTAGTAGCG
Rpl13A	TCTCAAGGTTGTTCGGCTGAA	GCCAGACGCCCCAGGTA
OXTR (PCR)	CTGGACGCCTTTCTTCTTC	CGAGGATGGTTGAGAACAG
RPE65 (PCR)	CGGACTTGGGTTGAATCACT	GCTCACCACCACACTCAGAA

Table 2: Antibodies used for IHC in Chapter 4			
Antibody	Description	Source	Product Number
Anti-OXTR	Rabbit Polyclonal	Novus Biologicals	NBP1-02410
Anti-Kir7.1 (extracellular)-ATTO-488	Rabbit Polyclonal	Alomone Labs	APC-124-AG
Lectin PNA, Alexa Flour 488 Conjugate	From *Arachis hypogaea*	ThermoFisher	L21409
Alexa Fluor 594 goat anti-rabbit lgG (H+L)	Goat Polyclonal	ThermoFisher	A-11012

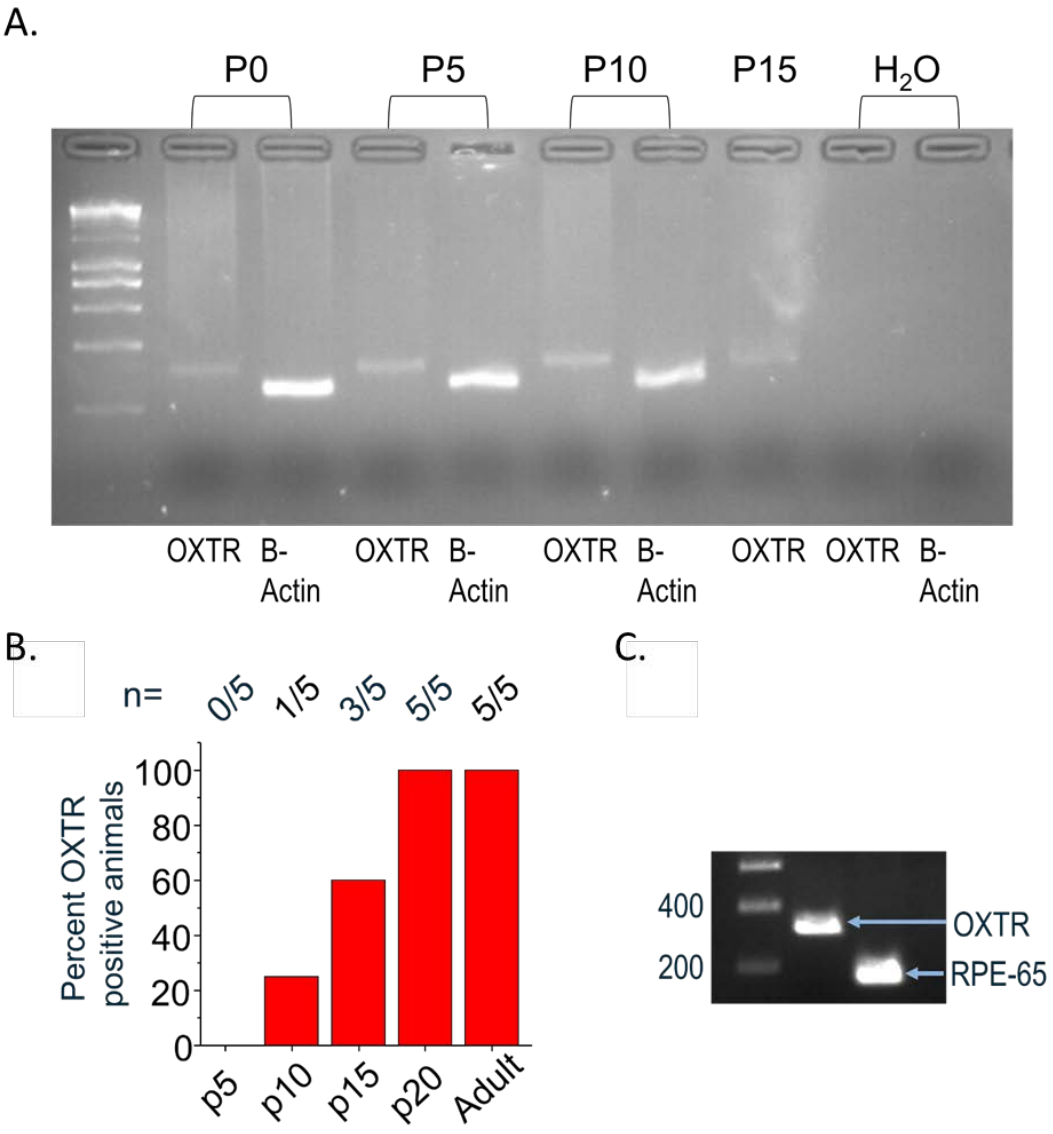

Figure 1: Expression of OXTR was found in the whole eye but not in the RPE prior to 10 days postnatal age using traditional PCR. (A) Expression of OXTR bands in whole eye is present from birth on. (B) Percent of animals with observed expression of OXTR. Sample size listed above as (OXTR-positive / total). (C) Representative bands showing OXTR and RPE-65 bands as observed.

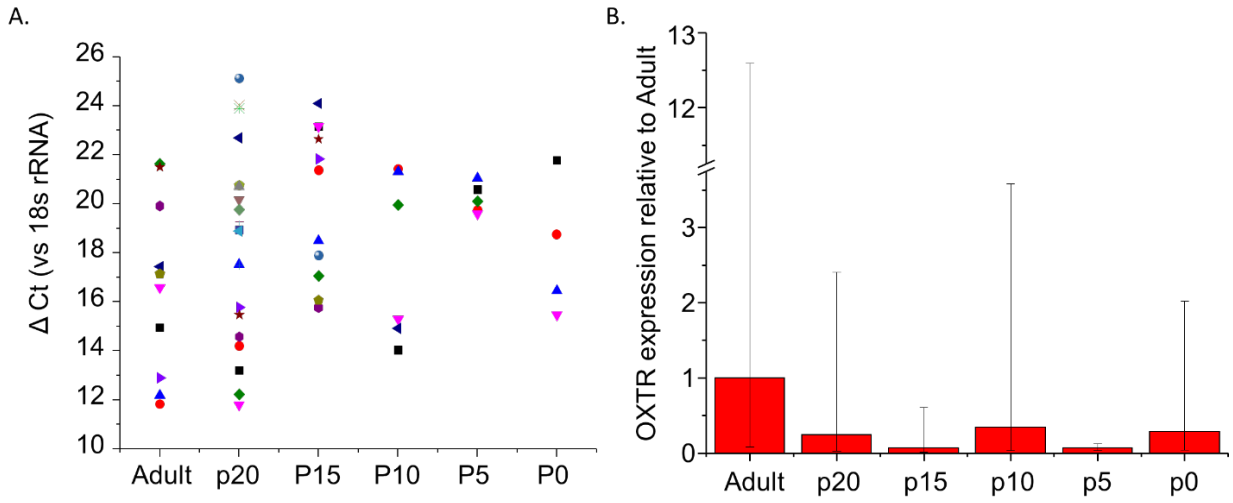

Figure 2: qPCR of OXTR expression relative to 18s rRNA during retinal vascular development in mice. (A) Scatterplot of ΔCt values for each mouse studied. The sample sizes were as follows, P0 (n=4), P5 (n=5), P 10 (n=6), P15 (n=11), P20 (n=22), Adult (n=6). ΔCt values were determined by subtracting Ct for 18srRNA from Ct for OXTR within each tested sample. Within each studied time point there was a large amount of variability in the observed ΔCt. (B) Comparison of OXTR expression, relative to the adult across all timepoints. There was no significant change in expression observed between the time points although on average the adult expression was higher than any other time point.

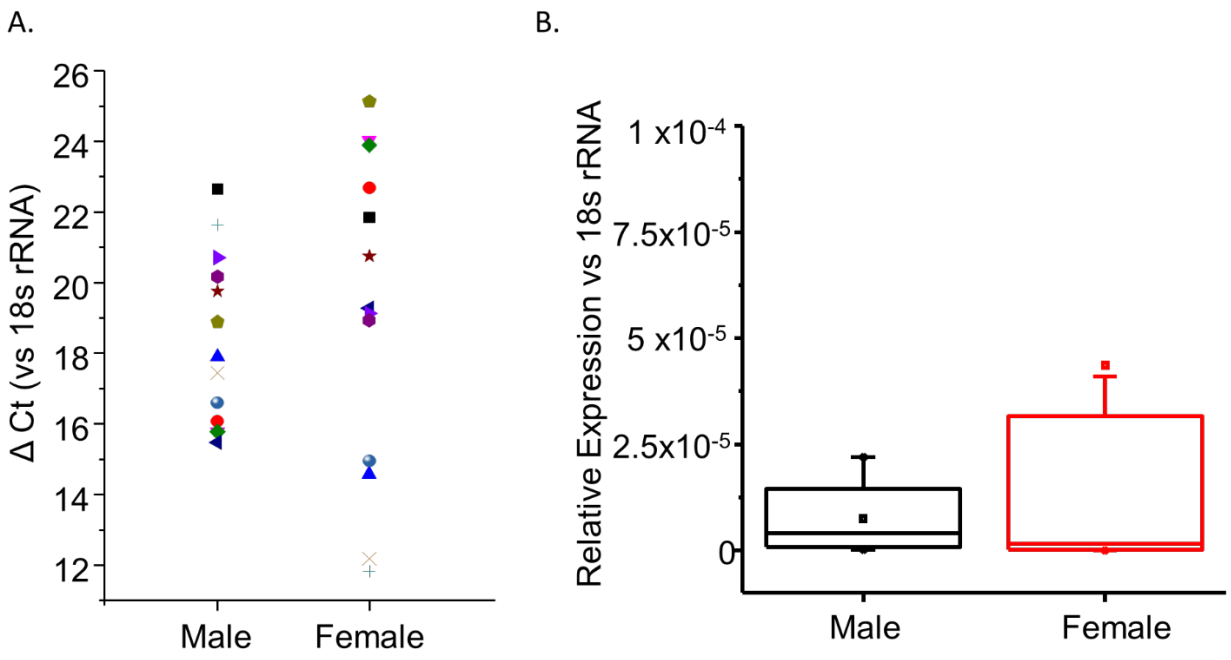

Figure 3: Comparison of OXTR expression between male and female mice. (A) Scatterplot of ΔCt values for each mouse studied. ΔCt values were determined by subtracting Ct for 18srRNA from Ct for OXTR within each tested sample. A large degree of variability was found in the ΔCt within each sex, similar to what was observed when grouping mice by age. (B) Box plot of average relative expression of OXTR observed. Male and female mice were compared and no significant difference was found between the two.

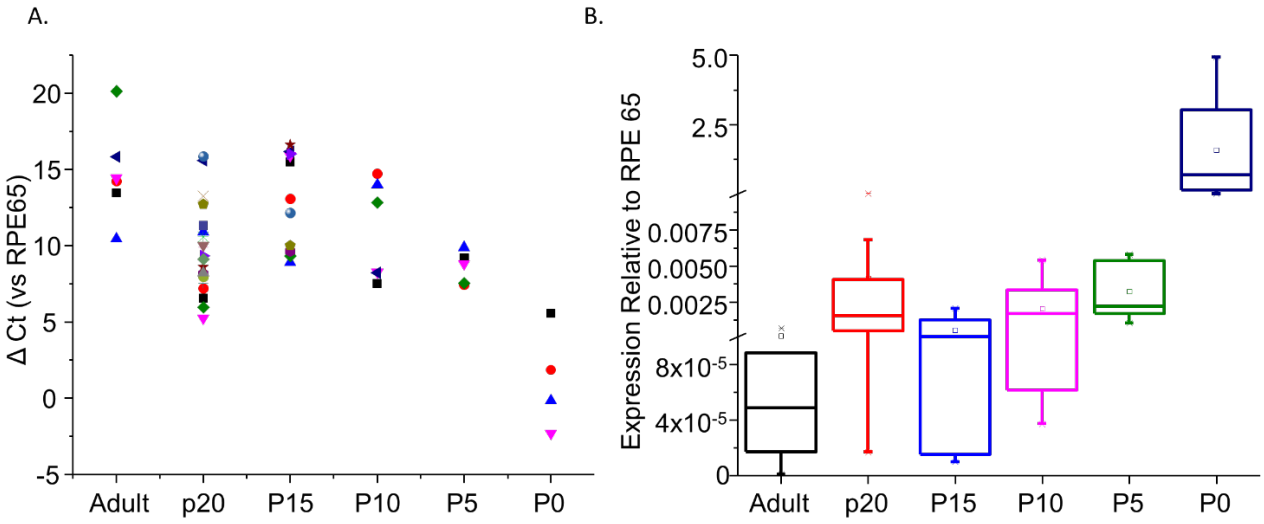

Figure 4: Comparison of OXTR expression by age, relative to RPE65 expression. (A) Scatterplot of ΔCt values for each mouse studied. ΔCt values were determined by subtracting Ct for RPE65 from Ct for OXTR within each tested sample. (B) Box plot of average relative expression of OXTR observed, relative to RPE65. Due to the large difference in expression across age, the y axis contains 2 breaks, with altered scales, to ensure all samples are visible.

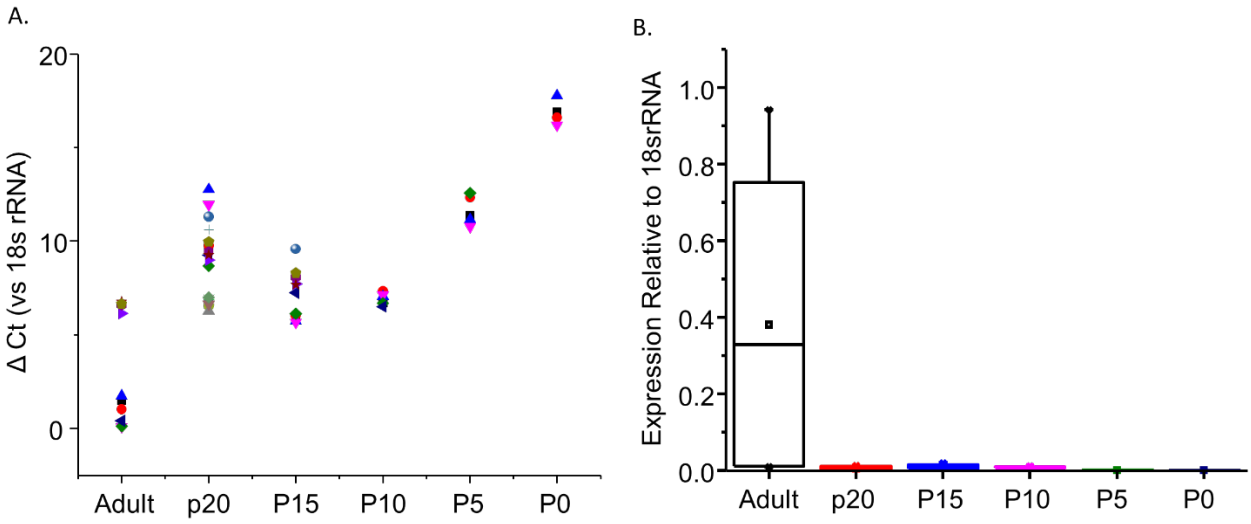

Figure 5: Expression of RPE 65, compared to 18s rRNA, in mouse retina. (A) Scatterplot of ΔCt values for each mouse studied. ΔCt values were determined by subtracting Ct for 18s rRNA from Ct for RPE65 within each tested sample. (B) Box plot of relative expression of RPE65, showing dramatic decrease in expression with reduced gestational age.

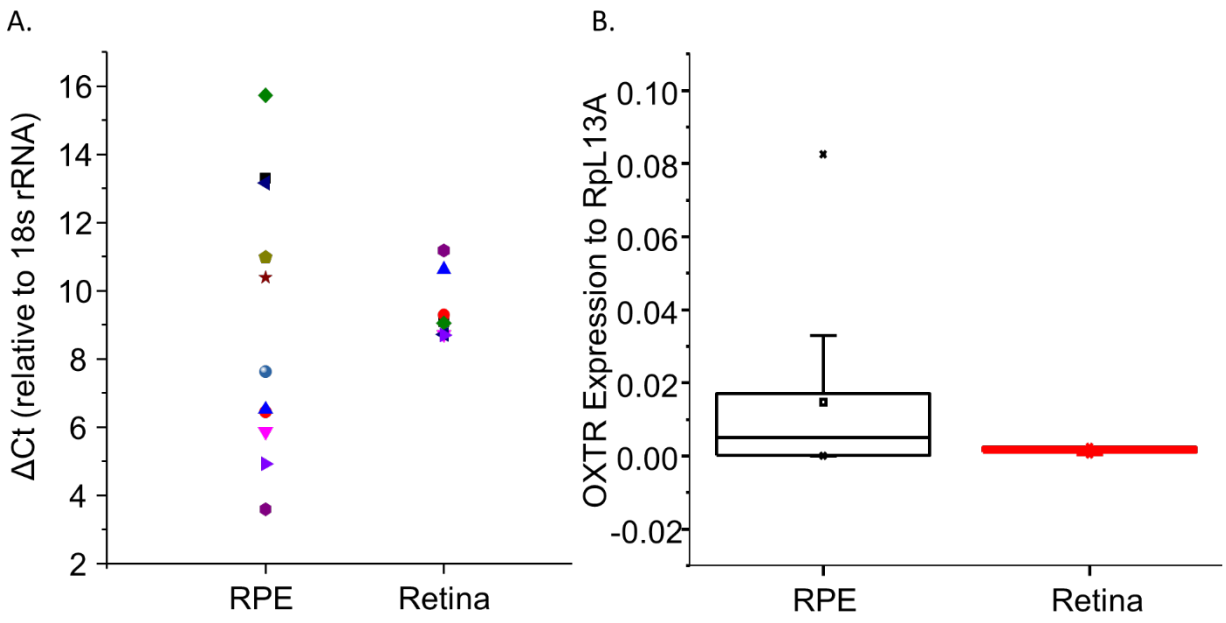

Figure 6: Expression of OXTR in the mouse retina. (A) ΔCt, relative to RpL13A, of each sample tested is shown. N=6 for RPE and N=4 for Retina. (B) Relative expression ($2^{-\Delta Ct}$) of OXTR in RPE and retina is shown.

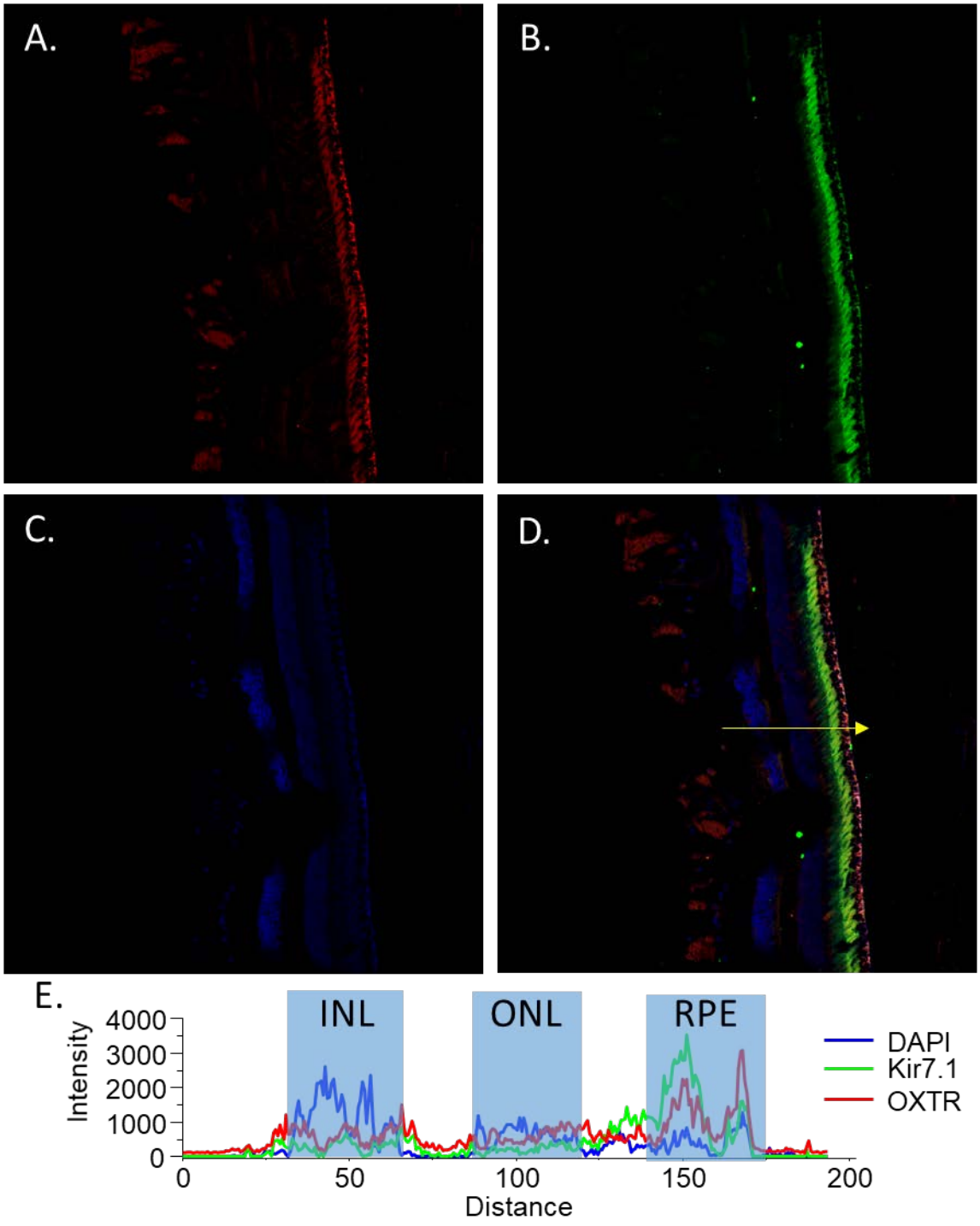

Figure 7: OXTR expression in the rhesus retina co-localizes with Kir7.1 in the RPE. (A) Single channel image showing OXTR staining in rhesus retina. (B) Single channel image showing Kir7.1 staining. (C) Single channel image showing DAPI staining. (D) Merged image of rhesus retina from A-C combined. E. Intensity profile of fluorescent intensity along arrow shown in Panel D. OXTR and Kir7.1 co-localization can be observed in the RPE, in both the outer segments and cell body.

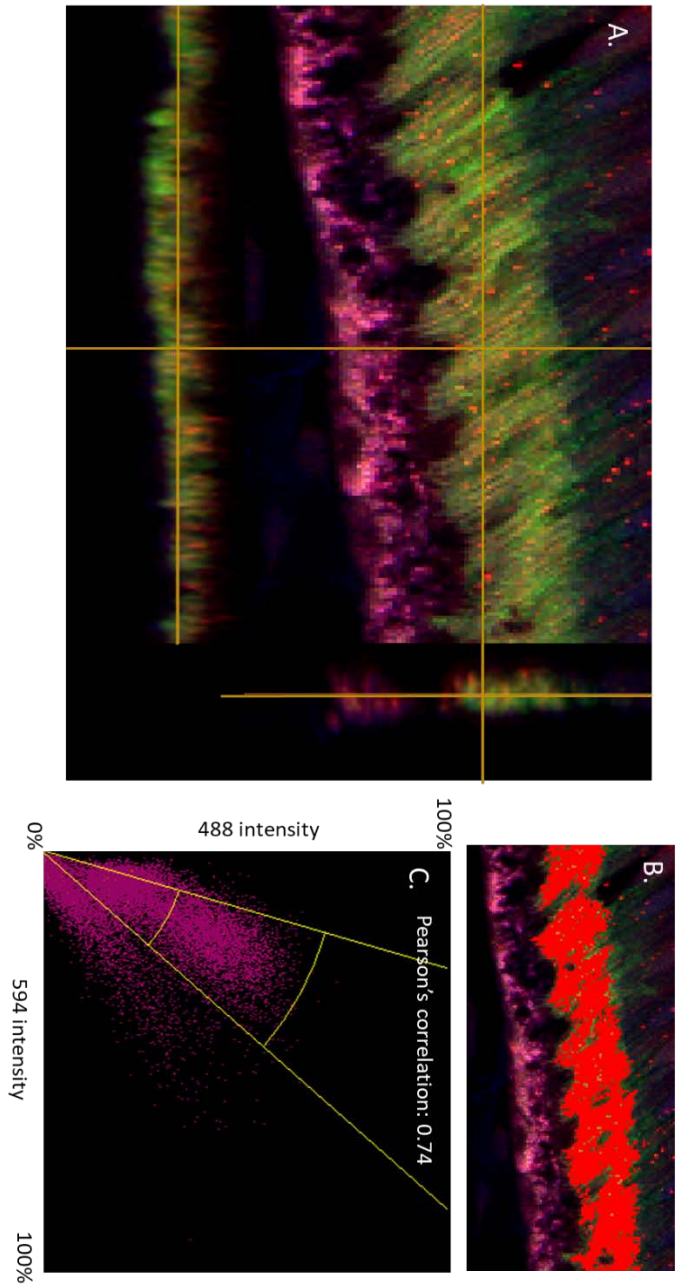

Figure 8: Enlarged image of RPE from rhesus retina showing co-localization of Kir7.1 and OXTR. (A) Maximum intensity projection, taken from a z-stack of rhesus retina, with slices view along the x and y axis. Yellow color indicates co-localization between OXTR and Kir7.1. (B) Region of co-localization was detected and highlighted in red using NIS elements AR software. (C) Fluorescent intensity was plotted and the region of highest intensity for both wavelengths was selected and the corresponding region was highlighted in Panel B. Pearson's correlation was calculated for the entire image to be 0.74.

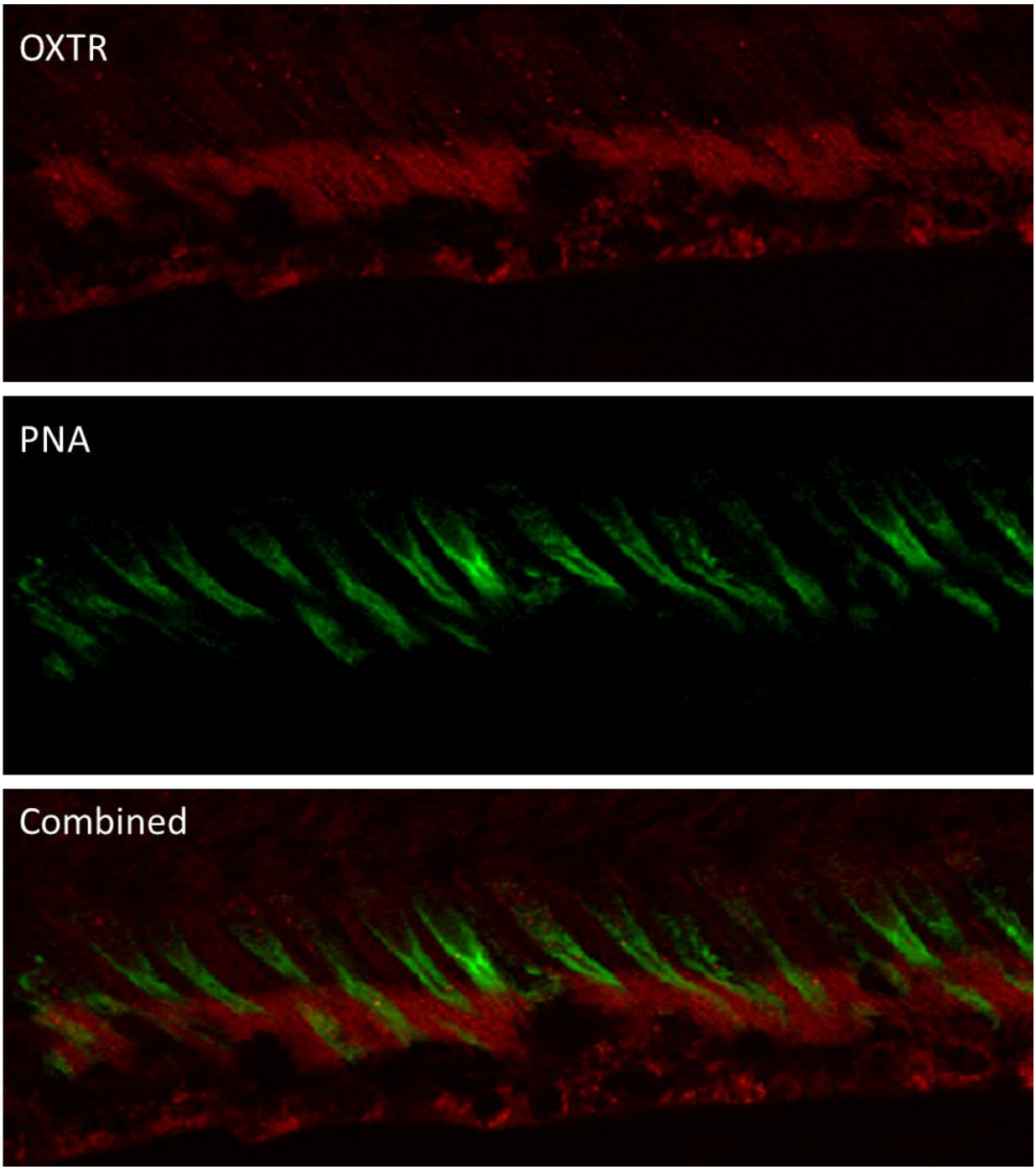

Figure 9: OXTR in the apical processes surrounds cone POS. OXTR, labeled in red, is shown in the outer segments of the RPE, which surround the cone photoreceptor outer segments, tagged with Peanut agglutinin (PNA) shown in green. OXT has been found in these outer segments, and this close spatial relationship further supports oxytocinergic signaling in the primate RPE.

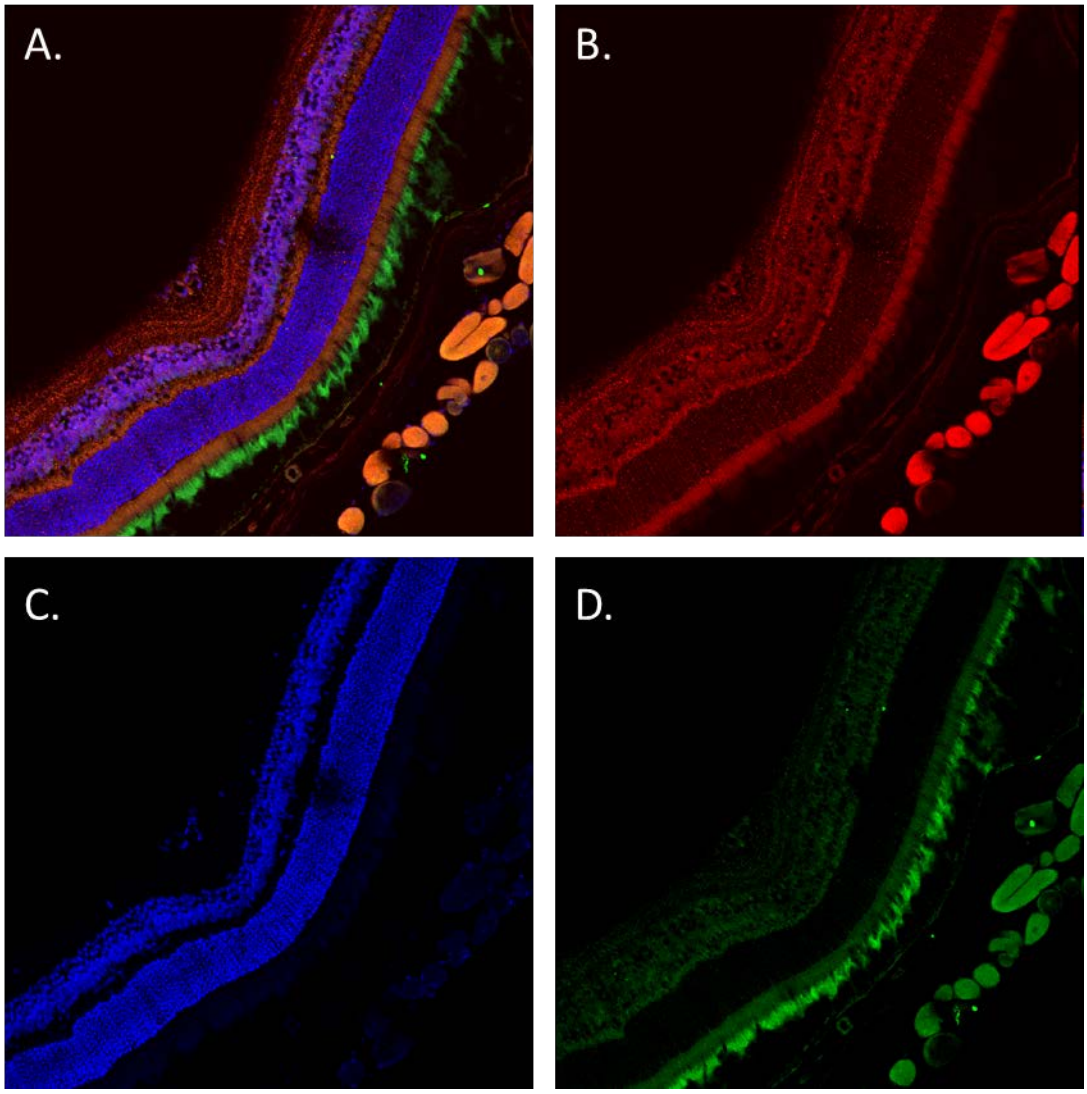

Figure 10: OXTR is expressed throughout the mouse retina. (A) Merged image of IHC staining of adult mouse retina. OXTR (Red), Kir7.1 (green), DAPI (blue) are shown. (B) OXTR staining is shown. (C) Nuclear staining (DAPI) is shown. (D) Kir7.1 staining is shown.

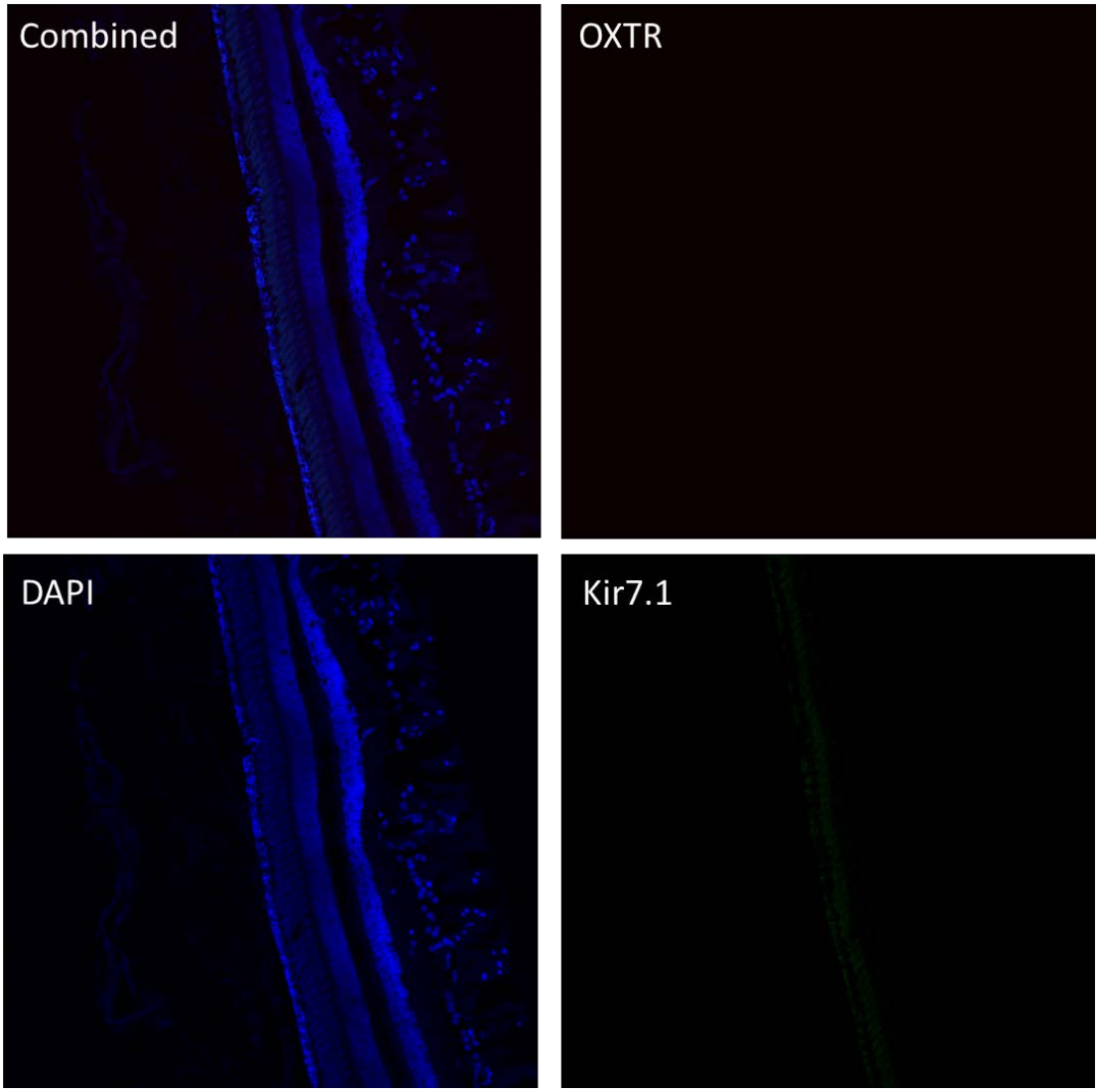

Figure 11: Negative control for staining in rhesus. IHC procedure was followed without Anti-OXTR or anti-Kir7.1 antibodies, demonstrating that staining observed was specific to the proteins assayed.

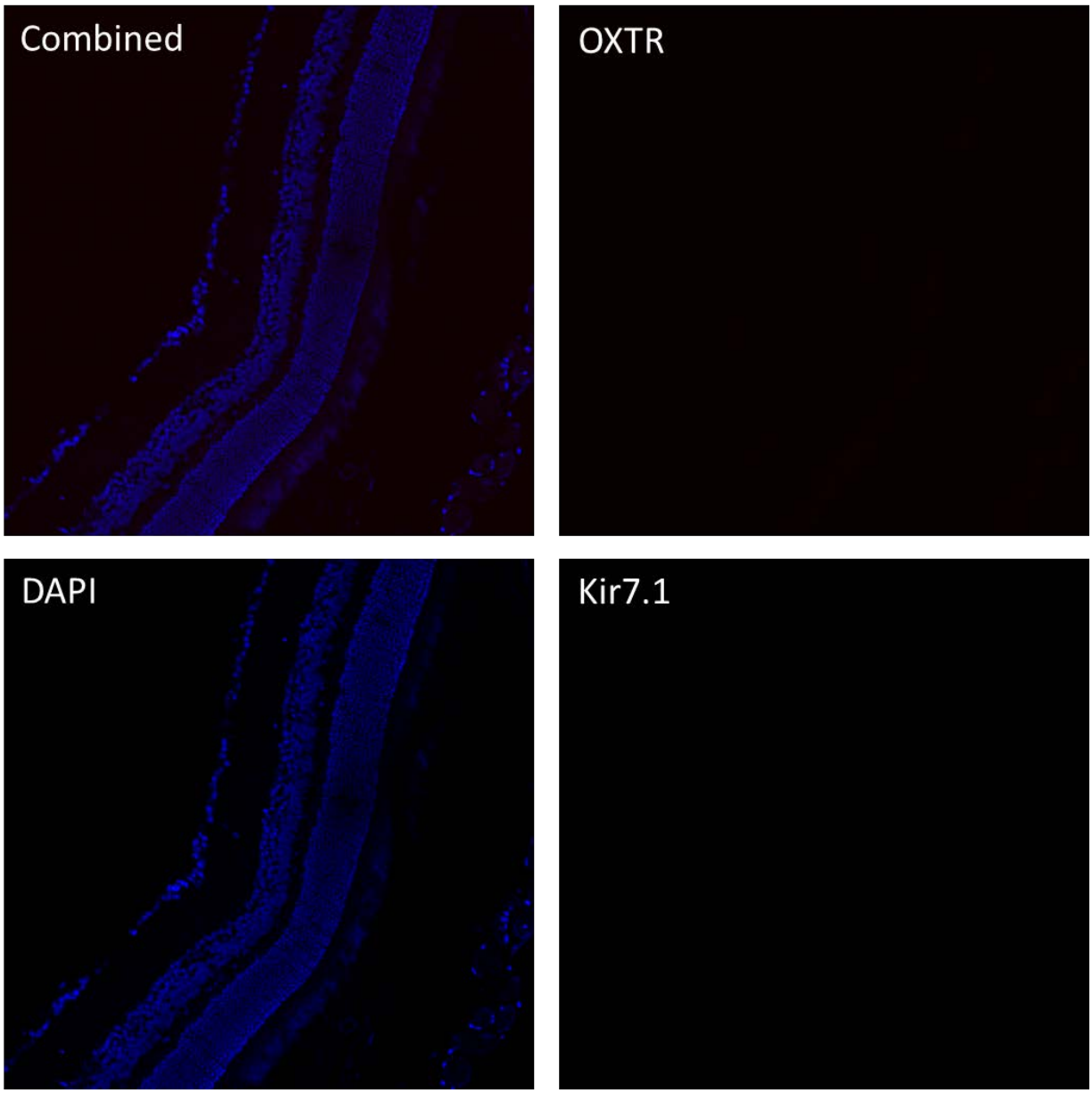

Figure 12: Negative control for staining in mouse. IHC procedure was followed without Anti-OXTR or anti-Kir7.1 antibodies, demonstrating that staining observed was specific to the proteins assayed.

Chapter 5: Final Discussion

5.1 Summary of Key Findings

Oxytocin has a diverse and ever-expanding list of roles throughout the body. In this study I have added to this list, characterizing the expression and function of oxytocin and its receptor in the RPE. The localization of OXTR to the RPE in primates has already been demonstrated by our lab and we have previously shown that OXT can induce a Ca^{2+} response in hfRPE cells (Halbach et al., 2015). I have expanded on these findings in **chapter 2** by characterizing the signaling pathway at work in the RPE and detailing the regulation of the important ion channel Kir7.1. While the mechanism of OXTR signaling in other tissues has been described previously I have taken a pharmacological approach to describing this signaling for the first time in the RPE. I have shown that OXT binds to OXTR in the RPE and induces the G-protein mediated activation of PLC. PLC then hydrolyzes PIP_2 into IP_3 and DAG and IP_3 goes on to induce release of Ca^{2+} from the endoplasmic reticulum. In the process of this characterization I have addressed some of the outstanding debate over the mechanism of OXTR signaling. Principle amongst these is the role played by extracellular $[Ca^{2+}]$ ($[Ca^{2+}]_e$) after OXT stimulation of OXTR. My data are in agreement with those who have suggested that the rise in OXT mediated $[Ca^{2+}]_I$ is nifedipine insensitive, however the reduced amplitude of the Ca^{2+} response both during nifedipine and 0 Ca^{2+} treatment demonstrate that an influx of $[Ca^{2+}]_e$ does occur, even if the response to OXT does not rely on it (Arrowsmith & Wray, 2014; Inoue et al., 1992). I have also addressed the potential for OXT to induce a response in the RPE through other mechanisms than its interaction with OXTR, for example through cross reactivity with the vasopressin receptor (Kimura et al., 1994). I was able to abolish the OXT mediated $[Ca^{2+}]_i$

response in the presence of an OXTR specific antagonist, showing that the RPE cells response to OXT is specifically mediated by OXTR.

Having established the mechanism of OXTR signaling in the RPE I shifted my focus to addressing the first aim of this thesis, exploring the impact this signaling has on RPE physiology. The regulation of Kir channels by PIP_2 has been extensively shown and it was this regulation that brought my focus to Kir7.1 (Hatcher-Solis et al., 2014; Pattnaik & Hughes, 2009; Rohács et al., 2003). In **chapter 2** I have demonstrated that OXT can inhibit Kir7.1, both in HEK-OXTR cells expressing Kir7.1 eGFP as well as in freshly isolated mouse RPE. This result was consistent with what we would expect, given the hydrolysis of PIP_2 by PLC, however the kinetics of the inhibition revealed a more complicated picture. Previous work has demonstrated that PIP_2 depletion following inhibition of phosphoinositide 3-kinase (PI3K) is immediately reversible once P13K inhibition is removed and membrane PIP_2 can be replenished (Pattnaik & Hughes, 2009). My results show a time course of current inhibition that is consistent with PIP_2 depletion, however I do not observe any recovery of current inhibition following washing of the cells with OXT free HR solution.

To eliminate the potential for this result to be due to disruption of the intracellular environment during whole cell recordings, possibly altering PIP_2 regeneration, I recorded from Kir7.1 expressing HEK-OXTR cells using the perforated patch clamp configuration. Again I observed a persistent inhibition of Kir7.1 following OXT treatment. The lack of recovery I observed brought into question whether the inhibition was in fact due to PIP_2 hydrolysis at all or if I was observing a potential G-protein independent inhibition similar to the inhibition of Kir7.1 described in MC4R neurons (Ghamari-Langroudi et al., 2015). To address this possibility I

used the same pharmacological inhibitor of G-protein function, GDPβS, which was utilized in the study on MC4R cells. In whole cell patch clamp recordings, with GDPβS in the internal solution, I found that the OXT mediated inhibition was completely abolished, demonstrating that unlike the inhibition observed in MC4R neurons the OXT induced inhibition was dependent on G-protein coupling. These results suggest a mechanism that begins with a G-protein mediated inhibition of Kir7.1, likely by the hydrolysis of PIP_2, but which persists through despite the replenishment of membrane PIP_2.

I can hypothesize about the cause of this prolonged inhibition but further study will have to be done to clearly delineate its causes. One possibility that should be explored is that OXTR activation is resulting in the internalization of Kir7.1. The internalization of OXTR has been described before and is suggested to occur in a clathrin dependent manner (Conti et al., 2009; Smith et al., 2006). While this type of internalization has not been described yet for Kir7.1, the protein structure contains a consensus motif (YSHI [244-247 aa]) that has been shown in other proteins to favor association with clathrin coated vesicles (Kumar & Pattnaik, 2014). Perhaps then when OXTR is activated and internalized Kir7.1 is internalized as well through the same mechanism. Additionally, work on K-ATP channels has shown that those channels can be internalized in a caveolin dependent manner as the result of PKC activation (Jiao et al., 2008). Not only has OXTR also been described to localize to caveolin domains but OXTR activation leads to the activation of PKC, hinting at a second possible mechanism for the internalization and subsequent prolonged inhibition of Kir7.1 (Guzzi et al., 2002). In **chapter 4** I have been able to demonstrate the co-localization of both Kir7.1 and OXTR to the apical projections of the rhesus RPE which provides some support for this hypothesis although further sub-membrane

localization will need to be established. This would explain the results we are observing as you would expect to see fast inhibition of Kir7.1 through PIP_2 hydrolysis followed by the internalization of the channel preventing the recovery of current when PIP_2 is regenerated by PI3K. Hopefully, this and other explanations can be explored in the future.

Having demonstrated this potential mechanism for OXTR to modulate the function of the RPE through alteration of ion homeostasis and membrane potential I turned my focus to the potential downstream implications of OXTR activation, looking at the impact of oxytocinergic signaling on the transcription and secretion of vascular growth factors. The reason for this focus centers on a desire to find a cause for the persistence of ROP in infants described in more detail in **chapter 1.6**. As we currently understand the pathogenesis of ROP is driven by initial hyperoxia in the retina on birth in premature infants despite the regulation of oxygen delivery. As modern medicine allows younger and younger infants to survive we are seeing an increase in the incidences of ROP suggesting that factors arising from prematurity itself play a role in the development of the disease (Sahin et al., 2014). Oxytocin has not only been shown to induce blood vessel growth but its production also increases towards the end of gestation indicating that premature infants will likely lack OXT (Cattaneo et al., 2008; Schubert et al., 1981). Given these two facts I hypothesized that the lack of OXT in premature infants could be a causal factor in the development of ROP. Having previously demonstrated the apparent exclusive expression of OXTR in the RPE within the posterior retina of the rhesus and human we set out to determine whether OXT could induce a change in RPE production of angiogenic factors, primarily those associated with ROP. In **chapter 3** I first looked at the effect of OXT treatment of human fetal RPE cells on the expression of 88 different genes that have

been associated with angiogenesis, including VEGF and IGF-1. While I found some changes in the assayed genes, detailed in **chapter 3**, no genes previously implicated in ROP pathogenesis were significantly altered. To address the potential immaturity of the fetal cells used, I isolated and cultured mouse RPE and determined whether these mature cells had any alteration in the expression of VEGF or IGF-1 following treatment with OXT. My results from these mouse cells agreed with what I found with my human cells, indicating that OXT does not alter the transcription of our genes of interest.

I then shifted my focus from changes in expression to actual changes in secretion. Focusing on VEGF I utilized an ELISA assay to determine the level of VEGF in cell culture media following 16 hours of exposure to RPE cells, either in the presence or absence of OXT. I looked at the concentration of VEGF in the apical and basal media separately and found that there was a small increase in apical VEGF concentration with increasing concentrations of OXT and this increase was significant when comparing 10 μM OXT to untreated cells. The increase in VEGF was not observed in the basal medium suggesting that OXT may be inducing a polarized secretion of VEGF, preferring growth factor release towards the subretinal space and the retina. VEGF secretion by the RPE has previously been shown to be in the basal direction so this inversion of that secretion is a novel finding. The polarized secretion of VEGF would support a role for OXT in mediating retinal vasculature specifically without interfering with the role played by the RPE in choroidal development and maintenance (Marneros et al., 2005). To determine whether the change in VEGF I observed could actually modulate angiogenesis I utilized two functional angiogenesis assays, the capillary morphogenesis assay and the endothelial cell migration assay. In both assays I used retinal endothelial cells (REC). Despite the statistically

significant increase in VEGF concentration in the apical media with 10 μM OXT, I observed no alteration in capillary morphogenesis when comparing REC's incubated in the conditioned media from OXT treated cells to those that did not receive OXT treatment. This lack of effect was further demonstrated when I looked at REC migration, again showing no change in the level of migration when comparing conditioned media from OXT treated cells to those that had not received OXT. These results demonstrate that while there is a small but significant increase in VEGF released by the RPE in response to OXT treatment the increased VEGF concentration in the cell culture media is not sufficient to induce an angiogenic response by endothelial cells that make up retinal vasculature.

In total the data presented in **chapter 3** suggests that oxytocinergic signaling in the RPE is not likely a major driver of retinal vascular growth and it is unlikely that it plays a major role in the pathogenesis of ROP. I have not, however, addressed the potential for OXT to affect vessel growth through stimulation of retinal cells expressing the receptor. Prior to the work presented in this thesis I had not identified OXTR expression beyond the retina. However, in **chapter 4**, I have shown that OXTR transcript is present in the mouse retina and that mouse retinal tissue contains abundant OXTR protein. The fact that I see a change in the secretion of VEGF by the RPE could also apply to cells of the retina and provides a way for OXT to mediate VEGF in much closer proximity to the retinal vasculature. To further explore the role of OXT in the retina it will be imperative to first characterize the cell types that are specifically expressing the receptor. Once this is done the role of OXT in regulating retinal vascular growth or other retinal functions can be further explored.

In addition to demonstrating the expression of OXTR in the mouse retina I have also explored the ontogeny of OXTR expression by the RPE in **chapter 4**. Given our hypothesized role for OXT in the development of retinal vasculature knowing the timeline of OXTR expression during development was imperative to understanding when OXT action could be present. To determine this ontogeny I utilized the mouse as the majority of its retinal vascular development occurs postnatally and along a well-defined timeline. I collected mouse RPE from mice aged from postnatal day 0 (p0) to p20, at five-day intervals, as well as from adult mice. Following mRNA isolation from the RPE of these mice I performed qPCR to quantify OXTR expression and found an interesting and complicated picture. I found no significant change in the relative expression of OXTR across all age groups when that expression was compared to 18s rRNA. However, when I compared the expression of OXTR to the RPE specific gene, RPE65, I found a dramatic reduction in OXTR expression with increased age. These data suggest that OXTR expression overall remains constant but that its expression relative to the RPE population is much higher during early development than in the mature retina. As the RPE continues to proliferate during the period I was studying it is possible that what I observed is a mechanism through which the RPE works to keep total expression of OXTR in the RPE consistent, independent of the number of cells present. As the retina matures and the RPE cells divide the individual cell expression of OXTR would decrease to ensure the total population of OXTR remains the same. Another possibility is that I observed a consistent level of OXTR expression despite changes in the RPE population because my mRNA is not exclusively from the RPE and instead contains mRNA from the retina as well. The level of expression I observed in the retina was consistent with the average level of expression I detected in the RPE which would support

this conclusion. This might explain the some of the variation across mice of the same age. It is clear that the mouse RPE does exhibit some expression though, independent of the retina, as I have demonstrated that Kir7.1 in mouse RPE cells responds to OXT treatment and in isolated mouse RPE cells I showed that OXTR can be detected.

The significant variation in RPE cell expression is consistently observed at all ages and I did not observe any correlation between the level of expression and the sex of the mice that the RPE were isolated from. All mice studied were sacrificed at approximately the same time of day (12PM), eliminating the possibility of circadian changes in OXTR expression. It is also possible that there are distinct sub-populations of RPE that express OXTR at different levels, perhaps because of the populations of photoreceptors they serve. However, I did not observe any differential expression in the IHC performed on mouse retinas, where I found little to no actual OXTR protein present in the RPE. The source of this variability then remains undiscovered. Given the difference in OXTR expression within the mouse retina when compared to the primate retina where we find little OXTR in the retina and robust staining of OXTR in the RPE it is likely that this variation is a present only in the mouse and not the primate. Perhaps in the mouse the function of OXTR is fulfilled by retinal cells making expression by the RPE less important while in the primate the role falls more directly on the RPE.

In conclusion then, in this thesis I have looked at OXTR expression in the RPE, characterized its signaling and looked at two potential implications of that signaling on retinal development and function. I have shown that OXTR acts through the G-protein mediated activation of PLC and the subsequent hydrolysis of PIP_2. Through this G-protein mediated signaling, OXT can induce the inhibition of the inwardly rectifying channel Kir7.1 resulting in an

immediate and prolonged depolarization of the RPE cell. This inhibitory effect was observed in a heterologous system as well as in mouse cells despite an apparent reduced expression of OXTR in these cells relative to the primate. I have also demonstrated that OXTR can induce an increase in the secretion of VEGF from human RPE cells but that this secretion is not the result of alterations in gene expression. Furthermore, this increased secretion does not appear to be adequate to induce angiogenesis in RECs. In addition to these findings I have demonstrated a persistent gross level of average OXTR expression in the mouse RPE and retina independent of the number of RPE cells, as determined by RPE65 expression. In individual mice the OXTR expression of the RPE varies greatly, a phenomenon not observed in the retina. Finally, the expression observed in the mouse appears to differ from that of the primate, with the mouse showing robust expression of OXTR in the retina with variation in the expression in the RPE while the primate shows limited to no expression of OXTR in the retina with robust staining of the RPE. I was also able to localize this RPE expression in the primate to the apical processes where it co-localizes with Kir7.1 and surrounds the cone photoreceptors. The implications of these findings will be discussed in the next section.

5.2 Implications of Key findings

The goal of this project was to explore the expression of OXTR and the impacts of oxytocinergic signaling in the RPE. The key findings I have made in pursuit of this goal have numerous implications both within the eye and beyond. I have determined that OXTR can inhibit Kir7.1 and that this inhibition results in a prolonged depolarization of the cells membrane. This has clear implications for retinal physiology as Kir7.1 is an important regulator

of several RPE functions including the transport of fluid from the subretinal space and maintenance of subretinal ion homeostasis. Kir7.1 function is integral to maintaining RPE health as evidenced by development of retinal dysfunction and disease in patients with non-functional Kir7.1 mutations (Pattnaik et al., 2015; Shahi et al., 2017). Given this important role for Kir7.1 the regulation we demonstrate here is the first example of oxytocin having a functional impact on retinal cells. Furthermore, I demonstrated that the mechanism of inhibition is G-protein dependent. This might be expected given the broader literature on PIP_2 regulation of Kir channels, however recent work has shown that in the case of Kir7.1 GPCR inhibition can occur in a G-protein independent manner (Ghamari-Langroudi et al., 2015). The data presented here demonstrates that this mechanism of inhibition is not shared across all GPCRs but is specific to the MC4R.

In the RPE Kir7.1 inhibition by OXT has implications for our understanding of the function of oxytocinergic signaling in the RPE. The prolonged inhibition that I observed hints at a possible functional role for OXT as well as a possible mechanism for this inhibition, both of which will help guide future work. The fact that the inhibition I see is prolonged suggests that the role played by OXT may be in the induction of an extended phenomenon. Given the previously observed localization of OXTR to cone photoreceptor outer segments it is possible that this inhibition of Kir7.1 and prolonged depolarization plays a role in the maintenance of phagocytosis. The process of phagocytosis occurs over a period of hours, followed by a refractory period in which no phagocytosis can occur. Membrane depolarization has been found to play a role in the initiation of phagocytosis in other cell types so it is possible the same is true for the RPE (Link et al., 2010). As for the mechanistic implications of this discovery, the

inhibition of Kir7.1 is consistent with the kinetics of inhibition by PIP_2 hydrolysis, however I did not observe any recovery. This suggests that Kir7.1 might be lost from the membrane following inhibition, either internalized with OXTR or through an alternative pathway. Both of these findings require further exploration and impact our understanding of RPE physiology and the broader regulation of Kir channels.

The implications of Kir7.1 inhibition by OXT are not limited to the eye but extend to anywhere that both Kir7.1 and OXTR are co-expressed. Perhaps the most intriguing of these places is the uterus, where Kir7.1 and OXTR have both been shown to play a role in the initiation of parturition (McCloskey et al., 2014). In this study it was shown that reduced expression of Kir7.1 occurs prior to the onset of parturition and that this results in an increase in the contractility of uterine myometrium. They further demonstrate that this increase in contractility is a result of membrane depolarization and that prolonged and powerful contractions can be induced through application of the specific Kir7.1 inhibitor, VU-590 (McCloskey et al., 2014). Additionally, they were able to demonstrate a synergistic effect of OXT and Kir7.1 inhibition on uterine contractility. OXT has a well described role in the initiation of parturition and OXTR expression increases dramatically as parturition approaches. I therefore propose that the OXTR mediated inhibition of Kir7.1 plays a role in increasing uterine contractility and inducing prolonged contractions during parturition.

The work in this thesis also impacts the field by supporting earlier literature and demonstrating a lack of OXT effect on retinal angiogenesis through the RPE. OXT initially appeared to be a promising potential factor in mediating early retinal development. The presence of such a factor is hinted at by the increase in instances of retinopathy of prematurity

(ROP) as infants of ever decreasing gestational age can survive with modern medicine. The potential for OXT to fill this role is discussed in the previous section as well as **chapter 1**. My data, however, demonstrates that OXT does not likely play a role in regulation of retinal vasculature, at least not through oxytocinergic signaling in the RPE. This supports previous literature which describes the choroidal vasculature as the target of RPE mediated angiogenesis while the effect of the RPE on the retina is primarily an anti-angiogenic protective role through the secretion of PEDF (Dawson et al., 1999; Marneros et al., 2005). The alterations I did observe in the expression of various angiogenic genes though, including a significant increase in angiogenin expression and a decrease in hepatocyte growth factor, have implications for any future work looking at the role of angiogenesis throughout the body. OXTR is expressed in many tissues and cell types and the information obtained from this study will help guide others as they study the potential role of OXT in those tissues.

The implications of my work on the ontogeny of OXTR in the RPE are more local, bringing our focus back to the retina and the RPE. In this study I have revealed that there is a difference in the pattern of OXTR expression between the mouse and the primate. The difference between the two suggests that the role played by OXT in the eye might be different between species and demonstrates that the mouse may not be an accurate model for the effects of oxytocinergic signaling on vision in the primate. Despite this difference in expression we know that OXTR is expressed in the RPE of mice, both through PCR and my studies showing that OXT can induce the inhibition of Kir7.1 in freshly isolated mouse RPE. However, I have shown that this expression is variable, with some populations of RPE showing little to no expression while others exhibit robust expression. Perhaps this variability is a result of

differential expression in RPE because of the populations of photoreceptors they associate with. I have only been able to observe OXT expression in cone photoreceptor outer segments so perhaps only populations of RPE associated with cones are expressing the OXTR receptor. We know that RPE cells form photoreceptor type specific apical sheaths, supporting the possibility variable gene expression between different RPE cell populations (Strauss, 2005). This is only one possibility though and I did not observe a difference in expression across the frozen mouse retina sections we used for IHC so there may be some alternative explanation and this variability needs to be further explored.

5.3 Limitations of this study

As with any scientific work, the scope of this study is limited and, in many cases, creates more questions than it answers. To acknowledge these questions and address other limitations of the study I will discuss them here.

This thesis focuses primarily on characterizing OXTR signaling and expression within the RPE. However, I do not address or explore the source of retinal OXT. The source of the peptide is the key component in the development of any theory on the role of OXT in the retina. I cannot determine whether OXT is used by the photoreceptors to initiate phagocytosis without knowing whether OXT is produced by the photoreceptors at all, nor can I understand the role played by OXT in retinal development without knowing whether retinal OXT is coming from the hypothalamus or if it is produced locally. It is a distinct possibility that while OXT is not produced in the fetal hypothalamus until relatively late in pregnancy it could very well be expressed earlier in the developing fetal eye (Schubert et al., 1981). For any true understanding

of the role played by OXT in the eye, we must first understand the source of OXT in that eye. Prior to this work I had only demonstrated that OXTR was expressed in the primate RPE and that OXT could induce a $[Ca^{2+}]_I$ response from hfRPE cells. This study represents only a second step into our understanding of OXT in the retina and a significant amount of future work is needed to expand on this knowledge.

There are other limitations of the work presented here as well, tied both to available resources and practical considerations when undergoing scientific experimentation. My studies on the mechanism of OXTR signaling as well as the work characterizing the effect of OXT on angiogenesis both utilize hfRPE cells. These cells represent one major limitation of this study because they are not mature RPE cells developed in the retinal environment. The development of the RPE is heavily reliant on the retina and as such these cells may not exhibit all characteristics of human RPE cells *in vivo*. We tried to maximize the similarities with *in vivo* counterparts by culturing the cells on transwells in a monolayer and ensuring pigmentation but nevertheless it cannot be guaranteed they are truly representative of *in vivo* RPE. To further validate our results I looked at the effect of OXT on gene expression in *ex vivo* mouse RPE. However, as I demonstrate in **chapter 4**, the mouse and human RPE and retina show different expression of OXTR and as such the mouse are not likely to be representative of the human. In addition to the use of hfRPE cells I also performed many of our electrophysiology studies in a heterologous system, with HEK-293 cells expressing OXTR and Kir7.1 eGFP. These studies were again validated in *ex vivo* mouse RPE but the previously mentioned concerns remain with that model. HEK cells are commonly used for electrophysiology because they lack significant endogenous current and there is no reason to doubt the applicability of our observations in

these cells to other cell types expressing both Kir7.1 and OXTR but nevertheless it should be mentioned.

Another limitation of this thesis lies in the isolation of RPE to analyze OXTR expression. While I took steps to try to separate the RPE from the retina the possibility of contamination of mRNA from one tissue with the other exists simply by the nature of their proximity. I address this, in part, by looking at gene expression of groups of RPE and retinal cells dissociated and then isolated with a glass capillary under a microscope. I found similar characteristics to the gene expression in these populations as I found in the whole RPE and retina, with equivalent average OXTR expression but a much higher level of variability in the RPE, however this comparative analysis cannot definitively rule out the potential for cross contamination in the whole RPE and retina samples. Another issue with the method of isolation used is that I have no control over the populations of RPE being collected. The RPE is separated from the eye cup through mechanical disruption and as such I have no idea of the origin of the RPE that detached or the photoreceptors to which that RPE was associated. This may be a reason for the variability I observe in RPE expression and a closer look at single cell expression between different populations of RPE should be done in the future.

5.4 Future Studies

In the content of this chapter I have mentioned several future directions I can see to address questions brought up by the data presented in this thesis. As I have stated, this work has answered only a few questions and given rise to many others. In this section I will outline

the future directions that might be taken to answer some of these questions with unlimited time and resources.

Identify Source of Retinal Oxytocin

As I mentioned in **section 6.3** one of the leading barriers to expanding our understanding of the role played by OXT in the retina is the fact that we don't know what the source of retinal OXT is. This is a clear future direction that should be pursued. I have generated preliminary evidence that shows that OXT mRNA can be found in the whole eye but I have not successfully localized that expression to any one tissue or cell type. I attempted to address this question through the development of a fluorescent *in-situ* hybridization (FISH) probe for OXT which would allow us to visualize the presence of OXT mRNA within the retina. However, despite some early promising results I was not able to generate a successful probe. In the future this direction should be continued. Once the source of OXT is identified the temporal expression and secretion pattern of the gene should be determined. Oxytocin in the eye has been shown to follow a diurnal pattern with higher OXT levels during the day (Gauquelin et al., 1983). Our discovery of OXT around the outer segments of the cone photoreceptors could explain this daytime increase as this would be the time when cone PR are most active. Alternatively, hypothalamic OXT has been shown to follow a circadian pattern of secretion and an increased release in response to light, meaning systemic OXT could also explain the variability in retinal OXT throughout the day (Devarajan et al., 2005). This ambiguity means that successful pursuit of this direction is necessary, as identifying the true source of OXT can not

only provide context to the work we have already done but it will go a long way to determining the role of OXT in the retina.

Determine mechanism of prolonged Kir7.1 inhibition

Another important future direction that should be pursued is exploring the cause of the prolonged inhibition that I observe for Kir7.1. As I have discussed, one possible reason for this inhibition could be the internalization of the channel. OXTR is internalized after activation in a clathrin dependent manner and Kir7.1 has been suggested to associate with clathrin, so perhaps they are internalized together (Kumar & Pattnaik, 2014; Smith et al., 2006). The non-clathrin mediated internalization of Kir channels has also been described previously where PKC has been shown to mediate the caveolin dependent internalization of K-ATP channels (Jiao et al., 2008). Given this information I think that the potential internalization of Kir7.1 should be explored. To determine whether internalization occurs live cell imaging could be performed on HEK-OXTR cells expressing Kir7.1 e-GFP. Following treatment any translocation of Kir7.1 from the membrane to the cytoplasm should be visible. Additionally, following OXT treatment membrane proteins could be extracted and separated from cytosolic proteins and quantified using western blot to identify whether there is any change in their ratio. These two tests should be able to demonstrate whether internalization is occurring and, depending on the results, the mechanism of that internalization could be further explored or alternative explanations could be discussed. In addition to looking at the internalization of Kir7.1 it would also be beneficial to look at the localization of the channel relative to OXTR. The interaction between the receptor and the K^+ channel suggest that they are close together and I have demonstrated their apical localization in **chapter 4.** However, describing their sub membrane localization would be helpful

not only in characterizing their interaction but in identifying the mechanism of inhibition. For example, localization of Kir7.1 to caveolae could point to PKC mediated endocytosis as shown with K-ATP channels (Jiao et al., 2008).

Characterizing OXTR expression within Mouse Retina

One of the key findings presented in this work is the presence of OXTR expression in the mouse retina, a phenomenon that I have not observed previously in primate retinas. From my IHC sections the expression appears to be relatively homogenous, however a closer look at the cell specific expression needs to be done. It is necessary to know specifically which cells are expressing the receptor so that we can direct our focus in studying what the role of the receptor might be within the retina. Dissociation of the retina as I performed in **chapter 4**, followed by isolation of single cells, could be repeated and single cell-PCR should be performed. To accomplish this the single cell is frozen at -80˚C to lyse the cell membrane and release mRNA. Then cDNA synthesis is performed on the single cell followed by multiplex PCR to amplify the gene of interest. This process requires two steps of PCR, with two sets of gene specific primers, one set that corresponds to a sequence that lies within the product of the other. The first set of primers (external primers) are used in the initial round of PCR and the product from that reaction is taken and PCR is run again, this time using the second set of primers, allowing for further amplification without loss of specificity. I have successfully used this technique in the past, shown in **appendix 1**, and it will give targeted information on the cell specific expression of OXTR (Phillips et al., 2018; Shahi et al., 2017).

Explore alternative models of retinal OXT signaling *in vivo*

As I have shown the mouse is not an ideal model for the OXTR signaling as it occurs in humans. For that reason it is important to identify another species which not only serves as a more accurate model but can be reliable and easily housed in a cost-effective manner. One possible candidate is the ground squirrel. While larger then mice, these animals are small and relatively inexpensive when compared to nonhuman primates. Additionally they could potentially be a powerful model as their retinas are extremely cone heavy, with 7.5 million cones to only 1.2 million rods (Kryger et al., 1998). Given our localization of OXT to the cone photoreceptor outer segments these animals provide a unique opportunity to explore the potential retinal production of OXT and to determine whether that production is photoreceptor specific. In addition to this we would also need to determine whether OXTR is expressed in the retina and whether this expression follows the pattern observed in primates. If that is the case these animals may serve as a good model for future studies.

Chapter 6: Bibliography

Adachi, S., & Oku, M. (1995). The regulation of oxytocin receptor expression in human myometrial monolayer culture. *J Smooth Muscle Res, 31*(4), 175-187.

Adamis, A. P., Shima, D. T., Yeo, K. T., Yeo, T. K., Brown, L. F., Berse, B., . . . Folkman, J. (1993). Synthesis and secretion of vascular permeability factor/vascular endothelial growth factor by human retinal pigment epithelial cells. *Biochem Biophys Res Commun, 193*(2), 631-638.

Agathocleous, M., & Harris, W. A. (2009). From progenitors to differentiated cells in the vertebrate retina. *Annu Rev Cell Dev Biol, 25*, 45-69. doi:10.1146/annurev.cellbio.042308.113259

Anand-Apte, B., & Hollyfield, J. (2010). Developmental Anatomy of the Retinal and Choroidal Vasculature. Cleveland, OH, USA: Elsevier Ltd.

Arrowsmith, S., & Wray, S. (2014). Oxytocin: its mechanism of action and receptor signalling in the myometrium. *J Neuroendocrinol, 26*(6), 356-369. doi:10.1111/jne.12154

Arshavsky, V. (2002). Like night and day: rods and cones have different pigment regeneration pathways. *Neuron, 36*(1), 1-3.

Ashton, N. (1970). Retinal angiogenesis in the human embryo. *Br Med Bull, 26*(2), 103-106.

Asselin, E., Drolet, P., & Fortier, M. A. (1997). Cellular mechanisms involved during oxytocin-induced prostaglandin F2alpha production in endometrial epithelial cells in vitro: role of cyclooxygenase-2. *Endocrinology, 138*(11), 4798-4805. doi:10.1210/endo.138.11.5527

Autrata, R., Krejcírová, I., Senková, K., Holoušová, M., Doležel, Z., & Borek, I. (2012). Intravitreal pegaptanib combined with diode laser therapy for stage 3+ retinopathy of prematurity in zone I and posterior zone II. *Eur J Ophthalmol, 22*(5), 687-694. doi:10.5301/ejo.5000166

Baehr, W., Wu, S. M., Bird, A. C., & Palczewski, K. (2003). The retinoid cycle and retina disease. *Vision Res, 43*(28), 2957-2958.

Bakall, B., Marmorstein, L. Y., Hoppe, G., Peachey, N. S., Wadelius, C., & Marmorstein, A. D. (2003). Expression and localization of bestrophin during normal mouse development. *Invest Ophthalmol Vis Sci, 44*(8), 3622-3628.

Barberis, C., Mouillac, B., & Durroux, T. (1998). Structural bases of vasopressin/oxytocin receptor function. *J Endocrinol, 156*(2), 223-229.

Barnard, E. A., Burnstock, G., & Webb, T. E. (1994). G protein-coupled receptors for ATP and other nucleotides: a new receptor family. *Trends Pharmacol Sci, 15*(3), 67-70.

Bialek, S., Joseph, D. P., & Miller, S. S. (1995). The delayed basolateral membrane hyperpolarization of the bovine retinal pigment epithelium: mechanism of generation. *J Physiol, 484 (Pt 1)*, 53-67.

Bialek, S., & Miller, S. S. (1994). K+ and Cl- transport mechanisms in bovine pigment epithelium that could modulate subretinal space volume and composition. *J Physiol, 475*(3), 401-417.

Blanco, R., & Gerhardt, H. (2013). VEGF and Notch in tip and stalk cell selection. *Cold Spring Harb Perspect Med, 3*(1), a006569. doi:10.1101/cshperspect.a006569

Blanks, A. M., & Thornton, S. (2003). The role of oxytocin in parturition. *BJOG, 110 Suppl 20*, 46-51.

Bockaert, J., & Pin, J. P. (1999). Molecular tinkering of G protein-coupled receptors: an evolutionary success. *EMBO J, 18*(7), 1723-1729. doi:10.1093/emboj/18.7.1723

Bodenstein, L., & Sidman, R. L. (1987). Growth and development of the mouse retinal pigment epithelium. I. Cell and tissue morphometrics and topography of mitotic activity. *Dev Biol, 121*(1), 192-204.

Bok, D. (1993). The retinal pigment epithelium: a versatile partner in vision. *J Cell Sci Suppl, 17*, 189-195.

Boulton, M., & Dayhaw-Barker, P. (2001). The role of the retinal pigment epithelium: topographical variation and ageing changes. *Eye (Lond), 15*(Pt 3), 384-389. doi:10.1038/eye.2001.141

Brown, C. H., Russell, J. A., & Leng, G. (2000). Opioid modulation of magnocellular neurosecretory cell activity. *Neurosci Res, 36*(2), 97-120.

Brownstein, M. J., Russell, J. T., & Gainer, H. (1980). Synthesis, transport, and release of posterior pituitary hormones. *Science, 207*(4429), 373-378.

Cai, X., Conley, S. M., & Naash, M. I. (2009). RPE65: role in the visual cycle, human retinal disease, and gene therapy. *Ophthalmic Genet, 30*(2), 57-62. doi:10.1080/13816810802626399

Cambell, K. (1951). Intensive oxygen therapy as a possible cause of retrolental fibroplasia; a clinical approach. *Med J Aust, 2*(2), 48-50.

Cattaneo, M. G., Chini, B., & Vicentini, L. M. (2008). Oxytocin stimulates migration and invasion in human endothelial cells. *Br J Pharmacol, 153*(4), 728-736. doi:10.1038/sj.bjp.0707609

Cavallaro, G., Filippi, L., Bagnoli, P., La Marca, G., Cristofori, G., Raffaeli, G., . . . Mosca, F. (2014). The pathophysiology of retinopathy of prematurity: an update of previous and recent knowledge. *Acta Ophthalmol, 92*(1), 2-20. doi:10.1111/aos.12049

Che, T., Sun, H., Li, J., Yu, X., Zhu, D., Xue, B., . . . Liu, C. (2012). Oxytocin hyperpolarizes cultured duodenum myenteric intrinsic primary afferent neurons by opening BK(Ca) channels through IP(3) pathway. *J Neurochem, 121*(4), 516-525. doi:10.1111/j.1471-4159.2012.07702.x

Chen, J., Joyal, J. S., Hatton, C. J., Juan, A. M., Pei, D. T., Hurst, C. G., . . . Smith, L. E. (2012). Propranolol inhibition of β-adrenergic receptor does not suppress pathologic neovascularization in oxygen-induced retinopathy. *Invest Ophthalmol Vis Sci, 53*(6), 2968-2977. doi:10.1167/iovs.12-9691

Chen, M. L., Guo, L., Smith, L. E., Dammann, C. E., & Dammann, O. (2010). High or low oxygen saturation and severe retinopathy of prematurity: a meta-analysis. *Pediatrics, 125*(6), e1483-1492. doi:10.1542/peds.2009-2218

Chen, P., Hao, W., Rife, L., Wang, X. P., Shen, D., Chen, J., . . . Fong, H. K. (2001). A photic visual cycle of rhodopsin regeneration is dependent on Rgr. *Nat Genet, 28*(3), 256-260. doi:10.1038/90089

Chibbar, R., Miller, F. D., & Mitchell, B. F. (1993). Synthesis of oxytocin in amnion, chorion, and decidua may influence the timing of human parturition. *J Clin Invest, 91*(1), 185-192. doi:10.1172/JCI116169

Chowers, I., Banin, E., Hemo, Y., Porat, R., Falk, H., Keshet, E., . . . Panet, A. (2001). Gene transfer by viral vectors into blood vessels in a rat model of retinopathy of prematurity. *Br J Ophthalmol, 85*(8), 991-995.

Cochran, W. G. (1977). *Sampling techniques* (3d ed.). New York: Wiley.

Collin, J., Mellough, C. B., Dorgau, B., Przyborski, S., Moreno-Gimeno, I., & Lako, M. (2016). Using Zinc Finger Nuclease Technology to Generate CRX-Reporter Human Embryonic Stem Cells as a Tool to Identify and Study the Emergence of Photoreceptors Precursors During Pluripotent Stem Cell Differentiation. *Stem Cells, 34*(2), 311-321. doi:10.1002/stem.2240

Connolly, S. E., Hores, T. A., Smith, L. E., & D'Amore, P. A. (1988). Characterization of vascular development in the mouse retina. *Microvasc Res, 36*(3), 275-290.

Conti, F., Sertic, S., Reversi, A., & Chini, B. (2009). Intracellular trafficking of the human oxytocin receptor: evidence of receptor recycling via a Rab4/Rab5 "short cycle". *Am J Physiol Endocrinol Metab, 296*(3), E532-542. doi:10.1152/ajpendo.90590.2008

Copland, J. A., Jeng, Y. J., Strakova, Z., Ives, K. L., Hellmich, M. R., & Soloff, M. S. (1999). Demonstration of functional oxytocin receptors in human breast Hs578T cells and their up-regulation through a protein kinase C-dependent pathway. *Endocrinology, 140*(5), 2258-2267. doi:10.1210/endo.140.5.6723

Crankshaw, D. J., Branda, L. A., Matlib, M. A., & Daniel, E. E. (1978). Localization of the oxytocin receptor in the plasma membrane of rat myometrium. *Eur J Biochem, 86*(2), 481-486.

D'Avanzo, N., Lee, S. J., Cheng, W. W., & Nichols, C. G. (2013). Energetics and location of phosphoinositide binding in human Kir2.1 channels. *J Biol Chem, 288*(23), 16726-16737. doi:10.1074/jbc.M113.452540

Dascal, N., Schreibmayer, W., Lim, N. F., Wang, W., Chavkin, C., DiMagno, L., . . . Trollinger, D. (1993). Atrial G protein-activated K+ channel: expression cloning and molecular properties. *Proc Natl Acad Sci U S A, 90*(21), 10235-10239.

Dawson, D. W., Volpert, O. V., Gillis, P., Crawford, S. E., Xu, H., Benedict, W., & Bouck, N. P. (1999). Pigment epithelium-derived factor: a potent inhibitor of angiogenesis. *Science, 285*(5425), 245-248.

Del Rio-Tsonis, K., & Tsonis, P. A. (2003). Eye regeneration at the molecular age. *Dev Dyn, 226*(2), 211-224. doi:10.1002/dvdy.10224

Devarajan, K., Marchant, E. G., & Rusak, B. (2005). Circadian and light regulation of oxytocin and parvalbumin protein levels in the ciliated ependymal layer of the third ventricle in the C57 mouse. *Neuroscience, 134*(2), 539-547. doi:10.1016/j.neuroscience.2005.04.034

Devost, D., & Zingg, H. H. (2003). Identification of dimeric and oligomeric complexes of the human oxytocin receptor by co-immunoprecipitation and bioluminescence resonance energy transfer. *J Mol Endocrinol, 31*(3), 461-471.

Döring, F., Derst, C., Wischmeyer, E., Karschin, C., Schneggenburger, R., Daut, J., & Karschin, A. (1998). The epithelial inward rectifier channel Kir7.1 displays unusual K+ permeation properties. *J Neurosci, 18*(21), 8625-8636.

Dornonville de la Cour, M. (1993). Ion transport in the retinal pigment epithelium. A study with double barrelled ion-selective microelectrodes. *Acta Ophthalmol Suppl*(209), 1-32.

Du Vigneaud, V., Ressler, C., & Trippett, S. (1953). The sequence of amino acids in oxytocin, with a proposal for the structure of oxytocin. *J Biol Chem, 205*(2), 949-957.

Du, X., Zhang, H., Lopes, C., Mirshahi, T., Rohacs, T., & Logothetis, D. E. (2004). Characteristic interactions with phosphatidylinositol 4,5-bisphosphate determine regulation of kir channels by diverse modulators. *J Biol Chem, 279*(36), 37271-37281. doi:10.1074/jbc.M403413200

Edelman, J. L., Lin, H., & Miller, S. S. (1994). Acidification stimulates chloride and fluid absorption across frog retinal pigment epithelium. *Am J Physiol, 266*(4 Pt 1), C946-956. doi:10.1152/ajpcell.1994.266.4.C946

Edwards, M. M., McLeod, D. S., Grebe, R., Heng, C., Lefebvre, O., & Lutty, G. A. (2011). Lama1 mutations lead to vitreoretinal blood vessel formation, persistence of fetal vasculature, and epiretinal membrane formation in mice. *BMC Dev Biol, 11*, 60. doi:10.1186/1471-213X-11-60

Elabd, C., Cousin, W., Upadhyayula, P., Chen, R. Y., Chooljian, M. S., Li, J., . . . Conboy, I. M. (2014). Oxytocin is an age-specific circulating hormone that is necessary for muscle maintenance and regeneration. *Nat Commun, 5*, 4082. doi:10.1038/ncomms5082

Evans, J. J., Forrest-Owen, W., & McArdle, C. A. (1997). Oxytocin receptor-mediated activation of phosphoinositidase C and elevation of cytosolic calcium in the gonadotrope-derived alphaT3-1 cell line. *Endocrinology, 138*(5), 2049-2055.

Fahrenholz, F., Klein, U., & Gimpl, G. (1995). Conversion of the myometrial oxytocin receptor from low to high affinity state by cholesterol. *Adv Exp Med Biol, 395*, 311-319.

Fanelli, F., Barbier, P., Zanchetta, D., de Benedetti, P. G., & Chini, B. (1999). Activation mechanism of human oxytocin receptor: a combined study of experimental and computer-simulated mutagenesis. *Mol Pharmacol, 56*(1), 214-225.

Fierson, W. M., Ophthalmology, A. A. o. P. S. o., Ophthalmology, A. A. o., Strabismus, A. A. f. P. O. a., & Orthoptists, A. A. o. C. (2013). Screening examination of premature infants for retinopathy of prematurity. *Pediatrics, 131*(1), 189-195. doi:10.1542/peds.2012-2996

Finnemann, S. C., & Silverstein, R. L. (2001). Differential roles of CD36 and alphavbeta5 integrin in photoreceptor phagocytosis by the retinal pigment epithelium. *J Exp Med, 194*(9), 1289-1298.

Fisher, T. E., & Bourque, C. W. (2001). The function of Ca(2+) channel subtypes in exocytotic secretion: new perspectives from synaptic and non-synaptic release. *Prog Biophys Mol Biol, 77*(3), 269-303.

Frambach, D. A., Roy, C. E., Valentine, J. L., & Weiter, J. J. (1989). Precocious retinal adhesion is affected by furosemide and ouabain. *Curr Eye Res, 8*(6), 553-556.

Friedman, Z., Delahunty, T. M., Linden, J., & Campochiaro, P. A. (1991). Human retinal pigment epithelial cells possess V1 vasopressin receptors. *Curr Eye Res, 10*(9), 811-816.

Fruttiger, M. (2007). Development of the retinal vasculature. *Angiogenesis, 10*(2), 77-88. doi:10.1007/s10456-007-9065-1

Fuhrmann, S., Zou, C., & Levine, E. M. (2014). Retinal pigment epithelium development, plasticity, and tissue homeostasis. *Exp Eye Res, 123*, 141-150. doi:10.1016/j.exer.2013.09.003

Gainer, H. (1998). Cell-specific gene expression in oxytocin and vasopressin magnocellular neurons. *Adv Exp Med Biol, 449*, 15-27.

Gallemore, R. P., Griff, E. R., & Steinberg, R. H. (1988). Evidence in support of a photoreceptoral origin for the "light-peak substance". *Invest Ophthalmol Vis Sci, 29*(4), 566-571.

Gallemore, R. P., & Steinberg, R. H. (1990). Effects of dopamine on the chick retinal pigment epithelium. Membrane potentials and light-evoked responses. *Invest Ophthalmol Vis Sci, 31*(1), 67-80.

Gariano, R. F. (2010). Special features of human retinal angiogenesis. *Eye (Lond), 24*(3), 401-407. doi:10.1038/eye.2009.324

Gariano, R. F., Sage, E. H., Kaplan, H. J., & Hendrickson, A. E. (1996). Development of astrocytes and their relation to blood vessels in fetal monkey retina. *Invest Ophthalmol Vis Sci, 37*(12), 2367-2375.

Gauquelin, G., Geelen, G., Louis, F., Allevard, A. M., Meunier, C., Cuisinaud, G., . . . et al. (1983). Presence of vasopressin, oxytocin and neurophysin in the retina of mammals, effect of light and darkness, comparison with the neuropeptide content of the neurohypophysis and the pineal gland. *Peptides, 4*(4), 509-515.

Gauquelin, G., Gharib, C., Ghaemmaghami, F., Allevard, A. M., Cherbal, F., Geelen, G., . . . Legros, J. J. (1988). A day/night rhythm of vasopressin and oxytocin in rat retina, pineal and harderian gland. *Peptides, 9*(2), 289-293.

Gerhardt, H., Golding, M., Fruttiger, M., Ruhrberg, C., Lundkvist, A., Abramsson, A., . . . Betsholtz, C. (2003). VEGF guides angiogenic sprouting utilizing endothelial tip cell filopodia. *J Cell Biol, 161*(6), 1163-1177. doi:10.1083/jcb.200302047

Ghamari-Langroudi, M., Digby, G. J., Sebag, J. A., Millhauser, G. L., Palomino, R., Matthews, R., . . . Cone, R. D. (2015). G-protein-independent coupling of MC4R to Kir7.1 in hypothalamic neurons. *Nature, 520*(7545), 94-98. doi:10.1038/nature14051

Gilbert, C., & Foster, A. (2001). Childhood blindness in the context of VISION 2020--the right to sight. *Bull World Health Organ, 79*(3), 227-232.

Gimpl, G., Burger, K., & Fahrenholz, F. (1997). Cholesterol as modulator of receptor function. *Biochemistry, 36*(36), 10959-10974. doi:10.1021/bi963138w

Gimpl, G., Burger, K., Politowska, E., Ciarkowski, J., & Fahrenholz, F. (2000). Oxytocin receptors and cholesterol: interaction and regulation. *Exp Physiol, 85 Spec No*, 41S-49S.

Gimpl, G., & Fahrenholz, F. (2000). Human oxytocin receptors in cholesterol-rich vs. cholesterol-poor microdomains of the plasma membrane. *Eur J Biochem, 267*(9), 2483-2497.

Gimpl, G., & Fahrenholz, F. (2001). The Oxytocin Receptor System: Structure, function, and regulation. *Physiol Rev, 81*(2), 629-683.

Gimpl, G., & Fahrenholz, F. (2002). Cholesterol as stabilizer of the oxytocin receptor. *Biochim Biophys Acta, 1564*(2), 384-392.

Gimpl, G., Klein, U., Reilander, H., & Fahrenholz, F. (1995). Expression of the human oxytocin receptor in baculovirus-infected insect cells: high-affinity binding is induced by a cholesterol-cyclodextrin complex. *Biochemistry, 34*(42), 13794-13801.

Gonzalez-Fernandez, F. (2003). Interphotoreceptor retinoid-binding protein--an old gene for new eyes. *Vision Res, 43*(28), 3021-3036.

Gramage, E., Li, J., & Hitchcock, P. (2014). The expression and function of midkine in the vertebrate retina. *Br J Pharmacol, 171*(4), 913-923. doi:10.1111/bph.12495

Gregory, C. Y., Abrams, T. A., & Hall, M. O. (1994). Stimulation of A2 adenosine receptors inhibits the ingestion of photoreceptor outer segments by retinal pigment epithelium. *Invest Ophthalmol Vis Sci, 35*(3), 819-825.

Griff, E. R., Shirao, Y., & Steinberg, R. H. (1985). Ba2+ unmasks K+ modulation of the Na+-K+ pump in the frog retinal pigment epithelium. *J Gen Physiol, 86*(6), 853-876.

Gross, G. A., Imamura, T., Luedke, C., Vogt, S. K., Olson, L. M., Nelson, D. M., . . . Muglia, L. J. (1998). Opposing actions of prostaglandins and oxytocin determine the onset of murine labor. *Proc Natl Acad Sci U S A, 95*(20), 11875-11879.

Grynkiewicz, G., Poenie, M., & Tsien, R. Y. (1985). A new generation of Ca2+ indicators with greatly improved fluorescence properties. *J Biol Chem, 260*(6), 3440-3450.

Gupta, T., Kapoor, K., Sahni, D., & Singh, B. (2016). Mapping the Time Line of Development in Each Layer of Human Foetal Retina. *J Clin Diagn Res, 10*(3), AC04-07. doi:10.7860/JCDR/2016/14936.7372

Guzzi, F., Zanchetta, D., Cassoni, P., Guzzi, V., Francolini, M., Parenti, M., & Chini, B. (2002). Localization of the human oxytocin receptor in caveolin-1 enriched domains turns the receptor-mediated inhibition of cell growth into a proliferative response. *Oncogene, 21*(11), 1658-1667. doi:10.1038/sj.onc.1205219

Hagiwara, S., & Takahashi, K. (1974). The anomalous rectification and cation selectivity of the membrane of a starfish egg cell. *J Membr Biol, 18*(1), 61-80.

Halbach, P. (2013). *Oxytocin signaling in the retinal pigment epithelium.* (Masters), University of Wisconsin-Madison.

Halbach, P., Pillers, D. A., York, N., Asuma, M. P., Chiu, M. A., Luo, W., . . . Pattnaik, B. R. (2015). Oxytocin expression and function in the posterior retina: a novel signaling pathway. *Invest Ophthalmol Vis Sci, 56*(2), 751-760. doi:10.1167/iovs.14-15646

Hall, M. O., & Abrams, T. (1987). Kinetic studies of rod outer segment binding and ingestion by cultured rat RPE cells. *Exp Eye Res, 45*(6), 907-922.

Hall, M. O., Abrams, T. A., & Mittag, T. W. (1991). ROS ingestion by RPE cells is turned off by increased protein kinase C activity and by increased calcium. *Exp Eye Res, 52*(5), 591-598.

Hall, M. O., Abrams, T. A., & Mittag, T. W. (1993). The phagocytosis of rod outer segments is inhibited by drugs linked to cyclic adenosine monophosphate production. *Invest Ophthalmol Vis Sci, 34*(8), 2392-2401.

Hatcher-Solis, C., Fribourg, M., Spyridaki, K., Younkin, J., Ellaithy, A., Xiang, G., . . . Logothetis, D. E. (2014). G protein-coupled receptor signaling to Kir channels in Xenopus oocytes. *Curr Pharm Biotechnol, 15*(10), 987-995.

Hayasaka, S., Shiono, T., Hara, S., & Mizuno, K. (1981). Regional distribution of lysosomal enzymes in the retina and choroid of human eyes. *Albrecht Von Graefes Arch Klin Exp Ophthalmol, 216*(4), 269-273.

Hejtmancik, J. F., Jiao, X., Li, A., Sergeev, Y. V., Ding, X., Sharma, A. K., . . . Edwards, A. O. (2008). Mutations in KCNJ13 cause autosomal-dominant snowflake vitreoretinal degeneration. *Am J Hum Genet, 82*(1), 174-180. doi:10.1016/j.ajhg.2007.08.002

Hellström, A., Smith, L. E., & Dammann, O. (2013). Retinopathy of prematurity. *Lancet, 382*(9902), 1445-1457. doi:10.1016/S0140-6736(13)60178-6

Heth, C. A., & Marescalchi, P. A. (1994). Inositol triphosphate generation in cultured rat retinal pigment epithelium. *Invest Ophthalmol Vis Sci, 35*(2), 409-416.

Hibino, H., Inanobe, A., Furutani, K., Murakami, S., Findlay, I., & Kurachi, Y. (2010). Inwardly rectifying potassium channels: their structure, function, and physiological roles. *Physiol Rev, 90*(1), 291-366. doi:10.1152/physrev.00021.2009

Ho, K., Nichols, C. G., Lederer, W. J., Lytton, J., Vassilev, P. M., Kanazirska, M. V., & Hebert, S. C. (1993). Cloning and expression of an inwardly rectifying ATP-regulated potassium channel. *Nature, 362*(6415), 31-38. doi:10.1038/362031a0

Hughes, B. A., & Takahira, M. (1996). Inwardly rectifying K+ currents in isolated human retinal pigment epithelial cells. *Invest Ophthalmol Vis Sci, 37*(6), 1125-1139.

Hughes, S., & Chang-Ling, T. (2000). Roles of endothelial cell migration and apoptosis in vascular remodeling during development of the central nervous system. *Microcirculation, 7*(5), 317-333.

Husch, A., Cramer, N., & Harris-Warrick, R. M. (2011). Long-duration perforated patch recordings from spinal interneurons of adult mice. *J Neurophysiol, 106*(5), 2783-2789. doi:10.1152/jn.00673.2011

Imamoto, Y., Kojima, K., Oka, T., Maeda, R., & Shichida, Y. (2015). Helical rearrangement of photoactivated rhodopsin in monomeric and dimeric forms probed by high-angle X-ray scattering. *Photochem Photobiol Sci, 14*(11), 1965-1973. doi:10.1039/c5pp00175g

Inoue, Y., Shimamura, K., & Sperelakis, N. (1992). Oxytocin actions on voltage-dependent ionic channels in pregnant rat uterine smooth muscle cells. *Can J Physiol Pharmacol, 70*(12), 1597-1603.

Ishida, S., Yamashiro, K., Usui, T., Kaji, Y., Ogura, Y., Hida, T., . . . Adamis, A. P. (2003). Leukocytes mediate retinal vascular remodeling during development and vaso-obliteration in disease. *Nat Med, 9*(6), 781-788. doi:10.1038/nm877

Ivell, R. (1986). Biosynthesis of Oxytocin in the Brain and Peripheral Organs. (Vol. 6). Berlin, Heidelberg: Springer.

Jablonski, M. M., Tombran-Tink, J., Mrazek, D. A., & Iannaccone, A. (2000). Pigment epithelium-derived factor supports normal development of photoreceptor neurons and opsin expression after retinal pigment epithelium removal. *J Neurosci, 20*(19), 7149-7157.

Jeffery, G. (1998). The retinal pigment epithelium as a developmental regulator of the neural retina. *Eye (Lond), 12 (Pt 3b)*, 499-503. doi:10.1038/eye.1998.137

Jiao, J., Garg, V., Yang, B., Elton, T. S., & Hu, K. (2008). Protein kinase C-epsilon induces caveolin-dependent internalization of vascular adenosine 5'-triphosphate-sensitive K+ channels. *Hypertension, 52*(3), 499-506. doi:10.1161/HYPERTENSIONAHA.108.110817

Karl, M. O., Kroeger, W., Wimmers, S., Milenkovic, V. M., Valtink, M., Engelmann, K., & Strauss, O. (2008). Endogenous Gas6 and Ca2+ -channel activation modulate phagocytosis by retinal pigment epithelium. *Cell Signal, 20*(6), 1159-1168. doi:10.1016/j.cellsig.2008.02.005

Katz, B. (1949). Les constantes electriques de la membrane du muscle (Vol. 3, pp. 285-299): Arch Sci Physiol

Kenyon, E., Yu, K., La Cour, M., & Miller, S. S. (1994). Lactate transport mechanisms at apical and basolateral membranes of bovine retinal pigment epithelium. *Am J Physiol, 267*(6 Pt 1), C1561-1573. doi:10.1152/ajpcell.1994.267.6.C1561

Kimura, T., Makino, Y., Bathgate, R., Ivell, R., Nobunaga, T., Kubota, Y., . . . Kinoshita, M. (1997). The role of N-terminal glycosylation in the human oxytocin receptor. *Mol Hum Reprod, 3*(11), 957-963.

Kimura, T., Makino, Y., Saji, F., Takemura, M., Inoue, T., Kikuchi, T., . . . Tokugawa, Y. (1994). Molecular characterization of a cloned human oxytocin receptor. *Eur J Endocrinol, 131*(4), 385-390.

King, G. L., & Suzuma, K. (2000). Pigment-epithelium-derived factor--a key coordinator of retinal neuronal and vascular functions. *N Engl J Med, 342*(5), 349-351. doi:10.1056/NEJM200002033420511

Klein, U., & Fahrenholz, F. (1994). Reconstitution of the myometrial oxytocin receptor into proteoliposomes. Dependence of oxytocin binding on cholesterol. *Eur J Biochem, 220*(2), 559-567.

Kong, L., Mintz-Hittner, H. A., Penland, R. L., Kretzer, F. L., & Chévez-Barrios, P. (2008). Intravitreous bevacizumab as anti-vascular endothelial growth factor therapy for retinopathy of prematurity: a morphologic study. *Arch Ophthalmol, 126*(8), 1161-1163. doi:10.1001/archophthalmol.2008.1

Krapivinsky, G., Medina, I., Eng, L., Krapivinsky, L., Yang, Y., & Clapham, D. E. (1998). A novel inward rectifier K+ channel with unique pore properties. *Neuron, 20*(5), 995-1005.

Kryger, Z., Galli-Resta, L., Jacobs, G. H., & Reese, B. E. (1998). The topography of rod and cone photoreceptors in the retina of the ground squirrel. *Vis Neurosci, 15*(4), 685-691.

Kubo, Y., Baldwin, T. J., Jan, Y. N., & Jan, L. Y. (1993). Primary structure and functional expression of a mouse inward rectifier potassium channel. *Nature, 362*(6416), 127-133. doi:10.1038/362127a0

Kumar, M., & Pattnaik, B. R. (2014). Focus on Kir7.1: physiology and channelopathy. *Channels (Austin), 8*(6), 488-495. doi:10.4161/19336950.2014.959809

La Cour, M. (1992). Cl- transport in frog retinal pigment epithelium. *Exp Eye Res, 54*(6), 921-931.

la Cour, M., Lund-Andersen, H., & Zeuthen, T. (1986). Potassium transport of the frog retinal pigment epithelium: autoregulation of potassium activity in the subretinal space. *J Physiol, 375*, 461-479.

Lavine, J. A., Sang, Y., Wang, S., Ip, M. S., & Sheibani, N. (2013). Attenuation of choroidal neovascularization by β(2)-adrenoreceptor antagonism. *JAMA Ophthalmol, 131*(3), 376-382. doi:10.1001/jamaophthalmol.2013.1476

Leake, R. D., Weitzman, R. E., Glatz, T. H., & Fisher, D. A. (1981). Plasma oxytocin concentrations in men, nonpregnant women, and pregnant women before and during spontaneous labor. *J Clin Endocrinol Metab, 53*(4), 730-733. doi:10.1210/jcem-53-4-730

Lefebvre, D. L., Giaid, A., Bennett, H., Larivière, R., & Zingg, H. H. (1992). Oxytocin gene expression in rat uterus. *Science, 256*(5063), 1553-1555.

Leng, G., & Brown, D. (1997). The origins and significance of pulsatility in hormone secretion from the pituitary. *J Neuroendocrinol, 9*(7), 493-513.

Leng, G., Caquineau, C., & Sabatier, N. (2005). Regulation of oxytocin secretion. *Vitam Horm, 71*, 27-58. doi:10.1016/S0083-6729(05)71002-5

Leng, G., Shibuki, K., & Way, S. A. (1988). Effects of raised extracellular potassium on the excitability of, and hormone release from, the isolated rat neurohypophysis. *J Physiol, 399*, 591-605.

Lievremont, J. P., Bird, G. S., & Putney, J. W., Jr. (2005). Mechanism of inhibition of TRPC cation channels by 2-aminoethoxydiphenylborane. *Mol Pharmacol, 68*(3), 758-762. doi:10.1124/mol.105.012856

Lincoln, D. W., & Wakerley, J. B. (1974). Electrophysiological evidence for the activation of supraoptic neurones during the release of oxytocin. *J Physiol, 242*(2), 533-554.

Link, T. M., Park, U., Vonakis, B. M., Raben, D. M., Soloski, M. J., & Caterina, M. J. (2010). TRPV2 has a pivotal role in macrophage particle binding and phagocytosis. *Nat Immunol, 11*(3), 232-239. doi:10.1038/ni.1842

Logothetis, D. E., Jin, T., Lupyan, D., & Rosenhouse-Dantsker, A. (2007). Phosphoinositide-mediated gating of inwardly rectifying K(+) channels. *Pflugers Arch, 455*(1), 83-95. doi:10.1007/s00424-007-0276-5

Lopatin, A. N., & Nichols, C. G. (1996). [K+] dependence of open-channel conductance in cloned inward rectifier potassium channels (IRK1, Kir2.1). *Biophys J, 71*(2), 682-694. doi:10.1016/S0006-3495(96)79268-8

Ludwig, M., & Leng, G. (2006). Dendritic peptide release and peptide-dependent behaviours. *Nat Rev Neurosci, 7*(2), 126-136. doi:10.1038/nrn1845

Maeda, T., Van Hooser, J. P., Driessen, C. A., Filipek, S., Janssen, J. J., & Palczewski, K. (2003). Evaluation of the role of the retinal G protein-coupled receptor (RGR) in the vertebrate retina in vivo. *J Neurochem, 85*(4), 944-956.

Marmor, M. F. (1990). Control of subretinal fluid: experimental and clinical studies. *Eye (Lond), 4 (Pt 2)*, 340-344. doi:10.1038/eye.1990.46

Marneros, A. G., Fan, J., Yokoyama, Y., Gerber, H. P., Ferrara, N., Crouch, R. K., & Olsen, B. R. (2005). Vascular endothelial growth factor expression in the retinal pigment epithelium is essential for choriocapillaris development and visual function. *Am J Pathol, 167*(5), 1451-1459. doi:10.1016/S0002-9440(10)61231-X

McCloskey, C., Rada, C., Bailey, E., McCavera, S., van den Berg, H. A., Atia, J., . . . Blanks, A. M. (2014). The inwardly rectifying K+ channel KIR7.1 controls uterine excitability throughout pregnancy. *EMBO Mol Med, 6*(9), 1161-1174. doi:10.15252/emmm.201403944

McLeod, D. S., Hasegawa, T., Prow, T., Merges, C., & Lutty, G. (2006). The initial fetal human retinal vasculature develops by vasculogenesis. *Dev Dyn, 235*(12), 3336-3347. doi:10.1002/dvdy.20988

Mens, W. B., Witter, A., & van Wimersma Greidanus, T. B. (1983). Penetration of neurohypophyseal hormones from plasma into cerebrospinal fluid (CSF): half-times of disappearance of these neuropeptides from CSF. *Brain Res, 262*(1), 143-149.

Mergler, S., & Strauss, O. (2002). Stimulation of L-type Ca(2+) channels by increase of intracellular InsP3 in rat retinal pigment epithelial cells. *Exp Eye Res, 74*(1), 29-40. doi:10.1006/exer.2001.1128

Mintz-Hittner, H. A. (2010). Avastin as monotherapy for retinopathy of prematurity. *J AAPOS, 14*(1), 2-3. doi:10.1016/j.jaapos.2009.12.002

Mironneau, J. (1976). Effects of oxytocin on ionic currents underlying rhythmic activity and contraction in uterine smooth muscle. *Pflugers Arch, 363*(2), 113-118.

Mitchell, B. F., & Chibbar, R. (1995). Synthesis and metabolism of oxytocin in late gestation in human decidua. *Adv Exp Med Biol, 395*, 365-380.

Mitchell, C. H. (2001). Release of ATP by a human retinal pigment epithelial cell line: potential for autocrine stimulation through subretinal space. *J Physiol, 534*(Pt 1), 193-202.

Miyazaki, S. I., Takahashi, K., Tsuda, K., & Yoshii, M. (1974). Analysis of non-linearity observed in the current-voltage relation of the tunicate embryo. *J Physiol, 238*(1), 55-77.

Moiseyev, G., Chen, Y., Takahashi, Y., Wu, B. X., & Ma, J. X. (2005). RPE65 is the isomerohydrolase in the retinoid visual cycle. *Proc Natl Acad Sci U S A, 102*(35), 12413-12418. doi:10.1073/pnas.0503460102

Murtazina, D. A., Chung, D., Ulloa, A., Bryan, E., Galan, H. L., & Sanborn, B. M. (2011). TRPC1, STIM1, and ORAI influence signal-regulated intracellular and endoplasmic reticulum calcium dynamics in human myometrial cells. *Biol Reprod, 85*(2), 315-326. doi:10.1095/biolreprod.111.091082

Mutlu, F. M., & Sarici, S. U. (2013). Treatment of retinopathy of prematurity: a review of conventional and promising new therapeutic options. *Int J Ophthalmol, 6*(2), 228-236. doi:10.3980/j.issn.2222-3959.2013.02.23

Nakamura, N., Suzuki, Y., Sakuta, H., Ookata, K., Kawahara, K., & Hirose, S. (1999). Inwardly rectifying K+ channel Kir7.1 is highly expressed in thyroid follicular cells, intestinal epithelial cells and choroid plexus epithelial cells: implication for a functional coupling with Na+,K+-ATPase. *Biochem J, 342 (Pt 2)*, 329-336.

Nakamura, T. (1991). Structure and function of hepatocyte growth factor. *Prog Growth Factor Res, 3*(1), 67-85.

Nash, M., Flanigan, T., Leslie, R., & Osborne, N. (1999). Serotonin-2A receptor mRNA expression in rat retinal pigment epithelial cells. *Ophthalmic Res, 31*(1), 1-4.

Nash, M. S., & Osborne, N. N. (1997). Pharmacologic evidence for 5-HT1A receptors associated with human retinal pigment epithelial cells in culture. *Invest Ophthalmol Vis Sci, 38*(2), 510-519.

Naug, H. L., Browning, J., Gole, G. A., & Gobé, G. (2000). Vitreal macrophages express vascular endothelial growth factor in oxygen-induced retinopathy. *Clin Exp Ophthalmol, 28*(1), 48-52.

Neumann, I. D., & Landgraf, R. (2008). Advances in vasopressin and oxytocin--from genes to behaviour to disease. Preface. *Prog Brain Res, 170*, xi-xiii. doi:10.1016/S0079-6123(08)00448-2

Nichols, C. G., & Lopatin, A. N. (1997). Inward rectifier potassium channels. *Annu Rev Physiol, 59*, 171-191. doi:10.1146/annurev.physiol.59.1.171

Nishijima, K., Ng, Y. S., Zhong, L., Bradley, J., Schubert, W., Jo, N., . . . Shima, D. T. (2007). Vascular endothelial growth factor-A is a survival factor for retinal neurons and a critical neuroprotectant during the adaptive response to ischemic injury. *Am J Pathol, 171*(1), 53-67. doi:10.2353/ajpath.2007.061237

Nishimori, K., Young, L. J., Guo, Q., Wang, Z., Insel, T. R., & Matzuk, M. M. (1996). Oxytocin is required for nursing but is not essential for parturition or reproductive behavior. *Proc Natl Acad Sci U S A, 93*(21), 11699-11704.

Nordmann, J. J. (1977). Ultrastructural morphometry of the rat neurohypophysis. *J Anat, 123*(Pt 1), 213-218.

O'Keefe, M., & Kirwan, C. (2006). Diode laser versus cryotherapy in treatment of ROP. *Br J Ophthalmol, 90*(4), 402-403. doi:10.1136/bjo.2005.086330

Oakley, B., 2nd. (1977). Potassium and the photoreceptor-dependent pigment epithelial hyperpolarization. *J Gen Physiol, 70*(4), 405-425.

Oancea, E., Teruel, M. N., Quest, A. F., & Meyer, T. (1998). Green fluorescent protein (GFP)-tagged cysteine-rich domains from protein kinase C as fluorescent indicators for diacylglycerol signaling in living cells. *J Cell Biol, 140*(3), 485-498.

Ookata, K., Tojo, A., Suzuki, Y., Nakamura, N., Kimura, K., Wilcox, C. S., & Hirose, S. (2000). Localization of inward rectifier potassium channel Kir7.1 in the basolateral membrane of distal nephron and collecting duct. *J Am Soc Nephrol, 11*(11), 1987-1994.

Pattnaik, B., Jellali, A., Sahel, J., Dreyfus, H., & Picaud, S. (2000). GABAC receptors are localized with microtubule-associated protein 1B in mammalian cone photoreceptors. *J Neurosci, 20*(18), 6789-6796.

Pattnaik, B. R., & Hughes, B. A. (2009). Regulation of Kir channels in bovine retinal pigment epithelial cells by phosphatidylinositol 4,5-bisphosphate. *Am J Physiol Cell Physiol, 297*(4), C1001-1011. doi:10.1152/ajpcell.00250.2009

Pattnaik, B. R., & Hughes, B. A. (2012). Effects of KCNQ channel modulators on the M-type potassium current in primate retinal pigment epithelium. *Am J Physiol Cell Physiol, 302*(5), C821-833. doi:10.1152/ajpcell.00269.2011

Pattnaik, B. R., Shahi, P. K., Marino, M. J., Liu, X., York, N., Brar, S., . . . Traboulsi, E. I. (2015). A Novel KCNJ13 Nonsense Mutation and Loss of Kir7.1 Channel Function Causes Leber Congenital Amaurosis (LCA16). *Hum Mutat, 36*(7), 720-727. doi:10.1002/humu.22807

Pattnaik, B. R., Tokarz, S., Asuma, M. P., Schroeder, T., Sharma, A., Mitchell, J. C., . . . Pillers, D. A. (2013). Snowflake vitreoretinal degeneration (SVD) mutation R162W provides new insights into Kir7.1 ion channel structure and function. *PLoS One, 8*(8), e71744. doi:10.1371/journal.pone.0071744

Phillips, M. J., Jiang, P., Howden, S., Barney, P., Min, J., York, N. W., . . . Gamm, D. M. (2018). A Novel Approach to Single Cell RNA-Sequence Analysis Facilitates In Silico Gene Reporting of Human Pluripotent Stem Cell-Derived Retinal Cell Types. *Stem Cells, 36*(3), 313-324. doi:10.1002/stem.2755

Pliska, V., Heiniger, J., Muller-Lhotsky, A., Pliska, P., & Ekberg, B. (1986). Binding of oxytocin to uterine cells in vitro. Occurrence of several binding site populations and reidentification of oxytocin receptors. *J Biol Chem, 261*(36), 16984-16989.

Pliska, V., & Kohlhauf Albertin, H. (1991). Effect of Mg2+ on the binding of oxytocin to sheep myometrial cells. *Biochem J, 277 (Pt 1)*, 97-101.

Prematurity, I. C. f. t. C. o. R. o. (2005). The International Classification of Retinopathy of Prematurity revisited. *Arch Ophthalmol, 123*(7), 991-999. doi:10.1001/archopht.123.7.991

Provis, J. M. (2001). Development of the primate retinal vasculature. *Prog Retin Eye Res, 20*(6), 799-821.

Quehenberger, O., Prossnitz, E. R., Cochrane, C. G., & Ye, R. D. (1992). Absence of G(i) proteins in the Sf9 insect cell. Characterization of the uncoupled recombinant N-formyl peptide receptor. *J Biol Chem, 267*(28), 19757-19760.

Quinn, R. H., & Miller, S. S. (1992). Ion transport mechanisms in native human retinal pigment epithelium. *Invest Ophthalmol Vis Sci, 33*(13), 3513-3527.

Quinn, R. H., Quong, J. N., & Miller, S. S. (2001). Adrenergic receptor activated ion transport in human fetal retinal pigment epithelium. *Invest Ophthalmol Vis Sci, 42*(1), 255-264.

Ramsay, D. T., Kent, J. C., Owens, R. A., & Hartmann, P. E. (2004). Ultrasound imaging of milk ejection in the breast of lactating women. *Pediatrics, 113*(2), 361-367.

Rao, V. V., Löffler, C., Battey, J., & Hansmann, I. (1992). The human gene for oxytocin-neurophysin I (OXT) is physically mapped to chromosome 20p13 by in situ hybridization. *Cytogenet Cell Genet, 61*(4), 271-273.

Redmond, T. M., Yu, S., Lee, E., Bok, D., Hamasaki, D., Chen, N., . . . Pfeifer, K. (1998). Rpe65 is necessary for production of 11-cis-vitamin A in the retinal visual cycle. *Nat Genet, 20*(4), 344-351. doi:10.1038/3813

Reese, B. R. (2011). Development of the Retina and Optic Pathway. *Vision Research, 51*(7), 613-632.

Richard, S., & Zingg, H. H. (1990). The human oxytocin gene promoter is regulated by estrogens. *J Biol Chem, 265*(11), 6098-6103.

Richard, S., & Zingg, H. H. (1991). Identification of a retinoic acid response element in the human oxytocin promoter. *J Biol Chem, 266*(32), 21428-21433.

Risau, W. (1997). Mechanisms of angiogenesis. *Nature, 386*(6626), 671-674. doi:10.1038/386671a0

Ristori, C., Filippi, L., Dal Monte, M., Martini, D., Cammalleri, M., Fortunato, P., . . . Bagnoli, P. (2011). Role of the adrenergic system in a mouse model of oxygen-induced retinopathy: antiangiogenic effects of beta-adrenoreceptor blockade. *Invest Ophthalmol Vis Sci, 52*(1), 155-170. doi:10.1167/iovs.10-5536

Rohacs, T., Chen, J., Prestwich, G. D., & Logothetis, D. E. (1999). Distinct specificities of inwardly rectifying K(+) channels for phosphoinositides. *J Biol Chem, 274*(51), 36065-36072.

Rohács, T., Lopes, C. M., Jin, T., Ramdya, P. P., Molnár, Z., & Logothetis, D. E. (2003). Specificity of activation by phosphoinositides determines lipid regulation of Kir channels. *Proc Natl Acad Sci U S A, 100*(2), 745-750. doi:10.1073/pnas.0236364100

Rosenthal, R., Heimann, H., Agostini, H., Martin, G., Hansen, L. L., & Strauss, O. (2007). Ca2+ channels in retinal pigment epithelial cells regulate vascular endothelial growth factor secretion rates in health and disease. *Mol Vis, 13*, 443-456.

Russell, J. A., Leng, G., & Douglas, A. J. (2003). The magnocellular oxytocin system, the fount of maternity: adaptations in pregnancy. *Front Neuroendocrinol, 24*(1), 27-61.

Ryan, J. S., Baldridge, W. H., & Kelly, M. E. (1999). Purinergic regulation of cation conductances and intracellular Ca2+ in cultured rat retinal pigment epithelial cells. *J Physiol, 520 Pt 3*, 745-759.

Sabatier, N., Caquineau, C., Dayanithi, G., Bull, P., Douglas, A. J., Guan, X. M., . . . Leng, G. (2003). Alpha-melanocyte-stimulating hormone stimulates oxytocin release from the dendrites of hypothalamic neurons while inhibiting oxytocin release from their terminals in the neurohypophysis. *J Neurosci, 23*(32), 10351-10358.

Sahin, A., Sahin, M., Türkcü, F. M., Cingü, A. K., Yüksel, H., Cınar, Y., . . . Caça, I. (2014). Incidence of retinopathy of prematurity in extremely premature infants. *ISRN Pediatr, 2014*, 134347. doi:10.1155/2014/134347

Sakamoto, T., Sakamoto, H., Murphy, T. L., Spee, C., Soriano, D., Ishibashi, T., . . . Ryan, S. J. (1995). Vessel formation by choroidal endothelial cells in vitro is modulated by retinal pigment epithelial cells. *Arch Ophthalmol, 113*(4), 512-520.

Sakmann, B., & Trube, G. (1984). Conductance properties of single inwardly rectifying potassium channels in ventricular cells from guinea-pig heart. *J Physiol, 347*, 641-657.

Salom, D., Lodowski, D. T., Stenkamp, R. E., Le Trong, I., Golczak, M., Jastrzebska, B., . . . Palczewski, K. (2006). Crystal structure of a photoactivated deprotonated intermediate of rhodopsin. *Proc Natl Acad Sci U S A, 103*(44), 16123-16128. doi:10.1073/pnas.0608022103

Samuels, I. S., Sturgill, G. M., Grossman, G. H., Rayborn, M. E., Hollyfield, J. G., & Peachey, N. S. (2010). Light-evoked responses of the retinal pigment epithelium: changes accompanying photoreceptor loss in the mouse. *J Neurophysiol, 104*(1), 391-402. doi:10.1152/jn.00088.2010

Sanborn, B. M., Ku, C. Y., Shlykov, S., & Babich, L. (2005). Molecular signaling through G-protein-coupled receptors and the control of intracellular calcium in myometrium. *J Soc Gynecol Investig, 12*(7), 479-487. doi:10.1016/j.jsgi.2005.07.002

Schubert, F., George, J. M., & Rao, M. B. (1981). Vasopressin and oxytocin content of human fetal brain at different stages of gestation. *Brain Res, 213*(1), 111-117.

Sergouniotis, P. I., Davidson, A. E., Mackay, D. S., Li, Z., Yang, X., Plagnol, V., . . . Webster, A. R. (2011). Recessive mutations in KCNJ13, encoding an inwardly rectifying potassium channel subunit, cause leber congenital amaurosis. *Am J Hum Genet, 89*(1), 183-190. doi:10.1016/j.ajhg.2011.06.002

Sermasi, E., & Coote, J. H. (1994). Oxytocin acts at V1 receptors to excite sympathetic preganglionic neurones in neonate rat spinal cord in vitro. *Brain Res, 647*(2), 323-332.

Shah, P. K., Prabhu, V., Karandikar, S. S., Ranjan, R., Narendran, V., & Kalpana, N. (2016). Retinopathy of prematurity: Past, present and future. *World J Clin Pediatr, 5*(1), 35-46. doi:10.5409/wjcp.v5.i1.35

Shahi, P. K., Liu, X., Aul, B., Moyer, A., Pattnaik, A., Denton, J., . . . Pattnaik, B. R. (2017). Abnormal Electroretinogram after Kir7.1 Channel Suppression Suggests Role in Retinal Electrophysiology. *Sci Rep, 7*(1), 10651. doi:10.1038/s41598-017-11034-1

Shimura, M., Yuan, Y., Chang, J. T., Zhang, S., Campochiaro, P. A., Zack, D. J., & Hughes, B. A. (2001). Expression and permeation properties of the K(+) channel Kir7.1 in the retinal pigment epithelium. *J Physiol, 531*(Pt 2), 329-346.

Sinclair, M. S., Perea-Martinez, I., Dvoryanchikov, G., Yoshida, M., Nishimori, K., Roper, S. D., & Chaudhari, N. (2010). Oxytocin signaling in mouse taste buds. *PLoS One, 5*(8), e11980. doi:10.1371/journal.pone.0011980

Smith, L. E. (2004). Pathogenesis of retinopathy of prematurity. *Growth Horm IGF Res, 14 Suppl A*, S140-144. doi:10.1016/j.ghir.2004.03.030

Smith, M. P., Ayad, V. J., Mundell, S. J., McArdle, C. A., Kelly, E., & Lopez Bernal, A. (2006). Internalization and desensitization of the oxytocin receptor is inhibited by Dynamin and clathrin mutants in human embryonic kidney 293 cells. *Mol Endocrinol, 20*(2), 379-388. doi:10.1210/me.2005-0031

Soloff, M. S., & Fields, M. J. (1989). Changes in uterine oxytocin receptor concentrations throughout the estrous cycle of the cow. *Biol Reprod, 40*(2), 283-287.

Sonoda, S., Sreekumar, P. G., Kase, S., Spee, C., Ryan, S. J., Kannan, R., & Hinton, D. R. (2009). Attainment of polarity promotes growth factor secretion by retinal pigment epithelial cells: relevance to age-related macular degeneration. *Aging (Albany NY), 2*(1), 28-42.

Stahl, A., Connor, K. M., Sapieha, P., Chen, J., Dennison, R. J., Krah, N. M., . . . Smith, L. E. (2010). The mouse retina as an angiogenesis model. *Invest Ophthalmol Vis Sci, 51*(6), 2813-2826. doi:10.1167/iovs.10-5176

Stalmans, I., Ng, Y. S., Rohan, R., Fruttiger, M., Bouche, A., Yuce, A., . . . D'Amore, P. A. (2002). Arteriolar and venular patterning in retinas of mice selectively expressing VEGF isoforms. *J Clin Invest, 109*(3), 327-336. doi:10.1172/JCI14362

Stamer, W. D., Bok, D., Hu, J., Jaffe, G. J., & McKay, B. S. (2003). Aquaporin-1 channels in human retinal pigment epithelium: role in transepithelial water movement. *Invest Ophthalmol Vis Sci, 44*(6), 2803-2808.

Steinberg, R. H., Linsenmeier, R. A., & Griff, E. R. (1983). Three light-evoked responses of the retinal pigment epithelium. *Vision Res, 23*(11), 1315-1323.

Stone, J., Itin, A., Alon, T., Pe'er, J., Gnessin, H., Chan-Ling, T., & Keshet, E. (1995). Development of retinal vasculature is mediated by hypoxia-induced vascular endothelial growth factor (VEGF) expression by neuroglia. *J Neurosci, 15*(7 Pt 1), 4738-4747.

Strauss, O. (2005). The retinal pigment epithelium in visual function. *Physiol Rev, 85*(3), 845-881. doi:10.1152/physrev.00021.2004

Strauss, O., Mergler, S., & Wiederholt, M. (1997). Regulation of L-type calcium channels by protein tyrosine kinase and protein kinase C in cultured rat and human retinal pigment epithelial cells. *FASEB J, 11*(11), 859-867.

Strick, D. J., Feng, W., & Vollrath, D. (2009). Mertk drives myosin II redistribution during retinal pigment epithelial phagocytosis. *Invest Ophthalmol Vis Sci, 50*(5), 2427-2435. doi:10.1167/iovs.08-3058

Tao, L., Shen, D., Pandey, S., Hao, W., Rich, K. A., & Fong, H. K. (1998). Structure and developmental expression of the mouse RGR opsin gene. *Mol Vis, 4*, 25.

Tao, Q., & Kelly, M. E. (1996). Calcium-activated potassium current in cultured rabbit retinal pigment epithelial cells. *Curr Eye Res, 15*(3), 237-246.

Taugourdeau-Raymond, S., Rouby, F., Default, A., Jean-Pastor, M. J., & Centers, F. N. o. P. (2012). Bevacizumab-induced serious side-effects: a review of the French pharmacovigilance database. *Eur J Clin Pharmacol, 68*(7), 1103-1107. doi:10.1007/s00228-012-1232-7

Teirstein, P. S., Goldman, A. I., & O'Brien, P. J. (1980). Evidence for both local and central regulation of rat rod outer segment disc shedding. *Invest Ophthalmol Vis Sci, 19*(11), 1268-1273.

Terrillon, S., Durroux, T., Mouillac, B., Breit, A., Ayoub, M. A., Taulan, M., . . . Bouvier, M. (2003). Oxytocin and vasopressin V1a and V2 receptors form constitutive homo- and heterodimers during biosynthesis. *Mol Endocrinol, 17*(4), 677-691. doi:10.1210/me.2002-0222

Tsuboi, S. (1987). Measurement of the volume flow and hydraulic conductivity across the isolated dog retinal pigment epithelium. *Invest Ophthalmol Vis Sci, 28*(11), 1776-1782.

Varnai, P., & Balla, T. (1998). Visualization of phosphoinositides that bind pleckstrin homology domains: calcium- and agonist-induced dynamic changes and relationship to myo-[3H]inositol-labeled phosphoinositide pools. *J Cell Biol, 143*(2), 501-510.

Versaux-Botteri, C., Gibert, J. M., Nguyen-Legros, J., & Vernier, P. (1997). Molecular identification of a dopamine D1b receptor in bovine retinal pigment epithelium. *Neurosci Lett, 237*(1), 9-12.

Wallace, V. A. (2011). Concise review: making a retina--from the building blocks to clinical applications. *Stem Cells, 29*(3), 412-417. doi:10.1002/stem.602

Whorton, M. R., Bokoch, M. P., Rasmussen, S. G., Huang, B., Zare, R. N., Kobilka, B., & Sunahara, R. K. (2007). A monomeric G protein-coupled receptor isolated in a high-density lipoprotein particle efficiently activates its G protein. *Proc Natl Acad Sci U S A, 104*(18), 7682-7687. doi:10.1073/pnas.0611448104

Willermain, F., Libert, S., Motulsky, E., Salik, D., Caspers, L., Perret, J., & Delporte, C. (2014). Origins and consequences of hyperosmolar stress in retinal pigmented epithelial cells. *Front Physiol, 5*, 199. doi:10.3389/fphys.2014.00199

Wilson, T., Liggins, G. C., & Whittaker, D. J. (1988). Oxytocin stimulates the release of arachidonic acid and prostaglandin F2 alpha from human decidual cells. *Prostaglandins, 35*(5), 771-780.

Wong, L. L., & Rapaport, D. H. (2009). Defining retinal progenitor cell competence in Xenopus laevis by clonal analysis. *Development, 136*(10), 1707-1715. doi:10.1242/dev.027607

Wray, S. (2007). Insights into the uterus. *Exp Physiol, 92*(4), 621-631. doi:10.1113/expphysiol.2007.038125

Xin-Zhao Wang, C., Zhang, K., Aredo, B., Lu, H., & Ufret-Vincenty, R. L. (2012). Novel method for the rapid isolation of RPE cells specifically for RNA extraction and analysis. *Exp Eye Res, 102*, 1-9. doi:10.1016/j.exer.2012.06.003

Yang, D., Pan, A., Swaminathan, A., Kumar, G., & Hughes, B. A. (2003). Expression and localization of the inwardly rectifying potassium channel Kir7.1 in native bovine retinal pigment epithelium. *Invest Ophthalmol Vis Sci, 44*(7), 3178-3185.

Yang, J., Jan, Y. N., & Jan, L. Y. (1995). Determination of the subunit stoichiometry of an inwardly rectifying potassium channel. *Neuron, 15*(6), 1441-1447.

York, N., Halbach, P., Chiu, M. A., Bird, I. M., Pillers, D. M., & Pattnaik, B. R. (2017). Oxytocin (OXT)-stimulated inhibition of Kir7.1 activity is through PIP2-dependent Ca2+ response of the oxytocin receptor in the retinal pigment epithelium in vitro. *Cell Signal, 37*, 93-102. doi:10.1016/j.cellsig.2017.06.005

Young, R. W. (1978). The daily rhythm of shedding and degradation of rod and cone outer segment membranes in the chick retina. *Invest Ophthalmol Vis Sci, 17*(2), 105-116.

Young, W. S., Shepard, E., Amico, J., Hennighausen, L., Wagner, K. U., LaMarca, M. E., . . . Ginns, E. I. (1996). Deficiency in mouse oxytocin prevents milk ejection, but not fertility or parturition. *J Neuroendocrinol, 8*(11), 847-853.

Yuan, Y., Shimura, M., & Hughes, B. A. (2003). Regulation of inwardly rectifying K+ channels in retinal pigment epithelial cells by intracellular pH. *J Physiol, 549*(Pt 2), 429-438. doi:10.1113/jphysiol.2003.042341

Zeng, W. Z., Babich, V., Ortega, B., Quigley, R., White, S. J., Welling, P. A., & Huang, C. L. (2002). Evidence for endocytosis of ROMK potassium channel via clathrin-coated vesicles. *Am J Physiol Renal Physiol, 283*(4), F630-639. doi:10.1152/ajprenal.00378.2001

Zhang, W., Zitron, E., Bloehs, R., Müller-Krebs, S., Scholz, E., Zeier, M., . . . Schwenger, V. (2008). Dual regulation of renal Kir7.1 potassium channels by protein Kinase A and protein Kinase C. *Biochem Biophys Res Commun, 377*(3), 981-986. doi:10.1016/j.bbrc.2008.10.110

Zhang, X., & Hughes, B. A. (2013). KCNQ and KCNE Potassium Channel Subunit Expression in Bovine Retinal Pigment Epithelium. *Exp Eye Res*. doi:10.1016/j.exer.2013.10.013

Zhong, M., Yang, M., & Sanborn, B. M. (2003). Extracellular signal-regulated kinase 1/2 activation by myometrial oxytocin receptor involves Galpha(q)Gbetagamma and epidermal growth factor receptor tyrosine kinase activation. *Endocrinology, 144*(7), 2947-2956.

Appendix 1: Characterization of iPS derived photoreceptors

Work published as part of the following collaboration:

A Novel Approach to Single Cell RNA-Sequence Analysis Facilitates In Silico Gene Reporting of Human Pluripotent Stem Cell-Derived Retinal Cell Types

M. Joseph Phillips, Peng Jiang, Sara Howden, Patrick Barney, Jee Min, Nathaniel W. York, Li-Fang Chu, Elizabeth E. Capowski, Abigail Cash, Shivani Jain, Katherine Barlow, Tasnia Tabassum, Ron Stewart, Bikash R. Pattnaik, James A. Thomson, David M. Gamm.

Published in Stem Cells, Volume 36(2), November 2017, Pages 313-324 (Phillips et al., 2018)

Introduction

During my time in the Pattnaik lab I had the opportunity to collaborate with other researchers on campus. This work was the product of one such collaboration in which I worked with Dr. Joseph Phillips and Dr. David Gamm to identify whether human induced pluripotent stem cells (hPSC) derived photoreceptors that they had developed exhibited the electrophysiological properties associated with rods and cones. This served as part of a broader project focused on evaluating the composition of hPSC derived optic vesicles (hPSC-OV) during their differentiation. While RPE cells derived from these cultures can be identifies and cultured with relative ease the neural retina is much more complex. Using single cell RNA-seq, Phillips et al. set out to identify the diversity and authenticity of cell types during hPSC-OV differentiation. To support this study they developed an hPSC reporter line that expressed the *tdTomato* gene under the control of the *CRX* promoter. This promoter is active in PR's from early retinogenesis through maturity allowing identification of photoreceptors during all stages of development (Collin et al., 2016). My contribution to this work was to assay the functional maturity of differentiated photoreceptors from early and late stage hPSC-OV cultures. Utilizing whole cell patch clamp electrophysiology I recorded whole cell current from single CRX positive cells. I retrieved cytoplasm from a subset of cells and identified rod vs cone identity using RT-PCR. I determined that PRs from the earlier time points were predominately cones whereas cells from the later time point where predominately rods. These observations are consistent with previous mouse studies and suggests that these hPSC-OV derived PR are authentic (Pattnaik et al., 2000).

This work, while not directly applicable to the aims of my thesis, will have an impact on future studies of retinal development and PR-RPE interactions and therefore oxytocinergic

signaling within the retina. Developing and characterizing a working hPSC-OV culture will allow us for future *in vitro* studies on the development and function of the neural retina and RPE in a much more accessible way then is currently possible. Showing that the progeny of these OV's are authentic helps to legitimize this culture as a model for this future work.

Methods

Complete methods used can be found in the full paper (Phillips et al., 2018). Here I have listed the methods I used for my contribution to the study.

Electrophysiology *–T*dtomato fluorescence positive cells were recorded in the standard whole-cell patch-clamp mode using an upright FN1 microscope (Nikon, Melleville, NY). Hepes buffered Ringer's solution was used to perfuse the recording chamber (135mM NaCl, 5 mM KCl, 1.8mM $CaCl_2$, 1mM $MgCl_2$, 10mM HEPES and 10mM glucose with pH adjusted to 7.4 using NaOH). The patch pipettes used measured 3-7 MΩ, when filled with a solution (83 K-gluconate, 30 KCL, 0.5 $CaCl_2$, 4 $MgCl_2$, 5.5 EGTA-KOH, 10 HEPES, 4 K_2-ATP in mM with pH adjusted to 7.2 using KOH at 22^{o}C). Current responses were measured by applying a 2 sec voltage ramp protocol (from -150 to 50 mV while holding the cells at -60 mV during the inter-pulse interval). Data were acquired using p-Clamp10 (Axopatch 200B and Digidata 1440 from Molecular Devices, CA) and analyzed off-line using Clampfit-10, and Microsoft Excel or Origin-9.

Single-Cell RNA Isolation and RT-PCR**-** Following electrophysiological recording the patch pipette was used to collect and deposit the cell in a PCR tube, where it was stored at -80^{o}C. The same day, amplification of mRNA was performed by reverse transcription using the SuperScript III First-Strand Synthesis System (Life technologies). The collected cell was

incubated for 5 minutes at 65^{o}C in a 10 µL solution containing 5µM oligo(dT)$_{20}$ and 1mM dNTP mix. After a minimum of 1 minute at 4^{o}C, 10µL of cDNA synthesis mixture containing 2X RT buffer, 10mM $MgCl_2$, .02 M DTT, 40 U RNaseOUT and 200 U SuperScript III was added. Reverse transcription was performed using the ProFlex PCR system (Life technologies) at 50^{o}C for 50 minutes, followed by termination 85^{o}C for 5 minutes and chilling at 4^{o}C. 1 µL of RNase H was added and the mixture was incubated at 37^{o}C for 20 min, after which cDNA was stored at -20^{o}C or used immediately for PCR.

***PCR on single-cell cDNA*-** To probe for expression of THRB or NRL by recorded cells a 2 step nested PCR was utilized. In the first step each PCR reaction used 1X MyTaw HS Mix (Bioline, Taunton, MA, USA), 200nM external forward primer, 200nM external reverse primer, between 2 and 15 µL of RT-PCR Product, brought to a total volume of 50 µL with RNase-free water. PCR began with one cycle at 95 ^{o}C for 1 min, followed by denaturing, annealing and extension for 35 cycles at 95^{o}C for 15 s, 51^{o}C for 15s and 72^{o}C for 10s, respectively. The second step used 1X MyTaw HS Mix (Bioline, Taunton, MA, USA), 200nM internal forward primer, 200nM internal reverse primer, 2-3 µL of the product from step one, brought to a total volume of 50 µL with RNase-free water. The same cycling conditions were used for this step, with the exception of the annealing temperature, which was changed to 52^{o}C. The second step PCR product was resolved in a 3% agarose gel (Bioline, Taunton, MA, USA) and documented using the FOTO Dual Trans-illuminator (FOTODYNE, Hartland, WI, USA)

Results

To determine whether a physiological distinction was present between photoreceptors expressing rod and cone markers whole cell electrophysiological current was recorded from each population. Cells were identified by their expression of tdTomato (Figure 1b) and cytoplasm was collected following recording for so that cells could later be identified by single cell PCR. Expression of neural retina leucine zipper protein (NRL) or thyroid hormone receptor β2 (THRB), key transcription factors in the differentiation of rods and cones respectively, were used to determine the identity of recorded cells (Figure 1c). In later cultures I observed NRL positive cells with a current profile consistent with previous literature. From this time point I found THRB cells but they did not exhibit current consistent with what would be expected of cones (Figure 1a). However, cones are known to mature prior to rods so we repeated recordings using an earlier culture. In these cells THRB positive cells did exhibit characteristic cone current (Figure 1a).

Discussion

Electrophysiology demonstrated a significant difference in the current profiles of CRX positive cells identified as rods or cones by the presence of genetic markers for each. In the differentiated population NRL positive cells appear to have a current profile that is characteristic of rod photoreceptors, supporting the hypothesis that these iPS derived cells are physiologically mature rods. As cones develop earlier than rods I looked at cells from an earlier culture and found THRB positive cells that express current characteristic of cones. This evidence not only demonstrates that CRX positive cells generated from this iPS culture are in fact functional rods and cones it also shows that they follow the same differentiation timeline with

cones maturing earlier than rods. It also suggests that mature photoreceptors degenerate over time in this culture model.

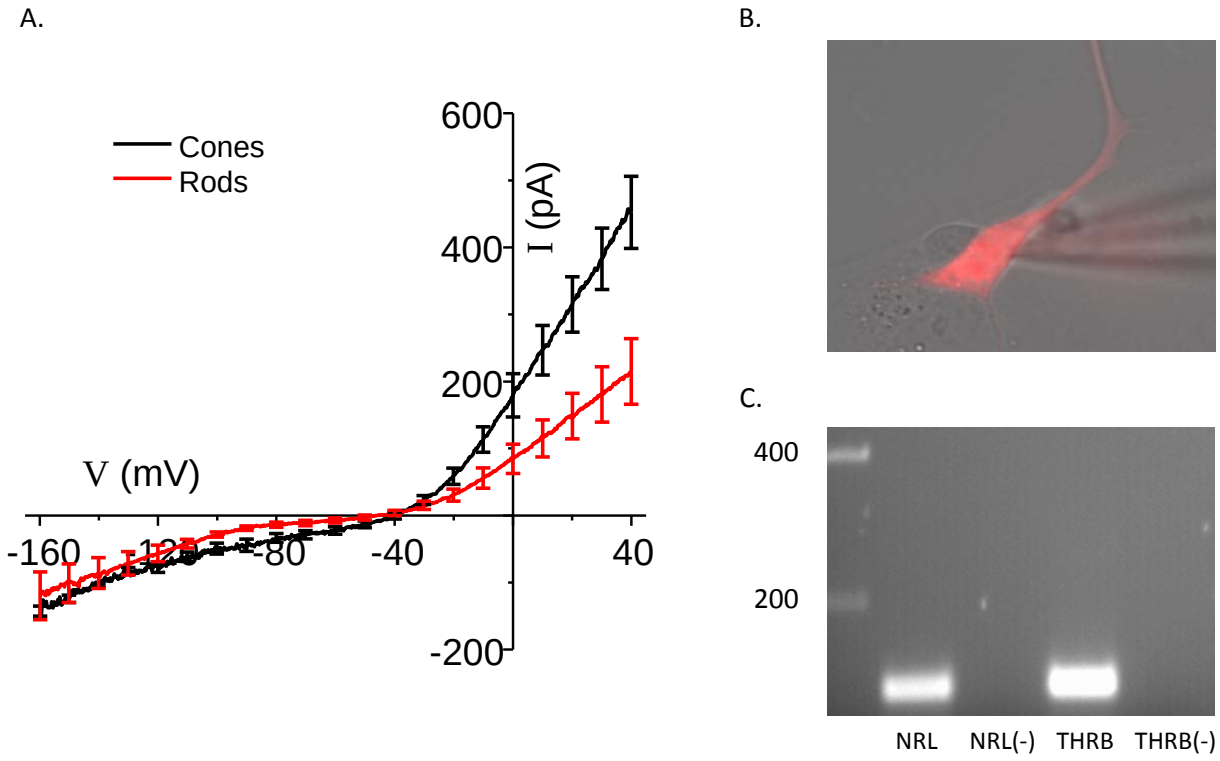

Figure A1.1: Electrophysiology of hPSC derived photoreceptors A. Average current-voltage plot is shown from cone marker positive (n=5) and rod marker positive (n=5). B. Photoreceptor identified by tdTomato flouresense and morphology, including neuronal projections, superimposed as bright field and fluorescence image. C. Agarose gel electrophoresis of Single cell PCR results shows NRL positive cell in Lane 2 and THRB positive cell in Lane 4 with respective negative control adjacent.

Appendix II: Original Manuscript, Oxytocin (OXT)-stimulated inhibition of Kir7.1 activity is modulated by PIP_2-dependent Ca^{2+} response of the Oxytocin receptor in the Retinal Pigment Epithelium in vitro, as published

Cellular Signalling 37 (2017) 93–102

Contents lists available at ScienceDirect

Cellular Signalling

journal homepage: www.elsevier.com/locate/cellsig

Oxytocin (OXT)-stimulated inhibition of Kir7.1 activity is through PIP_2-dependent Ca^{2+} response of the oxytocin receptor in the retinal pigment epithelium in vitro

Nathaniel York[a,b,c,g,1], Patrick Halbach[a,b,c,g,1], Michelle A. Chiu[b,c,g], Ian M. Bird[a,d], De-Ann M. Pillers[b,c,e,g], Bikash R. Pattnaik[a,b,c,f,g,*]

[a] Endocrinology-Reproductive Physiology Program, The University of Wisconsin, Madison, WI 53715, United States
[b] Division of Neonatology & Newborn Nursery, The University of Wisconsin, Madison, WI 53715, United States
[c] Departments of Pediatrics, The University of Wisconsin, Madison, WI 53715, United States
[d] Obstetrics & Gynecology, The University of Wisconsin, Madison, WI 53715, United States
[e] Medical Genetics, The University of Wisconsin, Madison, WI 53715, United States
[f] Ophthalmology & Visual Sciences, The University of Wisconsin, Madison, WI 53715, United States
[g] The McPherson Eye Research Institute, The University of Wisconsin, Madison, WI 53715, United States

ARTICLE INFO

Keywords:
Calcium imaging
Cell signaling
Hormone receptor
Inositol 1,4,5-trisphosphate (IP3)
Ion-channel
Retina
Oxytocin
RPE
Oxytocin receptor

ABSTRACT

Oxytocin (OXT) is a neuropeptide that activates the oxytocin receptor (OXTR), a rhodopsin family G-protein coupled receptor. Our localization of OXTR to the retinal pigment epithelium (RPE), in close proximity to OXT in the adjacent photoreceptor neurons, leads us to propose that OXT plays an important role in RPE-retinal communication. An increase of RPE $[Ca^{2+}]_i$ in response to OXT stimulation implies that the RPE may utilize oxytocinergic signaling as a mechanism by which it accomplishes some of its many roles. In this study, we used an established human RPE cell line, a HEK293 heterologous OXTR expression system, and pharmacological inhibitors of Ca^{2+} signaling to demonstrate that OXTR utilizes capacitative Ca^{2+} entry (CCE) mechanisms to sustain an increase in cytoplasmic Ca^{2+}. These findings demonstrate how multiple functional outcomes of OXT-OXTR signaling could be integrated via a single pathway. In addition, the activated OXTR was able to inhibit the Kir7.1 channel, an important mediator of sub retinal waste transport and K^+ homeostasis.

1. Introduction

Oxytocin (OXT) is a cyclic nonapeptide produced in the paraventricular and supraoptic nuclei of the hypothalamus [1]. Although best known for its association with parturition and lactation, OXT also has numerous central and peripheral effects, including, but not limited to, the modulation of sexual and social behavior, influence over metabolic activity in adipose tissues, and skeletal muscle maintenance [1,2].

The RPE is a monolayer of polarized cells that serve as a physical and protective blood-retina barrier and act as a facilitator of phototransduction in the photoreceptors [3]. The RPE also mediates the bidirectional transport of nutrients between the choroid and photoreceptors, maintains the ionic composition of the subretinal fluid, and facilitates phagocytosis of photoreceptor outer segments that are shed on a daily basis. It is not fully understood how the RPE and photoreceptors coordinate their function. What is known, however, is that autocrine and paracrine signaling in the RPE involves G protein-coupled receptors (GPCR), including the dopaminergic, adrenergic, P_{2Y}-purinergic, and serotoninergic receptors [4–9].

We have shown that OXT is a potential mediator of retinal physiology given its presence in the cone photoreceptor extracellular matrix [10]. Moreover, the oxytocin receptor (OXTR) is expressed in the retinal pigment epithelium (RPE) where we have shown that OXT can induce an increase in $[Ca^{2+}]_i$, leading to our hypothesis that oxytocinergic signaling may serve as a means for communication between cone photoreceptors and the RPE [10]. OXTR is a GPCR and like the aforementioned receptors, it activates a phospholipase C (PLC)-mediated signaling pathway, thereby stimulating PIP_2 hydrolysis and resulting in a rise in $[Ca^{2+}]_i$ [11].

Facing the photoreceptor outer segments on the apical membrane of

* Corresponding author at: Division of Neonatology and Newborn Nursery, Department of Pediatrics, University of Wisconsin School of Medicine and Public Health, SMI 112, 1300 University Avenue, Madison, WI 53706, United States.
E-mail address: pattnaik@wisc.edu (B.R. Pattnaik).
[1] These authors contributed equally to this work.

http://dx.doi.org/10.1016/j.cellsig.2017.06.005
Received 20 January 2017; Received in revised form 28 May 2017; Accepted 5 June 2017
Available online 08 June 2017
0898-6568/ Published by Elsevier Inc.

the RPE cell is the inwardly rectifying potassium (Kir7.1) channel [3,12]. As its name suggests, Kir7.1 exhibits a large inward K^+ current at hyperpolarized membrane potentials. However, at physiological membrane potentials, the channel facilitates the efflux of intracellular K^+ [13,14]. This, combined with its co-localization with Na^+-K^+-ATPase, makes Kir7.1 integral to the maintenance of the K^+ transport needed for transepithelial fluid transport [15–17]. Kir7.1 function is also directly mediated by PIP_2, supporting the possible regulation of Kir7.1 by OXTR through PLC-activated PIP_2 hydrolysis [18]. Understanding how Kir7.1 is regulated is clinically important, as disrupted Kir7.1 function is a known cause of the retinal diseases of Snowflake Vitreoretinal Degeneration and Lebers Congenital Amaurosis – Type 16 (LCA16) [19,20]. A direct impact of Kir7.1 on retinal function and vision can be clearly seen following RNA interference (RNA_i) knockdown of Kir7.1 in mice, resulting in a characteristic and abnormal electroretinogram (ERG) [21].

In the present study we sought to delineate the mechanism by which OXT elicits an increase in $[Ca^{2+}]_i$ and how this may affect Kir 7.1 function in the RPE by using cultured hfRPE cells. We also studied a human embryonic kidney (HEK293) cell line with heterologous expression of human OXTR to study the effects of OXTR on the Kir7.1 channel without the complex interactions inherent in the intact RPE cell. Lastly, we used adult mouse RPE cells to demonstrate the link between Kir7.1 channel function and OXT-OXTR signaling.

2. Materials and methods

2.1. Reagents

All chemical reagents were purchased from Sigma-Aldrich (Sigma-Aldrich, St. Louis, MO), Thermo Fisher Scientific (Thermo Fisher Scientific, Waltham, MA), or Gibco (Grand Island, NY), unless otherwise specified.

2.2. Solutions

HEPES Ringers (HR) extracellular bath solution was prepared using (mM) 135 NaCl, 5 KCl, 1.8 $CaCl_2$, 1 $MgCl_2$, 10 HEPES, 10 glucose, and adjusted to pH 7.4 with NaOH. K^+ inhibition solutions require the same composition with 115 mM NaCl and the addition of 20 mM $BaCl_2$ or $CsCl_2$. Ca^{2+}-free extracellular bath solution was prepared using (mM) 135 NaCl, 5 KCl, 1 $MgCl_2$, 10 glucose, 10 HEPES, 2 EGTA-KOH, and adjusted to pH 7.4 with NaOH. Final concentrations of 0.01, 0.1, 1, 6, 10, or 100 μM OXT were prepared in either HR or Ca^{2+}-free extracellular solutions. Extracellular solution containing the Ca^{2+} channel blocker nifedipine was prepared by diluting to 10 μM final concentration in HR. A final concentration of 60 μM 2-APB (Tocris Bioscience, Bristol, UK), an IP_3R inhibitor, was prepared in HR.

2.3. Cell culture

Passages 1–3 cryopreserved Primary Clonetics™ Human RPE cells (hfRPE) (LONZA, Walkersville, WA) were cultured using a previously published protocol [10].

HEK293 cells were obtained from ATCC (Manassas, VA). To generate HEK-OXTR line, cells were transfected with a pcDNA6/HisC plasmid-containing human OXTR via nucleofection (4-D Nucleofector, LONZA) as per the manufacturer's instructions. Cells were cultured in a 60 mm culture dish in complete growth medium (DMEM + 10% Fetal Bovine Serum + 1% Pen-Strep). Twenty-four hours after transfection, culture media was supplemented with 10 μg/mL blasticidin (Thermo Fisher Scientific) to select for cells expressing the OXTR-containing plasmid. Individual surviving cell colonies were selected and grown in culture media containing blasticidin in 24-well plates. OXTR expression was verified by indirect immunofluorescence and Ca^{2+} imaging. OXTR positive cells were cryo-preserved and subcultured for experimental usage.

hfRPE culture media was prepared using MEM alpha base medium, 1% N-2 supplement, 1% glutamine, 1% pen-strep, 1% MEM non-essential amino acids, taurine, hydrocortisone, and 3, 3′, 5-triiodothryonine. HEK cell culture complete growth media was prepared using 10% FBS and 1% PenStrep diluted in DMEM.

2.4. Ca^{2+} imaging

hfRPE cells were grown on coverslips and incubated in 5 μM FURA-2 penta-acetoxymethyl ester (AM) in hfRPE culture media + 0% FBS for 30 min in a dark environment. Selective Oxytocin antagonist, desGly-NH_2-d$(CH_2)_5$[D-Tyr^2,Thr^4]OVT, (OTA) was generously provided by Dr. Maurice Manning (University of Toledo, OH). 100 μM OTA was included in FURA incubation solution as well as perfusion solution. HEK-OXTR cells grown on coverslips were incubated with 5 μM Fura-2 AM in serum-free DMEM under the same conditions. Following incubation with FURA-2 AM, coverslips were rinsed × 3 in HR solution and transferred to the recording chamber (Warner Instruments, Hamden, CT) on the microscope stage (Nikon FN1, Nikon Instruments Inc., New York, NY). hfRPE cells were continuously perfused with HR or Ca^{2+}-free solution containing tested compounds (OXT, nifedipine, 2-APB, OTA) and were exchanged using a gravity-feed 8-valve solution exchange system with a ValveLink Pinch Valve (Automate Scientific, Berkeley, CA) controlled through ValveLink8.2 (Automate Scientific, Berkeley, CA). HEK-OXTR cells were continuously perfused with HR, and HR solution containing OXT or ATP was exchanged using the same system.

Images were acquired every 10 s using a 20× water immersion objective (NA = 0.5) and Lambda LS lamp (Shutter Instruments, Novato, CA). The 300 ms shutter speed and 340 and 380 nm excitation wavelengths were controlled by the Lambda 10–2 controller (Sutter Instruments), and emission was set to 518 nm. Image frames from the CoolSnap HQ Photonics camera (Nikon) were digitized and stored for off-line analysis. Background and calibration images were similarly acquired and used to obtain absolute changes in fluorescence values. All distinct, visible cells in a visual field had regions of interest defined using NIS-elements software thresholding intensity feature to identify cells by intensity at 380 nM excitation and the amplitude of the R (340/380) was measured.

The calcium concentration was calculated using the equation: $[Ca] = K_d * (R - R_{min})/(R_{max} - R)(F_{max}{}^{380}/F_{min}{}^{380})$, assuming the K_d to be 225 nM in the cytosolic environment [22]. Calibration values were determined using 10 μM ionomycin to permeabilize cells to Ca^{2+} and exposing them to [0] Ca^{2+} solution or HR to obtain min and max values, respectively. Values were determined separately for hRPE and HEK-OXTR cells.

2.5. Live-cell fluorescence imaging

Plasmids encoding the PH domain of phospholipase Cd1 fused to GFP (PH-GFP kindly provided by T. Balla, NIH) or GFP fused to C1 domains from protein kinase C (PKC-GFP kindly provided by T. Meyer, Stanford) were used for live-cell fluorescence imaging [23,24]. After 24 h of plasmid transfection into HEK-OXTR cells using TransIT-LT1 (Mirus Bio, Madison, WI), cells were dissociated and plated onto laminin-coated coverslips (12 mm #1; Thermo Fischer Scientific).

Imaging was performed between 48 and 72 h post-transfection while cells were perfused with HR alone and OXT dissolved in HR. Using 470 nm excitation and 525 nm emission, images were acquired every 10 s. 10 μM OXT was used to stimulate cells. The images were analyzed off-line using scans of either membrane or cytoplasmic 'regions of interest' (ROI).

2.6. Animal handling and RPE isolation

Mouse RPE was isolated from 6 to 8 wk old C57BL6 mice (The

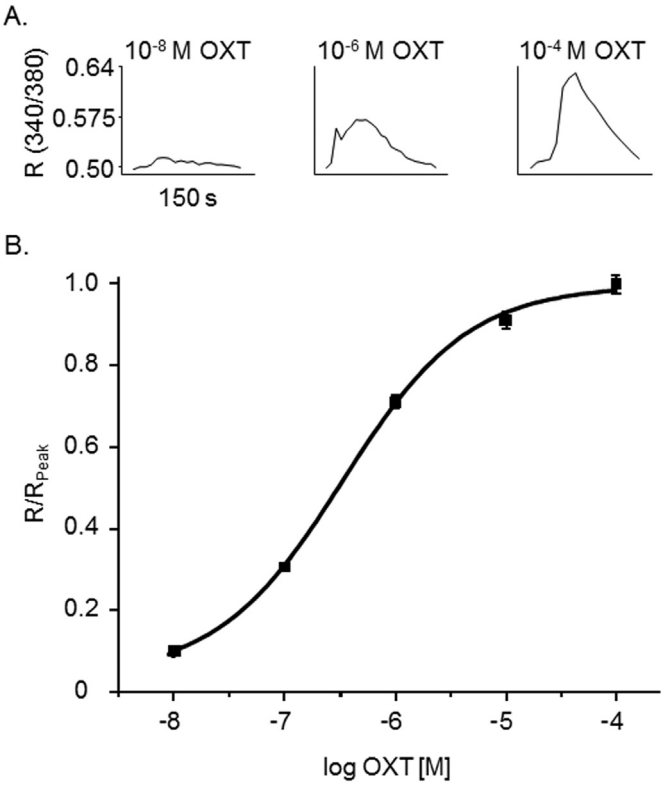

Fig. 1. OXT activation of OXTR in hfRPE cells. (A) Representative traces of individual hfRPE cells during 0.01, 1, or 100 μM OXT bath solution showing a change in R (340/380). (B) OXT-activated increase in intracellular Ca^{2+}-response curve normalized (R/R_{peak}) to the average peak R (340/380), 0.18 ± 0.01, acquired at 100 μM OXT as a function of OXT concentration. Scatter plots represent the average of five experiments (n = 150 cells for each dose, 0.01, 0.1, 1, 10, and 100 μMOXT) and are reported as mean ± SEM. The curve shown is the best fit of the data using the Hill equation. Values obtained for EC_{50} and Hill coefficient were 341 nM and 0.77 ± 0.07, respectively.

Jackson Laboratory, Bar Harbor, ME) used for research in accordance with the recommendations of the guide for the care and use of laboratory animals by Association for Research in Vision and Ophthalmology (ARVO) with housing and care reviewed and approved by the UW-Madison Animal Care Committee. Mice were anesthetized and sacrificed by cervical dislocation. The eyes were enucleated, immediately placed in chilled 0 Na, Ca-Mg free (0Na-CMF) solution (135 mM NMDG-Cl, 5 mM KCl 10 mM HEPES, 10 mM Glucose, 2 mM EDTA-KOH and pH adjusted to 7.4) and washed two times. An incision was made in the scleral buckle with a sharp needle. Vannas scissors were used to cut along the scleral buckle to open the eye, and the anterior cornea, iris and lens were discarded. With the use of surgical forceps, the thin layer of retina was removed. The posterior eye cup with the intact retinal cells was then transferred to an enzymatic solution (0.375 mg/mL Adenosine, 0.3 mg/mL L-Cysteine, 0.25 mg/mL Glutathione, 0.05 mg/mL Taurine, 2.5 μl/mL papain and 5 μL/mL DNAse (0.8 mg/mL-stock) dissolved in 0Na-CMF solution for digestion and incubated in 2 mL tube at 37 °C for 30 mins. The reaction was stopped using 0.01% BSA solution and the eye cups were washed gently with warm HEPES ringer solution (135 mM NaCl, 5 mM KCl, 10 mM HEPES, 10 mM Glucose, 1.8 mM $CaCl_2$, 2 mM $MgCl_2$ and pH adjusted to 7.4).

2.7. Electrophysiology

For electrophysiology using HEK-OXTR cells, 1.8×10^5 cells were plated in a 35 mm dish overnight. The following day, cells were transfected with an N-terminal GFP-labeled Kir7.1 plasmid using a standard TransIT LT-1 protocol at 37 °C for 24 h, after which the cells were transferred to coverslips and placed in reduced-serum media at 37 °C overnight. Cells were selected for recording by the presence of GFP fluorescence in the membrane.

For electrophysiology using murine RPE cells, cells were isolated from 8wk old C57BL/6 mice by enzymatic digestion of the eye cup. Following digestion, RPE cells were identified by their morphology. All recordings were performed in whole-cell patch-clamp configuration. During the recording, HR was used in the bath. Once current was stable, RPE cells were perfused with 10 μM OXT whereas HEK-OXTR cells were perfused with 100–500 nM OXT. Potassium ion current in cells was blocked using 20 mM $CsCl_2$ to identify the proportion of total current for which Kir channel was responsible. The pipette solution contained 30 mM KCl, 83 mM K-gluconate, 5.5 mM EGTA-KOH, 0.5 mM $CaCl_2$, 0.5 mM $MgCl_2$ and 10 mM HEPES. All recordings were performed using an electrophysiology rig built around a Nikon FN1 microscope and consisting of a fixed stage (Nikon, USA), PATCHSTAR micropositioner (Scientifica, East Sussex, UK), low noise amplifier, D/A convertor, and pClamp-10 software (all from Molecular Devices, Sunnyvale, CA). We used a micropipette with a 5–7 MΩ tip and recordings were made using a 2 s ramp protocol from − 150 mV to 50 mV to monitor Kir7.1 current while holding cells at − 60 mV in the inter-pulse interval.

2.8. Statistical analyses

Data from the Ca^{2+} imaging and electrophysiology experiments were analyzed using the Student's t-test. All curve fitting, statistical tests, and plotting of data was performed with Origin (OriginLab Corporation, MA). The dose-response was calculated with the equation $y = R_{min} + (R_{max} - R_{min}) / (1 + 10\hat{}((LogEC_{50} - x) * HillSlope))$. Ca^{2+} response decay was fit with the exponential equation $y = y_0 + Ae^{R0x}$ using Origin. Confidence interval for the ratio of means was calculated using method described by Cochran (1977, Section 6.4, Eq. 6.13) [25]. Data are expressed as mean ± SEM. Significance was determined to be present at $P < 0.05$.

3. Results

3.1. Dose-response effects of OXT in activating hfRPE cell $[Ca^{2+}]_i$

We have previously shown that OXT induces an increase in hfRPE $[Ca^{2+}]_i$, so we used $[Ca^{2+}]_i$ as a variable to determine the dose-dependent response to OXT [10]. hfRPE cells were stimulated by OXT concentrations ranging from 0.01 to 100 μM, and $[Ca^{2+}]_i$ represented by R (340/380), was measured. OXT concentrations of 0.01, 1, and 100 μM showed a progressive increase in $[Ca^{2+}]_i$ (Fig. 1A). 100 μM OXT induced an average increase in R (340/380) of 0.2 (Fig. 1A). Using R values normalized to R_{peak} (0.63; R/R_{peak}), a dose-response curve was generated (Fig. 1B). The dose-response curve exhibited a sigmoidal shape with EC_{50} 0.341 μM OXT and Hill coefficient 0.77 ± 0.07.

3.2. Selective inhibition of hfRPE Ca^{2+} response by selective OXTR antagonist

To demonstrate that the observed Ca^{2+} response was specifically mediated by OXTR we utilized the potent selective OXTR antagonist, desGly-NH_2-d$(CH_2)_5$[D-Tyr^2,Thr^4]OVT (OTA). Following pre incubation with 100 μM OTA we observed a severe reduction of response relative to HR controls performed on the same day (Fig. 2A/B). On average, while 10 μM OXT was able to elicit a 4 ± 0.5 (n = 39/2 coverslips) fold increase in intracellular calcium, pretreatment of cells with 100 μM OTA significantly reduced the Ca^{2+} response to merely 1.3 ± 0.1 (n = 55/3 coverslips) fold increase ($P < 0.001$, Fig. 2B).

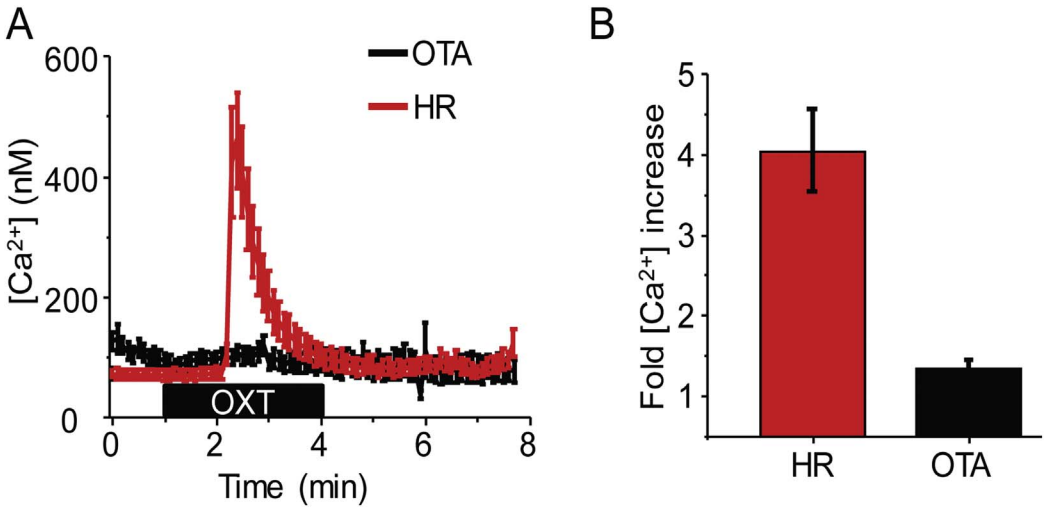

Fig. 2. OXT mediated calcium response is specifically through OXTR activation. (A) Average Ca^{2+} mobilization in response to 10 μM OTA from all hfRPE cells in a visual field on a coverslip incubated with OTA (black trace) or HR (red trace) only. (B) Average fold increase in calcium in HR (Red bar, $n = 39$ ROI/2 coverslips) or after OTA incubation (Black bar, $n = 55$ ROI/3 coverslips) ($P < 0.005$).

3.3. The OXT-induced initial increase of hfRPE $[Ca^{2+}]_i$ is not dependent on extracellular Ca^{2+}

In addition to mobilizing stored intracellular Ca^{2+} via IP_3R, activation of OXTR is thought to stimulate CaV channels, thereby causing an influx of extracellular Ca^{2+} [26–28]. Thus, to determine whether extracellular Ca^{2+} contributed to the OXT-induced transient increase in hfRPE $[Ca^{2+}]_i$, hfRPE cells were exposed to OXT in HR, the CaV specific inhibitor nifedipine in HR and to Ca^{2+}-free extracellular solution. (Fig. 3). We found that 10 μM OXT induced an increase of 1.3 ± 0.2 μM $[Ca^{2+}]_i$ in cells tested using HR solution and 611 ± 130 nM in cells perfused with HR solution including nifedipine. Ca^{2+}-free solution was used to determine the gross effect of extracellular Ca^{2+}, including CaV channels. Stimulation of hfRPE cells in Ca^{2+}-free extracellular solution with 10 μM OXT induced a 685 ± 106 nM increase in $[Ca^{2+}]_i$ (Fig. 3C). We compared the average $[Ca^{2+}]_i$ response to OXT in HR, Ca^{2+} free medium and HR-nifedipine (Fig. 3D), and fit a 1st order equation for the average Ca^{2+} time to decay from peak response. Elevated Ca^{2+} returned

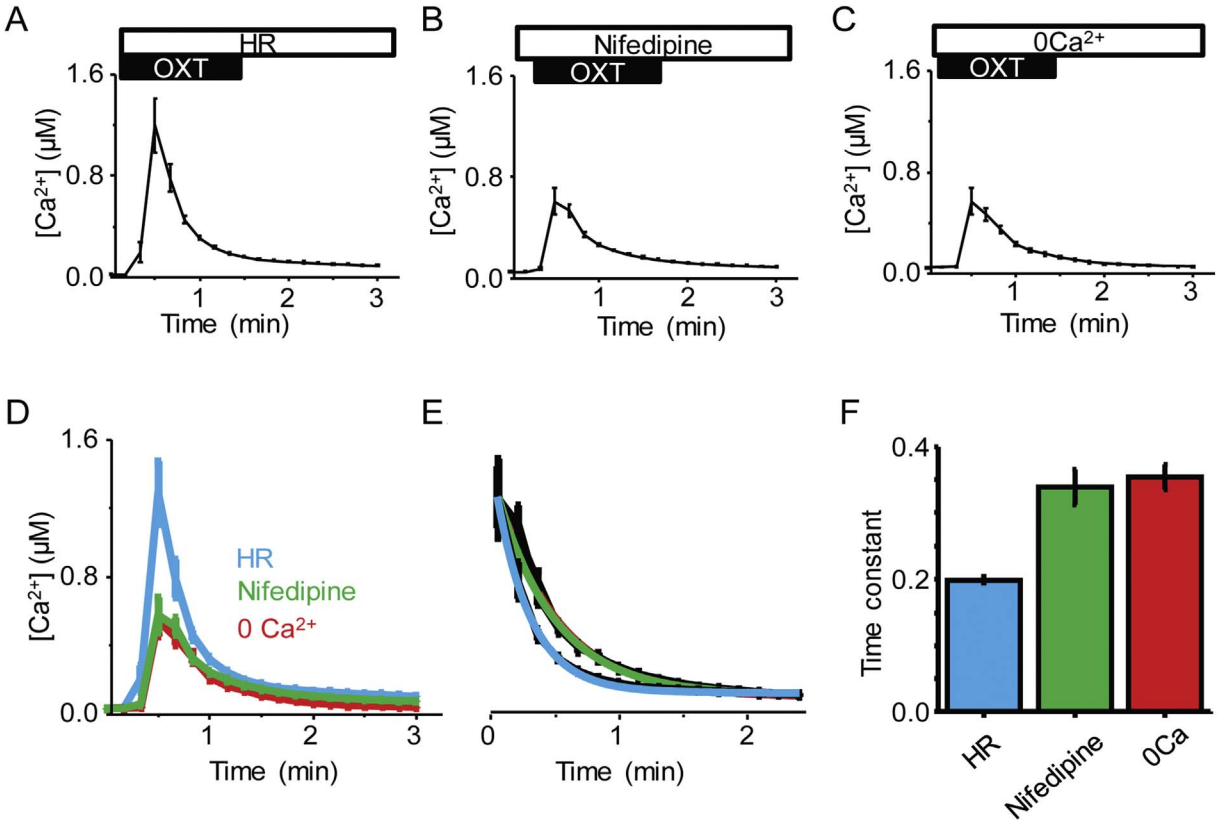

Fig. 3. A) Average time course of hfRPE $[Ca^{2+}]_i$ in response to OXT treatment during incubation with HR solution ($n = 79$ ROI/2 coverslips). B) Average time course of $[Ca^{2+}]_i$ in response to OXT treatment during incubation with nifedipine ($n = 158$ ROI/3 coverslips). C) Average time course of $[Ca^{2+}]_i$ in response to OXT treatment during incubation with 0 Ca^{2+} solution ($n = 174$ ROI/4 coverslips). D) Recordings in all three conditions aligned by their pre-treatment baseline to allow comparison of rise time and amplitude. E) Rate of decay of each treatment, normalized to HR peak with exponential fit included in color. F) Time constant for decay rate in the presence of these three treatments.

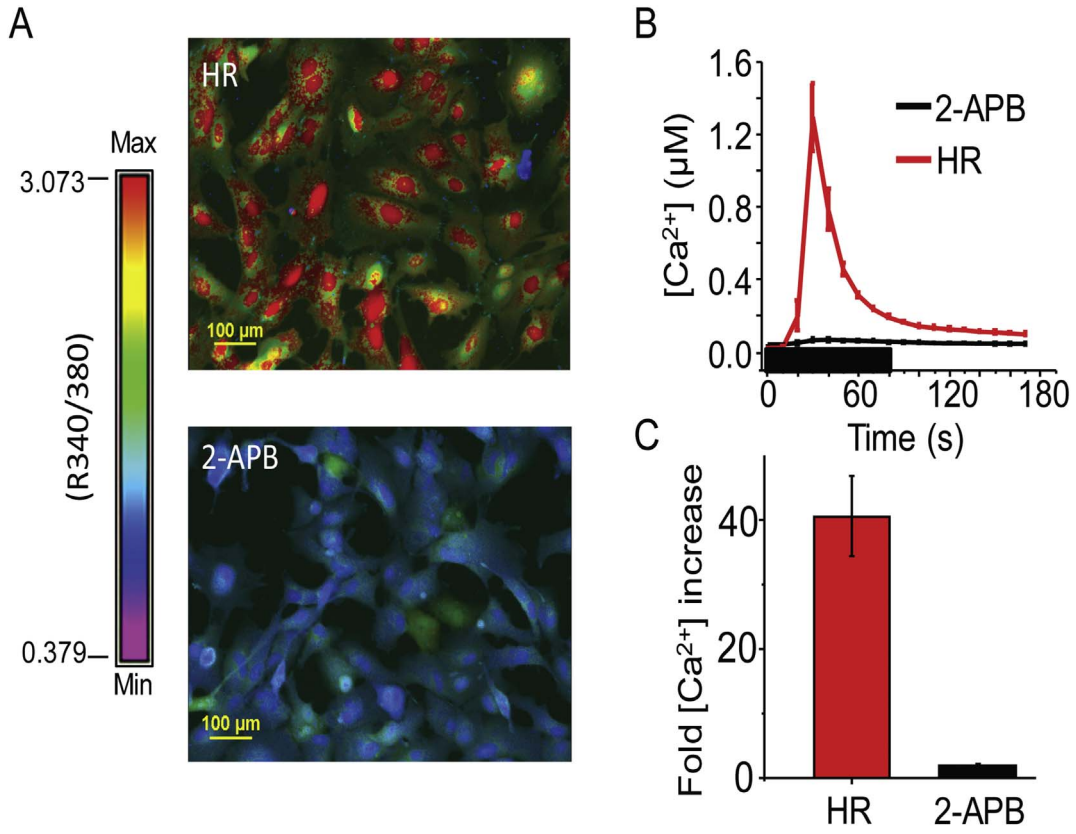

Fig. 4. hfRPE OXT response is inhibited by the IP_3R antagonist, 2-APB. A) Example of Ca^{2+} response to OXT in HR solution compared to OXT response in 2-APB treated cells. Color spectrum with max and min R (340/390) used to calculate $[Ca^{2+}]_i$ provided. (B) An average trace taken from an entire (20 ×) visual field of hfRPE cells showing the change in $[Ca^{2+}]_i$ when stimulated with 10 μM OXT in HR (pink) and 10 μM OXT in 60 μM 2-APB (black). (C) Fold increase in $[Ca^{2+}]_i$ after 10 μM OXT treatment in HR (black) or 60 μM 2-APB (red), relative to baseline taken by averaging five points prior to treatment. This plot demonstrates a significant inhibition ($P < 0.0001$) in the Ca^{2+} response in hfRPE cells following treatment with 2-APB. (For interpretation of the references to color in this figure legend, the reader is referred to the web version of this article.)

to baseline, with time constants (τ) of 0.35 ± 0.02 (r [2] = 0.99), 0.34 ± 0.03 (r [2] = 0.99), and 0.20 ± 0.005 (r [2] = 0.99) min for Ca^{2+}-free, nifedipine, and Ringer's solution, respectively (Fig. 3E).

3.4. 2-APB reduces the OXT-induced increase of hfRPE $[Ca^{2+}]_i$

In non-retinal tissues, OXTR activation by OXT is known to cause the PLC-mediated generation of IP_3, IP_3-IP_3R binding and an increase in $[Ca^{2+}]_i$ due to IP_3R-mediated mobilization of Ca^{2+} from intracellular stores [29]. To determine whether the OXT-induced increase of hfRPE $[Ca^{2+}]_i$ is similarly initiated through the IP_3R-mediated mobilization, we used the IP_3R antagonist, 2-APB. In the presence of 60 μM 2-APB we found that the Ca^{2+} response to 10 μM OXT was virtually abolished in hfRPE cells (Fig. 4). Fig. 4B demonstrates the significance of this inhibition by comparing the average $[Ca^{2+}]_i$ response to 10 μM OXT response from an entire visual field of hfRPE cells, captured with a 20 × objective, in a coverslip exposed to 60 μM 2-APB versus one exposed to OXT alone. The fold increase in $[Ca^{2+}]_i$ relative to pre-OXT baseline supports that there is a significant inhibition of OXT effect by 2-APB ($P < 0.0001$) (Fig. 4C). While 2-APB has also been shown to inhibit TRP channels, the maintenance of a $[Ca^{2+}]_i$ response in the presence of Ca-free solution suggests that TRP channels are not required for the OXT-mediated response, supporting that our observation that inhibition is through IP_3R.

3.5. Development of HEK-OXTR cell line

To facilitate further study of OXTR signaling, we generated a stably-transfected HEK293-OXTR cell-line. In three independent experiments, we measured intracellular $[Ca^{2+}]_i$ during stimulation with 10 μM OXT or 100 μM ATP, in a total of 947 cells. OXT increased $[Ca^{2+}]_i$ 6.0 ± 0.2 fold relative to baseline ($P < 0.001$, Fig. 5C). This was similar to the effect of ATP, which increased $[Ca^{2+}]_i$ by 5.6 ± 0.1 fold relative to baseline ($P < 0.001$, Fig. 5C). HEK293 cells not expressing OXTR were used as a negative control and displayed an increase in intracellular Ca^{2+} when stimulated with ATP, but not with OXT (Fig. 5C). These observations are consistent with our work identifying OXT-OXTR signaling in hfRPE cells [10].

3.6. Visualization of OXT-induced GPCR signaling

To support our findings in hfRPE and provide visual evidence that OXTR activation by OXT induced the PLC-mediated hydrolysis of PIP_2 to generate IP_3, we used live-cell fluorescence imaging to visualize the production of IP_3 and DAG. GFP probes to the Plekstrin Homology domain (PH-GFP) were used to detect membrane PIP_2, and PKC-GFP was used to detect DAG, as both signaling molecules are used by the GPCR-PLC activation pathway. When HEK-OXTR cells were treated with OXT, PH-GFP fluorescence translocated from the membrane micro-environment to the cytoplasm, an indication of PIP_2 hydrolysis by PLC to form IP_3. Fig. 6A is a plot of cytoplasmic fluorescence intensity measured over time in a single PH-GFP expressing cell exposed to 10 μM OXT. In Fig. 6B left panel upper picture, PH-GFP localized to cytoplasmic membrane of two cells. Immediately following OXT treatment, there was an increase in cytoplasmic fluorescence (Fig. 6A, upward deflection; Fig. 6B left panel middle; Video 1) followed by slow return to the baseline level (Fig. 6B left panel lower). On average, OXT treatment of cells resulted in a 1.2 ± 0.2 fold reversible increase of cytoplasmic fluorescence (Fig. 6B right panel, $p < 0.001$, $n = 35$).

We performed a similar experiment using PKC-GFP transfected cells.

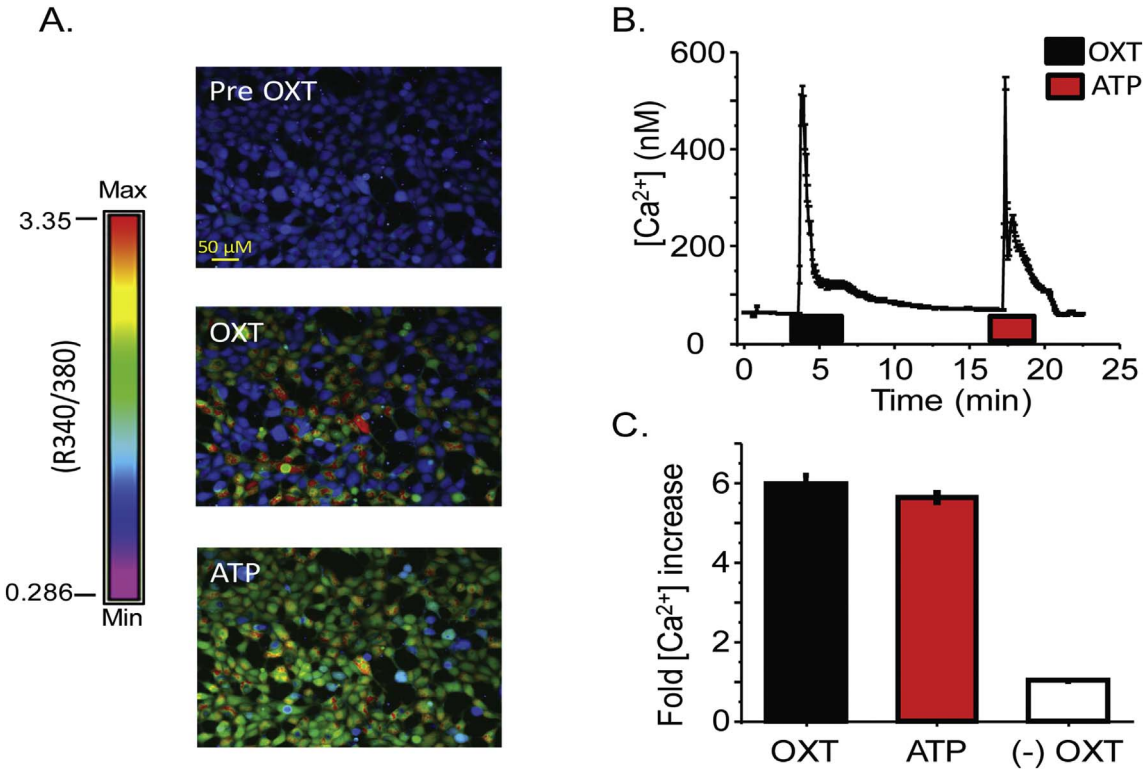

Fig. 5. The $[Ca^{2+}]_i$ response upon OXT stimulation of HEK293-OXTR cells. A) Representative images demonstrating $[Ca^{2+}]_i$ response to OXT and ATP. Color spectrum with max and min R (340/390) used to calculate $[Ca^{2+}]_i$ provided. B) An average time course, from one coverslip, of change in $[Ca^{2+}]_i$ when stimulated with 10 µM OXT or 100 µM ATP. Horizontal bars indicate duration of agonist application. C) Average fold increase in $[Ca^{2+}]_i$ in response to OXT or ATP taken from three independent experiments (n = 947) HEK293 cells without OXTR expression are used as a negative control for OXT mediated $[Ca^{2+}]_i$ response (n = 139).

Plotting of fluorescence intensity in the cytoplasm (Fig. 6C) versus time indicated a reversible decrease (Fig. 6C, downward deflection) in fluorescence intensity upon treatment of HEK-OXTR cells with OXT. As shown in Fig. 6D left panel, one representative cell shows cytoplasmic GFP before (upper image), and after (lower image) OXT treatment. During the treatment with 10 µM OXT, GFP fluorescence was noticed primarily in the membrane microenvironment and cell nucleus (Fig. 6D left panel middle image; Video 2). Measurement of the average fluorescence intensity showed that OXT treatment resulted in a decrease in the cytoplasmic fluorescence level to 0.80 ± 0.02 fold of that in non-treated cells ($p < 0.0001$, $n = 8$) which recovered to 0.9 ± 0.03 fold upon washing of OXT (Fig. 6D, right panel).

3.7. OXTR activation inhibits RPE Kir7.1 channel function

Kir7.1 channels are present in the RPE apical membrane and are regulated by membrane PIP_2 [30]. Given the importance of Kir7.1 to RPE-Retina interaction and our demonstration of its contribution to an OXTR signaling mechanism, we were keen to test whether these two signaling pathways are connected [31]. As the RPE cell contains a complex microenvironment that could mask the interaction between Kir7.1 and OXTR, we first used the HEK-OXTR stably transfected cell line model. An N-terminal GFP-fused Kir7.1 protein was transiently expressed. Whole cell current was recorded in bath solution, and during treatment with 100 nM OXT and 20 mM $BaCl_2$ or 20 mM $CsCl_2$. Fig. 7A shows the time course of a whole-cell recording from a single transfected HEK-OXTR cell. A large inward current at − 160 mV, characteristic of Kir7.1, was observed, was subsequently reduced following OXT treatment (green bar), and almost completely blocked by Cs^{2+} (blue bar). Depolarization of the membrane was also observed (red trace) following OXT treatment in this single cell. Fig. 7B is an IV plot in which we observed an average whole-cell (n = 9) current of − 22.0 ± 2.6 pA/pF (black trace) which was reduced to − 6.6 ± 0.6 pA upon treatment with OXT (Fig. 7B, red trace) measured at − 160 mV. This 68 ± 3% decrease in total current corresponds to a 72 ± 3% decrease in K^+ current and was statistically significant (Fig. 7F, P < 0.001). Despite what was observed in Fig. 7A, on average there was no significant alteration of membrane potential. Chinese hamster ovary cells stably expressing the muscarinic (M1) receptor GPCR were used as a positive control. These cells displayed a similar reduction in inward Kir7.1 current amplitude when exposed to the M1-receptor agonist carbachol (66% decrease; $P < 0.001$ results not shown), suggesting that the inhibition is GPCR-dependent.

To validate the physiologic relevance of our results showing inhibition of Kir 7.1 by OXT in a heterologous expression system, whole-cell patch clamp recordings were performed on RPE cells freshly dissociated from mouse eye cups. An example of the morphology of selected cells can be seen in Fig. 7C. In 7 cells we observed an average membrane potential of − 58.7 ± 1.9 mV. As illustrated in Fig. 7D, a plot of whole-cell current amplitude at -160 mV shows the reduction of inward current in response to 10 µM OXT (Fig. 7D, black bar). In the same figure, depolarization of the cell can also be observed in response to OXT and Cs^{2+} treatment. A plot of the current-voltage curve shows the average whole cell current in HR before and after 10 µM OXT treatment (Fig. 7E, n = 7). The three treatment conditions show equal current at a voltage consistent with E_k (~ − 88 mV), further demonstrating that the observed effect is through modulation of K^+ channels. This plot demonstrated a 22 ± 2% decrease in whole cell current following OXT treatment, corresponding to a 62 ± 5% decrease in K^+ current ($p < 0.005$) and an average depolarization by 11.4 ± 3.3 mV ($p < 0.005$).

In Fig. 7F, we compare the proportion of the K^+ current following OXT treatment to the K^+ current before treatment in mouse RPE (n = 3), and HEK-OXTR (n = 9) cells. The overexpression of OXTR and Kir7.1 compared to that in the mouse RPE cells is likely the reason for the greater decrease in current observed in HEK-OXTR cells.

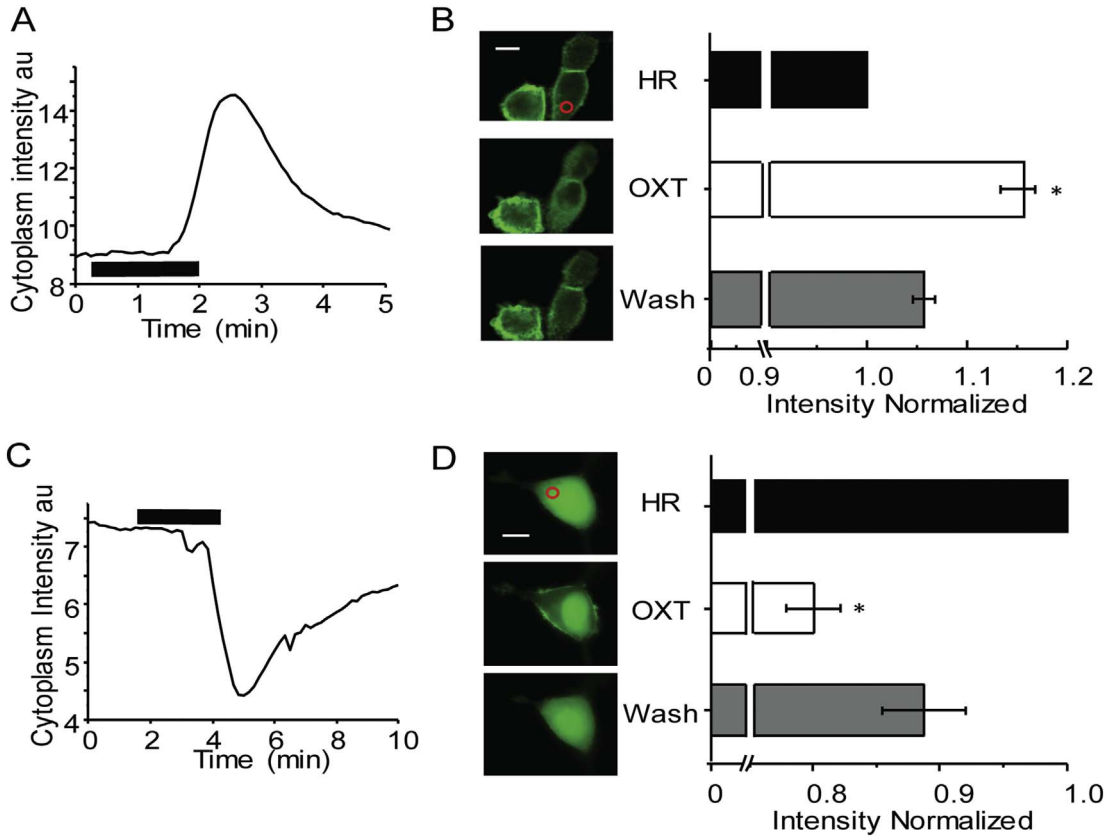

Fig. 6. OXT activation of OXTR results in PIP2 hydrolysis in HEK-OXTR cells. A) Representative GFP fluorescence time course within the cytoplasmic region shows OXTR receptor activation by 6 μM OXT (horizontal line) induced a translocation of the PIP2 indicator PH-GFP from the plasma membrane to the cytosol that completely reversed upon removal of OXT. B) On the left PH-GFP transfected cells shown before (top), during (middle) and after (bottom) OXT treatment with ROI indicated as red circle. The average of normalized fluorescence intensity change within the cytoplasmic domain is shown on the right from four experiments. C) Representative GFP fluorescence time course within the cytoplasmic ROI shows OXTR receptor activation by 6 μM OXT (horizontal line) induced a translocation of the PKC-GFP (indicator of DAG) from the cytosol to the plasma membrane that completely reversed upon removal of OXT. D) On the left images of PKC-GFP expressing cell shown before (top), during (middle) and after (bottom) OXT treatment with ROI indicated as red circle. On the right average plot of normalized fluorescence intensity values within the cytoplasmic domain from three experiments and reported as mean ± SEM. Scale bar in B and D is 10 μm and * indicates $P < 0.001$. (For interpretation of the references to color in this figure legend, the reader is referred to the web version of this article.)

4. Discussion

Oxytocin is present in the cone photoreceptor extracellular matrix and OXTR is expressed in the adjacent RPE cells, leading us to suggest that oxytocinergic signaling may be of physiologic significance in the retina [10]. In the present study, we show that OXT increases hfRPE $[Ca^{2+}]_i$ through a GPCR-mediated mechanism whereby the OXT binding to OXTR causes downstream activation of PLC and PIP_2 hydrolysis. In addition, we have shown that heterologously expressed Kir7.1 channels in HEK-OXTR cells, as well as endogenous mouse RPE cell Kir7.1 channels are subject to OXTR inhibition. We propose a model by which OXT-OXTR signaling between photoreceptor and RPE cells may also occur in vivo, as summarized in Fig. 8.

The dose-response curve of $[Ca^{2+}]_i$ induced by OXT in hfRPE exhibited a sigmoidal profile similar to previously reported dose-response curves for OXT, indicating that OXT-OXTR signaling may be of physiologic relevance [32,33]. In the present study, hfRPE had a reported EC_{50} of approximately 341 nM OXT. Previously reported K_d values for OXTR range from 0.96 to 215 nM OXT [12,34–37]. Within this range, however, there exist distinct high- and low-affinity subgroups of OXTR. As demonstrated by Gimpl and colleagues (1995), the affinity state of OXTR is cholesterol-dependent, such that addition of exogenous cholesterol can promote a shift of about 20% of the low affinity OXTR to an approximately 200-fold higher affinity state (K_d = 0.96 nM) [38]. Our finding of an EC_{50} of 341 nM OXT in hfRPE suggests that OXTR was in a low affinity state under our experimental conditions. Variable OXTR K_d values have been shown with alterations in culture media cholesterol, serum, and Mg^{2+} concentrations [39–42]. The hfRPE cells were cultured in non-FBS containing media and thus did not contain adequate exogenous cholesterol to promote the high affinity variant of the OXTR. It is also true that RPE cells are highly polarized cells with a distinct plasma-membrane composition when compared to other epithelial cells, and thus they may demonstrate sensitivity to OXT that could be unique [3].

Although OXT likely increases hfRPE $[Ca^{2+}]_i$ by binding and activating the OXTR, OXT also has some affinity, albeit low, for the vasopressin V_{1a} receptor, which when activated, can also stimulate an increase in $[Ca^{2+}]_i$ [43,44]. In addition to being highly homologous and closely related to OXTR, vasopressin V_{1a} is known to be present and functional in the RPE. We have shown previously that the OXT-induced increase in hfRPE $[Ca^{2+}]_i$ was reduced by 87% in the presence of 500 nM of the OXTR-specific antagonist, L-371,257, providing strong evidence that the OXT-induced increase in hfRPE $[Ca^{2+}]_i$ was mediated through the OXTR, even when a supraphysiologic dose (6 μM) was used [10]. The other specific OXTR antagonist, OTA, in this paper also significantly (> 85%) reduced the Ca^{2+} response to OXT (10 μM), further supporting the explicit activation of OXTR in the RPE. Based on these finding, we used 10 μM OXT to ensure maximal activation of cells during perfusion experiments.

Studies in the myometrium and OXTR-COSM6 cells have demonstrated activation of a Gßγ-mediated pathway as a consequence of GPCR activation, resulting in increased ERK1/2 phosphorylation [1,45,46]. This suggests that OXT may be stimulating the increase in $[Ca^{2+}]_i$ through mechanisms other than the $G\alpha_q$-mediated activation of

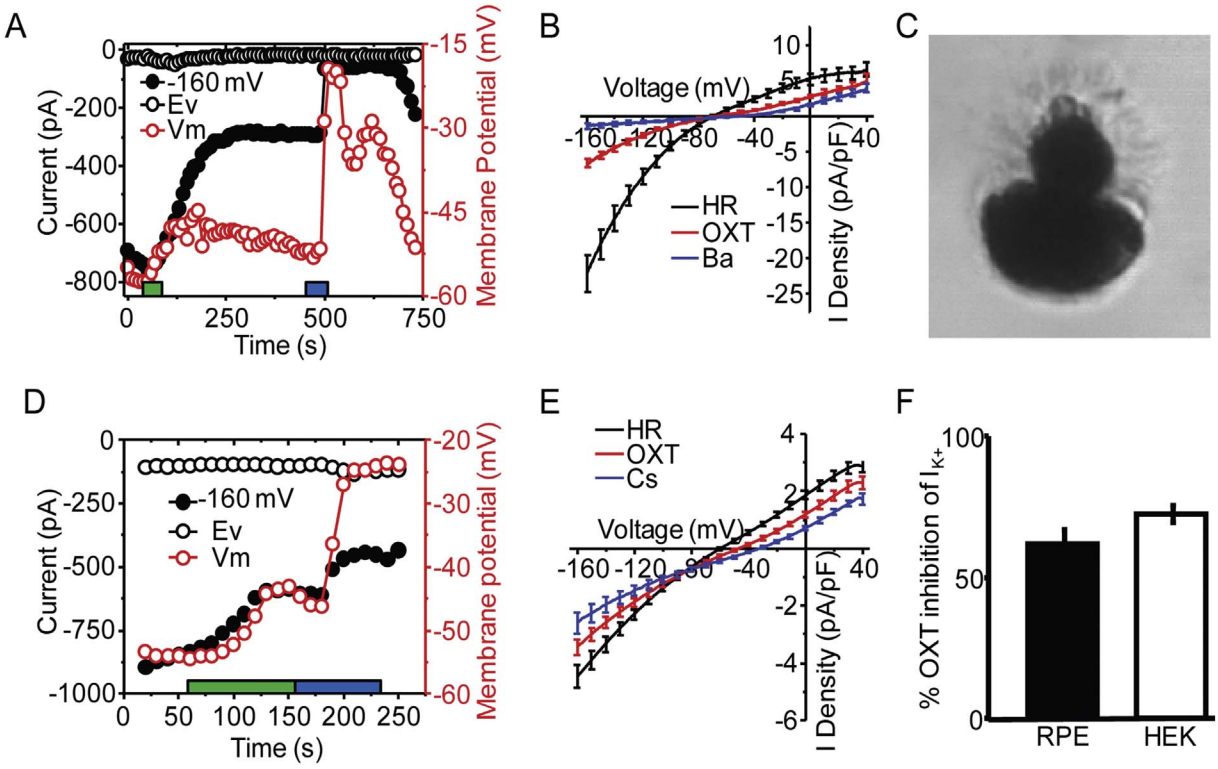

Fig. 7. OXT activation of OXTR inhibits Kir7.1 channel. A) Representative HEK-OXTR whole-cell current time course measured at cell potentials − 68 mV (Ev) and − 160 mV during application of a ramp voltage protocol from − 160 to − 40 mV every 10 s while holding the cell at − 10 mV. In addition, the membrane potential of the cell (Vm) is plotted over the time course of the experiment. The duration of OXT (red) and Kir7.1 blocker Cs^{2+} (blue) application is indicated. B) Average plot of I–V whole cell current at baseline (Black; $n = 9$), and after application of OXT (Red; $n = 9$), Cs^{2+} (Blue; $n = 9$). C) Image of dissociated mouse RPE cell with polarized morphology representative of cells selected for recording. D) Representative mouse RPE whole-cell current time course measured at cell potentials − 62 (Ev), and − 160 mV during application of the same ramp protocol as in A. The membrane potential of the cell is plotted over the time course of the experiment. Duration of application of OXT (red) and Cs2 + (blue) is indicated. The duration of OXT (red) and Kir7.1 blocker Cs^{2+}(blue) application is indicated. E) Average plot of I–V whole cell current before (Black; $n = 7$), and after application of OXT (Red; $n = 7$) or Cs^{2+} (Blue; $n = 3$). F) Comparison of ratio of Cs^{2+} sensitive current during OXT treatment relative to current in HR in murine RPE and HEK-OXTR cells. Data is from at least three independent experiments and represented as mean ± SEM. (For interpretation of the references to color in this figure legend, the reader is referred to the web version of this article.)

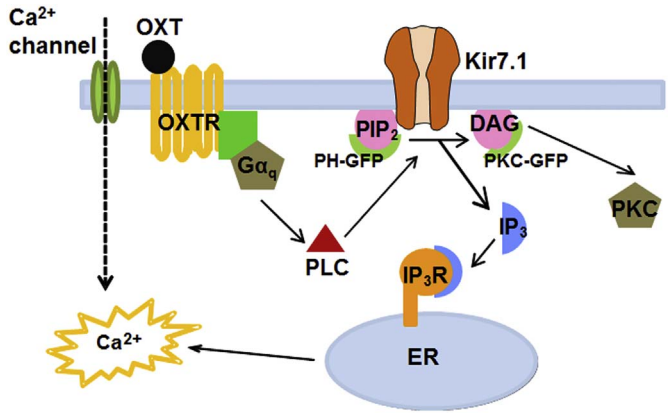

Fig. 8. Summary of our findings regarding OXT-OXTR initiated cellular signaling events in the RPE. Binding of OXT ligand, either from cone photoreceptors or choroidal vasculature, to OXTR receptor in the RPE causes cytoplasmic membrane leaflet PIP2 to hydrolyze to IP3 and DAG. PIP2 hydrolysis inhibits RPE Kir7.1 channel to depolarize the membrane potential while IP3 binding to its receptor leads to the increase in cytoplasmic Ca^{2+}. These transient intracellular signaling responses neither involve Ca^{2+} channels nor does extracellular Ca^{2+} influence them in any substantive way.

PLC. Our data, however, support the $G\alpha_q$-mediated mechanism of oxytocinergic signaling in the RPE (Fig. 8). We propose that binding of OXT from the retina leads to OXTR-mediated hydrolysis of the RPE membrane PIP_2 by PLC and generates two cellular responses: 1) the inhibition of Kir7.1 channels in the RPE apical membrane, and 2) IP_3 binding to the IP_3R that causes release of Ca^{2+} from intracellular stores. The effect is abolished in the presence of 2-APB, in agreement with published work on OXTR signaling in myenteric neurons [47]. 2-APB has also been described as a TRPC inhibitor, however, the sustained Ca^{2+} response in Ca^{2+}-free solution we have described shows that the 2-APB mediated inhibition demonstrated found in our system is through the IP_3R [48].

The association of OXTR activation with extracellular Ca^{2+} influx through CaV is somewhat controversial in uterine function, the best characterized model of OXT signaling to-date. In our RPE work, the rapid initial OXT-induced increase in $[Ca^{2+}]_i$ occurs consistently in the presence of nifedipine, as well as Ca^{2+}-free solution, demonstrating nifedipine insensitivity in agreement with work published by Inoue and colleagues [49,50]. However, we observed a reduction in the amplitude of the Ca^{2+} response from HR to nifedipine and Ca^{2+}-free solution, which corresponds to an increase in time constant (Fig. 3D–E). This suggests that extracellular calcium is involved in part in the OXT-mediated response after the initial IP_3-mediated Ca^{2+} release. We suggest that this response is likely mediated by voltage-activated Ca^{2+} channels, given the lack of distinction between the responses observed in Ca^{2+}-free solution and nifedipine.

Utilizing HEK-OXTR cells exposed to OXT, we were able to demonstrate by live cell fluorescence imaging that PLC hydrolysis of PIP_2 is a source of IP_3 and DAG using PH-GFP and PKC-GFP, supporting our observations and hypothesis about its role in the RPE. Using this heterologous system we also investigated whether a loss of PIP_2 affects direct gating of RPE Kir7.1 channels [31]. In development of our Kir7.1 eGFP, we generated both N-terminal and C-terminal fused constructs. The N-terminal fused construct exhibited measurable current whereas the C-terminal fused construct did not, suggesting that the C-terminal

GFP, but not the N-terminal GFP, interfered with Kir7.1 channel function [21]. The activation of OXTR with OXT therefore inhibits Kir7.1 channel in both HEK-OXTR cells and the mouse RPE and the N-terminal GFP does not interfere with the cellular signaling events explored in this study.

All Kir channels demonstrate PIP binding to the same general cytoplasmic location; however, the affinity of Kir channels for PIP_2 and other PIP groups is determined by differences in the amino acid sequence mediating interaction with the lipid tail group [51,52]. Relative to other Kir channels, Kir 7.1 has a weak affinity for PIP_2 which results in a more pronounced inhibition by PIP_2 hydrolysis compared to other Kir channels [18,53]. We observed an OXT-mediated decrease in the Kir7.1 channel current by 15.5 pA/pF or 68 ± 3% in HEK-OXTR cells (Fig. 7B) and a smaller but still significant decrease in whole cell current in mouse RPE cells. After removing non-K^+ current by subtracting the Cs^{2+}-insensitive component, the percent inhibition between the two cell types was identical, with the remaining difference likely due to overexpression of Kir7.1 in the HEK-OXTR cells (Fig. 7E). Furthermore, mouse RPE was significantly depolarized in response to OXT treatment. The RPE membrane potential regulates the ion and waste transport functions of the RPE, making oxytocin a potential regulator of outer retina function. In view of the discovery by Ghamari-Langroudi and colleagues (2015) that Kir7.1 can be inhibited by a GPCR independently of G-protein coupling, our future studies will determine if this also occurs in OXT-mediated OXTR activation in the RPE [54]. Given the recent discovery of a role for Kir7.1 in the initiation of uterine contractions by McCloskey and colleagues (2014), we propose that the signaling mechanism discovered in our study is also involved in parturition [55].

In summary, we have provided evidence of the following:1) OXT specifically activated OXTR in RPE cells, 2) OXT-induced $[Ca^{2+}]_i$ response is not dependent on extracellular Ca^{2+}, 2) the OXT-induced $[Ca^{2+}]_i$ response is not blocked by the CaV blocker nifedipine, and 3) the IP_3R inhibitor 2-APB inhibits the OXT-mediated $[Ca^{2+}]_i$ increase. Using a model in which OXTR is stably expressed in HEK-OXTR cells, we have demonstrated an OXT-induced $[Ca^{2+}]_i$ increase, associated with PIP_2 hydrolysis through PH-GFP and PKC-GFP can be visualized in response to OXT. We have also shown that Kir7.1 is inhibited by OXT in both heterologous HEK-OXTR cells and in physiological RPE cells isolated from the mouse eye, resulting in depolarization of the RPE membrane potential. Tight regulation of membrane potential via Kir7.1 regulates the ion and waste transport functions of the RPE, and supports our hypothesis that oxytocin is a potential regulator of outer retina function.

Supplementary data to this article can be found online at http://dx.doi.org/10.1016/j.cellsig.2017.06.005.

Statement of conflicts of interest

The authors declare that they have no conflicts of interest.

Author contributions

Study concept and design: all authors. Acquisition, analysis and interpretation of data: NY, PJH, MC, BRP. Drafting of manuscript: NY, PJH, MC, DMP, BRP. Critical revision of manuscript: NY, IB, DMP, BRP. Final approval: DMP, BRP. Study supervision: BRP.

Acknowledgments

We thank Dr. Barbara Sanborn (Colorado State University) for the gift of the OXTR plasmid and for helpful discussion, Dr. Thomas Balla (NICHD, NIH) for the gift of PH-GFP, Dr. Maurice Manning (University of Toledo) for providing the selective oxytocin receptor antagonist and Dr. Tobias Meyer (Stanford) for the gift of PKC-GFP expression plasmids. We would also like to thank Dr. Jens Eickhoff (University of Wisconsin-Madison) for the help he provided with our calcium imaging statistics. We acknowledge members of the Pillers-Pattnaik research team for helpful discussion and exchange of ideas. These studies were supported by the Meriter Foundation (BRP), McPherson Eye Research Institute M.D. Mathews Research Professorship (BRP), and the University of Wisconsin Department of Pediatrics (DMP, BRP). BRP is supported by NIH grant EY24995, and a core grant P30EY16665.

References

[1] G. Gimpl, F. Fahrenholz, The oxytocin receptor system: structure, function, and regulation, Physiol. Rev. 81 (2001) 629–683.
[2] C. Elabd, et al., Oxytocin is an age-specific circulating hormone that is necessary for muscle maintenance and regeneration, Nat. Commun. 5 (2014) 4082, http://dx.doi.org/10.1038/ncomms5082.
[3] O. Strauss, The retinal pigment epithelium in visual function, Physiol. Rev. 85 (2005) 845–881, http://dx.doi.org/10.1152/physrev.00021.2004.
[4] R.P. Gallemore, R.H. Steinberg, Effects of dopamine on the chick retinal pigment epithelium. Membrane potentials and light-evoked responses, Invest. Ophthalmol. Vis. Sci. 31 (1990) 67–80.
[5] C. Versaux-Botteri, J.M. Gibert, J. Nguyen-Legros, P. Vernier, Molecular identification of a dopamine D1b receptor in bovine retinal pigment epithelium, Neurosci. Lett. 237 (1997) 9–12.
[6] R.H. Quinn, J.N. Quong, S.S. Miller, Adrenergic receptor activated ion transport in human fetal retinal pigment epithelium, Invest. Ophthalmol. Vis. Sci. 42 (2001) 255–264.
[7] E.A. Barnard, G. Burnstock, T.E. Webb, G protein-coupled receptors for ATP and other nucleotides: a new receptor family, Trends Pharmacol. Sci. 15 (1994) 67–70.
[8] M.S. Nash, N.N. Osborne, Pharmacologic evidence for 5-HT1A receptors associated with human retinal pigment epithelial cells in culture, Invest. Ophthalmol. Vis. Sci. 38 (1997) 510–519.
[9] M. Nash, T. Flanigan, R. Leslie, N. Osborne, Serotonin-2A receptor mRNA expression in rat retinal pigment epithelial cells, Ophthalmic Res. 31 (1999) 1–4.
[10] P. Halbach, et al., Oxytocin expression and function in the posterior retina: a novel signaling pathway, Invest. Ophthalmol. Vis. Sci. 56 (2015) 751–760, http://dx.doi.org/10.1167/iovs.14-15646.
[11] F. Fahrenholz, U. Klein, G. Gimpl, Conversion of the myometrial oxytocin receptor from low to high affinity state by cholesterol, Adv. Exp. Med. Biol. 395 (1995) 311–319.
[12] D. Yang, A. Pan, A. Swaminathan, G. Kumar, B.A. Hughes, Expression and localization of the inwardly rectifying potassium channel Kir7.1 in native bovine retinal pigment epithelium, Invest. Ophthalmol. Vis. Sci. 44 (2003) 3178–3185.
[13] M. Shimura, et al., Expression and permeation properties of the K(+) channel Kir7.1 in the retinal pigment epithelium, J. Physiol. 531 (2001) 329–346.
[14] B.A. Hughes, M. Takahira, Inwardly rectifying K + currents in isolated human retinal pigment epithelial cells, Invest. Ophthalmol. Vis. Sci. 37 (1996) 1125–1139.
[15] M. La Cour, Cl- transport in frog retinal pigment epithelium, Exp. Eye Res. 54 (1992) 921–931.
[16] S. Bialek, S.S. Miller, K + and Cl- transport mechanisms in bovine pigment epithelium that could modulate subretinal space volume and composition, J. Physiol. 475 (1994) 401–417.
[17] E.R. Griff, Y. Shirao, R.H. Steinberg, Ba2 + unmasks K + modulation of the Na + -K + pump in the frog retinal pigment epithelium, J. Gen. Physiol. 86 (1985) 853–876.
[18] B.R. Pattnaik, B.A. Hughes, Regulation of Kir channels in bovine retinal pigment epithelial cells by phosphatidylinositol 4,5-bisphosphate, Am. J. Phys. 297 (2009) C1001–C1011.
[19] J.F. Hejtmancik, et al., Mutations in KCNJ13 cause autosomal-dominant snowflake vitreoretinal degeneration, Am. J. Hum. Genet. 82 (2008) 174–180, http://dx.doi.org/10.1016/j.ajhg.2007.08.002.
[20] P.I. Sergouniotis, et al., Recessive mutations in KCNJ13, encoding an inwardly rectifying potassium channel subunit, cause leber congenital amaurosis, Am. J. Hum. Genet. 89 (2011) 183–190, http://dx.doi.org/10.1016/j.ajhg.2011.06.002.
[21] B.R. Pattnaik, et al., A novel KCNJ13 nonsense mutation and loss of Kir7.1 channel function causes Leber congenital Amaurosis (LCA16), Hum. Mutat. 36 (2015) 720–727, http://dx.doi.org/10.1002/humu.22807.
[22] G. Grynkiewicz, M. Poenie, R.Y. Tsien, A new generation of Ca2 + indicators with greatly improved fluorescence properties, J. Biol. Chem. 260 (1985) 3440–3450.
[23] P. Varnai, T. Balla, Visualization of phosphoinositides that bind pleckstrin homology domains: calcium- and agonist-induced dynamic changes and relationship to myo-[3H]inositol-labeled phosphoinositide pools, J. Cell Biol. 143 (1998) 501–510.
[24] E. Oancea, M.N. Teruel, A.F. Quest, T. Meyer, Green fluorescent protein (GFP)-tagged cysteine-rich domains from protein kinase C as fluorescent indicators for diacylglycerol signaling in living cells, J. Cell Biol. 140 (1998) 485–498.
[25] W.G. Cochran, Sampling Techniques, 3rd edn, Wiley, 1977.
[26] B.M. Sanborn, C.Y. Ku, S. Shlykov, L. Babich, Molecular signaling through G-protein-coupled receptors and the control of intracellular calcium in myometrium, J. Soc. Gynecol. Investig. 12 (2005) 479–487, http://dx.doi.org/10.1016/j.jsgi.2005.07.002.
[27] D.A. Murtazina, et al., TRPC1, STIM1, and ORAI influence signal-regulated intracellular and endoplasmic reticulum calcium dynamics in human myometrial cells, Biol. Reprod. 85 (2011) 315–326, http://dx.doi.org/10.1095/biolreprod.111.

091082.
[28] S. Wray, Insights into the uterus, Exp. Physiol. 92 (2007) 621–631, http://dx.doi.org/10.1113/expphysiol.2007.038125.
[29] S.A.a.S. Wray, Oxytocin: its mechanism of action and receptor signalling in the myometrium, J. Neuroendocrinol. 36 (14) (2014).
[30] D.E. Logothetis, T. Jin, D. Lupyan, A. Rosenhouse-Dantsker, Phosphoinositide-mediated gating of inwardly rectifying K(+) channels, Pflugers Arch. 455 (2007) 83–95, http://dx.doi.org/10.1007/s00424-007-0276-5.
[31] B.R. Pattnaik, B.A. Hughes, Regulation of Kir channels in bovine retinal pigment epithelial cells by phosphatidylinositol 4,5-bisphosphate, Am. J. Phys. Cell Phys. 297 (2009) C1001–C1011, http://dx.doi.org/10.1152/ajpcell.00250.2009.
[32] J.J. Evans, W. Forrest-Owen, C.A. McArdle, Oxytocin receptor-mediated activation of phosphoinositidase C and elevation of cytosolic calcium in the gonadotrope-derived alphaT3-1 cell line, Endocrinology 138 (1997) 2049–2055.
[33] M.S. Sinclair, et al., Oxytocin signaling in mouse taste buds, PLoS One 5 (2010) e11980, , http://dx.doi.org/10.1371/journal.pone.0011980.
[34] O. Quehenberger, E.R. Prossnitz, C.G. Cochrane, R.D. Ye, Absence of G(i) proteins in the Sf9 insect cell. Characterization of the uncoupled recombinant N-formyl peptide receptor, J. Biol. Chem. 267 (1992) 19757–19760.
[35] D.J. Crankshaw, L.A. Branda, M.A. Matlib, E.E. Daniel, Localization of the oxytocin receptor in the plasma membrane of rat myometrium, Eur. J. Biochem. 86 (1978) 481–486.
[36] G. Gimpl, K. Burger, F. Fahrenholz, Cholesterol as modulator of receptor function, Biochemistry 36 (1997) 10959–10974, http://dx.doi.org/10.1021/bi963138w.
[37] V. Pliska, J. Heiniger, A. Muller-Lhotsky, P. Pliska, B. Ekberg, Binding of oxytocin to uterine cells in vitro. Occurrence of several binding site populations and re-identification of oxytocin receptors, J. Biol. Chem. 261 (1986) 16984–16989.
[38] G. Gimpl, U. Klein, H. Reilander, F. Fahrenholz, Expression of the human oxytocin receptor in baculovirus-infected insect cells: high-affinity binding is induced by a cholesterol-cyclodextrin complex, Biochemistry 34 (1995) 13794–13801.
[39] G. Gimpl, K. Burger, E. Politowska, J. Ciarkowski, F. Fahrenholz, Oxytocin receptors and cholesterol: interaction and regulation, Exp. Physiol. 85 (2000) 41S–49S (Spec No).
[40] M.S. Soloff, M.J. Fields, Changes in uterine oxytocin receptor concentrations throughout the estrous cycle of the cow, Biol. Reprod. 40 (1989) 283–287.
[41] V. Pliska, H. Kohlhauf Albertin, Effect of Mg2 + on the binding of oxytocin to sheep myometrial cells, Biochem. J. 277 (Pt 1) (1991) 97–101.
[42] J.A. Copland, et al., Demonstration of functional oxytocin receptors in human breast Hs578T cells and their up-regulation through a protein kinase C-dependent pathway, Endocrinology 140 (1999) 2258–2267, http://dx.doi.org/10.1210/endo.140.5.6723.
[43] Z. Friedman, T.M. Delahunty, J. Linden, P.A. Campochiaro, Human retinal pigment epithelial cells possess V1 vasopressin receptors, Curr. Eye Res. 10 (1991) 811–816.
[44] E. Sermasi, J.H. Coote, Oxytocin acts at V1 receptors to excite sympathetic preganglionic neurones in neonate rat spinal cord in vitro, Brain Res. 647 (1994) 323–332.
[45] M. Zhong, M. Yang, B.M. Sanborn, Extracellular signal-regulated kinase 1/2 activation by myometrial oxytocin receptor involves Galpha(q)Gbetagamma and epidermal growth factor receptor tyrosine kinase activation, Endocrinology 144 (2003) 2947–2956.
[46] C.H. Mitchell, Release of ATP by a human retinal pigment epithelial cell line: potential for autocrine stimulation through subretinal space, J. Physiol. 534 (2001) 193–202.
[47] T. Che, et al., Oxytocin hyperpolarizes cultured duodenum myenteric intrinsic primary afferent neurons by opening BK(Ca) channels through IP(3) pathway, J. Neurochem. 121 (2012) 516–525, http://dx.doi.org/10.1111/j.1471-4159.2012.07702.x.
[48] J.P. Lievremont, G.S. Bird, J.W. Putney Jr., Mechanism of inhibition of TRPC cation channels by 2-aminoethoxydiphenylborane, Mol. Pharmacol. 68 (2005) 758–762, http://dx.doi.org/10.1124/mol.105.012856.
[49] S. Arrowsmith, S. Wray, Oxytocin: its mechanism of action and receptor signalling in the myometrium, J. Neuroendocrinol. 26 (2014) 356–369, http://dx.doi.org/10.1111/jne.12154.
[50] Y. Inoue, K. Shimamura, N. Sperelakis, Oxytocin actions on voltage-dependent ionic channels in pregnant rat uterine smooth muscle cells, Can. J. Physiol. Pharmacol. 70 (1992) 1597–1603.
[51] N. D'Avanzo, S.J. Lee, W.W. Cheng, C.G. Nichols, Energetics and location of phosphoinositide binding in human Kir2.1 channels, J. Biol. Chem. 288 (2013) 16726–16737, http://dx.doi.org/10.1074/jbc.M113.452540.
[52] T. Rohacs, J. Chen, G.D. Prestwich, D.E. Logothetis, Distinct specificities of inwardly rectifying K(+) channels for phosphoinositides, J. Biol. Chem. 274 (1999) 36065–36072.
[53] X. Du, et al., Characteristic interactions with phosphatidylinositol 4,5-bisphosphate determine regulation of kir channels by diverse modulators, J. Biol. Chem. 279 (2004) 37271–37281, http://dx.doi.org/10.1074/jbc.M403413200.
[54] M. Ghamari-Langroudi, et al., G-protein-independent coupling of MC4R to Kir7.1 in hypothalamic neurons, Nature (2015), http://dx.doi.org/10.1038/nature14051.
[55] C. McCloskey, et al., The inwardly rectifying K^+ channel KIR7.1 controls uterine excitability throughout pregnancy, EMBO Mol. Med. 6 (2014) 1105–1214.